BIOZENTRUM
Universität Basel

Thermodynamics and Kinetics of P-Glycoprotein-Substrate Interactions

INAUGURALDISSERTATION

zur

Erlangung der Würde eines Doktors der Philosophie vorgelegt der Philosophisch-Naturwissenschaftlichen Fakultät der Universität Basel

Von

Päivi Äänismaa

aus Finnland

Basel 2007

Genehmigt von der Philosophisch-Naturwissenschaftlichen Fakultät auf Antrag von

PD Dr. Anna Seelig
PD Dr. Jörg Huwyler
Prof. Dr. Joachim Seelig

Basel, den 27.03.2007

<div align="right">

Prof. Dr. Hans-Peter Hauri
(Dekan)

</div>

TABLE OF CONTENTS

1. Introduction

1.1   ATP-Binding Cassette Transporter Superfamily

The A̲TP-b̲inding c̲assette, ABC, transporter superfamily is one of the largest protein classes known. ABC-transporters are found in all cell types from archaebacteria to mammalian cells and they translocate different substrates, ranging from small ions to large polypeptides across the lipid bilayer either into or out of cell and organelles. ABC-transporters are involved in diverse cellular processes such as maintenance of osmotic homeostasis, nutrient uptake, resistance to xenotoxins, cell division, pathogenesis and sporulation, cholesterol and lipid trafficking, and developmental stem cell biology. ABC-transporters utilize the energy released from ATP hydrolysis for solute translocation (*1-4*).

Despite the differences in transported solutes and whether they are transported in or out of cells, all ABC-transporters appear to have a conserved domain structure which comprises two t̲ransm̲embrane d̲omains, TMDs, and two n̲ucleotide b̲inding d̲omains, NBDs. The TMDs contain several membrane-spanning α-helices and provide the specificity for the transported solute. The amino acid sequence of TMDs varies considerably trough ABC-transporters most likely due to the wide variety in transported solutes (*3, 4*).

The classification as ABC-transporters is based on the sequence and organization of the NBDs. The amino acid sequence in the NBDs is highly conserved through the whole superfamily (25-30 % identity) (*1*). The NBDs contain characteristic motifs (Walker A and B), and the signature C motif, also called as ABC- or LSGGQ-motif (*2*). The signature C motif is specific for ABC-transporters and distinguishes them from the other ATP-binding proteins. The hydrophilic NBDs are located in cytoplasm and function as molecular motors by transferring the energy of ATP binding and hydrolysis to the TMDs. Most ABC-transporters are unidirectional (*2, 3*).

In eukaryotes, most ABC-transporters move compounds from the cytoplasm to the outside of cell or into an intracellular compartment (endoplasmic reticulum, mitochondria, peroxisome) (*2*). At present 48 ABC-transporter genes are known in humans (*5*). They have been classified into seven subfamilies (A-G) by the Human Genome Organization. The human ABC-transporters are either full transporters where four domains are in one single polypeptide chain or half-transporters where one TMD is linked to one NBD. A half-transporter has to form a homo- or heterodimer to be a functional unity (*2*). *In bacteria,*

ABC-transporters are mainly involved in the import of essential compounds that cannot enter into the cell by diffusion (sugars, amino acids, vitamins, small peptides, metal, anions, vitamin B12 etc.). Prokaryote importers or permeases generally contain four separate subunits in the core configuration together with a periplasmic-binding protein, which binds and presents solute to the membrane-bound transporters (*3*).

Here we focus on one member of the ABC-transporter superfamily, namely P-glycoprotein (Pgp, ABCB1). Pgp is often described as a double-edged sword (*6*), since it has an important role in the cellular defense system protecting us from xenobiotic toxins (*7*). On the other hand it limits the bioavailability of drugs during chemotherapy and contributes to the multidrug resistance phenomenon (*6, 8*).

1.2   Multidrug Resistance and P-glycoprotein

Cancer cells have the ability to become simultaneously resistant to different drugs. After initial resistance to a single anticancer drug, cells may develop cross-resistance to other structurally and mechanistically unrelated drugs. This phenomenon is known as multidrug resistance, MDR. There are several ways how cancer cells can become resistant to anticancer drugs. i) One way is to reduce the accumulation of drugs into cancer cells. This can occur e.g. by increasing the activity of efflux transporters such as Pgp. ii) If the drug accumulation is unchanged, activation of drug metabolizing enzymes, cytochrome P450s, can promote drug resistance. iii) Cells can also activate drug-induced DNA damage repairing mechanisms or iv) disrupt the apoptotic signaling pathways which diminish the drug-induced cell death (*9*).

The best understood mechanism causing MDR is the reduced accumulation of hydrophobic anticancer drugs into cancer cells resulting from the overexpression of multidrug resistance proteins. The best known multidrug resistance protein is P-glycoprotein (Pgp, ABCB1) (for review cf. (*10, 11*)). Subsequently, other multidrug resistance proteins were discovered such as the mitoxantrone resistance protein (MXR, ABCG2) and a family of multidrug-resistance-associated proteins 1 which currently contains 10 members from which at least seven have shown to confer resistance to anticancer drugs (MRP1-7, ABCC1-6, ABCC10) (*12*). All these proteins prevent sufficient accumulation of hydrophobic anticancer drugs within cancer cells due to their ability to transport many anticancer drugs out of the cell membrane. The presence of multidrug

resistance proteins in various types of human cancers including leukemia and solid tumors has been demonstrated (*13-16*). The MDR phenomenon is not only restricted to cancer but it can also hamper the chemotherapy of HIV (*17, 18*), epilepsy (*19*), bacterial (*20*), fungal (*21*), and parasitic diseases (*22*).

To overcome MDR is a challenging area in pharmaceutical sciences. The pharmacological approach is to design molecules which are not recognized by multidrug resistance proteins or compounds which modulate or inhibit their activity. This can be achieved by using non-competitive or competitive inhibitors, which interact directly with the drug-binding site(s) of the proteins (*23*). A lot of effort has been made in order to find suitable Pgp-inhibitors for clinical use, but either due to their poor modulatory activity, toxicity at high concentration, or unpredictable pharmacokinetic interactions in the presence of chemotherapeutic agents (*24-28*), only a few significant advances have been made. Clinical trials with the third generation of Pgp-inhibitors developed specifically for MDR reversal are ongoing but a number of investigations have demonstrated that also they display cross-reactivity at least with MXR and drug-metabolizing enzymes (*29*).

The difficulty to design a suitable Pgp-inhibitor for clinical use has led to the search for other strategies to overcome MDR (*29, 30*). One of those is the MDR gene silencing method where the aim is selectively block the expression of individual multidrug resistance proteins in human cancer cells. Recently, the feasibility of RNA interference, RNAi, technology to 'knockdown' Pgp expression in mice was demonstrated (*31*). Immunological methods have also been applied to inhibit Pgp. Binding of the monoclonal antibody (e.g. UIC2) abolishes conformational changes required for drug transport and thus reduces the MDR phenotype of tumor cells (*32*). Monoclonal antibodies themselves effect also on the proliferation of Pgp-expressing tumor cells (*33*). One concept to overcome MDR is to introduce Pgp into the bone marrow cells which do not widely express Pgp. The idea is to protect bone marrow cells from the side effects of anticancer drugs, thus allowing the elevation in the doses of anticancer drugs during the chemotherapy treatment of cancer patients (*9*).

1.3   Tissue Distribution and Physiological Role of P-glycoprotein

The properties of Pgp, such as its tissue distribution and the drug transport activity, suggest that its physiological function is the protection of the organism against natural xenobiotics

(*7*). Pgp is found on the apical surface of endothelial cells at important physiological barriers, such as the blood-brain barrier, BBB, blood-testis barrier, blood-nerve barrier, and fetal-maternal barrier (*34-39*), where it limits the entry of xenobiotics. Furthermore, Pgp is highly expressed on the apical surface of the small and large intestine epithelium, on the biliary canalicular membrane of liver hepatocytes, and on the apical surface of epithelial cells of the kidney proximal tubules (*38*). In these locations Pgp contributes to the excretion of xenobiotics into the intestinal lumen, bile and, urine, respectively. The knockout mice studies support the idea of the protective function of Pgp. The mice lacking the *Abcb1a-* and *Abcb1b*-genes were hypersensitive to the several xenobiotic toxins but otherwise they did not show dramatic physiological abnormalities (*7, 40*). These studies revealed that even if Pgp has some further physiological roles they are not vital. As other possible physiological functions e.g. transport of lipids (*41*), regulation of apoptosis (*42*), indirect modulation of chloride channel activity (*43*), and involvement in cholesterol esterification (*44*) have been postulated.

Pgp is not only expressed in plasma membranes but it is also localized subcellularly. In cancer and in multi-drug resistance cells functional Pgp is found e.g. in the Golgi apparatus, mitochondrial, and nuclear membranes. It was proposed that the subcellular Pgp contributes to the protection of DNA (*45-48*).

1.4   Effect of P-glycoprotein on Pharmacokinetics

Pgp modulates the administration, distribution, metabolism and excretion of the drugs. After *oral administration* most drugs enter to the blood circulation mainly within the small intestine via passive diffusion. However, as discussed in Chapter 1.3 Pgp is highly expressed in the walls of small intestine thus hampering the absorption of drugs. Consequently, the net amount of drugs absorbed into the blood circulation is the difference between the amount absorbed by passive influx and the amount extruded by Pgp together with amount metabolized (*49*).

Absorbed drugs have to be transported from the site of administration to the site of action in order to be effective. The brain for example is frequently targeted by drugs. However, the brain is separated from the blood circulation by the BBB which is composed of tightly connected endothelial cells by tight junctions (*50*). The hydrophilic drugs therefore have to be small enough to pass the tight junctions by passive diffusion or they

need special carrier systems. In contrary, the hydrophobic drugs can freely diffuse across the BBB and enter the brain compartment (*7*). However, the penetration of hydrophobic drugs is limited mainly by two factors. One is the cross-sectional area of the drug molecule which has to be > 80 Å^2 (*51*) and the other is Pgp which is highly expressed in the BBB and thus exports its substrates back to the bloodstream (*52, 53*).

Drugs are *metabolized* mainly in the liver (*49, 54*). In addition, the small intestine and the kidney may contribute to the overall drug metabolism (*55*). The effect of Pgp on the metabolism of drugs in the liver and kidney is small because of its exit site localization in hepatocytes and renal epithelial cells. Therefore Pgp mostly interacts with compounds that have already undergone cellular uptake, intracellular distribution and metabolism. In contrary, in intestine Pgp is localized at the entrance site of epithelial cells and thus the drugs are exposed to Pgp prior to intracellular distribution and metabolism. The intestinal Pgp extrudes drugs from the inside of epithelial cells back to the intestinal lumen after the drugs have gained access across the luminal surface of the epithelial cells. However, a portion of the extruded drugs reabsorb back into the epithelial cells. In this way Pgp prolongs the intracellular residence time of drugs and increases the probability that drugs get caught by the metabolizing enzymes (*49, 56, 57*).

The elimination of the drugs from the body occurs generally via metabolism and/or *excretion*. Unchanged drugs and their metabolites are excreted by the liver and kidney. For biliary excretion drugs have to first diffuse passively or via hepatic uptake transporters through the basolateral membrane of hepatocytes. Once in the hepatocytes the drugs can diffuse to the apical membrane, where Pgp then transports them into bile. Similarly in renal excretion drugs at first cross the basolateral membrane of renal epithelial cells and then diffuse to the apical membrane where Pgp contributes to the excretion of drugs into the urine (*49, 57*).

1.5   P-glycoprotein – Structure and Function

The MDR phenomenon in cancer cells was first described in literature more than thirty years ago (*58-60*). The drug-resistant mammalian cell lines were established to study this phenomenon. The cell lines, which were initially selected for resistance to one anticancer drug showed cross-resistance to other structurally diverse drugs (*58, 60*). Some years later this phenomenon was linked to the overexpression of a surface phosphoglycoprotein in

multidrug resistance Chinese hamster ovary cells (*61*), which was named as a P-glycoprotein (P for permeability) (*62*). Subsequently, it was shown that P-glycoprotein transports structurally unrelated compounds out of the cell at the expense of ATP (*63*).

P-glycoprotein (Pgp, ABCB1), a member of ABC-transporter superfamily, is a transmembrane protein composed of 1280 amino acids (170 kDa). In humans Pgp is encoded by the *ABCB1*-gene (old nomenclature *MDR1*-gene) and in mice *Abcb1a*- and *Abcb1b*-genes (old nomenclature *Mdr1a* and *Mdr1b*-genes). The sequence analysis predicts that Pgp is composed of two homologues halves which are linked together by an intracellular flexible polypeptide loop (*63, 64*). Amino acid sequence identity of both halves is 43 % (*64*). Each half of the protein contains a transmembrane domain, TMD, which is composed of six hydrophobic α-helices and a hydrophilic cytoplasmically located nucleotide binding domain, NBD. TMDs form a pathway through which drug molecules cross the membrane. The necessity of both homologues halves and the intracellular linker region for drug transport and ATPase activity has been demonstrated (*65-67*).

Pgp is glycolysated at three sites, N91, N94, and N99, in the first extracellular loop but glycolysation is not required for drug transport (*68*). Pgp has also four phosphorylation sites, S661, S667, S671, and S683, located in the linker region. Phosphorylation sites have shown to be phosphorylated by several kinases eg. protein kinase C and cAMP-dependent kinase A (*69*). The functional significance of phosphorylation is not well understood. However, mutational studies where Pgp lacked all phosphorylation sites suggested that phosphorylation is not essential for the overall ability of Pgp to interact with different cytotoxic agents (*70*). The hypothetical 2D model of human Pgp is shown in Figure 1.
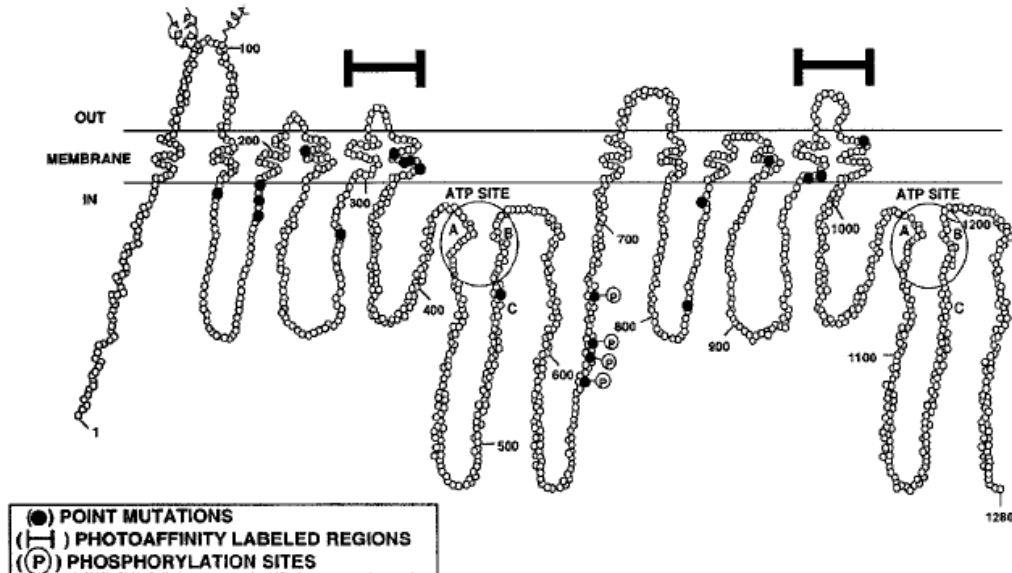
Figure 1. Hypothetical 2D-model of human P-glycoprotein. The N-linked glycolysation sites are shown as tortuous lines and the phosphorylation sites as a P surrounded with a circle. Conserved sequence motifs in NBDs, Walker A, Walker B and Signature C, are indicated as A, B, and C. Adapted from (*10*).

The high resolution crystal structure of Pgp is still unsolved but low- to medium resolution structures exist. Three dimensional structures with ~20 Å resolution were determined by electron crystallography of negatively stained 2D crystals in the absence of ATP and in the presence of non-hydrolysable analog of ATP (AMP-PNP) (*71*). Recently, also ~8 Å resolution 3D structure of Pgp in the presence of AMP-PNP was reported (*72*). These structures revealed that in the absence of ATP the TMDs form a single barrel within the membrane with a diameter of 5-6 nm and a depth of about 5 nm. The barrel contains a central pore which appeared to be open to the extracellular surface and spanning much of the membrane depth. Binding of non-hydrolysable ATP led to the repacking of TMDs and the opening the central pore along its length (*71*). Changes on the conformation at extracellular face of TMDs was also observed at vanadate, V_i-trapped state (Pgp·ADP·V_i) (*73*). V_i-trapped state is explained in more details in Chapter 1.5.2.

1.5.1 Substrate Binding to P-glycoprotein

Perhaps the most intriguing and long-lasting question related to Pgp is how a single transmembrane protein can bind and transport hundreds of structurally dissimilar compounds including chemotherapeutic drugs, natural products, detergents and peptides. Progress in this field has been made recently, but it is still far away from complete understanding. Typically Pgp substrates are hydrophobic, neutral or positively charged molecules, which often carry an aromatic ring, but not always. Recent surface activity measurements revealed that also hydrophilic compounds can function as Pgp substrates suggesting that not the hydrophobicity but the amphiphilicity is a requirement for Pgp substrates (*51*). Also the importance of the hydrogen bond acceptor groups in the substrate recognition has been reported recently (*74-78*).

The amphiphathic nature of Pgp substrates allows them to partition into the lipid bilayer. This is consistent with the fact that the drug-binding sites of Pgp are accessible from the lipid bilayer or more exactly from the intracellular leaflet of the lipid bilayer (*79-81*). This led to the proposal of two models which could partially explain the broad substrate specificity of Pgp (*82*). In the hydrophobic vacuum cleaner model Pgp binds its substrates from the inner leaflet of the lipid bilayer and transports them out to the extracellular bulk water phase. In the flippase model drugs are flipped from the inner to the outer leaflet of lipid bilayer where they can diffuse to the extracellular medium. Electron paramagnetic resonance studies with spin-labeled verapamil demonstrated that Pgp can actively generate a 25-fold aqueous phase gradient suggesting that the Pgp substrates are directly transported out of the lipid membrane (*83*). On to other hand, it has been shown that Pgp is able to carry out the ATP-driven flipping of NBD (nitrobenzo-2-oxa-1,3-diazole)-labelled phospholipids, NBD-derivatives of sphingomyelin, and simple glycosphingolipids supporting the flippase model (*84, 85*). Furthermore, the flippase model is supported by the fact that an isoform of Pgp, ABCB4, which shares >75 % sequence similarity with Pgp, functions as phosphotidylcholine (PC) flippase in liver canalicular cells (*86*). It is possible that Pgp functions as a transporter and a flippase depending on the hydrophobicity of the transported compound. However, to proof this further investigations are required.

It is important to consider the influence of the lipids as non-polar solvent on the drug-binding step since that is the environment where Pgp binds its substrates. The lipid bilayer accumulates drug molecules due to their lipid-water partitioning coefficient.

Therefore, the hydrophobic drugs are highly concentrated in lipid bilayer whereas in aqueous phase they are present at a low concentration. The lipid bilayer also orients amphiphilic molecules in such a way that the hydrophilic part of the molecule remains in the water-lipid head group interface whereas the hydrophobic part inserts into the membrane. Furthermore, the low dielectric constant of lipid environment, $\varepsilon \approx 2$, determines the nature of substrate-Pgp binding interactions. The electrostatic interactions are especially enhanced in a non-polar environment resulting also in weak electrostatic interactions such as the π-electrons of aromatic ring and a cation may play a role. Also hydrogen bonding can become relevant (*75, 78*). Sharom et al. (*87*) found a relationship between the octanol-water partition coefficient, LogP, and the concentration of half-maximum Pgp activity for three Pgp substrates suggesting that the lipid bilayer is important in drug recognition. LogP, however, did not sufficiently correlate with the large set of structurally unrelated compounds (*88*) but an excellent linear correlation was found between the concentration of half-maximum Pgp activity and the air-water partition coefficient (*77*). The air-water interface mimics better the lipid bilayer than the octanol-water system because it orders the compounds similarly as lipid bilayer and secondly, the dielectric constant of air ($\varepsilon \approx 1$) is closer to the dielectric constant of the hydrophocic core region of the membrane than the dielectric constant of octanol ($\varepsilon \approx 10$) (*78*).

The location and the number of drug-binding site(s) of Pgp has been the interest of many research groups. The site-directed mutagenesis and the photoaffinity labeling experiments suggested that the different substrates have different, but maybe overlapping binding sites and that the major sites of drug interactions are located in several transmembrane α-helices, especially clustered in TM5, TM6, TM11, and TM12 (*10, 12, 89-93*). However, the mutations that effected substrate specificity were found throughout the Pgp molecule including extra- and intracellular loops, and even NBDs (*10*). Similar findings were reported from the photoaffinity labeling studies (*90, 91*). Loo et al.(*94-97*) used cysteine-scanning mutagenesis to identify the amino acid residues which line the drug-binding site(s). In initial studies they worked with cysteine-less Pgp mutant and introduced systematically a single cysteine residue into the TMDs of Pgp and probed it with thiol-reactive Pgp substrates. Their results supported the photoaffinity and other site-directed mutagenesis studies suggesting that transmembrane α-helices TM4, TM5, TM6, TM10, TM11, and TM12 contribute to drug-binding. Recently, they reported that also TM1 and TM7 are contributing to the drug-binding domain (*98, 99*).

The clear consensus from the studies described above is that the drug-binding site(s) of Pgp are located within TMDs. However, the number and the nature of drug binding site(s) has been subject to much controversy. The results of some studies have suggested the existence of two drug-binding sites, some three and some even four binding sites (*80, 100, 101*). Shapiro et al. (*102*) showed that Pgp substrates <u>h</u>oechst 33342 and <u>r</u>hodamine 123 bound two different binding-sites (called as H- and R-site). H-site drugs stimulated transport of R-site drugs whereas two drugs which bind to the same site caused a mutual inhibition of transport. Progesterone and prazosin did not bind either site leading to the suggestion of the existence of a third binding site (*80*). As an alternative idea, compared to the distinct drug-binding sites, the existence of a single large binding site or broader binding regions has been proposed (*103-105*). Loo et al. (*105*) proposed that the drug-binding pocket involves amino acid residues from several transmembrane α-helices and the diverse substrates create their own binding sites by using a combination of residues from different TMs. Lugo et al. (*106*) showed that two R-site drugs, rhodamine 123 and LDS-751, which compete with each other for transport, are able to bind simultaneously within Pgp supporting further the idea of a large flexible drug binding site. The dimension of the drug-binding pocket has been estimated with the crosslinking studies. It was proposed that the drug-binding domain is funnel shaped and narrow in the cytoplasmic region. The central diameter of the drug-binding region was estimated as 9-25 Å, and at the extracellular side as ~50 Å (*95*).

The concept of broader binding regions is also supported by the quantitative structure-activity-relationship, QSAR, analysis. It was suggested that Pgp recognizes its substrates via specific hydrogen bond formation patterns (*75*). The concept was based on two facts. First, it was noticed that transmembrane α-helices of Pgp have a high density of hydrogen bond donor side chains which are arranged in amphiphathic manner. It was proposed that the hydrogen bonding side of TM helices are facing the drug transport route and the non-hydrogen bonding side is located in the lipid environment (*75, 76*). Secondly, three dimensional structural analysis of hundred Pgp-substrates revealed that all Pgp substrates carried at least two hydrogen bond acceptor groups in a specific distance of 2.5 ± 0.5 Å (type I unit) or three with a distance of 4.6 ± 0.6 Å between the two outer hydrogen bond acceptor groups (type II unit). The hydrogen bond acceptor patterns are shown in Figure 2. Furthermore, it was proposed that the strength of substrate binding to Pgp increases with the number and strength of individual hydrogen bond formed. The hydrogen bond hypothesis as recognition element between Pgp and its substrates is investigated further in the studies summarized in Chapters 3.1 and 3.6.
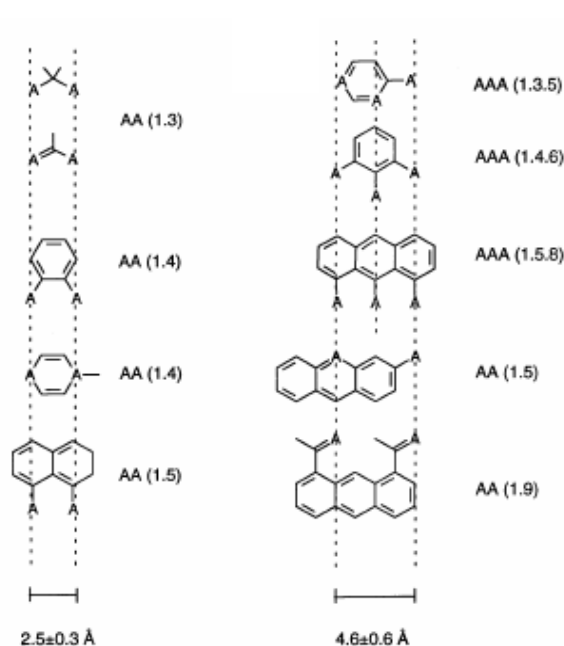
Figure 2. Hydrogen bond acceptor patters in Pgp substrates suggested functioning as binding modules with hydrogen bond donor rich transmembrane α-helices of Pgp. A represents a hydrogen bond acceptor (such as O, N, S, or X= F, Cl, and unsaturated system with π-electrons e.g. phenyl ring). Numbers in brackets shows 1st and n^{th} atom with free electron pair. Adopted from (75).

1.5.2 Nucleotide Binding to P-glycoprotein

Pgp requires ATP hydrolysis for its drug transport activity (107-109). ATP binding and hydrolysis occurs in two NBDs, which are located in cytosol. It has been shown that both NBDs can bind and hydrolyze ATP (110, 111) and that the binding affinity of ATP to Pgp is low ($K_m \approx$ (0.3–0.8) mM) (112-115). Mutations and covalent modifications that inactivated ATP hydrolysis in one NBD prevented the ATP hydrolysis also in other NBD (116-118). Similarly, vanadate, V_i, permitted ATP hydrolysis in one NBD, but after dissociation of inorganic phosphate, P_i, the vanadate entered the active site forming a stable complex with ADP (ATP·Pgp·ADP·V_i) and, thus, impeded ATP hydrolysis in other NBD (111). Moreover, photoaffinity labeling suggested that 1 mol of Mg-8-azido-ADP/1 mol Pgp is bound after hydrolysis of Mg-8-azido-ATP (119). All these experiments suggests that there is a strong catalytic cooperativity between two NBDs and based on these kinds of observations Senior et al. (119) proposed an alternating catalysis site model for Pgp, where

two NBDs alternate in carrying out ATP hydrolysis in such a way that only one NBD is active at a time.

In recent years considerable progress has been made in the understanding of the ATP binding pocket and the mechanism of how ATP is hydrolyzed since several crystal structures of isolated NBDs of ABC transporters have been solved (HisP (*120*), Rad50 (*121*), MJ0796 (*122*), and MutS (*123*)). All crystallized NBDs showed a similar tertiary structure which was also seen in the crystal structure of bacterial full-length ABC-transporter, BtuCD (*124*). An important observation from the structures was that a functional ATP binding site is formed by the interaction of amino acid residues from both NBDs. Moreover, the structures revealed that two NBDs form a ''nucleotide sandwich dimer'' with two ATP molecules bound between the dimer interface (Figure 3). Because NBDs of all ABC-transporters share an extensive amino acid sequence identity it was postulated that the tertiary structure may be conserved within the whole ABC-transporter superfamily (*4*). By merging now the structural, mutational and biochemical data together a more detailed picture of the ATP binding pocket of Pgp has started to evolve.
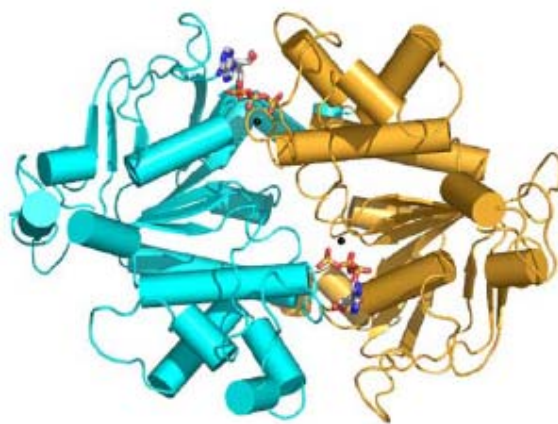
Figure 3. The closed NBD dimer with two ATP molecules and two Mg^{2+}-ions viewed from above trough the membrane and TMDs. TMDs are not shown for clarity. Two NBDs are colored as cyan and gold, the two ATP molecules are presented as stick models and two Mg^{2+}-ions as black spheres. The picture is adopted from (*4*).

Each NBD of Pgp consists of the highly conserved Walker A, Walker B, Signature C motifs, and the Q-, D-, and H-loops (*125*). Recently, the importance of tyrosine residues at positions 401 in N-terminal NBD and 1044 in C-terminal NBD of human Pgp to ATP binding and hydrolysis was demonstrated. Tyrosine was shown to form the π–π stacking interaction with an aromatic ring of ATP and therefore it was named the A-loop (aromatic

residue interacting with adenine ring of ATP). It was proposed that this conserved aromatic residue should be considered as an integral part of NBD (*126, 127*). Figure 4 displays in detail the major molecular interactions between ATP molecule and the conserved motifs. ATP is sandwiched between the Walker A, Walker B, H-loop, Q-loop and A-loop of one NBD on one side and the signature C motif and D-loop of the other NBD on the other side (*121, 122*). The structures of ABC proteins showed that Walker A binds to negatively charged triphosphate moiety of ATP and Walker B shows hydrogen bonding with a coordinating Mg^{2+}-cation (*120, 122*). There is no high-resolution structure of Pgp available yet but this kind of molecular architecture of NBDs is supported by biochemical studies (*128, 129*). Qu et al (*129*) showed with the FRET studies that NBDs are in close contact with each other. Loo et al. (*128*) demonstrated with the crosslinking studies that the signature C motif in each NBD is adjacent to the opposing Walker A sequence. Furthermore, the recent 8Å resolution electron crystallographic structure of Pgp confirmed the close proximity of NBDs (*72*). The physical contact of NBDs could explain the experimentally observed cooperation between two NBDs.
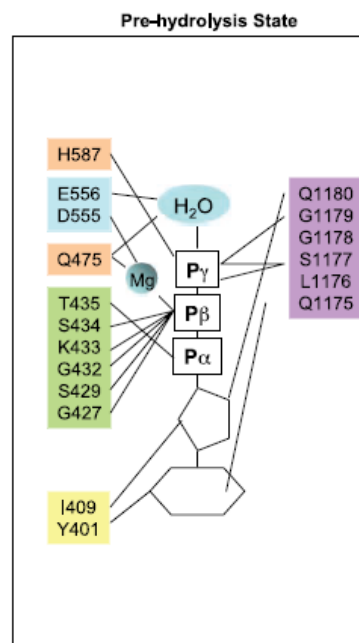
Figure 4.   Interactions between NBDs of Pgp and ATP, Mg^{2+} and H_2O based on the X-ray crystallographic structure of MJ0796 and HlyB. Adapted from (*130*). Amino acid residues which are part of conserved motifs are indicated with colors. Walker A motif (green), Walker B (blue), Q-loop glutamine (down lachs), H-loop histidine (upper lachs), A-loop (yellow) are part of one NBD and Signature motif (lila) is part of the other NBD.

1.6   Coupling of ATP hydrolysis to Drug Translocation

To fully understand the mechanism of Pgp knowledge of how ATP hydrolysis in the NBDs is coupled to the drug translocation through the TMDs is mandatory. The connection of these two processes is evident from the ability of Pgp substrates to stimulate the ATP hydrolysis rate (*107-109*). In order to mediate drug transport, Pgp has to couple the energy from drug binding, ATP binding and hydrolysis to the conformational changes that most probably alter the drug binding affinity and/or the accessibility of drug-binding sites (*131*). The technique of vanadate, V_i, trapping has been useful in dissecting the catalytic cycle of Pgp. V_i-trapping technique was created to solve the difficulties in kinetic analysis, which arose from the low affinity of ATP to Pgp (*111*). When ATP is hydrolyzed in the presence of V_i, that has a similar size and charge as P_i, a stable noncovalent complex with ADP is formed in one NBD of Pgp (Pgp·ADP·V_i) and the further ATP hydrolysis events are abolished. The geometry of V_i-complex is thought to mimic the transient catalytic transition state formed with ADP and P_i (*132*). The relatively long life-time of the V_i-trapped complex allows e.g to determine the dissociation constant for the drugs (*133*) and to study the conformational changes in Pgp during the different steps of the catalytic cycle of Pgp (*73, 134*). These types of measurements are usually coupled with the measurements done in the presence of non-hydrolysable ATP to determine the effect of ATP binding on the drug binding affinity and the tertiary structure of Pgp (*71, 135*).

The global changes in Pgp conformation upon ATP binding, ATP hydrolysis, V_i-trapping and upon drug binding has been detected with spectroscopic techniques (*134, 136*), with cross-linking experiments (*137*), with FACS analysis in the presence of monoclonal antibody UIC2 (*138*) as well as with cryoelectron microscopy (*71*). The conclusion from these studies was that Pgp possesses different conformations which are associated with the different steps in the drug transport process. In some studies the question was addressed how the conformational changes are effecting on the binding affinity of drugs (*133, 135, 139*). The goal was to identify the step at which the switch in drug-binding site from high to low affinity occurs. Different techniques have been used and the reported results are partially controversial. The initial photoaffinity labeling studies showed that the photolabeling of Pgp with Pgp-substrate analog [^{125}I]-iodoarylazidoprozosin, IAAP, was significantly reduced in V_i-trapped form (*139, 140*). This was intepretated that the drug-binding site is still in low affinity state and the model was proposed where two ATP are hydrolyzed per one drug transported. One ATP was used

to change the drug-binding site from high to low affinity and the second ATP was used to reset Pgp back to its high binding affinity conformation (*139, 140*). However, the liability of these results has been contradicted (*133, 141*). In contrast, Qu et al (*133, 142*) used several fluorescence spectroscopic approaches to study the changes in the drug-binding affinity to Pgp in V_i-trapped conformation compared to the resting state conformation. It was shown that the binding affinity of six different drugs was not changed in the V_i-trapped form and thus it was proposed that the drugs were released before the formation of post-hydrolysis transition state (Pgp·ADP·V_i). Furthermore, Qu et al (*133, 142*) suggested a mechanism which involves concerted conformational changes and predicted that the relaxation from the transition state drives simultaneous movement of the drug across the membrane. This mechanism is consistent with the alternative catalytic model (*119*). In the third study performed with the equilibrium radioligand binding assay it was demonstrated that the binding of the non-hydrolysable nucleotide caused a reduction in the fraction of transported substrate (vinblastine) bound to Pgp (*135*). V_i-trapped conformation showed a similar affinity for vinblastine than the nucleotide bound state suggesting that the change in the affinity of the drug-binding site from high to low occurred via the nucleotide binding. This led to the third possible model suggestion, the ''ATP switch model'' where the main differences being when compared to the two previous models is that the release of drug occurs via ATP binding and dimerization of NBDs and the energy from ATP hydrolysis is used for resetting Pgp back to its high affinity conformation (*4, 143*). As demonstrated above the clarification of the detailed steps in the drug transport cycle of Pgp is still a matter of intensive research. More experimental data is needed to judge which of the proposed models or whether any of them is correct. In the study summarized in Chapter 3.5 we addressed this question and studied the interplay between NBDs and TMDs of Pgp further.

2. Rationale and Aims of Research

2. Rationale and Aims of Research

As discussed in the Introduction (Chapter 1.3) Pgp has an important function to protect our sensitive and important organs such as the CNS against xenobiotics. Unfortunately, the overexpression of Pgp is also related to multidrug resistance, MDR, which is a serious problem in cancer chemotherapy (Chapter 1.2). Moreover, MDR also hampers the chemotherapy of other drug-treatable diseases such as AIDS, epilepsy, bacterial, parasital and fungal diseases. One strategy to overcome MDR is to design Pgp-inhibitors or eventually drugs that are not recognized by Pgp. In order to achieve this, it is mandatory to better understand the interactions between Pgp and its substrates better. Therefore, the main aim of this thesis was the quantitative characterization of the thermodynamics and the kinetics of Pgp-substrate interactions. Special emphasis was placed on better understanding of the effect of lipid bilayers on Pgp-substrate interactions.

Pgp is a transmembrane protein, which transports hundreds of structurally diverse compounds out of the cell membrane using the energy released in ATP hydrolysis. As pointed out in the Introduction (Chapter 1.5.1) it has been known already for years that Pgp extracts its substrates from the lipid bilayer and not from the aqueous phase, like many other membrane transporters. This complicated the determination of the *intrinsic* drug binding constants to Pgp (the binding constant of drug to Pgp from the lipid phase, K_{tl}), and consequently the evaluation of the strength of Pgp-substrate interactions. Drug binding constants to Pgp reported in literature are the products of two binding constants, namely the lipid-water partition coefficient, K_{lw}, and the binding constant of drug to Pgp from the lipid phase, K_{tl}. Thus, they are *apparent* values (the binding constants of drug to Pgp from the aqueous phase, K_{tw}). No *intrinsic* binding constants, K_{tl}, were available. Therefore the main goal in our first investigation was to separate the two binding constants and to determine the *intrinsic* drug binding constant to Pgp, K_{tl}, and the corresponding free energies, ΔG_{tl}^{0}, for the 15 structurally diverse Pgp-substrates (summarized in Chapter 3.1, full study in Chapter 7.1). Additionally, we tested the relevance of the hydrogen bond hypothesis as recognition mechanism between Pgp and its substrates (cf. Chapter 1.5.1).

It is also important to know how fast the drugs are transported by Pgp. Therefore, in the next three parts of this thesis (summarized in Chapters 3.2-3.4, full reports in Chapters 7.2-7.4) we studied the kinetics of Pgp and analyzed the influence of the physicochemical properties of drugs on Pgp activity. Recently, in our laboratory a new method was described where Pgp activity was studied for the first time in living *MDR1*-transfected cells

by monitoring the extracellular acidification rate, ECAR, with a Cytosensor microphysiometer (*144*). Previously, Pgp activity has been measured in inverted plasma membrane vesicles formed from *MDR1*-transfected cells or in reconstituted Pgp-proteoliposomes by determining the rate of ATP hydrolysis spectroscopically (*88, 114, 116*). The conventionally used spectroscopic assay detects directly the ATP dependent drug transport activity of Pgp, whereas the ECAR describes the efflux rate of acidic metabolites and, thus, reflects the overall energy metabolism of cells. Therefore the question arose, how the general mechanism of the ECAR under the conditions where Pgp is activated by drugs is related to the specific drug-stimulated ATP hydrolysis rate of Pgp. This question was mainly addressed in the studies summarized in Chapters 3.2-3.3 (full reports in Chapters 7.2-7.3).

In Chapter 3.2 (full report in Chapter 7.2) Pgp activity measured for a large set of structurally diverse Pgp substrates in plasma membrane vesicles was compared with the Pgp activity investigated in living cells (Chapter 7.1). In the present study the Pgp activity was determined in the same membrane environment in contrast to the previously reported results (*144*). This is relevant since Pgp activity depends on the lipid membrane (Chapter 7.1, (*87, 145*)). Moreover, we tested experimentally the soundness of the relationship reported earlier for the maximum Pgp activity, V_1, and for the hypothetical free energy of hydrogen bond formed (EU_H) between Pgp and drugs (Introduction, Chapter 1.5.1, (*26, 76, 78*)). It was shown previously for the smaller set of compounds that the maximum Pgp activity, V_1, is decreasing exponentially with increasing EU_H. In the present study the larger set of compounds were used with wider variation in their structures and hydrophobicity (Chapter 7.2).

The influence of the cell metabolic state on Pgp activity was described in Chapter 7.3. The results revealed a linear correlation between the basal and the verapamil-stimulated ECAR under low nutritional conditions. The correlation, however, flattened out under high nutritional conditions. To better understand this phenomenon we further studied the metabolic rate of cells with ^{13}C-NMR spectroscopy (summarized in Chapter 3.4, full report in Chapter 7.4). The advantages in the ^{13}C-NMR technique compared to the Cytosensor measurements are that all lactate molecules can be detected and that the measurements can be performed in a solution with a high buffer concentration. The Cytosensor microphysiometer only detects the extruded lactate molecules outside the cells.

The ultimate goal in understanding the drug transport mechanism of Pgp is to understand how ATP hydrolysis in the nucleotide binding domains of Pgp, NBDs, is

coupled to the drug translocation step through the transmembrane domains of Pgp, TMDs (Introduction, Chapter 1.6). In the study summarized in Chapter 3.5 (full report in Chapter 7.5) we aimed at getting further insight to the interplay between TMDs and NBDs by analyzing the transition state parameters (the activation enthalpy $\Delta H^{\ddagger}$, the activation entropy $\Delta S^{\ddagger}$, and the free energy of activation $\Delta G^{\ddagger}$) of ATP hydrolysis by Pgp in the absence and presence of several Pgp substrates. Furthermore, since the Pgp activity depends on the properties of the lipid bilayer (Chapter 7.1, (*87, 145*)), and Pgp is found in many organs that have significantly different membrane properties, we were interested in getting further information about the relationship between Pgp and lipids.

In the last part of this thesis we worked with four dyes, which are widely used in histological studies. Furthermore, the applicability of dyes as potential photosensitizers for the treatment of cancer and microbial infections together with photodynamic therapy has been tested. In this context it is important to know if the dyes are Pgp substrates. Furthermore, our aim was to test whether the established rules (*146*) for the intrinsic Pgp substrates holds for methylene blue, acridine orange, basic fuchsin, and ethyl eosin. The predictions were then tested experimentally.

3. Summary of Work Addressed

Reprints and Unpublished Manuscripts

3.1   Quantification   and   Characterization   of   P-glycoprotein-Substrate Interactions

Pgp binds its substrates from the inner leaflet of the lipid bilayer (Introduction Chapter 1.5). This means that drug molecules have to first partition into the lipid bilayer before they reach the site of interaction. After binding to Pgp they are exported either directly to the extracellular medium or flipped to the outer leaflet of the lipid bilayer. The first hints of the weak interactions between Pgp and its substrates came from the observation that Pgp transports hundreds of structurally diverse compounds and in general all of them were hydrophobic in their nature. This suggests that Pgp substrates accumulate inside the membrane and therefore the concentrations, which Pgp senses, are much higher than that in the aqueous phase. The two-step drug binding model to Pgp was introduced recently (*77, 78*), however, the quantitative evaluation for the drug binding constants from the lipid phase to Pgp, K_{tl}, and the corresponding free energies, ΔG_{tl}^{0}, were still missing.

Therefore in the first part of this thesis we separated the two binding processes, the lipid-water partition of the drug and the drug binding to Pgp from the lipid phase, and quantified for the first time the drug binding constants from the lipid phase to the activating (inhibitory) binding region of Pgp, $K_{tl(1)}$ ($K_{tl(2)}$), and the corresponding free energies $\Delta G_{tl(1)}^{0}$ ($\Delta G_{tl(2)}^{0}$). This was done for the 15 structurally diverse well-known Pgp substrates. The free energy of drug partitioning into the lipid phase, ΔG_{lw}^{0}, was determined from surface activity measurements (cf. Appendix 7.1.1) which allows estimation of the lipid-water partition coefficient of the drug, K_{lw}, when the packing density of the lipid bilayer, π_{M}, in which Pgp is embedded, is known. The free energy of the drug binding from the aqueous phase to the activating (inhibitory) binding region of Pgp, $\Delta G_{tw(1)}^{0}$ ($\Delta G_{tw(2)}^{0}$), was estimated from steady-state Pgp activity measurements. Pgp activity measurements were performed in living *MDR1*-transfected mouse embryo fibroblasts by monitoring the extracellular acidification rate, ECAR, with a Cytosensor microphysiometer. The free energy of drug binding from the lipid phase to the activating (inhibitory) binding region of Pgp, $\Delta G_{tl(1)}^{0}$ ($\Delta G_{tl(2)}^{0}$), was determined as the difference of $\Delta G_{tw(1)}^{0}$ ($\Delta G_{tw(2)}^{0}$) and ΔG_{lw}^{0}. Moreover, we evaluated the drug concentrations in the lipid phase at half-maximum Pgp activity, C_{b}, and tested the energetic soundness of the hydrogen bond hypothesis as a recognition mechanism between Pgp and its substrates (Introduction, Chapter 1.5).

The substrate concentrations in the lipid phase at half-maximum Pgp activity were $C_{b(1)} =$ (0.02 to 67) mM/L lipid. These are by a factor of 10^2 to 10^4 higher than that in the aqueous phase revealing that the interactions between Pgp and its substrates are relatively weak. The lowest value was determined for cyclosporin A and the highest for lidocaine. The free energy of drug binding from the aqueous phase to the transporter, the free energy of drug partitioning into the lipid phase, and the free energy of drug binding from the lipid phase to the activating binding region of Pgp for the 15 drugs studied ranged from ($\Delta G_{tw(1)}^0$ = (-30 to -54) kJ/mol), (ΔG_{lw}^0 = (-23 to -34 kJ/mol)), and ($\Delta G_{tl(1)}^0$ = (-7 to -27 kJ/mol)), respectively. For all drugs ΔG_{lw}^0 were more negative than $\Delta G_{tl(1)}^0$, however, $\Delta G_{tl(1)}^0$ varied more strongly suggesting that the drug-membrane interactions for the studied compounds are stronger than the Pgp-drug interactions. The Pgp-drug interactions, however, are more specific.

Knowledge of the free energy of the drug binding from the lipid phase to the activating binding region of Pgp, $\Delta G_{tl(1)}^0$, allowed to test the validity of the hydrogen bond hypothesis. The hydrogen bond hypothesis suggests that the hydrogen bonds can form between the hydrogen bond acceptor groups of the substrate and the hydrogen bond donor groups of transmembrane domains, TMDs, of Pgp and that hydrogen bond acceptor groups in specific distances in substrate molecules can thus serve as recognition element for Pgp (Introduction, Chapter 1.5). By dividing the experimentally determined $\Delta G_{tl(1)}^0$ values by the weighted number of hydrogen bond acceptors, the free energy per potential hydrogen bonds formed was estimated as (ΔG_{Hi}^0 = (-2.3 to -7.8) kJ/mol). These values are reasonable for weak hydrogen bonds and suggest that the hydrogen bond formation contributes significantly to the energetics of Pgp-substrate interactions within the lipid phase. Furthermore, the results presented here support the hypothesis that Pgp has a large binding region(s) rather than specific drug binding sites.

A difficulty in Pgp activity measurements with a Cytosensor microphysiometer is that the drug solutions have to flow through long tubing and along the debubbler membrane before they reach the cells. Considerable amount of drug was lost because of adsorption to the tubes and the debubbler membranes and therefore the drug concentrations had to be corrected. In the present study the drug adsorption for the 14 drugs studied was quantified by UV-spectroscopy. The adsorption varied from compound to compound and was especially high for the phenothiazines and relatively low for verapamil. The cyclosporin A concentration could not be corrected since it does not contain UV-detectable amino acid residues. The quantification of drug adsorption to the tubing of the Cytosensor

microphysiometer was my contribution to this work. I further contributed to the Pgp activity measurements with a Cytosensor microphysiometer for nine out of the fifteen drugs.

This study is described in detail in the following publication (Chapter 7.1, page 53): Gatlik-Landwojtowicz, E., Aanismaa, P., and Seelig, A. (2006), Quantification and Characterization of P-glycoprotein-Substrate Interactions. *Biochemistry*, 45(9), 3020-3032.

3.2   P-Glycoprotein Kinetics Measured in Plasma Membrane Vesicles and Living Cells

To understand Pgp in more detail it is important to elucidate its drug transport activity in the cellular ensemble as well as in an isolated environment. The drug transport rate of Pgp has been frequently assayed by means of transport measurement across the confluent cell monolayers that express high levels of Pgp. These measurements, however, reveal only the apparent drug transport rate of Pgp since they combine the passive influx rate of drug and the active efflux rate of drug by Pgp (*146*). The intrinsic drug transport rate of Pgp can be determined with greater reliability by monitoring the ATP hydrolysis rate because it is directly proportional to the intrinsic drug transport rate of Pgp.

Conventionally, the ATP hydrolysis rate of Pgp has been measured spectroscopically by detecting the ATP hydrolysis rate in inverted plasma membrane vesicles formed from *MDR1*-transfected cells or in reconstituted Pgp-proteoliposomes. Recently, our laboratory reported a new method where Pgp activity was studied in living *MDR1*-transfected cells by measuring the extracellular acidification rate, ECAR, with a Cytosensor microphysiometer (*144*). These two assays, however, bare distinct differences. In living cells drugs have to partition into the lipid bilayer and diffuse across the membrane to the cytosolic leaflet in order to reach the activating binding region of Pgp. In inverted plasma membrane vesicles the drugs merely have to intercalate between the lipids since the activating drug binding region of Pgp is now located towards extracellular medium. In an earlier investigation made by our laboratory the kinetics of Pgp activity measured in living *MDR1*-transfected pig kidney cell (*144*) was compared to Pgp activity measured in plasma membrane vesicles formed from Chinese hamster ovary cells (*88*). The results were in reasonable agreement. However, it is known that Pgp activity depends on the lipid

environment (Chapter 7.1, (*87, 145*)). Therefore, for a more rigorous comparison it is important to use Pgp embedded in the same membrane environment for both types of experiments.

In the second part of this thesis we characterized Pgp activity in living *MDR1*-transfected mouse embryo fibroblast cells and in plasma membrane vesicles formed from the same cells. In the study summarized in Chapter 3.3 this comparison was made only for the one well-known Pgp substrate, verapamil. Here, we extended the comparison for the same 15 drugs investigated earlier in living *MDR1*-transfected mouse embryo fibroblasts (summarized in Chapter 3.1). Furthermore, four other drugs were added in order to get an even broader range of drugs. Data was evaluated according to the modified Michaelis-Menten equation yielding the concentration of half-maximum Pgp activation (inhibition), K_1 (K_2), and maximum (minimum) Pgp activity, V_1 (V_2). The obtained kinetic parameters were then compared with the corresponding values determined in living cells.

The study revealed that the concentrations of half-maximum Pgp activation, K_1, determined in living cells and in plasma membrane vesicles were in good agreement provided that the two systems were at the same pH and that possible artifacts such as the drug adsorption, drug and vesicle association and cytotoxic effect of drugs could be eliminated. The concentrations of half-maximum Pgp activation, K_1, spread over a broad concentration range from ($K_1 = (10^{-8}$ to 10^3) M. The lower values were determined for hydrophobic drugs and the higher values for more hydrophilic drugs. A reasonably linear correlation was also found for the *relative* maximum Pgp activities, V_1, obtained in living cells and in plasma membrane vesicles. The deviations were mainly due to artifacts. In order to compare the *absolute* drug-stimulated rate enhancement the turnover numbers were calculated by dividing the maximum Pgp activity, V_1, by the estimated amount of Pgp molecules per sample. The turnover numbers from both systems were in reasonable agreement when the measurements in living cells performed in the presence of pyruvate. However, in the absence of pyruvate they seem to be higher in living cells. This issue is furthermore addressed in other parts of this thesis (Chapters 7.3-7.4).

Additionally, we tested the soundness of the relationship found previously between the maximum activity of Pgp, V_1, and the hypothetical hydrogen bonding energy of the drug (EU_H). It was shown earlier for a smaller set of compounds that the maximum Pgp activity, V_1, decreases exponentially with increasing EU_H (*26, 76, 78*). To this purpose we determined the total free energy of drug binding to Pgp from the aqueous phase, $\Delta G^0_{tw(1)}$, and from the lipid-phase, $\Delta G^0_{tl(1)}$, according to the two step-drug binding model. We found

that the logarithm of the maximum Pgp activity, $\ln V_1$, depends linearly on the binding affinity of drug to the transporter from the aqueous phase, $\Delta G^0_{tw(1)}$. The correlation between the logarithm of the maximum Pgp activity, $\ln V_1$, and the EU_H (or $\Delta G^0_{tl(1)}$) was valid for the compounds whose $\Delta G^0_{tw(1)}$ and $\Delta G^0_{tl(1)}$ were linearly correlated. The third generation inhibitor OC144-093 was an exception. It has a high affinity to the lipid phase but a low affinity from the lipid phase to Pgp. Its behavior was distinctly different than the behavior of the first-generation inhibitor, cyclosporin A, which has an intermediate affinity to the lipid phase but high affinity from the lipid phase to the transporter. Because both of them are effective inhibitors functioning already at low nM concentration this suggests that the inhibition mechanism for OC144-093 and cyclosporin A are different. Furthermore, the linear correlation found for the logarithm of maximum Pgp activity, $\ln V_1$ and the free energy of drug binding from the aqueous phase to the transporter, $\Delta G^0_{tw(1)}$, suggests that the drug release determines the rate of Pgp activity.

This study was the main topic of my PhD thesis. Details of these results are described in the following publication (Chapter 7.2, page 71):
Aanismaa, P., and Seelig, A. (2007), P-Glycoprotein Kinetics Measured in Plasma Membrane Vesicles and Living Cells. *Biochemistry*, 46(11), 3394-3404.

3.3   The Rate of P-glycoprotein Activation Depends on the Metabolic State of the Cell

In the first Pgp activity investigation performed in living cells by monitoring the extracellular acidification rate, ECAR, with a Cytosensor microphysiometer the molecular origin of the proton efflux was not known (*144*). All energy consuming processes in living cells produce acidic metabolites such as protons and the lactate molecules which need to be excreted outside of cells in order to maintain cellular homeostasis. The Cytosensor microphysiometer detects the changes in the acidity of the medium where cells are bathing and, thus, the ECAR reflects the overall energy metabolism of cells. Because measuring the changes in the ECAR is a rather indirect method to detect drug transport activity of Pgp the question raised how the general mechanism of the ECAR under the conditions where

Pgp is activated by drugs is related to the specific drug-stimulated ATP hydrolysis rate of Pgp. This was my main topic in the study reported in Chapter 7.3.

To answer this question a method had to be established by which the ATP hydrolysis rate of Pgp could be detected alone. Because this is not feasible in living cells another approach was necessary. To this purpose we established the conventional ATPase assay, where the rate of ATP hydrolysis by Pgp is measured spectroscopically in inverted plasma membrane vesicles. The plasma membrane vesicles were prepared from the same *MDR1*-transfected mouse embryo fibroblasts as used in the ECAR measurements since it is important to use Pgp embedded in same lipid environment in both assays. The comparison of the proton efflux rate in living *MDR1*-transfected cells and the phosphate release rate from ATP hydrolysis by Pgp revealed a reasonable agreement between the verapamil-stimulated ATP hydrolysis rate of Pgp and the verapamil-stimulated ECAR suggesting that ATP hydrolysis of Pgp is kinetically linked to the ECAR.

Details of this study are described in the following publication (Chapter 7.3, page 85): Gatlik-Landwojtowicz, E., Aanismaa, P., and Seelig, A. (2004), The Rate of P-glycoprotein Activation Depends on the Metabolic State of the Cell. *Biochemistry*, 43(46), 14840-14851.

3.4   Metabolic Rate of Mouse Embryo Fibroblasts Determined by ^{13}C-NMR

The metabolic rate of the mouse embryo fibroblast, wild-type and *MDR1*-transfected, cells was determined previously with a Cytosensor microphysiometer by monitoring the extracellular acidification rate, ECAR. It was shown that the ECAR is identical to the rate of lactate export via monocarboxylate transporters leading to the conclusion that the ECAR reflects the ATP synthesis rate via glycolysis (Chapter 7.3). The results further revealed that the basal ECAR of *MDR1*-transfected cells was linearly correlated with the verapamil-stimulated ECAR under the conditions where the metabolic state of cells was low, whereas under conditions where the metabolic state of cells was high the linear correlation flattened out. The increase in the verapamil-stimulated ECAR was suppressed compared to the increase in the basal ECAR.

Glycolysis is a highly regulated metabolic pathway which among other things is sensitive to pH. An increase in the extracellular proton concentration causes a reduction in

glycolysis probably through a reduced lactate efflux (*147*). Therefore, the question arose, whether the flattening of the linear correlation between the basal and verapamil-stimulated ECAR, observed under the conditions where the metabolic state of cells were high, is due to the acidification of the flow medium and to the suppression of glycolysis via feedback mechanism. Another possibility which could explain the decrease in the verapamil-stimulated ECAR under the conditions of the high metabolic state of cells is the limited transport capacity of the monocarboxylate transporters. If more lactate is produced than can be exported by the cell, the lactate accumulates inside the cells, the pH of the cytosol decreases leading to the inhibition of phosphofructokinase and hence glycolysis (*148*).

These questions were mainly addressed in the fourth part of this thesis. We used ^{13}C-NMR spectroscopy to determine the metabolic rate of wild-type and *MDR1*-transfected mouse embryo fibroblasts in the presence and absence of verapamil by monitoring the rate of glucose consumption and the lactate production. The measurements were carried out under anaerobic conditions in the presence of ^{13}C-labeled glucose. In contrast to the Cytosensor measurements, where the flow medium with the low buffer concentration has to be used in order to detect small changes in pH caused by extruded metabolites of cells, the ^{13}C-NMR measurements could be performed in solution with a high buffer concentration. Furthermore, because all lactate molecules can be detected with a ^{13}C-NMR whereas the Cytosensor only detects the extruded lactates outside the cells, the relationship between the intra- and extracellular lactate and the transport capacity of monocarboxylate transporters were addressed using a lactate specific shift reagent (Pr-DO3A). Pr-DO3A is a new shift-reagent and we thus simultaneously tested its bio-compatibility with living cells.

This study revealed that the *relative* enhancement in the lactate production of *MDR1*-transfected cells by verapamil measured with a ^{13}C-NMR was in good agreement with the values obtained earlier with a Cytosensor microphysiometer during longtime verapamil stimulation (~ 150-160 % relative to the basal metabolic rate). The *absolute* basal metabolic rate of the wild-type and the *MDR1*-transfected cells determined with ^{13}C-NMR was (~10·10^7 proton/cell/s). This value is about threefold higher than that determined earlier from the ECAR measurements (~3·10^7 proton/cell/s). Also the *absolute* rate enhancement stimulated by verapamil in *MDR1*-transfected cells was higher than that observed from the ECAR measurements. The shift reagent Pr-DO3A clearly separated the intra- and extracellular lactate NMR signals. The intracellular lactate concentration increased as the total lactate concentration increased. Furthermore, it was shown that the estimated intra- and extracellular lactate concentrations were similar suggesting that the

transmembrane lactate transport is fast enough to avoid accumulation of the lactate inside the cells.

Taking together these results demonstrates that the flattening of the linear correlation between the basal and the verapamil-stimulated ECAR, observed under the conditions where the metabolic state of cells were high, is due to the suppression of glycolysis by the feedback mechanism. The NMR results further suggest that the flattening does not arise from the saturated transport capacity of monocarboxylate carriers. However, further investigations are needed to confirm these arguments. Furthermore, we showed that the shift reagent Pr-DO3A can be used to observe the intracellular lactate concentration in living cells without effecting on the metabolic rate and the cell viability.

Details of this study are described in unpublished manuscripts (Chapter 7.4, page 99). This study was made in collaboration with Dr. Götz Kohler.

3.5   P-Glycoprotein Senses Its Substrates and the Lateral Membrane Packing Density: Consequences for the Catalytic Cycle

Pgp is composed of two homologous halves which are connected by a flexible linker region to a single functional unity. Each half contains a transmembrane domain, TMD, which is composed of six hydrophobic α-helices and a hydrophilic nucleotide binding domain, NBD (Introduction, Chapter 1.5). The TMDs are responsible for the substrate recognition and binding whereas the NBDs bind and hydrolyze ATP. The interplay between the TMDs and NBDs drives the substrate translocation across the lipid bilayer.

The first catalytic cycle model of Pgp known as a ''alternative catalytic cycle'' was proposed by Senior et al. (*119*). It hypothyzed that during the ATP hydrolysis, a transition state is generated and that the relaxation of transition state causes a change in the drug binding site from high to low affinity thus powering the extrusion of the drug. Recently, this model has been reevaluated and as a new possibility it was suggested that the change in the affinity of the drug to the binding site from high to low state is catalyzed by ATP binding and dimerization of the NBDs of Pgp (*4, 143*). The energy from ATP hydrolysis was proposed to be utilized for the transition of the NBDs from the closed dimer to the open dimer configuration (Introduction, Chapter 1.6). Therefore, our aim was to understand the interplay between the TMDs and the NBDs of Pgp during the drug transport cycle in

more detail. Furthermore, we aimed at getting additional information about the influence of the lipid environment, especially the lateral packing density of membrane, π_M, on the transition state parameters (the activation enthalpy $\Delta H^{\ddagger}$, the activation entropy $\Delta S^{\ddagger}$, and the free energy of activation $\Delta G^{\ddagger}$) of ATP hydrolysis by Pgp and thus on the mechanism of Pgp. It was shown in the study summarized in Chapter 3.1, that the lateral packing density of the membrane, π_M, has an important role in Pgp activity, since it determines the lipid-water partitioning step of the drug and, thus, it effects the concentration of half-maximum Pgp activity, K_1. Furthermore, Pgp has an important protective function in many organs that have different membrane packing densities, π_M, such as blood brain barrier ($\pi_M \cong 35$ mN/m) and intestine barriers ($\pi_M \cong 28$ mN/m) (*146*). It is, thus, relevant to understand better how the Pgp activity is affected by the lipid environment.

For this purpose we measured the temperature dependence of Pgp activity in plasma membrane vesicles obtained from *MDR1*-transfected mouse embryo fibroblasts. The measurements were done in the absence (= basal Pgp activity) and in the presence of exogenous Pgp substrates. Three different Pgp substrates where chosen (promazine, verapamil and PSC833) in order to study the effect of drug, its concentration and its binding affinity to the transporter on the transition state parameters of ATP hydrolysis by Pgp.

Data obtained from the temperature dependence measurement were evaluated with the Eyring's transition state theory. The Eyring's plots were apparently linear for ATP hydrolysis by Pgp in the absence and presence of drugs if measured in the plasma membrane vesicles in a relatively small temperature range (T = 25 – 37 $^{\circ}$C). From the linear fit of the Eyring's plots the activation enthalpy $\Delta H^{\ddagger}$, the activation entropy $\Delta S^{\ddagger}$, and the free energy of activation $\Delta G^{\ddagger}$ of ATP hydrolysis by Pgp were determined. The free energy of activation of ATP hydrolysis by Pgp, $\Delta G^{\ddagger}$, decreased slightly at low and increased at high verapamil and promazine concentration, whereas the free energy of activation, $\Delta G^{\ddagger}$, for PSC833 only increased, thus, revealing the mirror image of the Pgp activity profiles. The activation enthalpy of ATP hydrolysis by Pgp, $\Delta H^{\ddagger}$, did not correlate with the drug dependent ATP hydrolysis rate. It decreased in the presence of drugs independently whether the drug caused an increase or decrease in Pgp activity relative to the basal rate. By comparing the transition state parameters for basal Pgp activity measured in plasma membranes of NIH-MDR1-G185 cells with the literature data, it was found that the activation enthalpy, $\Delta H^{\ddagger}$, decreased significantly with the decreasing lateral membrane

packing density, π_M, whereas the decrease in the free energy of activation, $\Delta G^{\ddagger}$, was much smaller as expected from the rate measurements.

Taking together the present data and the results from our previous investigations (the study summarized in Chapter 3.2) we discussed two different catalytic cycle models proposed originally by Senior et al. (*119*) and Higgins et al. (*4, 143*). We assumed that the Pgp activity cycle consists of several steps where each step is described by a free energy of activation, $\Delta G^{\ddagger}_i$. The free energy of activation obtained from the steady-state Pgp activity measurements is a sum of all individual free energies of activation, $\Delta G^{\ddagger}$. Since it was observed that the drugs modulated the free energy of activation, $\Delta G^{\ddagger}$, in specific manner, the drugs have to be present at the rate-limiting step. Whether the rate-limiting step is the ATP hydrolysis or conformational change of Pgp driven by ATP binding, is not possible conclusively solve at the present. Therefore, further experiments are still needed.

These results are described in detail in the following manuscript (Chapter 7.5, page 115): Aanismaa, P., Gatlik-Landwojtowicz, E., and Seelig, A., P-Glycoprotein Senses Its Substrates and the Lateral Membrane Packing Density: Consequences for the Catalytic Cycle, *Biochemistry, in press*

3.6   Prediction and Validation of P-glycoprotein-Substrates Exemplified by Ehrlich´s Dyes

Synthetic dyes have been widely used in histological studies since they were invented in the 19th century. Furthermore, due to their selectivity and biological activity they formed a basis for chemotherapy initiated Paul Erlich. In 1891 methylene blue was used for the first time for the treatment of malaria in humans (*149*). Moreover, the applicability of dyes as photosensitizers to treat cancer and microbial infections with photodynamic therapy has been tested.

In this context it is important to know if dyes are Pgp substrates. Therefore, in the last part of this thesis we worked with four dyes, methylene blue, acridine orange, basic fuchsin, and ethyl eosin. By applying the established rules for intrinsic Pgp-substrates (*146*) we predicted that methylene blue, acridine orange, and basic fuchsin should be, whereas ethyl eosin should not be intrinsic substrates for Pgp. We tested the predictions by measuring the Pgp activity in plasma membrane vesicles formed from *MDR1*-trasfected

cells spectroscopically. Furthermore, their effect on Pgp activity was investigated in living *MDR1*-transfected mouse embryo fibroblasts by monitoring the ECAR with a Cytosensor microphysiometer. Simultaneously, the cytotoxicity of the dyes was tested.

Our results indicated that methylene blue, acridine orange, and basic fuchsin are intrinsic substrates for Pgp, whereas ethyl eosin most likely is not. The same conclusion was drawn from both assays and this was in good agreement with the prediction. However, by measuring the Pgp activity in living cells by monitoring the ECAR revealed that methylene blue, acridine orange, and ethyl eosin affect the energy metabolism of cells in a complex manner. Methylene blue and acridine orange increased the ECAR above basal values in the wild-type and in *MDR1*-transfected cells. However, a clear difference between the ECARs of wild-type and *MDR1*-transfected cells was observed demonstrating the protective function of Pgp. Ethyl eosin, on the other hand, caused a decrease in the ECARs of both cells to the similar extent. To give an conclusive answer, whether this is due to the interaction of eosin with NDBs of other ATPases or also with NBDs of Pgp, further experiments are needed.

These results are described in detail in unpublished manuscript (Chapter 7.6, page 149)

4. Summary

P-glycoprotein (Pgp, ABCB1) is a transmembrane protein, which extrudes a large number of structurally diverse compounds out of the cell membrane at the expense of ATP hydrolysis. The overexpression of Pgp strongly contributes to multidrug resistance, which hampers the chemotherapy of cancer and some other drug-treatable diseases. Therefore, the general aim of this thesis was to quantitatively characterize the thermodynamics and the kinetics of Pgp-substrate interactions. Specific emphasis was placed on the understanding the influence of the lipid bilayer since Pgp binds its substrates from the cytosolic leaflet of the membrane.

Drug binding to Pgp can be divided into two steps. The first step is the drug partitioning into the lipid bilayer described by the lipid-water partition coefficient, K_{lw}, and the second step is the drug binding to Pgp from the lipid phase depicted by the binding constant of drug to Pgp from the lipid phase, K_{tl}. The binding constant of the drug from the aqueous phase to Pgp, K_{tw}, is thus the product of these two binding constants. Since the separation of drug binding to the lipid bilayer and to Pgp from the lipid bilayer has not been done satisfactorily a question mark was still hanging above the strength of the Pgp-drug interactions. Therefore, the aim of the first part of this thesis was to quantify the binding constant of drugs to Pgp from the lipid phase, K_{tl} and furthermore to test the energetic soundness of the previously suggested hydrogen bond hypothesis. The lipid-water partition coefficient, K_{lw}, and the drug binding constant from water to Pgp, K_{tw}, were determined independently for the 15 drugs and for the first time the binding constant of drugs to Pgp from the lipid phase and the corresponding free energies ΔG_{tl}^{0} were reported. We found that the free energy of lipid-water partitioning ΔG_{lw}^{0} is more negative than the free energy of drug-binding to Pgp from the lipid phase ΔG_{tl}^{0} for all 15 drugs studied but ΔG_{tl}^{0} varied more strongly than ΔG_{lw}^{0}. This suggests that the drug interactions to Pgp are weaker but more specific than to the lipid bilayer. Furthermore, the higher concentration of drugs in the membrane than in the aqueous phase at the concentration of half-maximum Pgp activity supports the relative weak interactions. The results are well explained with the hydrogen bond hypothesis and they indicate the existence of large drug binding region(s) in transmembrane domains of Pgp. In addition, we demonstrated that the binding constant of drug to Pgp from the aqueous phase, K_{tw}, depends exponentially on the lateral packing density of the membrane, π_M. This finding can explain the diverse concentrations of half-

maximum Pgp activity, K_1, reported in literature for the same drug but determined in the different membrane environments.

The common aim of the next three parts of this thesis was to elucidate Pgp activity in the cellular ensemble as well as in an isolated environment. This was done by measuring the Pgp activity for 15 structurally diverse Pgp substrates in living *MDR1*-transfected mouse embryo fibroblasts by monitoring the extracellular acidification rate, ECAR, and in plasma membrane vesicles formed from the same cells by monitoring the rate of ATP hydrolysis. Because these two systems exhibit several differences such as the direction of drug approaching Pgp, it was interesting to compare the kinetics of Pgp activity measured in both systems. We found that the concentrations of half-maximum Pgp activation, K_1, for 15 drugs were identical as long as the pH of the environment was identical and the possible artifacts such as vesicle and the drug association in the phosphate release measurements and cytotoxic effects of drugs in the ECAR measurements could be excluded. We, therefore, concluded that whether the drugs approach Pgp from the extracellular or cytosolic side of the membrane does not play a role as long as the drugs can deprotonate and cross the membrane in their uncharged form. A reasonably linear correlation was also found for the *relative* maximum Pgp activities, V_1. The observed outliers were mainly due to artifacts. In order to compare the *absolute* rate enhancements stimulated by various drugs the turnover numbers were estimated. The drug-stimulated turnover numbers were in good agreement if the Pgp activity in living cells was measured in the presence of pyruvate. In the absence of pyruvate the turnover numbers in living cells is however higher. Furthermore, it was found that the logarithm of maximum Pgp activity, $\ln V_1$, decreases linearly with decreasing free energy of drug binding to Pgp from the aqueous phase, $\Delta G^0_{tw(1)}$. Thus, we concluded that the drug release to the extracellular leaflet of the lipid bilayer is the rate-determining step for Pgp activity.

The previous studies about the influence of the metabolic state of the cells on Pgp activity revealed that the verapamil-stimulated ECAR was linearly correlated with the basal ECAR under the nutritional condition where the metabolic state of cells was low. However, when the metabolic state of cells was high (in the presence of glucose) the drug-stimulated ECAR flattened out. The increase in the drug-stimulated ECAR was suppressed compared to the increase in the basal ECAR. To better understand the influence of the metabolic state of the cell on the basal and the drug-stimulated ECAR we further studied the metabolic rate of mouse embryo fibroblasts by measuring the glucose consumption and the lactate production rate by means of ^{13}C-NMR spectroscopy. We found that the *relative* verapamil-

stimulated enhancement in the metabolic rate of NIH-MDR1-G185 cells was in good agreement with the values obtained from the ECAR measurements upon longtime verapamil stimulation. However, the ^{13}C-NMR measurements revealed that the *absolute* metabolic rate of wild-type and *MDR1*-transfected cells in the absence of drugs were about three-fold higher than those observed by monitoring the ECAR of the same cells. Also the *absolute* metabolic rate of *MDR1*-transfected cells stimulated with verapamil was distinctly higher. Furthermore, it was demonstrated by separating the intra- and the extracellular lactate NMR signals with a novel shift reagent that the lactate concentrations inside and outside of *MDR1*-transfected cells were similar. These results support the assumption that the flattening observed between the basal and the verapamil-stimulated ECAR under conditions of high ECARs, is due to the suppression of glycolysis. The experiments further indicate that it is not due to the saturation of monocarboxylate transporters.

The drug transport activity of Pgp is coupled to ATP hydrolysis but how these two steps are connected is still a matter of debate. Therefore, the goal in the fifth part of this thesis was to study the interplay between the transmembrane domains, TMDs, of Pgp, which bind and release the drugs, and the nucleotide binding domains, NBDs, of Pgp, which bind and hydrolyze ATP. Moreover, we aimed at getting additional information about the influence of the lateral membrane packing density, π_M, on the transition state parameters of ATP hydrolysis by Pgp (the activation enthalpy $\Delta H^{\ddagger}$, the activation entropy $\Delta S^{\ddagger}$, and the free energy of activation $\Delta G^{\ddagger}$) and, thus, on the mechanism of Pgp activity. For this purpose we measured the temperature dependence of steady-state Pgp activity in the plasma membrane vesicles of NIH-MDR1-G185 cells in the absence and presence of several exogenous Pgp substrates and analyzed the transition state parameters for ATP hydrolysis by Pgp (the activation enthalpy $\Delta H^{\ddagger}$, the activation entropy $\Delta S^{\ddagger}$, and the free energy of activation $\Delta G^{\ddagger}$). We found that the activation enthalpy, $\Delta H^{\ddagger}$, of ATP hydrolysis by Pgp was relatively large for the basal and drug-stimulated Pgp activity and decreased in the presence of all drugs investigated, even in the presence of drugs that reduce Pgp activity. The free energy of activation, $\Delta G^{\ddagger}$, in contrary, decreased at low and increased at high drug concentrations of verapamil and promazine, whereas it only increased for PSC833. Thus, by plotting the free energy of activation, $\Delta G^{\ddagger}$, as function of drug concentration revealed the mirror images of Pgp activation profiles, in good agreement with the Eyring's transition state theory. Furthermore, by comparing the transition state parameters for basal Pgp in plasma membrane vesicles of NIH-MDR1-G185 cells with the

literature data measured in different membrane environments, we found that the activation enthalpy, $\Delta H^{\ddagger}$, of ATP hydrolysis by Pgp decreases significantly with decreasing lateral membrane packing density, π_{M}, whereas the free energy of activation, $\Delta G^{\ddagger}$, decreased only slightly. The Pgp activity cycle contains several steps and each step has its own free energy of activation, $\Delta G_{i}^{\ddagger}$. The sum of these individual free energies is the free energy of activation, $\Delta G^{\ddagger}$, obtained from the steady-state Pgp activity measurements. The experimental data revealed that the different drugs affected the free energy of activation, $\Delta G^{\ddagger}$, in characteristic manner. However, whether the rate-limiting step is the ATP hydrolysis or the conformational change of Pgp could not be decided conclusively from the present data and further experiments are needed.

In the last part of this thesis we aimed at identifying whether the dyes, methylene blue, acridine orange, basic fuchsin, and ethyl eosin are substrates for Pgp. This is relevant since they are widely used in histological studies. Furthermore, their applicability for the treatment of cancer and microbial infections with photodynamic therapy has been tested. In accordance with the established rules for the intrinsic Pgp substrates we predicted that methylene blue, acridine orange and basic fuchsin are intrinsic substrates for Pgp whereas ethyl eosin is not. The Pgp activity measurements in plasma membrane vesicles and in living *MDR1*-transfected mouse embryo fibroblasts supported the prediction. Furthermore, the Pgp activity measurements in living cells revealed that methylene blue, acridine orange and ethyl eosin influenced the energy metabolism of wild-type and *MDR1*-transfected mouse embryo fibroblasts in a complex manner. Thus, the evaluation of Pgp activity in living cells gave further valuable information about the cytotoxicity of drugs.

In conclusion. We evaluated the thermodynamics and the kinetics of Pgp-substrate interactions. Since Pgp binds its substrates from the lipid phase the influence of the lipid bilayer on both of them was emphasized. The intrinsic drug binding constants, the binding constants of drug to Pgp from lipid phase, K_{tl}, for the 15 Pgp-substrates were evaluated quantitatively for the first time and revealed the weak interactions between Pgp and its substrates. The thermodynamic evaluation further indicated that the hydrogen bonds contribute significantly on the energetics of Pgp-substrate interactions supporting the hydrogen bond hypothesis and the existence of large drug binding region(s). Furthermore, it was shown that the concentration of half-maximum Pgp activity, K_{1}, of a specific drug depends on the lipid-water partition coefficient of the drug, K_{lw}, which in turns depends on the lateral packing density of the membrane, π_{M}, and therefore is dependent on the lipid

membrane where Pgp activity is determined. The rate of Pgp activity evaluated in living cells and in inverted plasma membrane vesicles revealed that Pgp activity is controlled by the binding affinity of the drug to Pgp from the aqueous phase, $\Delta G^0_{tw(1)}$. In living cells the metabolic state of cells further affected the rate of Pgp activity. By evaluating the transition state parameters from the temperature dependence of Pgp activity in the absence and presence of Pgp substrates and comparing the data with the available literature values suggested that the membrane packing density seems to slightly affect the basal Pgp activity, whereas the effective drug transport rate seems not to be affected. Moreover, the mode of Pgp action changed from entropy-driven to enthalpy-driven in the membrane with decreasing membrane packing density suggesting that Pgp and the membrane form a functional unity.

5. Acknowledgements

This work was carried out from the April 2003 until February 2007 in the laboratory of PD Dr. Anna Seelig in the Department of Biophysical Chemistry at the Biozentrum of University of Basel, Switzerland.

There are many people who have contributed directly or indirectly to this work and I owe many thanks to all of them. At first I want to express my gratitude to my PhD supervisor PD Dr. Anna Seelig. I am grateful for her giving me the opportunity to work in her lab and to contribute to this interesting and very challenging field of research. I also want to thank her for the valuable advices, the continuous support, and the encouragement during the course of this work. I learned a lot from her.

I also want to express my gratitude to Professor Dr. Joachim Seelig, who gave me the opportunity to be a part of his research group. Even if the topic of my research was quite different compared to the research topics of his group, I learned a lot from him, too. Furthermore, I am grateful for Professor DP Dr. Jürg Huwyler who worked as a referee for this thesis.

I also want to thank warmly Ewa Gatlik-Landwojtowicz who was working in our lab at the beginning of my thesis. She was a great support teaching me how to work with the cells, how to handle a Cytosensor and how to perform the surface activity measurements. I am very grateful for her contribution to this work. Furthermore, I express my thanks to Götz Kohler who collaborated with us in the ^{13}C-NMR work. I also thank to following people who have in someway or another helped me with the practical work: Xiachung Li-Blatter, Thomas Ahrens, and Wolfgang Oppliger.

Many thanks also to my present and former lab mates for the nice atmosphere in the lab: Renate Reiter, Gabriela Klocek, Matthias Meier (thanks for the last minutes help and advices), Andre Ziegler, Gregori Gerebtzoff, Peter Ganz, Susanna Notz, Andreas Zumbühl, Christian Müller, Andreas Beck, Andreas Bruns, Therese Schultness, Alekos Tsamaloukas, Heiko Heerklotz, Halina Szadkowska, Elisabeth Golçalves, Tom Anderson, and Bernhard Steinbauer. The big thanks also to the people from our technical workshop Hans Vogt, Leo Faletti, Gernhard Hänisch, and Simon Saner.

The biggest thanks I want to say to Ilkka. Thank you Ilkka, that you always stood next to me during the good and the bad times and encouraged me to continue. Without you this would not been possible. Ilkka, olet minulle hyvin tärkeä. Olen erittäin onnellinen, että saan jakaa sinun kanssa elämäni tärkeimmät ja kauneimmat hetket. Kiitos sinulle kaikesta.

I also want to thank my family; my mother, my father, and my little sister. Thanks for your endless love and support. Äiti, isä ja Ulla: Kiitos teille kaikesta. Olette minulle erittäin rakkaita.

Furthermore, I want to say thanks to all my friends here in Switzerland and Finland. Your friendship is important for me. I hope you know it. Thanks for the nice moments which I have shared with you. Especially thanks for the time which I have spent with you in the Alps skiing, climbing, and cycling. Those moments in the amazing environment were my source of relaxation giving me the strength to go on.

6. References

1. Davidson, A. L., and Chen, J. (2004) ATP-binding cassette transporters in bacteria, *Annu. Rev. Biochem. 73*, 241-268.
2. Dean, M., Hamon, Y., and Chimini, G. (2001) The human ATP-binding cassette (ABC) transporter superfamily, *J. Lipid Res. 42*, 1007-1017.
3. Jones, P. M., and George, A. M. (2004) The ABC transporter structure and mechanism: perspectives on recent research, *Cell Mol Life Sci 61*, 682-699.
4. Linton, K. J., and Higgins, C. F. (2007) Structure and function of ABC transporters: the ATP switch provides flexible control, *Pflugers Arch. 453*, 555-567.
5. Dean, M., and Annilo, T. (2005) Evolution of the ATP-binding cassette (ABC) transporter superfamily in vertebrates, *Annu. Rev. Genomics Hum. Genet. 6*, 123-142.
6. Gottesman, M. M., and Pastan, I. (1988) The multidrug transporter, a double-edged sword, *J Biol Chem 263*, 12163-12166.
7. Schinkel, A. H. (1997) The physiological function of drug-transporting P-glycoproteins, *Semin. Cancer Biol. 8*, 161-170.
8. Gottesman, M. M., Pastan, I., and Ambudkar, S. V. (1996) P-glycoprotein and multidrug resistance, *Curr. Opin. Genet. Dev. 6*, 610-617.
9. Gottesman, M. M., Fojo, T., and Bates, S. E. (2002) Multidrug resistance in cancer: role of ATP-dependent transporters, *Nat. Rev. Cancer 2*, 48-58.
10. Ambudkar, S. V., Dey, S., Hrycyna, C. A., Ramachandra, M., Pastan, I., and Gottesman, M. M. (1999) Biochemical, cellular, and pharmacological aspects of the multidrug transporter, *Annu. Rev. Pharmacol. Toxicol. 39*, 361-398.
11. Litman, T., Druley, T. E., Stein, W. D., and Bates, S. E. (2001) From MDR to MXR: new understanding of multidrug resistance systems, their properties and clinical significance, *Cell. Mol. Life Sci. 58*, 931-959.
12. Ambudkar, S. V., Kimchi-Sarfaty, C., Sauna, Z. E., and Gottesman, M. M. (2003) P-glycoprotein: from genomics to mechanism, *Oncogene 22*, 7468-7485.
13. Broxterman, H. J., Sonneveld, P., Pieters, R., Lankelma, J., Eekman, C. A., Loonen, A. H., Schoester, M., Ossenkoppele, G. J., Lowenberg, B., Pinedo, H. M., and Schuurhuis, G. J. (1999) Do P-glycoprotein and major vault protein (MVP/LRP) expression correlate with in vitro daunorubicin resistance in acute myeloid leukemia?, *Leukemia 13*, 258-265.
14. Leith, C. P., Kopecky, K. J., Chen, I. M., Eijdems, L., Slovak, M. L., McConnell, T. S., Head, D. R., Weick, J., Grever, M. R., Appelbaum, F. R., and Willman, C. L. (1999) Frequency and clinical significance of the expression of the multidrug resistance proteins MDR1/P-glycoprotein, MRP1, and LRP in acute myeloid leukemia: a Southwest Oncology Group Study, *Blood 94*, 1086-1099.
15. Martin, C., Walker, J., Rothnie, A., and Callaghan, R. (2003) The expression of P-glycoprotein does influence the distribution of novel fluorescent compounds in solid tumour models, *Br. J. Cancer 89*, 1581-1589.
16. Trock, B. J., Leonessa, F., and Clarke, R. (1997) Multidrug resistance in breast cancer: a meta-analysis of MDR1/gp170 expression and its possible functional significance, *J. Natl. Cancer Inst. 89*, 917-931.
17. Huisman, M. T., Smit, J. W., and Schinkel, A. H. (2000) Significance of P-glycoprotein for the pharmacology and clinical use of HIV protease inhibitors, *AIDS 14*, 237-242.

18.   Lee, C. G., Gottesman, M. M., Cardarelli, C. O., Ramachandra, M., Jeang, K. T., Ambudkar, S. V., Pastan, I., and Dey, S. (1998) HIV-1 protease inhibitors are substrates for the MDR1 multidrug transporter, *Biochemistry 37*, 3594-3601.

19.   Loscher, W., and Potschka, H. (2002) Role of multidrug transporters in pharmacoresistance to antiepileptic drugs, *J Pharmacol Exp Ther 301*, 7-14.

20.   Van Bambeke, F., Balzi, E., and Tulkens, P. M. (2000) Antibiotic efflux pumps, *Biochem Pharmacol 60*, 457-470.

21.   Wolfger, H., Mamnun, Y. M., and Kuchler, K. (2001) Fungal ABC proteins: pleiotropic drug resistance, stress response and cellular detoxification, *Res. Microbiol. 152*, 375-389.

22.   Borst, P., and Ouellette, M. (1995) New mechanisms of drug resistance in parasitic protozoa, *Annu. Rev. Microbiol. 49*, 427-460.

23.   Litman, T., Zeuthen, T., Skovsgaard, T., and Stein, W. D. (1997) Competitive, non-competitive and cooperative interactions between substrates of P-glycoprotein as measured by its ATPase activity, *Biochim Biophys Acta 1361*, 169-176.

24.   Huisman, M. T., Smit, J. W., Wiltshire, H. R., Beijnen, J. H., and Schinkel, A. H. (2003) Assessing safety and efficacy of directed P-glycoprotein inhibition to improve the pharmacokinetic properties of saquinavir coadministered with ritonavir, *J Pharmacol Exp Ther 304*, 596-602.

25.   Krishna, R., and Mayer, L. D. (2000) Multidrug resistance (MDR) in cancer. Mechanisms, reversal using modulators of MDR and the role of MDR modulators in influencing the pharmacokinetics of anticancer drugs, *Eur. J. Pharm. Sci. 11*, 265-283.

26.   Seelig, A., and Gatlik-Landwojtowicz, E. (2005) Inhibitors of multidrug efflux transporters: their membrane and protein interactions, *Mini-Rev. Med. Chem. 5*, 135-151.

27.   Thomas, H., and Coley, H. M. (2003) Overcoming multidrug resistance in cancer: an update on the clinical strategy of inhibiting p-glycoprotein, *Cancer Control 10*, 159-165.

28.   Wandel, C., Kim, R. B., Kajiji, S., Guengerich, P., Wilkinson, G. R., and Wood, A. J. (1999) P-glycoprotein and cytochrome P-450 3A inhibition: dissociation of inhibitory potencies, *Cancer Res 59*, 3944-3948.

29.   Modok, S., Mellor, H. R., and Callaghan, R. (2006) Modulation of multidrug resistance efflux pump activity to overcome chemoresistance in cancer, *Curr. Opin. Pharmacol. 6*, 350-354.

30.   Borowski, E., Bontemps-Gracz, M. M., and Piwkowska, A. (2005) Strategies for overcoming ABC-transporters-mediated multidrug resistance (MDR) of tumor cells, *Acta Biochim. Pol. 52*, 609-627.

31.   Pichler, A., Zelcer, N., Prior, J. L., Kuil, A. J., and Piwnica-Worms, D. (2005) In vivo RNA interference-mediated ablation of MDR1 P-glycoprotein, *Clin. Cancer Res. 11*, 4487-4494.

32.   Mechetner, E. B., and Roninson, I. B. (1992) Efficient inhibition of P-glycoprotein-mediated multidrug resistance with a monoclonal antibody, *Proc Natl Acad Sci U S A 89*, 5824-5828.

33.   Tsuruo, T., Hamada, H., Sato, S., and Heike, Y. (1989) Inhibition of multidrug-resistant human tumor growth in athymic mice by anti-P-glycoprotein monoclonal antibodies, *Jpn. J. Cancer Res. 80*, 627-631.

34.   Ceckova-Novotna, M., Pavek, P., and Staud, F. (2006) P-glycoprotein in the placenta: expression, localization, regulation and function, *Reprod. Toxicol. 22*, 400-410.

35.   Cordon-Cardo, C., O'Brien, J. P., Boccia, J., Casals, D., Bertino, J. R., and Melamed, M. R. (1990) Expression of the multidrug resistance gene product (P-glycoprotein) in human normal and tumor tissues, *J. Histochem. Cytochem. 38*, 1277-1287.

36.   Holash, J. A., Harik, S. I., Perry, G., and Stewart, P. A. (1993) Barrier properties of testis microvessels, *Proc Natl Acad Sci U S A 90*, 11069-11073.

37.   Tanaka, Y., Abe, Y., Tsugu, A., Takamiya, Y., Akatsuka, A., Tsuruo, T., Yamazaki, H., Ueyama, Y., Sato, O., Tamaoki, N., and et al. (1994) Ultrastructural localization of P-glycoprotein on capillary endothelial cells in human gliomas, *Virchows Arch. 425*, 133-138.

38.   Thiebaut, F., Tsuruo, T., Hamada, H., Gottesman, M. M., Pastan, I., and Willingham, M. C. (1987) Cellular localization of the multidrug-resistance gene product P-glycoprotein in normal human tissues, *Proc Natl Acad Sci U S A 84*, 7735-7738.

39.   Thiebaut, F., Tsuruo, T., Hamada, H., Gottesman, M. M., Pastan, I., and Willingham, M. C. (1989) Immunohistochemical localization in normal tissues of different epitopes in the multidrug transport protein P170: evidence for localization in brain capillaries and crossreactivity of one antibody with a muscle protein, *J. Histochem. Cytochem. 37*, 159-164.

40.   Schinkel, A. H., Mol, C. A., Wagenaar, E., van Deemter, L., Smit, J. J., and Borst, P. (1995) Multidrug resistance and the role of P-glycoprotein knockout mice, *Eur. J. Cancer 31A*, 1295-1298.

41.   van Helvoort, A., Smith, A. J., Sprong, H., Fritzsche, I., Schinkel, A. H., Borst, P., and van Meer, G. (1996) MDR1 P-glycoprotein is a lipid translocase of broad specificity, while MDR3 P-glycoprotein specifically translocates phosphatidylcholine, *Cell 87*, 507-517.

42.   Johnstone, R. W., Ruefli, A. A., and Smyth, M. J. (2000) Multiple physiological functions for multidrug transporter P-glycoprotein?, *Trends Biochem Sci 25*, 1-6.

43.   Valverde, M. A., Diaz, M., Sepulveda, F. V., Gill, D. R., Hyde, S. C., and Higgins, C. F. (1992) Volume-regulated chloride channels associated with the human multidrug-resistance P-glycoprotein, *Nature 355*, 830-833.

44.   Luker, G. D., Nilsson, K. R., Covey, D. F., and Piwnica-Worms, D. (1999) Multidrug resistance (MDR1) P-glycoprotein enhances esterification of plasma membrane cholesterol, *J Biol Chem 274*, 6979-6991.

45.   Calcabrini, A., Meschini, S., Stringaro, A., Cianfriglia, M., Arancia, G., and Molinari, A. (2000) Detection of P-glycoprotein in the nuclear envelope of multidrug resistant cells, *Histochem. J. 32*, 599-606.

46.   Molinari, A., Calcabrini, A., Meschini, S., Stringaro, A., Del Bufalo, D., Cianfriglia, M., and Arancia, G. (1998) Detection of P-glycoprotein in the Golgi apparatus of drug-untreated human melanoma cells, *Int. J. Cancer 75*, 885-893.

47.   Munteanu, E., Verdier, M., Grandjean-Forestier, F., Stenger, C., Jayat-Vignoles, C., Huet, S., Robert, J., and Ratinaud, M. H. (2006) Mitochondrial localization and activity of P-glycoprotein in doxorubicin-resistant K562 cells, *Biochem Pharmacol 71*, 1162-1174.

48.   Solazzo, M., Fantappie, O., Lasagna, N., Sassoli, C., Nosi, D., and Mazzanti, R. (2006) P-gp localization in mitochondria and its functional characterization in multiple drug-resistant cell lines, *Exp. Cell Res. 312*, 4070-4078.

49.   Lin, J. H., and Yamazaki, M. (2003) Role of P-glycoprotein in pharmacokinetics: clinical implications, *Clin Pharmacokinet 42*, 59-98.

50.   Rubin, L. L., and Staddon, J. M. (1999) The cell biology of the blood-brain barrier, *Annu. Rev. Neurosci. 22*, 11-28.

51.   Fischer, H., Gottschlich, R., and Seelig, A. (1998) Blood-brain barrier permeation: molecular parameters governing passive diffusion, *J. Membr. Biol. 165*, 201-211.

52.   Tatsuta, T., Naito, M., Oh-hara, T., Sugawara, I., and Tsuruo, T. (1992) Functional involvement of P-glycoprotein in blood-brain barrier, *J Biol Chem 267*, 20383-20391.

53.   Schinkel, A. H., Wagenaar, E., Mol, C. A., and van Deemter, L. (1996) P-glycoprotein in the blood-brain barrier of mice influences the brain penetration and pharmacological activity of many drugs, *J. Clin. Invest. 97*, 2517-2524.

54.   Watkins, P. B. (1990) Role of cytochromes P450 in drug metabolism and hepatotoxicity, *Semin. Liver Dis. 10*, 235-250.

55.   Krishna, D. R., and Klotz, U. (1994) Extrahepatic metabolism of drugs in humans, *Clin Pharmacokinet 26*, 144-160.

56.   Hochman, J. H., Chiba, M., Nishime, J., Yamazaki, M., and Lin, J. H. (2000) Influence of P-glycoprotein on the transport and metabolism of indinavir in Caco-2 cells expressing cytochrome P-450 3A4, *J Pharmacol Exp Ther 292*, 310-318.

57.   Glavinas, H., Krajcsi, P., Cserepes, J., and Sarkadi, B. (2004) The role of ABC transporters in drug resistance, metabolism and toxicity, *Curr Drug Deliv 1*, 27-42.

58.   Biedler, J. L., and Riehm, H. (1970) Cellular resistance to actinomycin D in Chinese hamster cells in vitro: cross-resistance, radioautographic, and cytogenetic studies, *Cancer Res 30*, 1174-1184.

59.   Dano, K. (1972) Cross resistance between vinca alkaloids and anthracyclines in Ehrlich ascites tumor in vivo, *Cancer Chemother. Rep. 56*, 701-708.

60.   Ling, V. (1975) Drug resistance and membrane alteration in mutants of mammalian cells, *Can. J. Genet. Cytol. 17*, 503-515.

61.   Ling, V., and Thompson, L. H. (1974) Reduced permeability in CHO cells as a mechanism of resistance to colchicine, *J. Cell. Physiol. 83*, 103-116.

62.   Juliano, R. L., and Ling, V. (1976) A surface glycoprotein modulating drug permeability in Chinese hamster ovary cell mutants, *Biochim Biophys Acta 455*, 152-162.

63.   Gottesman, M. M., and Pastan, I. (1993) Biochemistry of multidrug resistance mediated by the multidrug transporter, *Annu. Rev. Biochem. 62*, 385-427.

64.   Chen, C. J., Chin, J. E., Ueda, K., Clark, D. P., Pastan, I., Gottesman, M. M., and Roninson, I. B. (1986) Internal duplication and homology with bacterial transport proteins in the mdr1 (P-glycoprotein) gene from multidrug-resistant human cells, *Cell 47*, 381-389.

65.   Hrycyna, C. A., Airan, L. E., Germann, U. A., Ambudkar, S. V., Pastan, I., and Gottesman, M. M. (1998) Structural flexibility of the linker region of human P-glycoprotein permits ATP hydrolysis and drug transport, *Biochemistry 37*, 13660-13673.

66.   Loo, T. W., and Clarke, D. M. (1994) Functional consequences of glycine mutations in the predicted cytoplasmic loops of P-glycoprotein, *J Biol Chem 269*, 7243-7248.

67.   Takada, Y., Yamada, K., Taguchi, Y., Kino, K., Matsuo, M., Tucker, S. J., Komano, T., Amachi, T., and Ueda, K. (1998) Non-equivalent cooperation between the two nucleotide-binding folds of P-glycoprotein, *Biochim Biophys Acta 1373*, 131-136.

68.   Schinkel, A. H., Kemp, S., Dolle, M., Rudenko, G., and Wagenaar, E. (1993) N-glycosylation and deletion mutants of the human MDR1 P-glycoprotein, *J Biol Chem 268*, 7474-7481.

69.   Fardel, O., Lecureur, V., and Guillouzo, A. (1996) The P-glycoprotein multidrug transporter, *Gen. Pharmacol. 27*, 1283-1291.

70.   Germann, U. A., Chambers, T. C., Ambudkar, S. V., Licht, T., Cardarelli, C. O., Pastan, I., and Gottesman, M. M. (1996) Characterization of phosphorylation-defective mutants of human P-glycoprotein expressed in mammalian cells, *J Biol Chem 271*, 1708-1716.

71.   Rosenberg, M. F., Kamis, A. B., Callaghan, R., Higgins, C. F., and Ford, R. C. (2003) Three-dimensional structures of the mammalian multidrug resistance P-glycoprotein demonstrate major conformational changes in the transmembrane domains upon nucleotide binding, *J Biol Chem 278*, 8294-8299.

72.   Rosenberg, M. F., Callaghan, R., Modok, S., Higgins, C. F., and Ford, R. C. (2005) Three-dimensional structure of P-glycoprotein: the transmembrane regions adopt an asymmetric configuration in the nucleotide-bound state, *J Biol Chem 280*, 2857-2862.

73.   Rosenberg, M. F., Velarde, G., Ford, R. C., Martin, C., Berridge, G., Kerr, I. D., Callaghan, R., Schmidlin, A., Wooding, C., Linton, K. J., and Higgins, C. F. (2001) Repacking of the transmembrane domains of P-glycoprotein during the transport ATPase cycle, *EMBO J. 20*, 5615-5625.

74.   Ecker, G., Huber, M., Schmid, D., and Chiba, P. (1999) The importance of a nitrogen atom in modulators of multidrug resistance, *Mol. Pharmacol. 56*, 791-796.

75.   Seelig, A. (1998) A general pattern for substrate recognition by P-glycoprotein, *Eur. J. Biochem. 251*, 252-261.

76.   Seelig, A., Blatter, X. L., and Wohnsland, F. (2000) Substrate recognition by P-glycoprotein and the multidrug resistance-associated protein MRP1: a comparison, *Int. J. Clin. Pharmacol. Ther. 38*, 111-121.

77.   Seelig, A., and Landwojtowicz, E. (2000) Structure-activity relationship of P-glycoprotein substrates and modifiers, *Eur. J. Pharm. Sci. 12*, 31-40.

78.   Seelig, A., Landwojtowicz, E., Fischer, H., and Li Blatter, X. (2003) Towards P-glycoprotein structure-activity relationships, in *Drug BioAvailability/Estimation of Solubility, Permeability and Absorption* (Van der Waterbeemd, L., Arthurson, Ed.), pp 461-492, Wiley-VCH Verlag GmbH.

79.   Chen, Y., Pant, A. C., and Simon, S. M. (2001) P-glycoprotein does not reduce substrate concentration from the extracellular leaflet of the plasma membrane in living cells, *Cancer Res. 61*, 7763-7769.

80.   Shapiro, A. B., Fox, K., Lam, P., and Ling, V. (1999) Stimulation of P-glycoprotein-mediated drug transport by prazosin and progesterone. Evidence for a third drug-binding site, *Eur. J. Biochem. 259*, 841-850.

81.   Shapiro, A. B., and Ling, V. (1997) Extraction of Hoechst 33342 from the cytoplasmic leaflet of the plasma membrane by P-glycoprotein, *Eur. J. Biochem. 250*, 122-129.

82.   Higgins, C. F., and Gottesman, M. M. (1992) Is the multidrug transporter a flippase?, *Trends Biochem. Sci. 17*, 18-21.

83.   Omote, H., and Al-Shawi, M. K. (2002) A novel electron paramagnetic resonance approach to determine the mechanism of drug transport by P-glycoprotein, *J Biol Chem 277*, 45688-45694.

84.   Eckford, P. D., and Sharom, F. J. (2005) The reconstituted P-glycoprotein multidrug transporter is a flippase for glucosylceramide and other simple glycosphingolipids, *Biochem J 389*, 517-526.

85.   Romsicki, Y., and Sharom, F. J. (2001) Phospholipid flippase activity of the reconstituted P-glycoprotein multidrug transporter, *Biochemistry 40*, 6937-6947.

86.   Ruetz, S., and Gros, P. (1994) Phosphatidylcholine translocase: a physiological role for the mdr2 gene, *Cell 77*, 1071-1081.

87.   Romsicki, Y., and Sharom, F. J. (1999) The membrane lipid environment modulates drug interactions with the P- glycoprotein multidrug transporter, *Biochemistry 38*, 6887-6896.

88.   Litman, T., Zeuthen, T., Skovsgaard, T., and Stein, W. D. (1997) Structure-activity relationships of P-glycoprotein interacting drugs: kinetic characterization of their effects on ATPase activity, *Biochim. Biophys. Acta 1361*, 159-168.

89.   Bruggemann, E. P., Currier, S. J., Gottesman, M. M., and Pastan, I. (1992) Characterization of the azidopine and vinblastine binding site of P-glycoprotein, *J Biol Chem 267*, 21020-21026.

90.   Demmer, A., Andreae, S., Thole, H., and Tummler, B. (1999) Iodomycin and iodipine, a structural analogue of azidopine, bind to a common domain in hamster P-glycoprotein, *Eur J Biochem 264*, 800-805.

91.   Demmer, A., Thole, H., Kubesch, P., Brandt, T., Raida, M., Fislage, R., and Tummler, B. (1997) Localization of the iodomycin binding site in hamster P-glycoprotein, *J Biol Chem 272*, 20913-20919.

92.   Greenberger, L. M. (1993) Major photoaffinity drug labeling sites for iodoaryl azidoprazosin in P-glycoprotein are within, or immediately C-terminal to, transmembrane domains 6 and 12, *J Biol Chem 268*, 11417-11425.

93.   Ueda, K., Taguchi, Y., and Morishima, M. (1997) How does P-glycoprotein recognize its substrates?, *Semin. Cancer Biol. 8*, 151-159.

94.   Loo, T. W., and Clarke, D. M. (1997) Identification of residues in the drug-binding site of human P-glycoprotein using a thiol-reactive substrate, *J Biol Chem 272*, 31945-31948.

95.   Loo, T. W., and Clarke, D. M. (2001) Determining the dimensions of the drug-binding domain of human P-glycoprotein using thiol cross-linking compounds as molecular rulers, *J Biol Chem 276*, 36877-36880.

96.   Loo, T. W., and Clarke, D. M. (2001) Cross-linking of human multidrug resistance P-glycoprotein by the substrate, tris-(2-maleimidoethyl)amine, is altered by ATP hydrolysis. Evidence for rotation of a transmembrane helix, *J Biol Chem 276*, 31800-31805.

97.   Loo, T. W., and Clarke, D. M. (2001) Defining the drug-binding site in the human multidrug resistance P-glycoprotein using a methanethiosulfonate analog of verapamil, MTS-verapamil, *J Biol Chem 276*, 14972-14979.

98.   Loo, T. W., Bartlett, M. C., and Clarke, D. M. (2006) Transmembrane segment 1 of human P-glycoprotein contributes to the drug-binding pocket, *Biochem J 396*, 537-545.

99.   Loo, T. W., Bartlett, M. C., and Clarke, D. M. (2006) Transmembrane segment 7 of human P-glycoprotein forms part of the drug-binding pocket, *Biochem J 399*, 351-359.

100.   Dey, S., Ramachandra, M., Pastan, I., Gottesman, M. M., and Ambudkar, S. V. (1997) Evidence for two nonidentical drug-interaction sites in the human P-glycoprotein, *Proc. Natl. Acad. Sci. U.S.A. 94*, 10594-10599.

101.   Martin, C., Berridge, G., Higgins, C. F., Mistry, P., Charlton, P., and Callaghan, R. (2000) Communication between multiple drug binding sites on P-glycoprotein, *Mol. Pharmacol. 58*, 624-632.

102.   Shapiro, A. B., and Ling, V. (1997) Positively cooperative sites for drug transport by P-glycoprotein with distinct drug specificities, *Eur J Biochem 250*, 130-137.

103.   Loo, T. W., and Clarke, D. M. (2002) Vanadate trapping of nucleotide at the ATP-binding sites of human multidrug resistance P-glycoprotein exposes different residues to the drug-binding site, *Proc. Natl. Acad. Sci. U.S.A. 99*, 3511-3516.

104.   Scala, S., Akhmed, N., Rao, U. S., Paull, K., Lan, L. B., Dickstein, B., Lee, J. S., Elgemeie, G. H., Stein, W. D., and Bates, S. E. (1997) P-glycoprotein substrates and antagonists cluster into two distinct groups, *Mol. Pharmacol. 51*, 1024-1033.

105.   Loo, T. W., Bartlett, M. C., and Clarke, D. M. (2003) Substrate-induced conformational changes in the transmembrane segments of human P-glycoprotein. Direct evidence for the substrate-induced fit mechanism for drug binding, *J Biol Chem 278*, 13603-13606.

106.   Lugo, M. R., and Sharom, F. J. (2005) Interaction of LDS-751 and rhodamine 123 with P-glycoprotein: evidence for simultaneous binding of both drugs, *Biochemistry 44*, 14020-14029.

107.   Al-Shawi, M. K., Polar, M. K., Omote, H., and Figler, R. A. (2003) Transition state analysis of the coupling of drug transport to ATP hydrolysis by P-glycoprotein, *J. Biol. Chem. 278*, 52629-52640.

108.   Ambudkar, S. V., Cardarelli, C. O., Pashinsky, I., and Stein, W. D. (1997) Relation between the turnover number for vinblastine transport and for vinblastine-stimulated ATP hydrolysis by human P-glycoprotein, *J. Biol. Chem. 272*, 21160-21166.

109.   Sharom, F. J., Yu, X., and Doige, C. A. (1993) Functional reconstitution of drug transport and ATPase activity in proteoliposomes containing partially purified P-glycoprotein, *J. Biol. Chem. 268*, 24197-24202.

110.   Loo, T. W., and Clarke, D. M. (1994) Reconstitution of drug-stimulated ATPase activity following co-expression of each half of human P-glycoprotein as separate polypeptides, *J Biol Chem 269*, 7750-7755.

111.   Urbatsch, I. L., Sankaran, B., Weber, J., and Senior, A. E. (1995) P-glycoprotein is stably inhibited by vanadate-induced trapping of nucleotide at a single catalytic site, *J Biol Chem 270*, 19383-19390.

112.   Ambudkar, S. V., Lelong, I. H., Zhang, J., Cardarelli, C. O., Gottesman, M. M., and Pastan, I. (1992) Partial purification and reconstitution of the human multidrug-resistance pump: characterization of the drug-stimulatable ATP hydrolysis, *Proc. Natl. Acad. Sci. U.S.A. 89*, 8472-8476.

113.   Kerr, K. M., Sauna, Z. E., and Ambudkar, S. V. (2001) Correlation between steady-state ATP hydrolysis and vanadate-induced ADP trapping in Human P-glycoprotein. Evidence for ADP release as the rate-limiting step in the catalytic cycle and its modulation by substrates, *J. Biol. Chem. 276*, 8657-8664.

114.   Sharom, F. J., Yu, X., Chu, J. W., and Doige, C. A. (1995) Characterization of the ATPase activity of P-glycoprotein from multidrug-resistant Chinese hamster ovary cells, *Biochem. J. 308 (Pt 2)*, 381-390.

115.   Urbatsch, I. L., al-Shawi, M. K., and Senior, A. E. (1994) Characterization of the ATPase activity of purified Chinese hamster P-glycoprotein, *Biochemistry 33*, 7069-7076.

116.   al-Shawi, M. K., and Senior, A. E. (1993) Characterization of the adenosine triphosphatase activity of Chinese hamster P-glycoprotein, *J Biol Chem 268*, 4197-4206.

117.   Loo, T. W., and Clarke, D. M. (1995) Covalent modification of human P-glycoprotein mutants containing a single cysteine in either nucleotide-binding fold abolishes drug-stimulated ATPase activity, *J Biol Chem 270*, 22957-22961.

118.   Urbatsch, I. L., Beaudet, L., Carrier, I., and Gros, P. (1998) Mutations in either nucleotide-binding site of P-glycoprotein (Mdr3) prevent vanadate trapping of nucleotide at both sites, *Biochemistry 37*, 4592-4602.

119.   Senior, A. E., al-Shawi, M. K., and Urbatsch, I. L. (1995) The catalytic cycle of P-glycoprotein, *FEBS Lett. 377*, 285-289.

120. Hung, L. W., Wang, I. X., Nikaido, K., Liu, P. Q., Ames, G. F., and Kim, S. H. (1998) Crystal structure of the ATP-binding subunit of an ABC transporter, *Nature 396*, 703-707.

121. Hopfner, K. P., Karcher, A., Shin, D. S., Craig, L., Arthur, L. M., Carney, J. P., and Tainer, J. A. (2000) Structural biology of Rad50 ATPase: ATP-driven conformational control in DNA double-strand break repair and the ABC-ATPase superfamily, *Cell 101*, 789-800.

122. Smith, P. C., Karpowich, N., Millen, L., Moody, J. E., Rosen, J., Thomas, P. J., and Hunt, J. F. (2002) ATP binding to the motor domain from an ABC transporter drives formation of a nucleotide sandwich dimer, *Mol. Cell 10*, 139-149.

123. Lamers, M. H., Perrakis, A., Enzlin, J. H., Winterwerp, H. H., de Wind, N., and Sixma, T. K. (2000) The crystal structure of DNA mismatch repair protein MutS binding to a G x T mismatch, *Nature 407*, 711-717.

124. Locher, K. P., Lee, A. T., and Rees, D. C. (2002) The E. coli BtuCD structure: a framework for ABC transporter architecture and mechanism, *Science 296*, 1091-1098.

125. Ambudkar, S. V., Kim, I. W., and Sauna, Z. E. (2006) The power of the pump: mechanisms of action of P-glycoprotein (ABCB1), *Eur. J. Pharm. Sci. 27*, 392-400.

126. Ambudkar, S. V., Kim, I. W., Xia, D., and Sauna, Z. E. (2006) The A-loop, a novel conserved aromatic acid subdomain upstream of the Walker A motif in ABC transporters, is critical for ATP binding, *FEBS Lett. 580*, 1049-1055.

127. Kim, I. W., Peng, X. H., Sauna, Z. E., FitzGerald, P. C., Xia, D., Muller, M., Nandigama, K., and Ambudkar, S. V. (2006) The conserved tyrosine residues 401 and 1044 in ATP sites of human P-glycoprotein are critical for ATP binding and hydrolysis: evidence for a conserved subdomain, the A-loop in the ATP-binding cassette, *Biochemistry 45*, 7605-7616.

128. Loo, T. W., and Clarke, D. M. (2000) Drug-stimulated ATPase activity of human P-glycoprotein is blocked by disulfide cross-linking between the nucleotide-binding sites, *J Biol Chem 275*, 19435-19438.

129. Qu, Q., and Sharom, F. J. (2001) FRET analysis indicates that the two ATPase active sites of the P-glycoprotein multidrug transporter are closely associated, *Biochemistry 40*, 1413-1422.

130. Sauna, Z. E., and Ambudkar, S. V. (2007) About a switch: how P-glycoprotein (ABCB1) harnesses the energy of ATP binding and hydrolysis to do mechanical work, *Mol Cancer Ther 6*, 13-23.

131. van Veen, H. W., Higgins, C. F., and Konings, W. N. (2001) Molecular basis of multidrug transport by ATP-binding cassette transporters: a proposed two-cylinder engine model, *J. Mol. Microbiol. Biotechnol. 3*, 185-192.

132. Smith, C. A., and Rayment, I. (1996) X-ray structure of the magnesium(II).ADP.vanadate complex of the Dictyostelium discoideum myosin motor domain to 1.9 A resolution, *Biochemistry 35*, 5404-5417.

133. Qu, Q., Chu, J. W., and Sharom, F. J. (2003) Transition state P-glycoprotein binds drugs and modulators with unchanged affinity, suggesting a concerted transport mechanism, *Biochemistry 42*, 1345-1353.

134. Sonveaux, N., Shapiro, A. B., Goormaghtigh, E., Ling, V., and Ruysschaert, J. M. (1996) Secondary and tertiary structure changes of reconstituted P-glycoprotein. A Fourier transform attenuated total reflection infrared spectroscopy analysis, *J Biol Chem 271*, 24617-24624.

135. Martin, C., Berridge, G., Mistry, P., Higgins, C., Charlton, P., and Callaghan, R. (2000) Drug binding sites on P-glycoprotein are altered by ATP binding prior to nucleotide hydrolysis, *Biochemistry 39*, 11901-11906.

136.   Sharom, F. J., Liu, R., Romsicki, Y., and Lu, P. (1999) Insights into the structure and substrate interactions of the P-glycoprotein multidrug transporter from spectroscopic studies, *Biochim Biophys Acta 1461*, 327-345.

137.   Loo, T. W., and Clarke, D. M. (1999) Determining the structure and mechanism of the human multidrug resistance P-glycoprotein using cysteine-scanning mutagenesis and thiol-modification techniques, *Biochim Biophys Acta 1461*, 315-325.

138.   Mechetner, E. B., Schott, B., Morse, B. S., Stein, W. D., Druley, T., Davis, K. A., Tsuruo, T., and Roninson, I. B. (1997) P-glycoprotein function involves conformational transitions detectable by differential immunoreactivity, *Proc Natl Acad Sci U S A 94*, 12908-12913.

139.   Ramachandra, M., Ambudkar, S. V., Chen, D., Hrycyna, C. A., Dey, S., Gottesman, M. M., and Pastan, I. (1998) Human P-glycoprotein exhibits reduced affinity for substrates during a catalytic transition state, *Biochemistry 37*, 5010-5019.

140.   Sauna, Z. E., and Ambudkar, S. V. (2000) Evidence for a requirement for ATP hydrolysis at two distinct steps during a single turnover of the catalytic cycle of human P-glycoprotein, *Proc. Natl. Acad. Sci. U.S.A. 97*, 2515-2520.

141.   Callaghan, R., Ford, R. C., and Kerr, I. D. (2006) The translocation mechanism of P-glycoprotein, *FEBS Lett. 580*, 1056-1063.

142.   Qu, Q., Russell, P. L., and Sharom, F. J. (2003) Stoichiometry and affinity of nucleotide binding to P-glycoprotein during the catalytic cycle, *Biochemistry 42*, 1170-1177.

143.   Higgins, C. F., and Linton, K. J. (2004) The ATP switch model for ABC transporters, *Nat Struct Mol Biol 11*, 918-926.

144.   Landwojtowicz, E., Nervi, P., and Seelig, A. (2002) Real-time monitoring of P-glycoprotein activation in living cells, *Biochemistry 41*, 8050-8057.

145.   Urbatsch, I. L., and Senior, A. E. (1995) Effects of lipids on ATPase activity of purified Chinese hamster P-glycoprotein, *Arch. Biochem. Biophys. 316*, 135-140.

146.   Seelig, A., and Gerebtzoff, G. (2006) Enhancement of drug absorption by noncharged detergents through membrane and P-glycoprotein binding, *Expert Opin Drug Metab Toxicol 2*, 733-752.

147.   Vezzoli, A., Gussoni, M., Greco, F., and Zetta, L. (2003) Effects of temperature and extracellular pH on metabolites: kinetics of anaerobic metabolism in resting muscle by 31P- and 1H-NMR spectroscopy, *J. Exp. Biol. 206*, 3043-3052.

148.   Halestrap, A. P., and Price, N. T. (1999) The proton-linked monocarboxylate transporter (MCT) family: structure, function and regulation, *Biochem J 343 Pt 2*, 281-299.

149.   Guttmann, P., and Erhlich, P. (1891) Ueber die Wirkung des Methylenblau bei Malaria., *Berlin Klin. Wochehschr. 28*, 953-956.

7. Reprints and Unpublished Manuscripts

7.1   Quantification and Characterization of P-glycoprotein-Substrate Interactions

Ewa Gatlik-Landwojtowicz, Päivi Äänismaa, and Anna Seelig*

Biophysical Chemistry, Biozentrum, University Basel, Klingelbergstrasse 70, CH-4056, Basel, Switzerland

*Corresponding author, Phone: +41-61-267-22-06. Fax: +41-61-267-2-89. E-mail: Anna.Seelig@unibas.ch

Quantification and Characterization of P-Glycoprotein−Substrate Interactions

Ewa Gatlik-Landwojtowicz, Päivi Äänismaa, and Anna Seelig*

Biophysical Chemistry, Biozentrum, University of Basel, Klingelbergstrasse 70, CH-4056, Basel, Switzerland

Received July 15, 2005; Revised Manuscript Received November 29, 2005

ABSTRACT: It is generally accepted that P-glycoprotein binds its substrates in the lipid phase of the membrane. Quantification and characterization of the lipid-transporter binding step are, however, still a matter of debate. We therefore selected 15 structurally diverse drugs and measured the binding constants from water to the activating (inhibitory) binding region of P-glycoprotein, $K_{tw(1)}$ ($K_{tw(2)}$), as well as the lipid−water partition coefficients, K_{lw}. The former were obtained by measuring the concentrations of half-maximum activation (inhibition), K_1 (K_2), in living NIH-MDR-G185 mouse embryo fibroblasts using a Cytosensor microphysiometer, and the latter were derived from surface activity measurements. This allowed determination of the membrane concentration of drugs at half-maximum P-glycoprotein activation ($C_{b(1)} = (0.02$ to $67)$ mmol/L lipid), which is much higher than the corresponding aqueous concentration ($K_1 = (0.02$ to $376)$ μM). Moreover we determined the free energy of drug binding from water to the activating binding region of the transporter ($\Delta G^{\circ}_{tw(1)} = (-30$ to $-54)$ kJ/mol), the free energy of drug partitioning into the lipid membrane ($\Delta G^{\circ}_{lw} = (-23$ to $-34)$ kJ/mol), and, as the difference of the two, the free energy of drug binding from the lipid membrane to the activating binding region of the transporter ($\Delta G^{\circ}_{tl(1)} = (-7$ to $-27)$ kJ/mol). For the compounds tested $\Delta G^{\circ}_{tl(1)}$ was less negative than ΔG°_{lw} but varied more strongly. The free energies of substrate binding to the transporter within the lipid phase, $\Delta G^{\circ}_{tl(1)}$, are consistent with a modular binding concept, where the energetically most efficient binding module comprises two hydrogen bond acceptor groups.

Various lines of evidence indicate that the P-glycoprotein-ATPase, Pgp[1] (ABCB1), binds its substrates within the plasma membrane (*1, 2*) and, more precisely, within the cytosolic lipid leaflet of the plasma membrane (*3−7*) (for review see ref *8*). Exogenous substrates such as drugs and toxins are thus caught by Pgp *after* partitioning into the plasma membrane but *before* reaching the cytosol and are then exported or flipped at the expense of ATP hydrolysis (*3, 4, 9*).

The environment from which substrates bind to the transporter is decisive for the type of binding interactions (*10, 11*). Little is known on the role of the lipid membrane for substrate−transporter interactions since most well-investigated transporters bind their substrates from the aqueous phase (e.g. fucose transporter (*12*)). To investigate the relationship between lipid partitioning and drug binding Romsicki and Sharom (*13*) reconstituted Pgp into various well-defined lipid bilayers and measured the transporter dissociation constants, K_d (i.e. the release of the drug from

Pgp into the aqueous phase), as well as the lipid−water partition coefficients, P_{lw}. For the three drugs investigated, the binding affinity to Pgp from the aqueous phase increased in parallel to the lipid−water partition coefficient, suggesting that the concentration of the drug in the membrane is important for the interaction with the transporter (*13*). A linear correlation between binding affinity to Pgp and membrane partitioning (estimated from the octanol−water partition coefficient, log P_{ow}) was also observed for propafenone analogues (*6*). However, for structurally more diverse drugs no correlation between binding affinity to Pgp and membrane affinity (log P_{ow}) was observed. Instead, an approximately linear dependence of the binding affinity to Pgp on the van der Waals surface area of drugs was noticed (*14*). For the same drugs, a linear correlation between drug affinity to Pgp and the logarithm of the air−water partition coefficient, log K_{aw}, was demonstrated (*15*), suggesting that both the lipid−water partition coefficient, K_{lw}, and the cross-sectional area, A_D, of a given drug molecule play a role for drug−Pgp interactions (*11*).

The question as to how Pgp accommodates molecules of different size is still a matter of debate. It has been suggested that Pgp has at least two substrate binding sites (*1, 13, 16*). Our kinetic data (*17, 18*) could be well fitted with a model (*14*) that assumes two binding sites, one for activation and one for inhibition. Evidence for three (*19*) and even four binding sites has also been reported (*20*). As an alternative to specific binding sites, broader binding regions have been proposed (*21*). The concept of binding regions is consistent with a search for possible drug interaction sites in the

---

* Corresponding author. Phone: +41-61-267-22-06. Fax: +41-61-267-21-89. E-mail: Anna.Seelig@unibas.ch.

[1] Abbreviations: DMPC, 1,2-dimyristoyl-*sn*-glycero-3-phosphatidylcholine; ECAR, extracellular acidification rate; K_1 (K_2), aqueous substrate concentration at half-maximum Pgp activation (inhibition); K_{aw}, air−water partition coefficient; K_{lw}, lipid−water partition coefficient; $K_{tl(1)}$ ($K_{tl(2)}$), binding constant of the drug from the lipid membrane to the activating (inhibitory) binding region of the transporter; $K_{tw(1)}$ ($K_{tw(2)}$), binding constant of the drug from water to the activating (inhibitory) binding region of the transporter; MDR, multidrug resistance; Pgp, P-glycoprotein-ATPase (MDR1, ABCB1); POPC, 1-palmitoyl-2-oleoyl-*sn*-glycero-3-phosphatidylcholine; π_M, lateral membrane packing density; V_1 (V_2), maximum (minimum) transporter activity.

predicted transmembrane sequences of Pgp (*22*). The latter investigation revealed a high density of amino acids with hydrogen bond donor side chains in the transmembrane sequences of Pgp which could interact with characteristic hydrogen bond acceptor patterns present in *all* Pgp substrates (*10*, *23*, *24*). Moreover, clusters of phenyl residues were observed which could interact either with π-electron systems ($\pi-\pi$ interactions) or with cationic residues in drugs (cation$-\pi$ interactions) (*22*). Recently, Sauna et al. (*25*) also suggested a variable number of binding interactions between substrate and transporter, however, without specifying the type of interactions. Concepts with a variable number of binding modules contrast with classical quantitative structure− activity relationship, QSAR, approaches (for review see refs *26*, *27*) or multivariant procedures (e.g. ref *28*) that are both based on "key-lock" concepts and consider one single "key" or "pharmacophore" per Pgp substrate.

Drug partitioning into the lipid membrane and drug binding to Pgp within the lipid membrane are tightly coupled processes which have not yet been deconvoluted satisfactorily. In the following we demonstrate that the binding constant of a given substrate in the lipid phase to the activating (inhibitory) binding region of Pgp, $K_{tl(1)}$ ($K_{tl(2)}$), can be calculated provided the corresponding lipid−water partition coefficient, K_{lw}, and the binding constant of the drug from the aqueous phase to the activating (inhibitory) binding region of Pgp, $K_{tw(1)}$ ($K_{tw(2)}$), are known. The binding constants from water to the transporter, $K_{tw(1)}$ ($K_{tw(2)}$), were determined in living NIH-MDR-G185 cells as the inverse of the concentrations of half-maximum Pgp activation, K_1 (inhibition, K_2) (*11*). The concentrations of half-maximum Pgp activation, K_1 (inhibition, K_2) were measured by means of a Cytosensor microphysiometer (*29*) that monitors the extracellular acidification rate, ECAR (*17*, *18*). As a control, we also measured the phosphate release rates upon drug-induced Pgp-ATPase activation in inside-out membrane vesicles and showed that the ECARs and the phosphate release rates are identical ((*18*), Äänismaa and Seelig, in preparation). The lipid−water partition coefficients, K_{lw}, were derived from the air−water partition coefficients, K_{aw}, and the cross-sectional area, A_D, of the drug taking into account the lateral packing density, π_M (*30*, *31*), and the surface potential, ψ, of the cytosolic membrane leaflet. The lipid− water partition coefficients, K_{lw}, obtained by means of this approach were in excellent agreement with the lipid−water partition coefficients obtained by means of isothermal titration calorimetry using model membranes of known lateral packing density (for the present compounds, Li-Blatter and Seelig, in preparation).

We selected 15 chemically diverse drugs (antidepressants, an antineoplastic, antipsychotics, a calcium channel blocker, local anesthetics, an immunosuppressant, a steroid hormone, a tyrosine kinase inhibitor) and report for the first time the binding constants of the drugs from the lipid membrane to the activating (inhibitory) binding region of the transporter in the lipid phase, $K_{tl(1)}$ ($K_{tl(2)}$). The corresponding free energies of binding, $\Delta G^{\circ}_{tl(1)}$ ($\Delta G^{\circ}_{tl(2)}$), reflect the *effective* interactions between the substrates and the activating (inhibitory) binding region of Pgp. We show that the substrate concentrations in the membrane are higher by a factor of 10^2 to 10^4 than those in the aqueous phase, which implies that the interactions between drugs and Pgp in the lipid membrane are relatively weak. Our results further indicate that binding of drugs to Pgp is not compatible with a classical "key-lock" or "one-pharmacophore" model but can be well explained with a modular binding concept, where the energetically most relevant binding module seems to consist of two hydrogen bond acceptor groups.

MATERIALS AND METHODS

Materials. Amitriptyline·HCl, *cis*-flupenthixol·2HCl, daunorubicin·HCl, dibucaine·HCl, diltiazem·HCl, lidocaine· HCl, progesterone, promazine·HCl, trifluoperazine·2HCl, and triflupromazine·HCl were from Sigma-Aldrich (Steinheim, Germany), and (*R/S*)-verapamil·HCl was from Fluka (Buchs, Switzerland). Chlorpromazine·HCl and reserpine·HCl·H$_2$O were generous gifts from Merck (Darmstadt, Germany), and cyclosporin A and glivec mesylate from Novartis AG (Basel, Switzerland). For Cytosensor measurements cyclosporin A, progesterone, reserpine, and (*R/S*)-verapamil were dissolved in DMSO, where the final DMSO concentration did not exceed 0.5% (v/v). The remaining drugs were directly dissolved in medium. To test the influence of DMSO on membrane partitioning and Pgp binding, (*R/S*)-verapamil and glivec were measured with and without DMSO. The results were identical within error limits (Äänismaa and Seelig, in preparation). Cell culture medium DMEM with pyruvate (liquid and dry, Cat. No. 21969 and Cat. No. 52100, respectively) as well as other compounds required for cell culture such as fetal bovine serum, FBS, L-glutamine, and antibiotics were from Gibco-BRL (Basel, Switzerland).

Buffers. Buffers were adjusted to pH 7.4 at ambient temperature. For Cytosensor measurements (performed at 37 °C), a flow medium with low buffer capacity is required. The flow medium was prepared from dry powder Dulbecco's modified Eagle medium (Gibco-BRL, Basel, Switzerland) which contains 0.91 mM phosphate but no sodium bicarbonate. Flow medium was supplemented with 1 mM sodium pyruvate to decrease the basal ECAR of cells and to enhance the relative ECAR changes due to Pgp activation in particular (*18*). In order to preserve osmotic balance the lacking sodium bicarbonate was replaced by sodium chloride (2.6 g/L of NaCl instead of 3.7 g/L of NaHCO$_3$).

Cell Lines and Cell Culture. The mouse embryo fibroblast cell lines NIH3T3 and NIH3T3 transfected with the human *MDR1* gene, NIH-MDR-G185 (grown in the presence of 0.15 μM colchicine), were generous gifts from Dr. M. M. Gottesman and Dr. S. V. Ambudkar (The National Institutes of Health, Bethesda, MD). Cells were maintained as described earlier (*17*, *18*).

Cytosensor Measurements. In short, the Cytosensor microphysiometer measures the rate of proton excretion from 10^4 to 10^6 cells in a flow chamber with diffusive contact to a pH sensitive silicon chip. Due to the flow chambers it is possible to maintain approximately constant drug concentrations, which allows the establishment of steady state conditions. Cytosensor measurements with NIH3T3 and NIH-MDR-G185 cells and the quantification of extracellular acidification are described elsewhere in detail (*17*, *18*). In the present study the drug concentrations were corrected for adsorption to the walls of the fluid supply tubes, the debubbler membranes, and the flexible tubing ($\sim$65 cm) which connect the fluid supply tubes with the Cytosensor
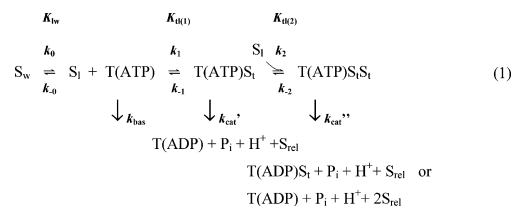
Gatlik-Landwojtowicz et al.

chamber. Corrections were made in separate control runs by sampling the drug solution just before entering the sensor chamber and measuring the drug concentration by UV spectroscopy. To mimic the time schedule of Cytosensor measurements the drug solutions were let to flow through Cytosensor tubing 6 min before the samples were collected during the 3 min. Adsorption varied strongly from compound to compound and was small for verapamil and high for phenothiazines. Cyclosporin A concentrations could not be corrected for adsorption by UV because the molecule does not contain UV-detectable amino acid residues.

Lipid−Water and Air−Water Partition Coefficient. Measurement of the lipid−water partition coefficient, K_{lw}, in intact cells is not possible since other structures e.g. the glycocalix or proteins also attract cationic compounds. We have therefore developed an approach that allows determination of the lipid−water partition coefficient, K_{lw}, from the air−water partition coefficient, K_{aw}, and the cross-sectional area, A_D, of the drug, by taking into account the relevant lateral membrane packing density, π_M (*30*, *31*), and the surface potential of the membrane, ψ. The air−water partition coefficient, K_{aw}, and the cross-sectional area, A_D, of the drug were derived from measurements of the surface pressure, π, as a function of concentration (Gibbs adsorption isotherm) as described previously ((*30*, *31*), for the present compounds, Li-Blatter and Seelig, in preparation).

The Kinetic Models. The kinetics of Pgp activation has been discussed in detail elsewhere (*11*, *17*) and is summarized briefly. The model used to analyze Pgp−drug interactions is outlined in the scheme depicted in eq 1. In

$$S_w \underset{k_{-0}}{\overset{k_0}{\rightleftharpoons}} S_l + T(ATP) \underset{k_{-1}}{\overset{k_1}{\rightleftharpoons}} T(ATP)S_t \underset{k_{-2}}{\overset{S_l \quad k_2}{\rightleftharpoons}} T(ATP)S_tS_t \qquad (1)$$

the *absence* of exogenous substrates Pgp shows basal activity, with k_{bas} as the catalytic rate constant (1st arrow down). Substrates in the aqueous phase, S_w, partition into the lipid membrane, where k_0 and k_{-0} are the partitioning rate constants, and $K_{lw} = k_0/k_{-0}$ is the lipid−water partition coefficient. The substrate in the lipid membrane, S_l, binds to the transporter, T, forming the transporter−ATP−substrate complex, $T(ATP)S_t$ (for simplicity only one ATP (ADP) molecule per Pgp is shown in eq 1); S_t is the substrate bound to the activating binding region of the transporter, k_1 and k_{-1} are the rate constants for association to and dissociation from the activating binding region, and $K_{tl(1)} = k_1/k_{-1}$ is the binding constant of the substrate for the activating binding region of the transporter within the lipid membrane. The 2nd arrow down shows the substrate transport step which is driven by hydrolysis of ATP to ADP and phosphate, P_i, where k_{cat}' denotes the catalytic rate constant and S_{rel} the substrate released. At high substrate concentrations a second substrate molecule is bound to the inhibitory binding region forming the complex $T(ATP)S_tS_t$, where k_2 and k_{-2} are the association and dissociation rate constants, respectively, $K_{tl(2)} = k_2/k_{-2}$ reflects the binding constant to the inhibitory binding

region of the transporter, and k_{cat}'' is the catalytic rate constant of the inhibitory binding step. The association/dissociation reactions are rapid compared to the catalytic steps (cf. ref *32*) (k_{-1} and $k_{-2} \gg k_{bas}, k_{cat}', k_{cat}''$). To a first approximation, the concentration of half-maximum (minimum) activation K_1 (K_2) can therefore be assumed to correspond to the dissociation constant of the activating (inhibitory) binding region of Pgp and the inverse, $1/K_1$ ($1/K_2$), to the transporter−water binding constant for the activating (inhibitory) binding region, $K_{tw(1)}$ ($K_{tw(2)}$).

Based on this mechanism the following rate equation for ATP hydrolysis has been developed by Litman et al. (*14*):

$$V_{sw} = \frac{K_1K_2V_{bas} + K_2V_1C_{sw} + V_2C_{sw}^2}{K_1K_2 + K_2C_{sw} + C_{sw}^2} \qquad (2)$$

where V_{sw} is the rate of P_i release as a function of the substrate concentration in aqueous solution, C_{sw}, V_{bas} is the basal activity of Pgp in the absence of drug, V_1 is the maximum transporter activity (if only activation occurred), and V_2 is the minimum activity at infinite substrate concentration. At a substrate concentration, $C_{sw} = K_1$, half-maximum binding of the activating binding region is reached, and at a substrate concentration, $C_{sw} = K_2$, half-maximum binding of the inhibitory binding region is reached. Equation 2 is thus based on the concept of substrate inhibition (or uncompetitive inhibition) which was extended to allow for basal activation in the absence of a substrate and for breakdown of the complex $T(ATP)S_tS_t$ (eq 1). The kinetic data given in Table 1 were analyzed using this model.

For comparison we discuss a simplified version of the above model (*14*) that does not allow for catalytic activity of the complex $T(ATP)S_tS_t$ ($V_2 = 0$) and shows the following rate equation:

$$V_{sw} = \frac{K_1K_2V_{bas} + K_2V_1C_{sw}}{K_1K_2 + K_2C_{sw} + C_{sw}^2} \qquad (3)$$

A related model was proposed by Al-Shawi et al. (*33*, *34*). It also considers basal activation of Pgp in the absence of drugs, drug activation, and drug inhibition. However, it is based on the concept of noncompetitive inhibition and shows the following rate equation:

$$V_{sw} = \frac{K_1K_2V_{bas} + K_2V_1C_{sw}}{K_1K_2 + K_1C_{sw} + K_2C_{sw} + C_{sw}^2} \qquad (4)$$

The influence of the different models on the kinetic data will be discussed.

The Thermodynamics of Substrate Binding. As shown previously (*11*), the binding constant of the drug from water to the transporter, $K_{tw(1)}$, is the product of the lipid−water partition coefficient, K_{lw}, and the binding constant of the drug from the lipid membrane to the transporter, $K_{tl(1)}$,

$$1/K_1 \cong K_{tw(1)} \cong K_{tl(1)}K_{lw} \qquad (5)$$

This leads to the corresponding free energy relationship

$$\Delta G°_{tw(1)} \cong \Delta G°_{tl(1)} + \Delta G°_{lw} \qquad (6)$$

where the degree symbol refers to a biological standard state

Table 1: Thermodynamic and Kinetic Parameters for 15 Drugs[a]

no.	compound	pK_a	K_{aw} [mM⁻¹] pH 7.4	A_D [Å²] pH 8.0	K_1 [µM]	K_2 [µM]	V_1 [fold]	V_2 [fold]	$X_{b(1)}$ [mmol/ mol]	$X_{b(2)}$ [mmol/ mol]	weighted number H-bond acceptors	$\Delta G°_{Hi}$ [kJ/mol]
1	amitriptyline	9.4[53]	7.1[30]	52[15]	6.4 ± 0.2	57.2 ± 11.3	1.9 ± 0.01	0.2 ± 0.2	3.6	33.5	2	−7.0
2	chlorpromazine	9.2[54]	21.5[30]	42[30] (pH 7.4)	5.7 ± 0.0	16.4 ± 3.0	2.0 ± 0.3	0.0 ± 0.0	20.2	58.1	2	−4.9
3	*cis*-flupenthixol	7.8[55]	453[30]	60[30]	3.0 ± 1.8	33.8 ± 18.1	1.4 ± 0.2	0.0 ± 0.0	47.0	523.0	2.5	−3.1
4	cyclosporin A	-	19952.6[15]	140	0.02 ± 0.01	1.5 ± 1.0	1.1 ± 0.1	0.8 ± 0.3	0.02	1.6	10.5	−2.6
5	daunorubicin	8.4[56]	588.8[15]	106[15]	0.6 ± 0.3	19.0 ± 4.0	1.1 ± 0.05	0.1 ± 0.1	0.6	19.1	7	−2.6
6	dibucaine	8.5[57]	11.3	52	10.9 ± 1.0	21.0 ± 7.8	2.0 ± 0.2	1.0 ± 0.1	9.4	18.2	1.5	−7.8
7	diltiazem	8.9[58]	26.9[15]	70[15]	3.5 ± 0.4	296.8 ± 107.6	1.8 ± 0.2	0.8 ± 0.2	2.2	182.0	3.5	−4.4
8	glivec	8.07	198	98	2.9 ± 2.7	117.8 ± 25.3	1.2 ± 0.1	0.0 ± 0.0	1.6	63.1	3	−5.4
9	lidocaine	7.6[59]	2.9[30]	50	375.6 ± 91.3	nd	1.5 ± 0.1	nd	66.7	nd	1.5	−4.5
10	progesterone	-	157	40[b]	5.0 ± 0.7	12.4 ± 1.9	1.7 ± 0.2	1.2 ± 0.2	47.4	117.9	1.5	−5.1
11	promazine	9.42[60]	4.8	42[31]	78.7 ± 22.0	131.5 ± 11.0	3.7 ± 0.6	0.0 ± 0.0	62.9	105.0	2	−3.5
12	(R/S)-verapamil	8.92[61]	166.0[15]	90	0.5 ± 0.1	37.3 ± 15.3	1.6 ± 0.1	1.1 ± 0.1	0.4	34.8	5	−3.9
13	reserpine	6.6[62]	2030	99	0.3 ± 0.1	10.7 ± 1.5	1.3 ± 0.1	0.6 ± 0.2	0.6	24.9	8	−2.3
14	trifluoperazine	8.09[63]	342	57.4[31]	3.6 ± 0.0	21.8 ± 3.2	1.6 ± 0.1	0.0 ± 0.0	57.4	349.0	2.5	−2.9
15	triflupromazine	9.1[64]	91.1	50[31]	2.0 ± 0.5	31.1 ± 1.6	1.7 ± 0.1	0.0 ± 0.0	17.0	266.3	2.5	−4.1

[a] The air−water partition coefficient, K_{aw}, and the cross-sectional area, A_D, were obtained by means of surface activity measurements. The concentration of half-maximum activation (inhibition), K_1 (K_2), and of maximum (minimum) transporter activity, V_1 (V_2), were measured in living NIH-MDR-G185 cells with a Cytosensor. The mole fraction of drugs in the membrane at half-maximum Pgp activation (inhibition), $X_{b(1)}$ ($X_{b(2)}$), was calculated according to eq 20 using the lipid−water partition coefficients, K_{lw} (Figure 4A), calculated by means of eq 12 assuming a membrane packing density of $\pi_M = 30$ mN/m and a surface potential of the cytosolic leaflet of $\psi = -30$ mV. The number of H-bond acceptors and the free energy of binding per H-bond, $\Delta G°_{Hi}$, was determined as described in Discussion. [b] The cross-sectional area of progesterone was estimated in analogy to the cross-sectional area of cholesterol. The error in the surface activity measurements is generally not larger than ±5%. However, for compounds with low amphiphilicity (e.g. daunorubicin, progesterone) the air−water partition coefficient as well as the cross-sectional area of the molecule can be affected by the association state of the molecule in solution which depends on the stock solution concentration and data variation can therefore be larger. Data presented in Table 1 correspond to average values of 1−4 data sets made with cells of different passages (cell passage number > 4), where one data set consists of 2−3 measurements made with cells of the same passage number as shown in Figure 3.

(pH 7.4 and 37 °C). The free energy of substrate binding from water to the transporter, $\Delta G°_{tw(1)}$, and the free energy of partitioning into the lipid membrane, $\Delta G°_{lw}$, are defined as

$$\Delta G°_{tw(1)} \cong -RT \ln(C_w K_{tw(1)}) \cong -RT \ln(C_w(1/K_1)) = RT \ln(C_w K_1) \quad (7)$$

and

$$\Delta G°_{lw} = -RT \ln(C_w K_{lw}) \quad (8)$$

respectively, where C_w corresponds to the molar concentration of water. Analogous equations can be formulated for the binding constant and the free energy of binding to the second binding region,

$$1/K_2 \cong K_{tw(2)} \cong K_{tl(2)} K_{lw} \quad (9)$$

and

$$\Delta G°_{tw(2)} \cong \Delta G°_{tl(2)} + \Delta G°_{lw} \quad (10)$$

where K_2 is the dissociation constant, $K_{tw(2)}$ and $K_{tl(2)}$ are the binding constant from water and from the lipid membrane to the inhibitory binding region of Pgp, respectively, and $\Delta G°_{tw(2)}$ and $\Delta G°_{tl(2)}$ are the corresponding free energies.

RESULTS

Drug-Induced Pgp Activation Measured in MDR1-Transfected and Wild-Type Cells. MDR1-transfected (NIH-MDR-G185) and wild type (NIH3T3) mouse embryo fibroblasts were exposed to 15 chemically diverse drugs (cf. Table 1), and the extracellular acidification rate, ECAR, was measured by means of the Cytosensor. Figure 1 shows a comparison of the raw data (A and B, where A is an enlargement of B)

and the rate data (C) obtained upon exposure of NIH-MDR-G185 and wild-type cells to chlorpromazine (3.4 µM). During each 120 s pump cycle, buffer was superfused for 100 s, then the pumps were switched off for the remaining 20 s, and the pH change was measured during 13 s within this time. When the pumps were on, the acidic metabolites excreted by the cells were washed away by the flow of medium, and the pH at the cell surface therefore remained constant and was identical to the pH of the flow medium. During pump-off periods (20 s) acidic products accumulated in the sensor chambers, causing a decrease of the pH. The ECAR was determined during 13 s of the pump-off period as the slope of a linear least-squares fit to voltage versus time data ($-\mu$V/s) (rate data), where -1 µV/s corresponds to an acidification rate of 1 mpH unit/min at pH 7.4 (Figure 1A). During the first four pump cycles cells were exposed to the flow medium without chlorpromazine and the basal ECAR was measured as seen in Figure 1B and 1C. Next NIH-MDR-G185 and NIH3T3 cells were exposed to a chlorpromazine-containing (3.4 µM) medium for a 40 s pulse and the ECAR was measured. Perfusion with chlorpromazine solution was continued for another 100 s and the ECAR was measured again. The hatched region in Figures 1B and 1C indicates the drug-stimulation period of 180 s comprising two measuring points. In the following, the second measuring point (filled symbol) was used for data evaluation for all compounds except cyclosporin A which was stimulated for a longer period of time (11 min). Drug stimulation for longer periods of time generally did not change the ECAR indicating that steady state conditions were reached.

After stimulation with drug-containing medium the cells were again perfused with flow medium and the ECAR measurements were continued every two minutes until basal
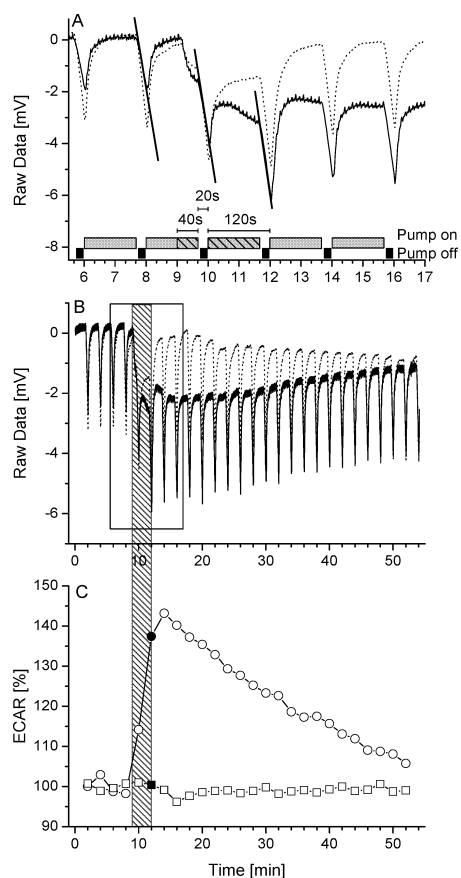
FIGURE 1: (A−C) ECAR measured by means of a Cytosensor microphysiometer. *MDR1*-transfected (NIH-MDR-G185) (solid lines in Figures 1A and B, circles in Figure 1C) and wild-type cells (NIH3T3) (dotted lines in Figures 1A and B, squares in Figure 1C) were exposed to 3.4 μM chlorpromazine. (A) Raw data show changes of the voltage (mV) with time, that are proportional to pH changes (-1 μV/s $= 0.001$ pH unit/min at pH 7.4). When the pumps are on (gray boxes), the pH in the measuring chamber corresponds to the pH of flow medium. When the pumps are off (black boxes), the pH drops due to an accumulation of acidic metabolites in the extracellular environment. Gray hatched boxes indicate the stimulation period of cells with chlorpromazine and comprise two measurements, where the second measurement (180 s) indicated by a filled symbol (C) is used for data evaluation. (B) Same data as in part A shown on a longer time scale. (C) Rate data show the acidification rate ($-\mu$V/s) in time, determined by a least-squares fit to the slope from the raw data when pumps are off. Values are normalized to the basal ECAR defined as 100%.

rates were reached again. The acidification rate was normalized to the basal acidification rate (average of the first four pump cycles before drug addition) which was defined as 100%. It has to be noted that the basal ECAR is the sum of the Pgp basal activity and other metabolic processes. The cellular response is given as the percentage of the basal activity (Figure 1C). As seen in Figures 1B and 1C addition of chlorpromazine to the flow medium leads to an ECAR increase in NIH-MDR-G185 cells, but not in wild-type cells.
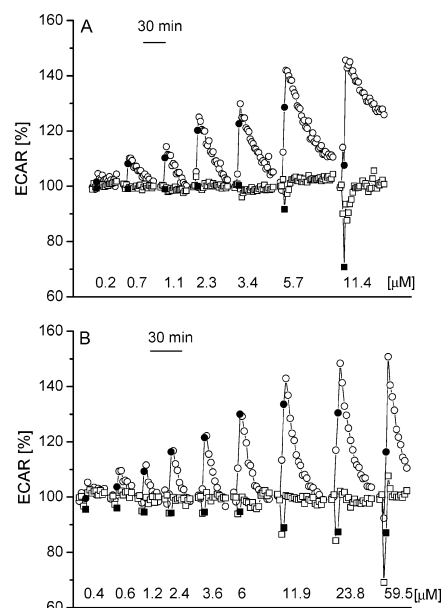

FIGURE 2: (A, B) Time-dependent ECAR of NIH-MDR-G185 (circles) and NIH3T3 (squares) cells in response to increasing concentrations of chlorpromazine (A) and dibucaine (B). The cells were stimulated with drugs for 180 s. Each segment is normalized to a basal acidification rate (the average of the two data points of the ECAR before drug addition defined as 100%). The second stimulation point obtained during the drug-stimulation period is indicated by a filled symbol and is used for data evaluation. The subsequent open circles correspond to measurements performed in the presence of drug-free medium. Measurements were continued until the ECAR returned to basal values. At low drug concentrations, where only the activating binding region of Pgp is occupied, the second stimulation point (filled symbol) corresponds to the ECAR maximum. At high drug concentrations the ECAR at the second stimulation point (180 s) is lower than the ECAR at the subsequent (third) stimulation point. This is due to the fact that reperfusion of the cells with drug-free medium lowers the membrane concentration of drugs which leads to the release of the substrate molecule at the inhibitory binding region of Pgp.

Figure 2 displays the ECAR changes relative to the basal acidification rates of NIH-MDR-G185 (circles) and NIH3T3 cells (squares) upon stimulation with either chlorpromazine (A) or dibucaine (B) at different concentrations as a function of time. The second measuring point at the end of the drug-stimulation period (at 180 s) is again indicated by a filled symbol (Figures 1C, 2A, and 2B).

The response of wild type cells (Figures 2A and 2B) was negligibly small for all drugs at low concentrations ($C < 10$ μM). Some drugs induced a fast transient decrease of the ECAR (to maximally $\sim$70%) at high concentrations as seen in Figures 2A and 2B. The largest transient effects were observed for chlorpromazine and dibucaine, which are given as examples in Figures 2A and 2B. Due to the protection of the cells by Pgp this effect was small in NIH-MDR-G185 cells. At high concentrations, $C > 10$ μM, the cytotoxic daunorubicin induced metabolic changes in wild-type cells which were similar to those in *MDR1*-transfected cells.

Analysis of Pgp Activation. Plotting the ECARs of NIH-MDR-G185 cells at the end of the drug-stimulation period
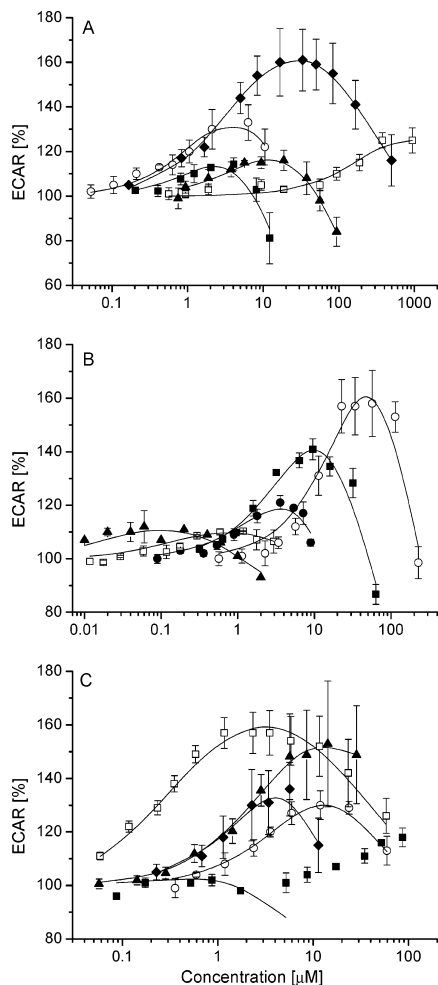
FIGURE 3: (A−C) Pgp activation profiles obtained by ECAR measurements in NIH-MDR-G185 cells stimulated by *cis*-flupentixol (■), diltiazem (◆), glivec (▲), lidocaine (□), triflupromazine (○) (A), amitriptyline (■), cyclosporin A (▲), promazine (○), reserpine (□), and trifluoperazine (●) (B), chlorpromazine (◆), daunorubicin (■) (data in the low concentration range $C < 5\ \mu M$ are fitted to eq 2, metabolic changes due to effects other than Pgp activation are observed at $C > 10\ \mu M$), dibucaine (○), progesterone (▲), and verapamil (□) (C). The solid lines are fits to eq 2 assuming activation with one and inhibition with two drug molecules bound to Pgp. Symbols represent average value of $n = 2−3$ measurements with cells of the same cell passage.

at 180 s (indicated by solid symbols in Figures 1C, 2A, and 2B) as a function of the logarithm of concentration yields activation profiles as displayed in Figure 3. The Pgp activation profiles of all drugs show a characteristic bell-shaped dependence on the logarithm of concentration, in agreement with previous investigations in other cell lines (*14*, *17*), as well as in reconstituted proteoliposomes (*33*). The solid lines are fits to the modified Michaelis−Menten equation (eq 2) assuming Pgp activation upon binding of a first drug molecule at low, and inhibition upon binding of a

second drug molecule at high, concentration. The error bars in Figures 3A−C correspond to the average of two to three measurements made with cells of the same passage (one data set). For compounds which are especially prone to aggregation, such as phenothiazines (e.g. chlorpromazine (*31*)) and progesterone, the quality of data decreases with increasing concentration as reflected in an increase in error bars. Data were evaluated using an automated fit program to eq 2 (described elsewhere, Äänismaa and Seelig, in preparation) yielding the concentration of half-maximum activation, K_1, and inhibition, K_2, as well as the maximum, V_1, and minimum rate, V_2, of Pgp activity. Data obtained with NIH-MDR-G185 are summarized in Table 1 and correspond to average values of one to four data sets made with cells of different passages. For the present study the cell passage number was $n > 4$ (*18*).

Binding to the Inhibitory Region of Pgp Is Reversible. A closer inspection of Figures 2A and 2B is now possible. It reveals that the data point at the end of the drug-stimulation period (at 180 s) is identical with the ECAR maximum at low drug concentrations. At higher drug concentrations the ECAR maximum is observed at the subsequent measuring point. At this point the cells have been reperfused with drug-free medium for 100 s (plus 20 s measuring stop) and the concentration of the drug in the membrane has therefore decreased below the value at which the inhibitory binding region is occupied. The increase in the ECAR is thus due to the release of the inhibitory substrate molecule from Pgp, which directly prooves the reversibility of the inhibitory binding step in eq 1.

Figure 2A further shows that more than 1 h can be required to reach the basal ECAR after reperfusion with drug-free medium. This implies that the membrane concentration of drugs in *MDR1*-transfected cells decreases only slowly (as discussed in detail elsewhere).

Drug Partitioning into the Lipid Membrane. For the electrically neutral extracellular lipid leaflet the lipid−water partition coefficient, K_{lw}, can be derived from the air−water partition coefficient, K_{aw}, and the cross-sectional area of the drug molecule in its amphiphilic orientation at the air−water interface, A_D ((*30*, *31*), for the present compounds, Li-Blatter and Seelig, in preparation),

$$K_{lw} = K_{aw}\ e^{-\pi_M A_D/kT} \tag{11}$$

where $\pi_M A_D$ is the energy required to create a cavity with a cross-sectional area, A_D, in a membrane exhibiting the lateral packing density, π_M, and kT is the thermal energy per molecule (*35*). The air−water partition coefficient, K_{aw}, was determined at pH 7.4. The cross-sectional area, A_D, was measured at pH 8.0 to minimize charge repulsion effects (*30*, *31*). The lateral packing density, π_M, of mouse embryo fibroblasts was determined as $\pi_M \approx 30$ mN/m (cf. next paragraph).

After insertion into the outer, electrically neutral membrane leaflet, the neutral fraction of drugs rapidly crosses the hydrophobic core region and accumulates in the inner, cytosolic membrane leaflet. The polar groups of the drug then reside in the headgroup region of the lipids, and the hydrophobic groups remain in the hydrophobic core. The cytosolic lipid leaflet contains ∼25% negatively charged lipids and thus exhibits a negative surface potential, ψ. Since

Gatlik-Landwojtowicz et al.

it is generally assumed that Pgp binds its substrates when they are inserted in the cytosolic membrane leaflet (although other binding locations have been proposed (*36*)), we calculated the appropriate cytosolic lipid−water partition coefficient by taking into account the charge, z, of the drug and the surface potential, ψ, of the cytosolic membrane leaflet,

$$K_{\text{lw}} = K_{\text{aw}}\, e^{-\pi_M A_D/kT}\, e^{-\psi Fz/RT} \qquad (12)$$

where RT is the thermal energy per mole, and F the Faraday constant.

The surface potential, ψ, depends not only on the lipid composition of the membrane but also on the cytosolic ion concentration. The cytosolic free magnesium concentration has been estimated to be in the range of $C = (0.5\ \text{to}\ 1)$ mM (*37*), and the concentration of monovalent cations is in the range of $C = (100\ \text{to}\ 150)$ mM. With a binding constant of $K = 10$ M^{-1} and $K = 0.6$ M^{-1} for magnesium and for monovalent cations, respectively (*38*), a surface potential in the range of $\psi \approx (-30\ \text{to}\ -20)$ mV is calculated using the Gouy−Chapman theory (*39*). Binding of cationic drugs also reduces the membrane surface potential. For most drugs it reaches a value of $\psi \approx 0$ mV at the concentration of half-maximum Pgp activation. To illustrate the effect of the surface potential we calculated the lipid water partition coefficients, K_{lw}, for the two extreme values, $\psi = 0$ mV, and $\psi = -30$ mV.[2] As seen in Figure 4A the lipid−water partition coefficients were in the range of $K_{\text{lw}} = (10^2\ \text{to}\ 10^4)$ M^{-1} and $K_{\text{lw}} = (2 \times 10^2\ \text{to}\ 2 \times 10^4)$ M^{-1} for $\psi = 0$ mV, and $\psi = -30$ mV, respectively. The lipid−water partition coefficients, K_{lw}, of the different drugs thus vary by 2 orders of magnitude under both conditions, whereas an increase of the negative surface potential from $\psi = 0$ mV to $\psi = -30$ mV increases the lipid−water partition coefficient only by maximally a factor of about two. If not otherwise stated the following data are calculated with a negative surface potential, $\psi = -30$ mV.

The Lateral Packing Density, π_M, of the Plasma Membrane of NIH-MDR-G185 Cells. The lateral packing density, π_M, of a membrane cannot be measured directly; however, it can be determined in relation to a monolayer or bilayer with a known lateral packing density (*40*). As seen from eq 11 the lipid−water partition coefficient, K_{lw}, decreases exponentially with increasing lateral packing density, π_M, of the membrane (*35, 41*). If the lipid−water partition coefficients, $K_{\text{lw(A)}}$ and $K_{\text{lw(B)}}$, and the surface potential difference, $\psi_B - \psi_A$, of two membranes, A and B, are known, the packing density difference between the two membranes, $\pi_{M(B)} - \pi_{M(A)}$, can be determined as

$$(\pi_{M(B)} - \pi_{M(A)}) = \frac{kT}{A_D}\left(\ln\!\left(\frac{K_{\text{lw(A)}}}{K_{\text{lw(B)}}}\right) - \frac{Fz}{RT}(\Psi_B - \Psi_A)\right) \quad (13)$$

In the comparison of cells the surface potential difference can be neglected to a first approximation and the last term in eq 13 thus cancels. With a reference membrane, A, of known packing density, $\pi_{M(A)}$, the packing density of the cell membrane, B, $\pi_{M(B)}$, can then be evaluated.

According to eq 5 the binding constant of the substrate from water to the transporter, $K_{\text{tw(1)}}$ (or $1/K_1$), corresponds to the product of the lipid−water partition coefficient and
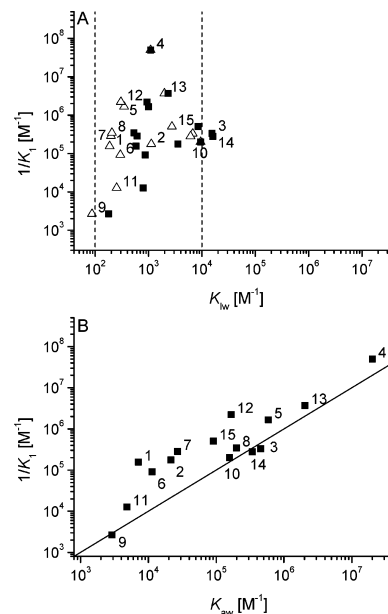

Figure 4: The inverse of the concentration of half-maximum Pgp activation, $(1/K_1)$, obtained by measurements of the ECAR in NIH-MDR-G185 cells, is plotted as a function of the lipid−water partition coefficient, K_{lw} (A), and as a function of the air−water partition coefficient, K_{aw} (B). Open triangles and filled squares in Figure 4A refer to a membrane surface potential, $\psi = 0$ mV and $\psi = -30$ mV, respectively. Surface activity measurements were performed at pH 7.4. (1) amitriptyline, (2) chlorpromazine, (3) *cis*-flupenthixol, (4) cyclosporin A, (5) daunorubicin, (6) dibucaine, (7) diltiazem, (8) glivec, (9) lidocaine, (10) progesterone, (11) promazine, (12) (R/S)-verapamil, (13) reserpine, (14) trifluopera-zine, and (15) triflupromazine. The straight line in Figure 4B exhibits a slope $m = 1$.

the binding constant of the substrate from the lipid membrane to the transporter, where $K_{\text{tl(1)}}$ is likely to be packing density independent (cf. Discussion). The binding constant of the substrate from water to the transporter, $K_{\text{tw(1)}}$, thus shows the same exponential dependence on the membrane packing density, π_M, as the lipid−water partition coefficient, K_{lw}. Therefore, the packing density difference, $\pi_{M(B)} - \pi_{M(A)}$, between two different cell membranes, A and B, can be evaluated by measuring the concentrations of half-maximum activation, $K_{1(A)}$ and $K_{1(B)}$, of Pgp embedded in two different membranes,

$$(\pi_{M(B)} - \pi_{M(A)}) = \frac{kT}{A_D}\left(\ln\!\left(\frac{K_{1(B)}}{K_{1(A)}}\right) - \frac{Fz}{RT}(\Psi_B - \Psi_A)\right) \quad (14)$$

where the surface potential difference can again be neglected

Table 2: The Lateral Membrane Packing Density, π_M, of Different Pgp Containing Membranes Estimated by Comparing Concentrations of Half-Maximum Pgp Activation K_1 (or K_m) by Verapamil[a]

membrane	rate equation	K_1 (or K_m) [μM]	Mg^{2+} [mM]	ATP [mM]	π_M [mN/m]	ψ [mV]	K_{lw} [M^{-1}]	$X_{b(1)}$ [mmol/mol]
lipid (DMPC)[13]	Michaelis−Menten equation	0.63[b]			30[42]	0	336	0.21
NIH-MDR-G185 cells	eq 2	0.5	cellular	cellular	30.5	−20	514	0.26
LLC-MDR1 cells[17]	eq 2	0.89[c]	cellular	cellular	33	−20	307	0.27
CR1R12 cells[14]	eq 2	2.5	2.5	3	35.5	−20	101	0.25
lipid mixture with E. coli lipids[d][43]	Michaelis−Menten equation	4.7	5	5−7.5	42	−20	51.3	0.24
lipid mixture with E. coli lipids[d][33,45]	eq 4	30	15	10	48	−5	8.3	0.25
		62.2	15	10	51	−5	4.4	0.27

[a] The K_1 (or K_m) values were taken from literature, and the corresponding experimental conditions (magnesium ion and ATP concentration, respectively, pH, and temperature) are given. The membrane packing density, π_M, was calculated according to eq 14 using the surface potential, ψ, estimated taking into account 25% negatively charged lipids and the free ion concentration in the different assays. The lipid−water partition coefficient, K_{lw}, was determined according to eq 12 using the relevant surface potential and lateral packing density. The mole fraction of drugs in the membrane at half-maximum Pgp activation, $X_{b(1)}$, was calculated according to eq 20. All measurements discussed were performed at T = 37 °C and pH 7.4 except those of ref. (13) (T > 30 °C), ref. (14) (pH 7.0) and ref. (43) (pH 6.8). K_1 values measured at lower pH were divided by a factor of 2 to correct for pH (cf. ref (45), and Äänismaa and Seelig, in preparation) and the Michaelis−Menten constant, K_m, in ref. (43) was doubled to adjust to a K_1 value. [b] Dissociation constant determined by fluorescence quenching. The corresponding concentration of half-maximum activation (13) obtained by means of an ATPase assay is slightly higher. [c] Corrected for adsorption to the Cytosensor tubes. [d] Lipid mixture (E. coli bulk phospholipids, phosphatidylcholine, phosphatidylserine, cholesterol) (60:17.5:10:12.5 w/w).

in most cases (cf. Table 2). To estimate the lateral packing density of the plasma membrane of different *MDR1*-transfected cell lines we used as reference membrane a DMPC bilayer for which the lateral packing density has been determined previously as $\pi_M = (30 \pm 1)$ mN/m (42). DMPC bilayers have been used to reconstitute Pgp and to measure the concentration of half-maximum Pgp activation, K_1, by verapamil (13). With the two reference values for DMPC bilayers (π_M and K_1 for verapamil) the lateral packing density of the plasma membranes of NIH-MDR-G185 cells was estimated as $\pi_M = 30.5 \pm 1$ mN/m. For comparison we estimated the packing density of two other cell membranes (LLC-MDR1 (17) and CR1R12 cells (14)) and of mixed lipid bilayers (~60% *Escherichia coli* lipids, ~17.5% egg phosphatidylcholine, 10% bovine brain phosphatidylserine and ~12.5% cholesterol) (34, 43) used for Pgp reconstitution (cf. Table 2). The membrane packing densities, π_M, estimated for the different membranes are summarized in Table 2. The type of assays, the kinetic models (rate equations), and the experimental conditions (e.g. pH, magnesium and ATP concentrations) differ in the different investigations.

The lateral packing densities of the mammalian plasma membranes investigated were found to be in the range of $\pi_M \cong (30$ to $35)$ mN/m, which is in good agreement with previous investigations (40). The lowest packing density was found for mouse embryo fibroblasts (NIH-MDR-G185), which is consistent with the low cholesterol content generally found in embryonic cell membranes (44), and the highest packing density was observed in *Ehrlich* ascites tumor cells, CR1R12. The packing density of lipid membranes containing a high percentage of *E. coli* lipids (33, 43, 45) was determined as $\pi_M = 46.5 \pm 4.5$ mN/m, which is distinctly higher than that of the mammalian plasma membranes. The high packing density is mainly due to the high percentage of phosphatidylethanolamines in *E. coli* lipids. Phosphatidylethanolamines exhibit smaller cross-sectional areas and therefore higher packing densities than the corresponding phosphatidylcholines (46). The high packing density of *E. coli* lipids is also reflected in their high phase transition temperature (47, 48).

Correlation between the Concentration of Half-Maximum Pgp Activation and the Lipid−Water Partition Coefficient. Figure 4A shows the inverse of the concentration of half-maximum Pgp activation, $1/K_1$ (log scale), versus the lipid−water partition coefficient, K_{lw} (log scale). No linear correlation is observed. Since $\log(1/K_1)$ is proportional to the free energy of binding from water to the activating binding region of Pgp, $\Delta G°_{tw(1)}$, and $\log K_{lw}$ is proportional to the free energy of drug partitioning from water to the membrane, $\Delta G°_{lw}$, it can be concluded that no correlation exists between the drug affinity from water to the transporter and the drug affinity to the lipid membrane for the present set of structurally diverse drugs. The same conclusion was drawn previously from octanol−water partition coefficients (14).

Correlation between the Concentration of Half-Maximum Pgp Activation and the Air−Water Partition Coefficient. If the $\log(1/K_1)$ (proportional to $\Delta G°_{tw(1)}$) is plotted versus the logarithm of the air−water partition coefficient, $\log K_{aw}$ (proportional to $\Delta G°_{aw}$) an approximately linear correlation is obtained as shown in Figure 4B. The air−water partition coefficients, K_{aw}, cover a broad range from $K_{aw} \sim 10^3$ M^{-1} (very hydrophilic compounds) to $K_{aw} \sim 10^7$ M^{-1} (very hydrophobic compounds). The straight line in Figure 4 corresponds to the product of the air−water partition coefficient and the concentration of half-maximum Pgp activation,

$$K_{aw}K_1 = 1 \tag{15}$$

The free energy of moving the drug from water to air, $\Delta G°_{aw} = -RT \ln(C_w K_{aw})$, is thus approximately identical to the free energy of substrate binding from water to the transporter, $\Delta G°_{tw}$,

$$\Delta G°_{aw} \approx \Delta G°_{tw} \tag{16}$$

Rewriting eq 11 in a logarithmic form and combining it with eq 8 yields

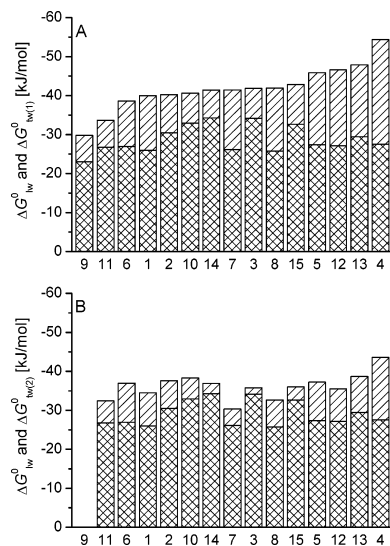$$\Delta G°_{aw} = \Delta G°_{lw} - \pi_M N_A A_D \tag{17}$$

FIGURE 5: (A) The free energy of drug binding from water to the activating binding region of Pgp, $\Delta G^{\circ}_{\text{tw}(1)}$ (hatched and crosshatched bars), in comparison to the free energy of drug partitioning from water to the lipid membrane, $\Delta G^{\circ}_{\text{lw}}$ (crossed-hatched bars). The difference between $\Delta G^{\circ}_{\text{tw}(1)}$ and $\Delta G^{\circ}_{\text{lw}}$ represents the free energy of drug binding from lipid membrane to the transporter, $\Delta G^{\circ}_{\text{tl}(1)}$ (hatched bar). (B) Analogous data for the inhibitory binding region of Pgp. Numbers correspond to those in Figure 4A. Lidocaine (9) is not included in Figure 5B since K_2 could not be precisely determined due to the high concentrations required (see Figure 3A).

where N_A is the Avogadro number. Equation 17 shows that the free energy of partitioning into the lipid−water interface, $\Delta G^{\circ}_{\text{lw}}$, corresponds to the free energy of partitioning into the air−water interface, $\Delta G^{\circ}_{\text{aw}}$, plus the additional work to penetrate into the lipid bilayers. Combining eqs 16 and 17 leads to the following approximation:

$$\Delta G^{\circ}_{\text{tw}} \approx \Delta G^{\circ}_{\text{aw}} = \Delta G^{\circ}_{\text{lw}} - \pi_M N_A A_D \qquad (18)$$

or

$$\Delta G^{\circ}_{\text{tl}(1)} \approx -\pi_M N_A A_D \qquad (19)$$

Equation 19 suggests that the free energy of binding to the transporter within the lipid membrane, $\Delta G^{\circ}_{\text{tl}(1)}$, is proportional to the cross-sectional area of the molecule, A_D, as will be further discussed below (Figure 6A).

DISCUSSION

The thermodynamic and kinetic methods applied here were able to reveal the free energy of binding from water to the activating (inhibitory) binding region of Pgp in its native lipid membrane, $\Delta G^{\circ}_{\text{tw}(1)}$ ($\Delta G^{\circ}_{\text{tw}(2)}$), and the corresponding free energy of partitioning into the lipid membrane, $\Delta G^{\circ}_{\text{lw}(1)}$, for 15 structurally diverse substrates. With this knowledge it is possible to determine two parameters which are not directly measurable, i.e., (i) the mole fraction of drugs in the membrane, $X_{\text{b}(1)}$ ($X_{\text{b}(2)}$), at half-maximum Pgp activation (inhibition) and (ii) the free energy of binding of the substrate from the lipid membrane to the activating, $\Delta G^{\circ}_{\text{tl}(1)}$ (inhibitory, $\Delta G^{\circ}_{\text{tl}(2)}$) binding region of Pgp. The latter reflects the direct

FIGURE 6: (A) The free energy of drug binding from the lipid membrane to the activating binding region of the transporter, $\Delta G^{\circ}_{\text{tl}(1)}$, plotted as a function of the cross-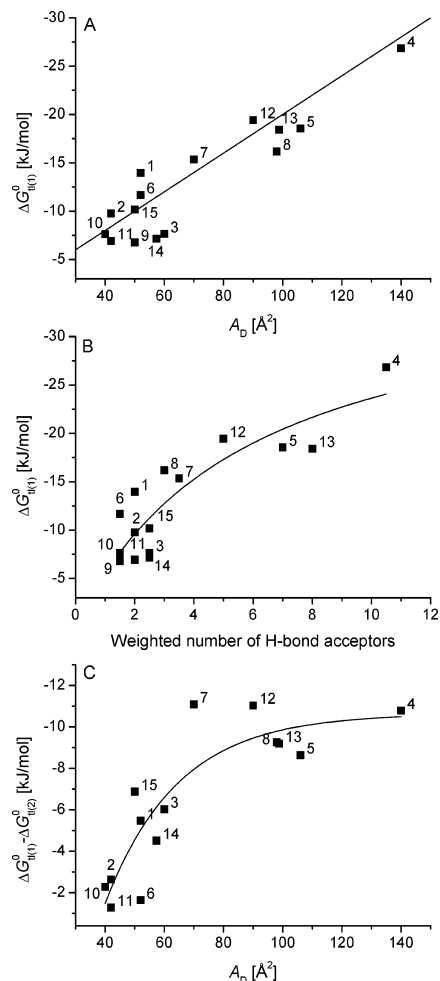sectional area, A_D, of the drug. A straight line corresponds to the diagonal. B: The free energy of drug binding from the lipid membrane to the activating binding region of the transporter, $\Delta G^{\circ}_{\text{tl}(1)}$, as a function of the weighted number of hydrogen bond acceptors in patterns determined according to refs *10* and *23*. Data were fitted to a hyperbolic saturation isotherm. (C) The difference in the free energy of binding from water to the activating and inhibitory binding region of Pgp, $\Delta G^{\circ}_{\text{tl}(1)} - \Delta G^{\circ}_{\text{tl}(2)}$, plotted as a function of the cross-sectional area, A_D, of the drug. Data were fitted to an exponential curve. Numbers correspond to those in Figure 4. Values of $\Delta G^{\circ}_{\text{tl}(1)}$ ($\Delta G^{\circ}_{\text{tl}(2)}$) were obtained by means of ECAR measurements. Lidocaine (9) is not included in Figure 6C since K_2 could not be precisely determined due to the high concentrations required (see Figure 3A).

interplay between the drug and the transporter and provides the basis for a discussion of the nature of the interactions between Pgp and its substrates.

The Membrane Concentration of Drugs That Elicits Half-Maximum Pgp Activation. Biological membranes of different origin differ in their lipid composition and as a consequence in their lateral membrane packing density, π_M. As seen in

Table 2 the packing density of mammalian plasma membranes were found to be in the range of $\pi_M \cong$ (30 to 35) mN/m, whereas the packing density of membranes with a high percentage of *E. coli* lipids was distinctly higher, $\pi_M = 46.5 \pm 4.5$ mN/m. The membrane packing density, π_M, determines the lipid−water partition coefficient, K_{lw}, as well as the concentration of half-maximum Pgp activation, K_1, whereby the former decreases (cf. eq 11) and the latter increases (cf. eq 5 and Table 2) with increasing membrane packing density, π_M. The mole fraction of drugs in the membrane, $X_{b(1)}$, that elicits half-maximum Pgp activation is the product of the concentration of half-maximum activation, K_1, and the lipid−water partition coefficient, K_{lw} (*11*),

$$X_{b(1)} = K_1 K_{lw} \tag{20}$$

and is thus *independent* of the membrane packing density, π_M, as illustrated in Table 2 (last column). The mole fraction of the different drugs in the membrane was estimated to be in the range of $X_{b(1)} =$ (0.02 to 67) mmol/mol lipid (cf. Table 1). If we assume that 1 mol of lipid corresponds approximately to 1 L of lipid, the membrane concentration corresponds to about $C_{b(1)} =$ (0.02 to 67) mmol/L lipid.

The high drug concentration in the membrane at half-maximum Pgp activation suggests relatively weak substrate−Pgp interactions. Similarly weak interactions have also been observed for transporters that bind their substrates in the aqueous phase at one side of the membrane and transport them to the aqueous phase at the other side of the membrane, such as the fucose transporter which exhibits a dissociation constant in the mM concentration range (*12*).

The membrane concentration for half-maximum inhibition ($X_{b(2)} = K_2 K_{lw}$) is even higher than that for half-maximum activation, $X_{b(1)}$. For small molecules (e.g. promazine) the mole fraction ratio is small ($X_{b(2)}/X_{b(1)} \approx 2$), and for large molecules (e.g. diltiazem, verapamil, cyclosporin A) the mole fraction ratio is large ($X_{b(2)}/X_{b(1)} \approx 80$), indicating that the accommodation of a second large molecule is more difficult.

The Free Energy of Drug-Binding from the Lipid Membrane to the Activating Binding Region of Pgp, $\Delta G°_{tl(1)}$. The free energy of drug binding from water to activating binding region of Pgp, $\Delta G°_{tw(1)}$, can be expressed as the sum of the free energy of drug partitioning into the lipid membrane, $\Delta G°_{lw}$, and the free energy of drug binding from the lipid phase to the activating binding region of Pgp, $\Delta G°_{tl(1)}$ (cf. eq 6). Figure 5A displays a comparison of $\Delta G°_{tw(1)} = (-30$ to $-54)$ kJ/mol (hatched plus crosshatched), the free energy of drug binding from water to the transporter, with $\Delta G°_{lw} = (-23$ to $-34)$ kJ/mol (crosshatched), the free energy of drug partitioning into the lipid membrane, and $\Delta G°_{tl(1)} = (-7$ to $-27)$ kJ/mol (hatched), the free energy of drug binding from the lipid membrane to the transporter determined for NIH-MDR-G185 cells. For the 15 drugs investigated, $\Delta G°_{lw}$, the free energy of drug partitioning into the lipid membrane, is generally somewhat larger than $\Delta G°_{tl(1)}$, the free energy of drug binding to the activating binding region of the transporter in the lipid phase. However, the variation in $\Delta G°_{tl(1)}$ is more pronounced (∼factor of 4.0) than the variation in $\Delta G°_{lw}$ (∼factor of 1.5).

Figure 5B displays the free energy of drug binding from water, $\Delta G°_{tw(2)} = (-23$ to $-44)$ kJ/mol (hatched plus crosshatched), and from the lipid membrane, $\Delta G°_{tl(2)} = (-1.6$ to $-16)$ kJ/mol (hatched), to the inhibitory binding region of Pgp. The values of $\Delta G°_{lw}$ (crosshatched) are identical to those in Figures 5A and 5B. The free energy of drug binding from water, $\Delta G°_{tw(2)}$, and from the lipid membrane, $\Delta G°_{tl(2)}$, to the inhibitory region of Pgp are thus less negative than the free energies of drug binding to the activating region of Pgp, $\Delta G°_{tw(1)}$ and $\Delta G°_{tl(1)}$.

Kinetic Models and Their Influence on the Estimated Free Energy of Binding to the Transporter. The kinetic data shown in Table 1 were evaluated using the rate eq 2 proposed by Litman et al. (*14*). It is based on the concept of uncompetitive inhibition (or substrate inhibition) which was extended to allow for basal activation in the absence of a substrate and for breakdown of the complex $T(ATP)S_tS_t$ (eq 1). For comparison we fitted our data to a simpler version of uncompetitive inhibition, assuming that the complex $T(ATP)$-S_tS_t (eq 1) is catalytically inactive ($V_2 = 0$) (rate eq 3). While the concentrations of half-maximum activation, K_1, obtained with the two models were similar, the concentrations of half-maximum inhibition, K_2, calculated with the latter model were generally higher. As a consequence the corresponding free energies of binding to the inhibitory binding region of Pgp, $\Delta G°_{tl(2)}$, were less negative (by maximally 15%). The model proposed by Al-Shawi et al. (*33, 34*) also considers basal activation of Pgp in the absence of drugs, drug activation, and drug inhibition, however, it is based on the concept of noncompetitive inhibition (rate eq 4). Rate eq 4 differs from rate eq 3 only by an additional term, $K_1 C_{sw}$, in the denominator which is small in comparison to the other terms. The free energies of binding, $\Delta G°_{tl(2)}$, obtained with the model of Al-Shawi et al. (*33, 34*) were therefore similar to those obtained with rate eq 3. The fits to all three models were of comparable quality.

Concentrations of half-maximum activation evaluated by means of a simple Michaelis−Menten equation, K_m (*43*), are generally smaller compared to those obtained with eqs 2−4 (by almost a factor of 2). In terms of free energies of binding, $\Delta G°_{tl(1)}$, the difference is, however, small.

The Nature of Drug−Transporter Interactions. The free energy of drug binding from water to the transporter, $\Delta G°_{tw(1)}$, was shown to be the sum of the free energy of drug partitioning into the lipid membrane, $\Delta G°_{lw}$, and the free energy of drug binding from the lipid phase to the activating binding region of Pgp, $\Delta G°_{tl(1)}$. The interactions which are relevant for binding of a drug from water to the transporter are thus the sum of all the interactions relevant for the two individual binding steps. Drug partitioning into the lipid membrane is dominated by hydrophobic and van der Waals interactions, respectively, with a potential contribution of electrostatic interactions (cf. Figure 4A). The possible nature of the substrate−transporter interactions within the lipid membrane will be discussed in the following. We have shown that the free energy of substrate binding to the transporter within the lipid membrane, $\Delta G°_{tl(1)}$, correlates with the cross-sectional area of the drug, A_D (cf. eq 19 and Figure 6A). However, substrate−transporter interactions are most likely not determined by the size of the substrate as such, but rather by a concomitant increase in residues which can undergo specific interactions with the amino acids in the *transmembrane* sequences of Pgp. Interactions which could play a role are electrostatic (ion−ion or dipole−dipole), hydrogen bonding (weak dipole−dipole), cation−π, π−π

stacking, and van der Waals interactions, respectively, listed in the order of decreasing free energy of binding. The X-ray structure of the multidrug transporter AcrB (at the resolution of (3.5 to 3.8) Å), crystallized with four different drugs bound (in the absence of lipids), suggested the presence of all the different interactions mentioned above (*49*). It has, however, to be considered that the energetic contributions of the diverse interactions differ. Moreover, it has to be considered that not all compounds which bind to Pgp are charged, or carry π-electron systems, but that all of them seem to carry at least one hydrogen bond acceptor pattern (i.e. two hydrogen bond acceptor groups in a distance of 2.5 Å or 4.6 Å) (*23*). Since the free energy contribution of hydrogen bond formation in a hydrophobic environment can be substantial (for review see ref *50*), hydrogen bonding is likely to contribute significantly to the energetics of drug transporter interactions. Hydrogen bond acceptor patterns were therefore suggested to serve as binding modules interacting with the hydrogen bond donor-rich transmembrane domains of Pgp. As a consequence the total free energy of binding of a drug from the lipid membrane to the transporter, $\Delta G^{\circ}_{\text{tl}(1)}$, can be assumed to be the sum of the free energies, $\Delta G^{\circ}_{\text{H}i}$, of the individual hydrogen bonds formed (*11, 22–24*),

$$\Delta G^{\circ}_{\text{tl}(1)} \approx \sum_{i=1}^{n} \Delta G^{\circ}_{\text{H}i} = \sum_{i=1}^{n} \Delta H^{\circ}_{\text{H}i} - T\Delta S^{\circ} \qquad (21)$$

where $\Delta H^{\circ}_{\text{H}i}$ is the enthalpy change for hydrogen bond formation and $T\Delta S^{\circ}$ the product of the entropy change upon drug binding and the absolute temperature.

To test whether the assumption made in eq 21 is energetically sound we estimated the free energy per potential hydrogen bond formed, $\Delta G^{\circ}_{\text{H}i}$, and compared it with literature values. Figure 6B shows the free energy of substrate binding from the lipid membrane to the transporter, $\Delta G^{\circ}_{\text{tl}(1)}$, as a function of the number of weighted hydrogen bond acceptor groups per drug. Since not all hydrogen bond acceptor groups will form hydrogen bonds with the same free energy, we arbitrarily divided them into three groups containing strong (oxygen atoms), intermediate (nitrogen and sulfur atoms as well as phenyl groups), and weak (fluorine atoms) hydrogen bond acceptors, weighted as 1, 0.5, and 0.25, respectively. The average free energy per hydrogen bond, $\Delta G^{\circ}_{\text{H}i}$, was then estimated by dividing the total free energy of binding, $\Delta G^{\circ}_{\text{tl}(1)}$, by the weighted number of hydrogen bond acceptor groups per drug. The most negative free energy of binding per hydrogen bond, $\Delta G^{\circ}_{\text{H}i} = -7.8$ kJ/mol, was observed for dibucaine (see Table 1), which exhibits one hydrogen bond acceptor pattern only (corresponding to two hydrogen bonds). For compounds with more than one hydrogen bond acceptor pattern the apparent free energy per hydrogen bond, $\Delta G^{\circ}_{\text{H}i}$, was less negative. For compounds with more than four hydrogen bond acceptor pattern the apparent free energy per hydrogen bond, $\Delta G^{\circ}_{\text{H}i}$, reached a limiting value ($\Delta G^{\circ}_{\text{H}i} \sim -2.5$ kJ/mol). The decrease in $\Delta G^{\circ}_{\text{H}i}$ with increasing number of hydrogen bond acceptors can be explained by a loss in residual motion after formation of more than one hydrogen bond leading to an entropy decrease (*51*). If appropriate membrane packing densities, π_{M}, are taken into account, comparable values of $\Delta G^{\circ}_{\text{H}i}$ are also obtained from other investigations (e.g. ref *14*). A similar conclusion was drawn previously for undefined

binding modules (*25*). The free energy of the first single hydrogen bond formed is therefore most likely $\Delta G^{\circ}_{\text{H}i} \geq -7.8$ kJ/mol. This value is larger than the free energy estimated for forming an amide hydrogen bond in water ($\Delta G \sim -4$ kJ/mol) and somewhat smaller than the free energy of forming a single hydrogen bond in alkane, determined as $\Delta G \sim -20$ kJ/mol without taking into account entropic effects (*52*). Considering the fact that different types of hydrogen bond acceptors are taken into account, and that possible steric effects are neglected, the resulting free energy value per hydrogen bond seems reasonable and supports the assumption of the modular binding concept proposed previously (eq 21).

The free energy of binding to the inhibitory binding region, $\Delta G^{\circ}_{\text{tl}(2)}$, is on average less negative than that for the activating binding region, $\Delta G^{\circ}_{\text{tl}(1)}$. Nevertheless, it can be assumed that the same type of interactions between drugs and Pgp take place. The less negative free energy of binding, $\Delta G^{\circ}_{\text{tl}(2)}$, is most likely due to conformational changes of the protein upon accommodation of a second molecule which may lead to a decrease in entropy. This is supported by the fact that the difference in free energy, $\Delta G^{\circ}_{\text{tl}(1)} - \Delta G^{\circ}_{\text{tl}(2)}$, increases with increasing the cross-sectional area, A_{D}, of the drug as seen in Figure 6C. This shows again that accommodation of a large molecule at the inhibitory binding region of Pgp is less favorable than accommodation a small molecule.

Conclusions. Binding of a drug from water to the activating binding region of Pgp occurs in two steps, a partitioning step from water to the lipid membrane, characterized by a lipid–water partition coefficient, K_{lw}, and a binding step from the lipid membrane to the transporter, characterized by a binding constant, $K_{\text{tl}(1)}$. The binding constant of a drug from water to the transporter, $K_{\text{tw}(1)}$, can thus be expressed as product of two individual binding constants K_{lw} and $K_{\text{tl}(1)}$, and the free energy of binding, $\Delta G^{\circ}_{\text{tw}(1)}$, as sum of two corresponding free energies, $\Delta G^{\circ}_{\text{lw}}$ and $\Delta G^{\circ}_{\text{tl}(1)}$. The free energies $\Delta G^{\circ}_{\text{tw}(1)}$ and $\Delta G^{\circ}_{\text{lw}}$ can be determined independently, which allows estimation of the free energy of binding from lipid to the transporter, $\Delta G^{\circ}_{\text{tl}(1)}$. For the 15 drugs investigated the free energy of drug partitioning into the lipid membrane, $\Delta G^{\circ}_{\text{lw}}$, was generally somewhat more negative than the free energy of drug binding to the transporter in the lipid phase, $\Delta G^{\circ}_{\text{tl}(1)}$. However, the variation in $\Delta G^{\circ}_{\text{tl}(1)}$ was more pronounced ($\sim$factor of 4.0) than the variation in $\Delta G^{\circ}_{\text{lw}}$ (less than a factor of 1.5). Drug affinity to the transporter in the lipid membrane was shown to increase with the cross-sectional area, A_{D}, of the drug. With increasing size of a drug the possibility for different types of interactions also increases. The present analysis suggests that hydrogen bond formation contributes significantly to the energetics of substrate–Pgp interactions within the lipid membrane. Data can be well explained with a modular binding concept, where the binding module in drugs consists of two hydrogen bond acceptor groups. Binding of a drug to Pgp (e.g. hydrogen bond formation) was assumed to be independent of the membrane packing density, π_{M}, to a first approximation. The mole fraction of drugs, $X_{\text{b}(1)}$, in the membrane at the concentration of half-maximum Pgp activation is thus constant, which implies that higher aqueous drug concentrations are required for membrane penetration and Pgp activation in the case of densely packed membranes (e.g.

P-Glycoprotein−Substrate Interactions

membranes of *E. coli* bacteria) than in the case of more loosely packed membranes (e.g. mouse embryo fibroblasts). Since the lipid membrane acts as a drug scavenger and interacts synergistically with Pgp, cells are well protected from intruding substrates despite the relatively weak Pgp−substrate interactions.

REFERENCES

1. Dey, S., Ramachandra, M., Pastan, I., Gottesman, M. M., and Ambudkar, S. V. (1997) Evidence for two nonidentical drug-interaction sites in the human P-glycoprotein, *Proc. Natl. Acad. Sci. U.S.A. 94*, 10594−10599.

2. Raviv, Y., Pollard, H. B., Bruggemann, E. P., Pastan, I., and Gottesman, M. M. (1990) Photosensitized labeling of a functional multidrug transporter in living drug-resistant tumor cells, *J. Biol. Chem. 265*, 3975−3980.

3. Chen, Y., Pant, A. C., and Simon, S. M. (2001) P-glycoprotein does not reduce substrate concentration from the extracellular leaflet of the plasma membrane in living cells, *Cancer Res. 61*, 7763−7769.

4. Shapiro, A. B., and Ling, V. (1997) Extraction of Hoechst 33342 from the cytoplasmic leaflet of the plasma membrane by P-glycoprotein, *Eur. J. Biochem. 250*, 122−129.

5. Shapiro, A. B., and Ling, V. (1998) Transport of LDS-751 from the cytoplasmic leaflet of the plasma membrane by the rhodamine-123-selective site of P-glycoprotein, *Eur. J. Biochem. 254*, 181−188.

6. Schmid, D., Ecker, G., Kopp, S., Hitzler, M., and Chiba, P. (1999) Structure−activity relationship studies of propafenone analogs based on P-glycoprotein ATPase activity measurements, *Biochem. Pharmacol. 58*, 1447−1456.

7. Lu, P., Liu, R., and Sharom, F. J. (2001) Drug transport by reconstituted P-glycoprotein in proteoliposomes. Effect of substrates and modulators, and dependence on bilayer phase state, *Eur. J. Biochem. 268*, 1687−1697.

8. Litman, T., Druley, T. E., Stein, W. D., and Bates, S. E. (2001) From MDR to MXR: new understanding of multidrug resistance systems, their properties and clinical significance, *Cell. Mol. Life Sci. 58*, 931−959.

9. Higgins, C. F., and Gottesman, M. M. (1992) Is the multidrug transporter a flippase?, *Trends Biochem. Sci. 17*, 18−21.

10. Seelig, A., Landwojtowicz, E., Fischer, H., and Li Blatter, X. (2003) in *Drug BioAvailability/Estimation of Solubility, Permeability and Absorption* (Van de Waterbeemd, H., Lennernäs, H., Artursson, P. Eds.) pp 461−492, Wiley-VCH Verlag GmbH, Weinheim.

11. Seelig, A., and Gatlik-Landwojtowicz, E. (2005) Inhibitors of multidrug efflux transporters: their membrane and protein interactions, *Mini-Rev. Med. Chem. 5*, 135−151.

12. Spooner, P. J., O'Reilly, W. J., Homans, S. W., Rutherford, N. G., Henderson, P. J., and Watts, A. (1998) Weak substrate binding to transport proteins studied by NMR, *Biophys. J. 75*, 2794−2800.

13. Romsicki, Y., and Sharom, F. J. (1999) The membrane lipid environment modulates drug interactions with the P−glycoprotein multidrug transporter, *Biochemistry 38*, 6887−6896.

14. Litman, T., Zeuthen, T., Skovsgaard, T., and Stein, W. D. (1997) Structure−activity relationships of P-glycoprotein interacting drugs: kinetic characterization of their effects on ATPase activity, *Biochim. Biophys. Acta 1361*, 159−168.

15. Seelig, A., and Landwojtowicz, E. (2000) Structure-activity relationship of P-glycoprotein substrates and modifiers, *Eur. J. Pharm. Sci. 12*, 31−40.

16. Garrigos, M., Mir, L. M., and Orlowski, S. (1997) Competitive and non-competitive inhibition of the multidrug-resistance-associated P-glycoprotein ATPase-further experimental evidence for a multisite model, *Eur. J. Biochem. 244*, 664−673.

17. Landwojtowicz, E., Nervi, P., and Seelig, A. (2002) Real-time monitoring of P-glycoprotein activation in living cells, *Biochemistry 41*, 8050−8057.

18. Gatlik-Landwojtowicz, E., Aanismaa, P., and Seelig, A. (2004) The rate of P-glycoprotein activation depends on the metabolic state of the cell, *Biochemistry 43*, 14840−14851.

19. Shapiro, A. B., Fox, K., Lam, P., and Ling, V. (1999) Stimulation of P-glycoprotein-mediated drug transport by prazosin and progesterone. Evidence for a third drug-binding site, *Eur. J. Biochem. 259*, 841−850.

20. Martin, C., Berridge, G., Higgins, C. F., Mistry, P., Charlton, P., and Callaghan, R. (2000) Communication between multiple drug binding sites on P-glycoprotein, *Mol. Pharmacol. 58*, 624−632.

21. Scala, S., Akhmed, N., Rao, U. S., Paull, K., Lan, L. B., Dickstein, B., Lee, J. S., Elgemeie, G. H., Stein, W. D., and Bates, S. E. (1997) P-glycoprotein substrates and antagonists cluster into two distinct groups, *Mol. Pharmacol. 51*, 1024−1033.

22. Seelig, A., Blatter, X. L., and Wohnsland, F. (2000) Substrate recognition by P-glycoprotein and the multidrug resistance-associated protein MRP1: a comparison, *Int. J. Clin. Pharmacol. Ther. 38*, 111−121.

23. Seelig, A. (1998) A general pattern for substrate recognition by P-glycoprotein, *Eur. J. Biochem. 251*, 252−261.

24. Ecker, G., Huber, M., Schmid, D., and Chiba, P. (1999) The importance of a nitrogen atom in modulators of multidrug resistance, *Mol. Pharmacol. 56*, 791−796.

25. Sauna, Z. E., Andrus, M. B., Turner, T. M., and Ambudkar, S. V. (2004) Biochemical basis of polyvalency as a strategy for enhancing the efficacy of P-glycoprotein (ABCB1) modulators: stipiamide homodimers separated with defined-length spacers reverse drug efflux with greater efficacy, *Biochemistry 43*, 2262−2271.

26. Pajeva, I. K., and Wiese, M. (2002) Pharmacophore model of drugs involved in P-glycoprotein multidrug resistance: explanation of structural variety (hypothesis), *J. Med. Chem. 45*, 5671−5686.

27. Stouch, T. R., and Gudmundsson, O. (2002) Progress in understanding the structure−activity relationships of P-glycoprotein, *Adv. Drug Delivery Rev. 54*, 315−328.

28. Cianchetta, G., Singleton, R. W., Zhang, M., Wildgoose, M., Giesing, D., Fravolini, A., Cruciani, G., and Vaz, R. J. (2005) A pharmacophore hypothesis for P-glycoprotein substrate recognition using GRIND-based 3D-QSAR, *J. Med. Chem. 48*, 2927−2935.

29. McConnell, H. M., Owicki, J. C., Parce, J. W., Miller, D. L., Baxter, G. T., Wada, H. G., and Pitchford, S. (1992) The cytosensor microphysiometer: biological applications of silicon technology, *Science 257*, 1906−1912.

30. Fischer, H., Gottschlich, R., and Seelig, A. (1998) Blood-brain barrier permeation: molecular parameters governing passive diffusion, *J. Membr. Biol. 165*, 201−211.

31. Gerebtzoff, G., Li-Blatter, X., Fischer, H., Frentzel, A., and Seelig, A. (2004) Halogenation of drugs enhances membrane binding and permeation, *ChemBioChem 5*, 676−684.

32. Ambudkar, S. V., Cardarelli, C. O., Pashinsky, I., and Stein, W. D. (1997) Relation between the turnover number for vinblastine transport and for vinblastine-stimulated ATP hydrolysis by human P-glycoprotein, *J. Biol. Chem. 272*, 21160−21166.

33. Al-Shawi, M. K., Polar, M. K., Omote, H., and Figler, R. A. (2003) Transition state analysis of the coupling of drug transport to ATP hydrolysis by P-glycoprotein, *J. Biol. Chem. 278*, 52629−52640.

34. Omote, H., Figler, R. A., Polar, M. K., and Al-Shawi, M. K. (2004) Improved energy coupling of human P-glycoprotein by the glycine 185 to valine mutation, *Biochemistry 43*, 3917−3928.

35. Boguslavsky, V., Rebecchi, M., Morris, A. J., Jhon, D. Y., Rhee, S. G., and McLaughlin, S. (1994) Effect of monolayer surface pressure on the activities of phosphoinositide-specific phospholipase C-beta 1, -gamma 1, and -delta 1, *Biochemistry 33*, 3032−3037.

36. Litman, T., Skovsgaard, T., and Stein, W. D. (2003) Pumping of drugs by P-glycoprotein: a two-step process?, *J. Pharmacol. Exp. Ther. 307*, 846−853.

37. Romani, A. M., and Scarpa, A. (2000) Regulation of cellular magnesium, *Front. Biosci. 5*, D720−D734.

38. Ohki, S., and Kurland, R. (1981) Surface potential of phosphatidylserine monolayers. II. Divalent and monovalent ion binding, *Biochim. Biophys. Acta 645*, 170−176.

39. Seelig, J., Nebel, S., Ganz, P., and Bruns, C. (1993) Electrostatic and nonpolar peptide-membrane interactions. Lipid binding and functional properties of somatostatin analogues of charge $z = +1$ to $z = +3$, *Biochemistry 32*, 9714−9721.

40. Seelig, A. (1987) Local anesthetics and pressure: a comparison of dibucaine binding to lipid monolayers and bilayers, *Biochim. Biophys. Acta 899*, 196−204.

41. Seelig, A., Alt, T., Lotz, S., and Holzemann, G. (1996) Binding of substance P agonists to lipid membranes and to the neurokinin-1 receptor, *Biochemistry 35*, 4365−4374.

42. Blume, A. (1979) A comparative study of the phase transitions of phospholipid bilayers and monolayers, *Biochim. Biophys. Acta 557*, 32−44.

Gatlik-Landwojtowicz et al.

43. Kerr, K. M., Sauna, Z. E., and Ambudkar, S. V. (2001) Correlation between steady-state ATP hydrolysis and vanadate-induced ADP trapping in Human P-glycoprotein. Evidence for ADP release as the rate-limiting step in the catalytic cycle and its modulation by substrates, *J. Biol. Chem. 276*, 8657−8664.

44. Hegner, D. (1980) Age-dependence of molecular and functional changes in biological membrane properties, *Mech. Ageing Dev. 14*, 101−118.

45. Figler, R. A., Omote, H., Nakamoto, R. K., and Al-Shawi, M. K. (2000) Use of chemical chaperones in the yeast Saccharomyces cerevisiae to enhance heterologous membrane protein expression: high-yield expression and purification of human P-glyco-protein, *Arch. Biochem. Biophys. 376*, 34−46.

46. Thurmond, R. L., Dodd, S. W., and Brown, M. F. (1991) Molecular areas of phospholipids as determined by 2H NMR spectroscopy. Comparison of phosphatidylethanolamines and phosphatidylcho-lines, *Biophys. J. 59*, 108−113.

47. Gally, H. U., Pluschke, G., Overath, P., and Seelig, J. (1979) Structure of Escherichia coli membranes. Phospholipid conforma-tion in model membranes and cells as studied by deuterium magnetic resonance, *Biochemistry 18*, 5605−5610.

48. Nichol, C. P., Davis, J. H., Weeks, G., and Bloom, M. (1980) Quantitative study of the fluidity of Escherichia coli membranes using deuterium magnetic resonance, *Biochemistry 19*, 451−7.

49. Yu, E. W., McDermott, G., Zgurskaya, H. I., Nikaido, H., and Koshland, D. E., Jr. (2003) Structural basis of multiple drug-binding capacity of the AcrB multidrug efflux pump, *Science 300*, 976−980.

50. Baldwin, R. L. (2005) in *Protein Folding Handbook. Part I* (Kiefhaber, J. B. a. T., Ed.) pp 127−162, Wiley-VCH Verlag GmbH & Co. KGaA, Weinheim.

51. Tobey, S. L., and Anslyn, E. V. (2003) Studies into the thermodynamic origin of negative cooperativity in ion-pairing molecular recognition, *J. Am. Chem. Soc. 125*, 10963−10970.

52. Ben-Tal, N., Sitkoff, D., Topol, I. A., Yang, A.-S., Burt, S. K., and Honig, B. (1997) Free Energy of Amide Hydrogen Bond Formation in Vacuum, in Water, and in Liquid Alkane Solution, *J. Phys. Chem. B 101*, 450−457.

53. Frisk-Holmberg, M., and van der Kleijn, E. (1972) The relationship between the lipophilic nature of tricyclic neuroleptics and antidepressants, and histamine release, *Eur. J. Pharmacol. 18*, 139−147.

54. Clarke, F. H. (1984) Ionization constants by curve fitting: application to the determination of partition coefficients, *J. Pharm. Sci. 73*, 226−230.

55. Tollenaere, J. P. (1977) Conformation of neuroleptic drugs in 3 aggregation states and their conformational resemblance to dopamine, *Eur. J. Med. Chem. 12*, 199−211.

56. Frézard, F., and Garnier-Suillerot, A. (1998) Permeability of lipid bilayer to anthracycline derivatives. Role of the bilayer composi-tion and of the temperature, *Biochim. Biophys. Acta 1389*, 13−22.

57. Ritchie, J. M., and Greengard, P. (1961) On the active structure of local anesthetics, *J. Pharmacol. Exp. Ther. 133*, 241−245.

58. Hwang, K. K., Martin, N. E., Jiang, L., and Zhu, C. (2003) Permeation prediction of M100240 using the parallel artificial membrane permeability assay, *J. Pharm. Pharm. Sci. 6*, 315−320.

59. Tenthorey, P. A., Block, A. J., Ronfeld, R. A., McMaster, P. D., and Byrnes, E. W. (1981) New antiarrhythmic agents. 6. Quantita-tive structure-activity relationships of aminoxylidides, *J. Med. Chem. 24*, 798−806.

60. Seiler, P. (1974) Interconversion of lipophilicities from hydrocarbon-water systems into octanol-water system, *Eur. J. Med. Chem. 9*, 473−479.

61. Hasegawa, J., Fujita, T., Hayashi, Y., Iwamoto, K., and Watanabe, J. (1984) pKa determination of verapamil by liquid-liquid partition, *J. Pharm. Sci. 73*, 442−445.

62. Budavari, S. (1996), Merck Research Laboratories Division of Merck & Co., Inc., New Jersey.

63. Clarke, F. H., and Cahoon, N. M. (1987) Ionization constants by curve fitting: determination of partition and distribution coef-ficients of acids and bases and their ions, *J. Pharm. Sci. 76*, 611−620.

64. Franke, U., Munk, A., and Wiese, M. (1999) Ionization constants and distribution coefficients of phenothiazines and calcium channel antagonists determined by a pH-metric method and correlation with calculated partition coefficients, *J. Pharm. Sci. 88*, 89−95.

7.1.1. Appendix: Surface Activity and Gibbs Adsorption Isotherm

Amphiphathic molecules, such as drugs, accumulate at the air-water interface from the interior of the solution which causes a decrease in the surface tension of buffer, γ_0, to the new value, γ. The difference is called as surface pressure, $\pi = \gamma_0 - \gamma$, and can be detected e.g. with a Wilhelmy plate in a monolayer trough.

The Gibbs adsorption isotherm describes the thermodynamics of adsorption of amphiphilic compound to the air-water interface

$$d\gamma = -RT\Gamma d\ln C_{Saq} = -d\pi \tag{1}$$

where R is the gas constant, T is the absolute temperature, C_{Saq} is the concentration of compound in bulk solution and Γ is the surface excess concentration. The surface excess concentration, Γ, describes the molar amount of accumulated solute per surface area (mol/m^2), and it can be written as

$$\Gamma = \frac{1}{A_0 N_A} = \frac{\Delta n}{A} \tag{2}$$

where Δn is the surface excess of molecules in the interface, A is the area of surface, A_0 is the surface area of compound required at the interface, and N_A is the Avogadro number.

The surface excess concentration, Γ, increases with C_{Saq} up to the limiting value Γ_∞. As long as Γ is constant a plot of π vs $\log C_{Saq}$ yields a straight line. The surface excess concentration, Γ, can be thus evaluated from the slope of the linear part of π versus $\log C_{Saq}$-plot and the surface area of compound required at the interface, A_0, from the eq. (2)

$$\Gamma_\infty = \frac{1}{RT} \frac{d\pi}{d\ln C_{Saq}} \tag{3}$$

The surface adsorption process can also described by a Langmuir adsorption isotherm

$$\Gamma = \Gamma_\infty \frac{K_{aw} C_{Saq}}{1 + K_{aw} C_{Saq}} \tag{4}$$

where K_{aw} is the air-water partition coefficient.

The air-water partition coefficient, K_{aw}, can be evaluated by using a Szyszkowski equation which is an integral version of the Gibbs adsorption isotherm (eq. (3)) and the Langmuir adsorption isotherm (eq. (4))

$$\pi = RT\Gamma_\infty \ln(K_{aw}C_{Saq} + 1) \qquad (5)$$

7.2 P-glycoprotein Kinetics Measured in Plasma Membrane Vesicles and Living Cells

Päivi Äänismaa and Anna Seelig*

Biophysical Chemistry, Biozentrum, University Basel, Klingelbergstrasse 70, CH-4056,

Basel, Switzerland

*Corresponding author, Phone: +41-61-267-22-06. Fax: +41-61-267-2-89. E-mail:

Anna.Seelig@unibas.ch

P-Glycoprotein Kinetics Measured in Plasma Membrane Vesicles and Living Cells

Päivi Äänismaa and Anna Seelig*

Biophysical Chemistry, Biozentrum, University of Basel, Klingelbergstrasse 70, Switzerland

Received September 20, 2006; Revised Manuscript Received January 11, 2007

ABSTRACT: P-glycoprotein (MDR1, ABCB1) is an ATP-dependent efflux transporter of a large variety of compounds. To understand P-glycoprotein in more detail, it is important to elucidate its activity in the cellular ensemble as well as in plasma membrane vesicles (under conditions where other ATP dependent proteins are blocked). We measured P-glycoprotein activity in inside-out vesicles formed from plasma membranes of *MDR1*-transfected mouse embryo fibroblasts (NIH-MDR1-G185) for comparison with previous measurements of P-glycoprotein activity in living NIH-MDR1-G185 cells. In plasma membrane vesicles activity was measured by monitoring phosphate release upon ATP hydrolysis and in living cells by monitoring the extracellular acidification rate upon ATP synthesis via glycolysis. P-glycoprotein was stimulated as a function of the concentration with 19 structurally different drugs, including local anesthetics, cyclic peptides, and cytotoxic drugs. The concentrations of half-maximum P-glycoprotein activation, K_1, were identical in inside-out plasma membrane vesicles and in living cells and covered a broad range of concentrations ($K_1 \sim (10^{-8}-10^{-3})$ M). The influence of the pH, drug association, and vesicle aggregation on the concentration of half-maximum P-glycoprotein activation was investigated. The turnover numbers in plasma membrane vesicles and in living cells were also approximately identical if the latter were measured in the presence of pyruvate. However, in the absence of pyruvate they were higher in living cells. The rate of ATP hydrolysis/ATP synthesis decreased exponentially with decreasing free energy of drug binding from water to the transporter, $\Delta G^0_{tw(1)}$ (or increasing binding affinity). This suggests that drug release from the transmembrane domains has to occur before ATP is hydrolyzed for resetting the transporter.

P-glycoprotein, Pgp[1] (MDR1, ABCB1), is an ATP-dependent efflux transporter of a large variety of structurally diverse compounds, including toxins, drugs, and metabolites. Together with metabolizing enzymes and other efflux transporters with partially overlapping functions Pgp significantly contributes to a sophisticated cellular defense and housekeeping system (for review see refs *3-5*). Pgp consists of two homologous parts, each comprising a cytosolic, nucleotide-binding domain, NBD (*6, 7*), and a drug-binding, transmembrane domain, TMD (*8*), which together form an integrated single entity as shown by preliminary X-ray data (*9*) and a recent homology model (*10*). Upon formation of the transition state each NBD carries one molecule of ATP which leads to a dimerization of the two domains. However, just one of the two ATP molecules seems to be hydrolyzed per dimerization event (*11*). The interplay between the NBDs and the TMDs upon drug stimulation is not yet fully understood. Whether ATP hydrolysis is required for driving the substrate across the membrane (*1*), or for resetting the

transporter to the open starting position (after a passive transport step) (*12*), or even for both (*13*) is still a matter of intensive research.

The difficulty in understanding Pgp arises to a large extent from the fact that substrates are bound from the cytosolic membrane leaflet (*8, 14*) (for review see refs *15, 16*) and not from the aqueous phase as is the case in most well-known transporters. To reach the site of interaction the substrate has therefore first to partition from the aqueous phase (w) into the lipid phase (l). This process is described by the lipid−water partition coefficient, K_{lw}. Second, the substrate binds from the lipid phase to the activating (1) region of the TMDs (t), which is described by the transporter−lipid binding constant, $K_{tl(1)}$. As a consequence, the binding constant describing substrate binding from the aqueous phase to the activating binding region of the transporter, $K_{tw(1)}$, can be expressed as the product of the lipid−water partition coefficient, K_{lw}, and the transporter−lipid binding constant, $K_{tl(1)}$ ($K_{tw(1)} = K_{lw} \cdot K_{tl(1)}$). Analogous binding constants can be defined for the inhibitory (2) binding region of the transporter. Substrate binding thus strongly depends on the lipid−water partition coefficient, K_{lw}, of the compound which in turn depends on the lateral packing density of the lipid membrane, π_M, and the pH of the environment (for detail see refs *5, 17*).

In inside-out membrane vesicles drugs merely have to intercalate between the lipids with the polar head group remaining in the head group region of the membrane, whereas in living cells they have to diffuse across the

---

* Corresponding author. Phone: +41-61-267 22 06. Fax: +41-61-267 21 89. E-mail: Anna.Seelig@unibas.ch.
[1] Abbreviations: CMC_D, critical micelle concentration of drug; ECAR, extracellular acidification rate; K_1 (K_2), aqueous substrate concentration at half-maximum Pgp activation (inhibition); K_{lw}, lipid−water partition coefficient; $K_{tl(1)}$ ($K_{tl(2)}$), binding constant of the drug from the lipid membrane to the activating (inhibitory) binding region of the transporter; $K_{tw(1)}$ ($K_{tw(2)}$), binding constant of the drug from water to the activating (inhibitory) binding region of the transporter; MDR, multidrug resistance; NBD, nucleotide binding domain; Pgp, P-glycoprotein-ATPase (MDR1, ABCB1); TMD, transmembrane domain; V_1 (V_2), maximum (minimum) Pgp activity.

membrane. Permanently charged cationic compounds such as spin labeled verapamil (*18*) can, therefore, reach the Pgp binding site in inside-out vesicles but not in living cells.

Pgp activity has generally been measured in plasma membrane vesicles of *MDR1*-transfected cells or in reconstituted proteoliposomes which both expose the NBDs to the extravesicular side and allow monitoring the release of inorganic phosphate (*1*, *19*, *20*) or ADP (*20*, *21*) upon drug stimulation. In living cells Pgp stimulation with drugs leads to intracellular ATP hydrolysis which entails enhanced ATP synthesis via glycolysis, whereby lactic acid is produced as waste product and is excreted by the cell (*22*). We exploited this process to monitor Pgp activity as a function of drug concentration in real time (*2*, *23*, *24*) using a Cytosensor microphysiometer (*25*). The experiments have shown that Pgp activity in living cells is not only controlled by the nature and the concentration of the drug, and the packing density of the membrane, but also by the metabolic state of the cell (*2*).

A comparison of Pgp activity in living cells and in inside-out membrane vesicles of the same cells has so far been published only for verapamil (*2*). Since the two systems bear distinct differences we extended the comparison to the 15 drugs measured previously in living mouse embryo fibroblasts (NIH-MDR1-G185) (*24*) and added four additional drugs to get an even broader selection of compounds. The 19 compounds range from local anesthetics (MW $\approx$ 200 g/mol) to cyclic peptides (MW $\approx$ 1200 g/mol) and include cytotoxic drugs. The wide variety of compounds allows, then, testing how the binding affinity of the drug for the TMDs influences the rate of nucleotide hydrolysis at the NBDs.

We show that the concentrations of half-maximum Pgp activation, K_1, in living *MDR1*-transfected mouse embryo fibroblasts (*24*) are identical to those in inside-out plasma membrane vesicles of the same cells, provided the two systems are at the same pH and possible artifacts due to drug and vesicle association are taken into account. The relative rates of activation are linearly correlated. The turnover numbers are practically identical if Pgp activity in living cells is measured in the presence of pyruvate (*2*, *24*). In the absence of pyruvate Pgp activity in living cells is higher. The maximum rate of Pgp activity, $\ln(V_1)$, decreased linearly with increasing affinity of the drug from water to the TMDs. Drug release is thus the rate-determining step and the transporter can only be reset if it is unloaded at the extracellular side.

MATERIALS AND METHODS

Materials. Amitriptyline·HCl, *cis*-flupenthixol·2HCl, daunorubicin·HCl, dibucaine·HCl, diltiazem·HCl, lidocaine·HCl, progesterone, promazine·HCl, trifluoperazine·2HCl, triflupromazine·HCl, and vinblastine·H_2SO_4 were from Sigma-Aldrich (Steinheim, Germany), and (*R/S*)-verapamil·HCl and colchicine were from Fluka (Buchs, Switzerland). Chlorpromazine·HCl and reserpine·HCl·H_2O were generous gifts from Merck (Darmstadt, Germany), and cyclosporin A, PSC-833, and glivec mesylate were generous gifts from Novartis AG (Basel, Switzerland). The inhibitor OC144-093 was a gift from Dr. T. Litman. Complete EDTA-free protease inhibitor cocktail tablets were obtained from Roche Diagnostics (Mannheim, Germany), 1,4-dithiol-DL-threitol, DTT,

from Applichem (Darmstadt, Germany), and bicinchoninic acid, BCA, protein assay reagents from Pierce (Rockford, IL). All other chemicals were from either Sigma, Fluka, or Merck. Cell culture media DMEM with and without pyruvate (liquid and dry, Cat. No. 21969 and Cat. No. 52100, respectively) as well as other compounds required for cell culture such as fetal bovine serum, FBS, L-glutamine, and antibiotics were from Gibco-BRL (Basel, Switzerland).

Cell Lines and Cell Culture. Wild-type (NIH3T3) and *MDR1*-transfected mouse embryo fibroblasts (NIH-MDR1-G185) were generous gifts from Dr. M. M. Gottesman and Dr. S. V. Ambudkar (The National Institutes of Health, Bethesda, MD). Cells were grown in the presence of 0.15 μM colchicine and were maintained as described previously (*2*, *23*).

Plasma Membrane Preparation. The crude plasma membrane vesicles were prepared as described previously with some modifications (*2*, *26*). Briefly, cells grown in 15 cm dishes were washed once with PBS buffer, and then scraped into ice-cold PBS (pH 7.0 at ambient temperature) supplemented with protease inhibitors (1 tablet/50 mL PBS). Next, cells were washed with ice-cold buffer A by centrifugation at $1000g_{max}$ for 10 min at 4 °C. Buffer A consisted of 10 mM Tris-HCl, 10 mM NaCl, 1 mM $MgCl_2$, protease inhibitors (1 tablet/50 mL), adjusted to pH 7.5 at ambient temperature. The pellet was resuspended in buffer A (5 mL/4*15 cm dishes) and was then kept on ice until disruption with a "One Shot" cell disrupter (Constant Systems Ltd, Warwickshire, U.K.) at 400 bar. The "One Shot" cell disrupter uses pressure to force a sample through a small fixed orifice at high speed. By transferring the cell sample from a region of high pressure to one of low pressure cells disrupt. The cell lysate was diluted 1:1 with ice-cold buffer B (10 mM Tris-HCl, 50 mM *N*-methyl-D-glucamine, NMDG, 120 mM sucrose, protease inhibitors (1 tablet/50 mL), adjusted to pH 7.4 at ambient temperature). The unbroken cells and nuclei were then precipitated by centrifugation at $800g_{max}$ for 10 min at 4 °C. Subsequently mitochondria were removed by centrifugation at $6000g_{max}$ for 10 min at 4 °C, and in the final centrifugation step ($100000g_{max}$, 1 h, 4 °C) the crude membranes were pelleted. The pellet was resuspended in buffer B and homogenized by repeated aspiration through a 23-gauge syringe. Aliquots were rapidly frozen in dry ice and stored at −80 °C until use.

The average protein content of the plasma membrane vesicles from five different preparations was determined as ((9.9 $\pm$ 1.7) mg/mL) using the BCA protein assay with bovine serum albumin (fraction V) as a standard. The initial number of cells per preparation varied from 5.7×10^8 to 1.1×10^9. Western immunoblots made with supernatants and pellets of the different centrifugation steps after cell disruption ($800g_{max}$, $6000g_{max}$, $100000g_{max}$) suggest a substantial loss of Pgp. Pgp was detected with monoclonal antibody C219. The total loss of plasma membrane Pgp during membrane vesicle preparation was estimated as approximately 20%. Taking into account the number of Pgp molecules in NIH-MDR1-G185 cells determined previously as $(1.95 \pm 0.53) \times 10^6$ Pgp/cell (*27*), the molecular weight (170 kDa), and a total loss of Pgp ($\sim$20%), the amount of Pgp per total protein concentration was estimated as (1.1 ± 0.3)% (average of five different membrane preparations).

Table 1: The Critical Micelle Concentration of Drugs, CMC_D, the Stock Solution Concentrations, and the Highest Drug Concentrations Measured in Phosphate Release (P_i) Assay and in ECAR Measurements

no.	compound	$CMC_D{}^a$ [mM]	stock solution ECAR [mM]	highest measd ECAR^d [mM]	stock solution P_i assay [mM]	highest measd P_i assay [mM]
1	amitriptyline	5.0	0.4[b]	0.064	10.6[e]	0.887
2	chlorpromazine	0.96	0.2[b]	0.011	2.6[e]	0.216
3	*cis*-flupenthixol	0.16	0.06[b]	0.012	1.5[e]	0.126
4	cyclosporin A	~0.001	0.002[c]	0.002	0.07,[f] 0.42[f]	0.001,[h] 0.007[h]
5	daunorubicin	0.06 − 0.3[j]	0.1[b]	0.087	0.096,[e] 0.48,[f] 0.9[e]	0.008, 0.008,[h] 0.075
6	dibucaine	2.4	0.2,[b] 1.0[b]	0.059	0.47,[e] 2.3[e]	0.039, 0.191
7	diltiazem	10	0.6[b]	0.498	10.2[e]	0.833
8	glivec	~1	0.1[b]	0.092	1.8[e]	0.151
9	lidocaine	60	1.0[b]	0.939	24,[e] 90[e]	2.0, 7.5
10	progesterone	0.08	0.2[c]	0.029	10[f]	0.167[h]
11	promazine	7	0.4[b]	0.227	3.45,[e] 27.8[e]	0.287, 2.3
12	(*R/S*)-verapamil	5	0.1[c]	0.058	0.66,[e] 1.9[e]	0.055, 0.160
13	reserpine	0.009	0.01,[c] 0.008[c]	0.003	0.55[f]	0.009[h]
14	trifluoperazine	0.18	0.1[b]	0.009	0.4,[e] 2.0[e]	0.033, 0.166
15	triflupromazine	0.47	0.1[b]	0.011	1.7,[e] 2.0[e]	0.143, 0.166
16	colchicine	2.6	nd	nd	200[f]	3.3[h]
17	OC144-093	~0.002	nd	nd	0.06[f]	0.001[h]
18	PSC-833	~0.001	nd	nd	0.2,[f] 0.8[f]	0.001[h]
19	vinblastine	0.1	0.1[c]	0.076	0.33[g]	0.027[i]

[a] CMC_D determined by surface activity measurements in 50 mM Tris-HCl, 114 mM NaCl, pH 7.4 at ambient temperature. [b] Stock solution in DMEM flow medium. [c] Stock solution in DMEM flow medium containing 0.5% (v/v) DMSO. [d] Drug concentrations after correction for adsorption. [e] Stock solution in water. [f] Stock solution in 100% (v/v) DMSO. [g] Stock solution in 6% (v/v) DMSO. [h] Drug concentration containing 1.7% (v/v) DMSO. [i] Drug concentration containing 0.5% (v/v) DMSO. [j] Depending on stock solution concentration.

The orientation of Pgp in plasma membrane vesicles was tested by permeabilizing the membranes with CHAPS in order to unmask the occluded nucleotide binding domains (*28*). Since increasing concentrations of CHAPS did not lead to an increase in the rate of ATP hydrolysis, we concluded that the vesicles obtained by the "One-Shot" procedure exhibited an essentially inside-out orientation.

Phosphate Release Assay. The Pgp associated ATPase activity was determined according to Litman et al. (*19*) in a 96-well microtiter plate (Nunc F96 MicroWell plate, non-treated) with small modifications. The plasma membrane vesicles were diluted to a protein concentration of 0.1 mg/mL in ice-cold phosphate release assay buffer which consisted of 25 mM Tris-HCl including 50 mM KCl, 3 mM ATP, 2.5 mM MgSO$_4$, 3 mM DTT, 0.5 mM EGTA, 2 mM ouabain, and 3 mM sodium azide, adjusted to pH 7.0 at 37 °C, unless stated otherwise. Each series of experiments contained 5 μg of protein per total assay volume of 60 μL (total protein concentration 84.7 μg/mL per sample). Incubation with the various drugs was started by transferring the plate from ice to a water bath at 37 °C for 1 h, and was terminated by rapidly cooling the plate on ice. The inorganic phosphate, P_i, released was determined by addition of ice-cold solution (200 μL) containing ammonium molybdate (0.2% (w/v)), sulfuric acid (1.43% (v/v)), freshly prepared ascorbic acid (1% (w/v)), and SDS (0.9% (w/v)) to each well. After incubation at room temperature (30 min), the phosphate released was quantified colorimetrically at 820 nm using a micro-plate reader Spectramax M2 (Molecular Device, Sunnyvale). Reference standards were included to each 96-well plate. Samples incubated with 0.5 mM vanadate to determine the vanadate-sensitive Pgp activation were obtained in parallel and were subtracted from the measured values.

Cytosensor Measurements. The rate of ATP synthesis in living cells was measured by monitoring the extracellular acidification rate, ECAR, using a Cytosensor (*25*). The

ECAR was shown to correspond to the rate of lactate efflux as a result of glycolysis (for details cf. refs *2*, *23*, *24*). The DMEM flow medium used was buffered with phosphate (0.91 mM) and thus exhibited a very low buffer capacity. Moreover, it contained pyruvate (1 mM) which reduces the basal activity of cells by (50−60)% (*2*). Measurements were performed at pH 7.4 and $T = 37$ °C. The transformation of the voltage per time data (μV·s^{-1}) to protons released per cell per second (H$^+$·cell^{-1}·s^{-1}) was performed as described previously (*2*).

Stock Solutions of Drugs. Stock solutions for the phosphate release assay were made with nanopure water or DMSO (cf. Table 1). Drug solutions were prepared by further dilution of the stock solution with either water or DMSO. The measured drug concentrations were then obtained by adding 5 μL of aqueous drug solution or 1 μL of DMSO drug solution into the phosphate release assay buffer (total sample volume per well = 60 μL). The final DMSO concentration was constant $c = 1.7\%$ (v/v).

Stock solutions for Cytosensor measurements were made with DMEM flow medium or DMSO which was diluted with flow medium to the final DMSO concentration (0.5% (v/v)). Upon further dilution the DMSO concentration was decreasing. Stock solution concentrations and the highest concentrations measured with the two assays are included in Table 1. At the concentrations applied DMSO affected neither the ECAR (*24*) nor the phosphate release rate.

All drugs investigated are amphiphilic and form micelle-like associates at high concentrations. The critical micelle concentrations of drugs, CMC_D, determined previously by surface activity measurements in 50 mM Tris-HCl buffer containing 114 mM NaCl (pH 7.4 at ambient temperature) are given in Table 1 (refs *29*, *30* and X. Li-Blatter and A. Seelig, unpublished results). For comparison the CMC_D value of triflupromazine was also measured in the phosphate release assay buffer (pH 7.4 at ambient temperature) and was found to be very similar. The stock solution concentra-

tions were below the critical micelle concentration, CMC_D, for most drugs in ECAR measurements but not in the phosphate release assay (see Table 1). The direct injection of the concentrated solutions into small volumes (60 μL) of ice-cold buffer containing the membrane vesicles generated high local drug concentrations. Since the pH of the buffer increases with decreasing temperature (pH 7.9 at $T = 4$ °C), this may have led to irreversible drug association in some cases which reduces membrane partitioning, and, in turn, binding to Pgp. Drugs which are especially prone to association are colchicine, progesterone, daunorubicin, and phenothiazines.

Drug Adsorption. Some drugs strongly adsorb to plastic surfaces (*31*). Drug solutions reaching the measuring cell in the Cytosensor were therefore corrected for adsorption using UV spectroscopy (for details see ref *24*). Adsorption varied strongly from compound to compound and was relatively small for verapamil ($\sim$21% for verapamil (20 μM)) and high for phenothiazines ($\sim$89.5% for triflupromazine (50 μM)). The corresponding values for adsorption to the test tubes (polypropylene) used in the phosphate release assay were also determined (as $\sim$3% (per 120 min) for verapamil (40 μM) and as $\sim$19.0% (per 130 min) for triflupromazine (23 μM)) but were not taken into account.
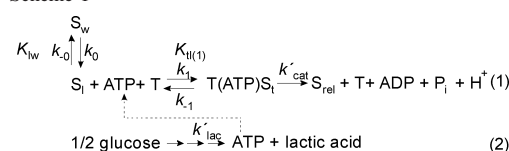
90° Light Scattering. Light scattering at 90° was measured with a Hitachi F-4500 spectrofluorometer under constant stirring at an excitation and emission wavelength of 550 nm ($T = 37$ °C). A quartz cuvette with a cell length of 1 cm and a volume of 3.5 mL was used. It was filled with 1.8 mL of phosphate release assay buffer (pH 7.0 at 37 °C) containing crude plasma membrane vesicles with the same protein concentration as used in the phosphate release assay (84.7 μg/mL). Aliquots (μL) of a promazine stock solution prepared in nanopure water (6.24, 12.4, 25.7, and 27.3 mM) were added into the buffer. The results were corrected for dilution (maximally $\sim$10%) upon promazine titration by titrating equal amounts of nanopure water into the membrane-containing phosphate release assay buffer.

The Kinetic Model. We used a modified Michaelis−Menten model (eq 1) proposed by Litman et al. (*19*) for data evaluation. It assumes basal Pgp activity in the absence of drugs, activation upon drug binding to a first binding region at low drug concentrations, and inhibition upon drug binding to a second binding region at high drug concentrations. The rate of Pgp activity, V_{sw}, is expressed as follows:

$$V_{sw} = \frac{K_1 K_2 V_0 + K_2 V_1 C_{sw} + V_2 C_{sw}^2}{K_1 K_2 + K_2 C_{sw} + C_{sw}^2} \qquad (1)$$

where C_{sw} is the substrate concentration in aqueous solution, V_0 is the basal activity in the absence of drugs, K_1 and K_2 are the concentrations of half-maximum activation and inhibition, respectively, V_1 is the maximum rate of ATP hydrolysis, and V_2 is the minimum rate of ATP hydrolysis at infinite substrate concentration. The corresponding reaction scheme was shown previously (*24*). At low substrate concentrations eq 1 reverts to the simple Michaelis−Menten kinetics which is illustrated in reaction 1, Scheme 1, where S_w is the substrate in the aqueous phase, S_l is the substrate in the lipid phase, k_0 and k_{-0} are the partitioning rate constants, and $K_{lw} = k_0/k_{-0}$ is the lipid−water partition

Scheme 1

$$K_{lw} \quad k_{-0} \Big\updownarrow k_0 \qquad K_{tl(1)}$$

$$S_l + ATP + T \underset{k_{-1}}{\overset{k_1}{\rightleftharpoons}} T(ATP)S_t \overset{k'_{cat}}{\rightleftharpoons} S_{rel} + T + ADP + P_i + H^+ \quad (1)$$

$$1/2 \text{ glucose} \overset{k_{lac}'}{\dashrightarrow} ATP + \text{lactic acid} \qquad (2)$$

coefficient. ATP and the substrate, S_l, bind to the transporter, T, to form the T(ATP)S_t complex. S_t is the substrate bound to the activating binding region of the transporter, k_1 and k_{-1} are the rate constants for association to and dissociation from the activating binding region, and $K_{tl(1)} = k_1/k_{-1}$ is the binding constant of the substrate for the activating binding region of the transporter within the lipid membrane, under the assumption that the association/dissociation reactions are rapid compared to catalytic step; k'_{cat} is the catalytic rate constant, and S_{rel} is the substrate released. For simplicity only one ATP (ADP) molecule per Pgp is shown. As seen in reaction 2 under the anaerobic conditions in the Cytosensor one molecule of glucose is transformed to two molecules of ATP and two molecules of lactic acid which is then exported out of the cell. The synthesis of ATP comprises several steps, and k'_{lac} is the over-all catalytic rate constant.

RESULTS

Basal Pgp Activity. For calibration, the time dependence of phosphate release upon Pgp activation at 37 °C was measured in plasma membrane vesicles of *MDR1*-transfected mouse embryo fibroblasts (NIH-MDR1-G185) in the presence and absence of 0.5 mM vanadate and 31.7 μM verapamil, respectively (Figure 1A,B). Samples were analyzed every 15 min, and the reaction was stopped by cooling the samples on ice. The amount of phosphate released was determined as described in Materials and Methods. ATP hydrolysis as a function of time was linear under each condition throughout the time period investigated (75 min). The phosphate release assay buffer contains sodium azide, ouabain, and EGTA to inhibit, e.g., Na/K- and Ca-ATPases, which reduced the basal activity of all ATP consuming enzymes by 75.1% in comparison to a buffer lacking these inhibitors. Sodium azide had the strongest effect (results not shown).

The ATPase activity of plasma membrane vesicles in phosphate release assay buffer is shown in Figure 1A (open triangles). Addition of verapamil (31.7 μM) increased the hydrolysis of ATP by Pgp (solid squares). In the presence of vanadate (0.5 mM) the release of phosphate was reduced (open down triangles) and remained at the same level upon addition of verapamil (open squares), indicating that Pgp activity was inhibited by vanadate (Figure 1A). The remaining phosphate released arises most likely from the ATPase activity of enzymes that are not sensitive to the inhibitors used. Figure 1B shows the vanadate-sensitive basal and verapamil-stimulated ATPase activity (assumed to correspond to the ATPase activity of Pgp) as a function of the incubation time at 37 °C. In the following, a single time point measurement (60 min) of Pgp activity was used. For five different plasma membrane preparations the average vanadate-sensitive basal Pgp activity expressed as phosphate released per total protein concentration and time was
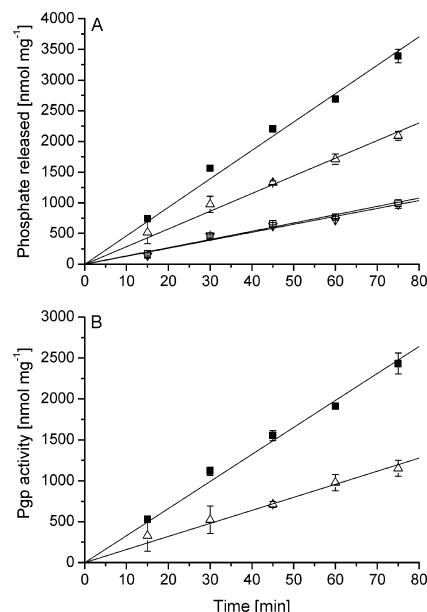
FIGURE 1: Time dependence of vanadate-sensitive Pgp activity in plasma membranes from NIH-MDR1-G185 cells in the presence of verapamil (31.7 μM) and vanadate (0.5 mM). A: Phosphate release measurements were made under four different conditions: in the absence of verapamil and vanadate ($\triangle$), in the presence of verapamil and in the absence of vanadate ($\blacksquare$), in the absence of verapamil and in the presence of vanadate ($\triangledown$), and in the presence of verapamil and vanadate ($\square$). B: Vanadate-sensitive Pgp activity in the presence ($\blacksquare$) and in the absence of verapamil ($\triangle$). Values are expressed as the mean of three measurements $\pm$ SD. The solid lines are the linear regressions to the data. For further analysis a single time point measurement (60 min) of Pgp activity was used.

determined as $V_0 = (12.3 \pm 1.3)$ nmol·mg^{-1}·min^{-1} ($n \approx$ 126).

Drug-Stimulated Pgp Activity Profiles Measured in Plasma Membrane Vesicles of MDR1-Transfected Mouse Embryo Fibroblasts. Pgp activity in inside-out plasma membranes vesicles of NIH-MDR1-G185 cells was measured for the 19 drugs listed in Tables 1 and 2. Figure 2A−D shows the rate of Pgp activity as a function of the substrate concentration in aqueous solution (Log scale). Drug-stimulated Pgp activity is expressed as percentage of the basal activity (taken as 100%).

Maximum Pgp activity requires high millimolar concentrations for very hydrophilic drugs, e.g., lidocaine (Figure 2A, filled squares) and colchicine (Figure 2C, filled down triangles), micromolar concentrations for more hydrophobic drugs, e.g., *cis*-flupentixol (Figure 2A, filled triangles) and verapamil (Figure 2B, filled squares), and nanomolar concentrations for even more hydrophobic drugs, e.g., OC144-093 (Figure 2D, open circles). Compounds of intermediate hydrophobicity show the characteristic bell-shaped Pgp activity profiles as a function of concentration observed previously in living NIH-MDR1-G185 cells (*24*). For very hydrophilic compounds inhibition could not be reached, whereas for the very hydrophobic compounds activation is barely visible or not present at all. The solid lines in Figure

2A−D are fits to the modified Michaelis−Menten model (eq 1) proposed by Litman et al. (*19*) (for details see ref *24*). The kinetic parameters derived from phosphate release measurements in plasma membrane vesicles are summarized in Table 2.

Vesicle Aggregation Can Hamper Measurement of the Inhibitory Part of the Pgp Activity Profile. The inhibitory part of the activity profile was easily reached in the ECAR assay (*24*). In the phosphate release assay this was more difficult since the highly concentrated drug solutions used in the phosphate release assay can lead to drug association as outlined in Materials and Methods; moreover, vesicle aggregation can occur as will be shown below.

In the absence of drugs inside-out membrane vesicles exhibit a negative surface potential, ψ, which prevents their aggregation. Upon partitioning of positively charged drugs, the negative surface potential decreases or even disappears (*24*, *32*), which can lead to vesicle aggregation. To investigate this phenomenon in more detail three compounds (verapamil, chlorpromazine, and promazine) with high lipid−water partition coefficients, K_{lw} (*24*), and high pK_a values were chosen and 90° light scattering measurements were performed in parallel to the spectroscopic phosphate release assay. Figure 3A−C displays the raw data of the phosphate release assay made with plasma membrane vesicles of *MDR1*-transfected and wild-type cells in the presence and absence of vanadate (0.5 mM) and drug. Plasma membrane vesicles of wild-type cells show some residual vanadate-sensitive activity in the presence of sodium azide, ouabain, and EGTA (Figure 3A−C) which is most likely due to a low concentration of Pgp (*2*). Nonenzymatic ATP hydrolysis was not observed.

At high drug concentrations the plasma membrane vesicles of wild-type and *MDR1*-transfected cells with and without vanadate both show a decrease in the optical density (820 nm). The effect increases in the order verapamil (pK_a 8.9) $\leq$ chlorpromazine (pK_a 9.2) < promazine (pK_a 9.4). As seen in Figure 3C a concomitant increase in light scattering intensity was observed at promazine concentrations, $C >$ 10^{-4} M. At even higher concentrations, $C > 7 \times 10^{-4}$ M, light scattering started to increase strongly not only with concentration but also with time, suggesting the formation of larger aggregates. As seen in Figure 3A−C the aggregation phenomenon was independent of the presence of Pgp and was merely a result of charge neutralization of inside-out cellular vesicles of wild-type and *MDR1*-transfected cells which exhibit approximately the same negative surface potential (cf. footnote 1 in ref *24*). Vesicle aggregation most likely hampered drug access to the membrane and ATP binding to the NBDs. Partitioning of electrically neutral drugs (progesterone, cyclosporin A, and PSC-833) or cationic drugs with low pK_a values (reserpine, glivec, daunorubicin, and OC144-093) (Figure 2A−D) induced no vesicle aggregation even at high concentrations (data not shown). Since problems due to drug association, as well as vesicle aggregation, are less pronounced at pH 7.0 than at pH 7.4, we chose the lower pH for the phosphate release assay despite the fact that the ECAR measurements were performed at pH 7.4.

The Influence of pH on the Kinetic Parameters of Drug-Stimulated Pgp Activity. To investigate the influence of the pH on Pgp activity we chose three representative examples, the electrically neutral progesterone and the cationic com-

Table 2: Kinetic Parameters of Pgp Activation for 19 Drugs. The Concentration of Half-Maximum Activation (Inhibition), K_1 (K_2), and the Maximum (Minimum) Transporter Activity, V_1 (V_2), Obtained from Phosphate Release Measurements in Plasma Membrane Vesicles of NIH-MDR1-G185 Cells[a]

no.	compound	MW_{base} [g/mol]	$pK_a{}^c$	K_1 [μM]	K_2 [μM]	V_1 [fold]	V_2 [fold]	no. of experiments
1	amitriptyline	277.4	9.4	14.2 ± 0.7	1239.5 ± 110.5	2.3 ± 0.1	1.1 ± 0.2	3
2	chlorpromazine	318.9	9.2	10.5 ± 0.5	125.0 ± 15.0	2.2 ± 0.1	1.2 ± 0.1	2
3	*cis*-flupenthixol	434.5	7.8	1.8 ± 0.6	28.3 ± 5.8	2.4 ± 0.1	0.3 ± 0.1	3
4	cyclosporin A	1202.6		0.02 ± 0.01	1.5 ± 1.0	0.9 ± 0.1	0.4 ± 0.2	3
5	daunorubicin	527.5	8.4	5.5 ± 1.5	43.5 ± 3.5	1.4 ± 0.1	0.8 ± 0.1	2
6	dibucaine[b]	343.5	8.5	4.1 ± 0.9	nd	2.9 ± 0.2	nd	4
7	diltiazem	414.5	8.9	6.7 ± 1.3	1678.5 ± 1.5	3.2 ± 0.1	1.0 ± 0.1	2
8	glivec	493.6	8.07	1.2 ± 0.3	241.8 ± 49.4	1.6 ± 0.1	0.10 ± 0.02	2
9	lidocaine	234.3	7.6	1630 ± 70	nd	2.7 ± 0.1	nd	4
10	progesterone	314.4		13.9 ± 0.4	144.7 ± 27.3	3.3 ± 0.2	0.7 ± 0.4	4
11	promazine	284.4	9.42	82.0 ± 10.0	2150 ± 200	2.5 ± 0.1	0.1 ± 0.0	2
12	(*R/S*)-verapamil	454.6	8.92	1.0 ± 0.3	843.6 ± 159.1	2.5 ± 0.1	1.0 ± 0.4	15
13	reserpine	608.7	6.6	0.2 ± 0.1	1.0 ± 0.2	1.7 ± 0.2	1.0 ± 0.1	2
14	trifluoperazine	407.5	8.09	2.3 ± 0.2	58.3 ± 14.4	2.4 ± 0.2	1.0 ± 0.2	5
15	triflupromazine	352.4	9.1	8.0 ± 2.7	140.0 ± 26.5	2.0 ± 0.1	1.0 ± 0.2	4
16	colchicine	399.4		227.6 ± 20.1	nd	1.7 ± 0.1	nd	2
17	OC144-093	494.7	6.3	0.008 ± 0.002	0.95 ± 0.15	0.9 ± 0.1	0.3 ± 0.1	2
18	PSC-833	1214.6		0.008 ± 0.001	2.6 ± 0.1	0.8 ± 0.1	0.4 ± 0.1	4
19	vinblastine	811.0	7.4	1.6 ± 0.2	40.5 ± 4.5	1.8 ± 0.1	0.9 ± 0.1	2

[a] Kinetic parameters for the inhibitory part of the Pgp activation profiles, K_2 and V_2, have to be taken as the estimates because for many compounds the inhibitory part is affected by vesicle aggregation and drug association appearing at high drug concentrations (discussed in detail in text). [b] Data fitted to simple Michaelis−Menten equation. [c] For references of pK_a values see ref *24*; the pK_a values for OC144-093 and vinblastine are taken from SciFinder and Merck Index, respectively.
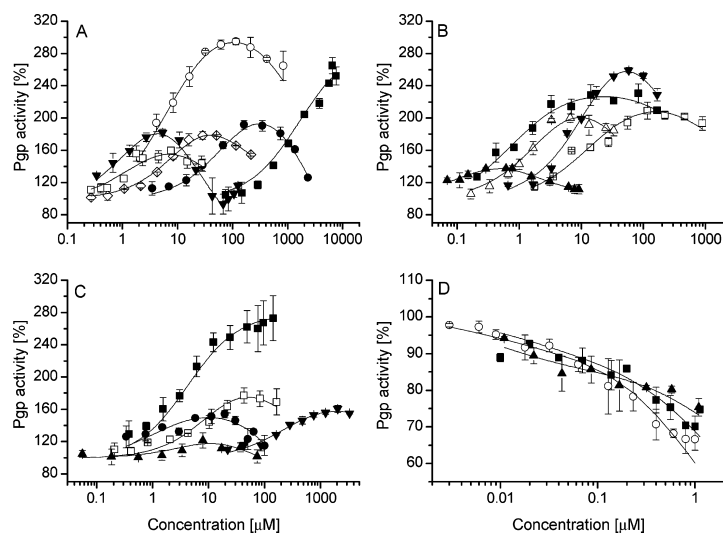

FIGURE 2: Vanadate-sensitive Pgp activity profiles obtained from phosphate release measurements in plasma membrane vesicles of NIH-MDR1-G185 cells. Measurements were performed at T = 37 °C and at pH 7.0. A: Chlorpromazine (◇), *cis*-flupenthixol (▼), diltiazem (○), lidocaine (■), promazine (●), and vinblastine (□). B: Amitriptyline (□), progesterone (▼), reserpine (▲), trifluoperazine (△), and verapamil (■). C: Daunorubicin (▲), dibucaine (■), colchicine (▼), glivec (●), and triflupromazine (□). D: Cyclosporin A (■), PSC-833 (▲), and OC144-093 (○). Data are expressed as the average of at least two measurements. Solid lines are fits to the modified Michaelis−Menten equation (eq 1), except for dibucaine, which is fitted to the simple Michaelis−Menten equation ($V_{sw} = V_0 + (V_{max} − V_0)C_{sw}/(K_M + C_{sw})$, where V_{max} is the maximum activity and K_M the Michaelis−Menten constant).

pounds, promazine (pK_a 9.4) and verapamil (pK_a 8.9). The pH dependence of Pgp activity as a function of concentration was investigated in the range of pH 6.2 to pH 7.4 at 37 °C using the phosphate release assay (Figure 4A,B). The basal Pgp activity, V_0, does barely change in the pH range investigated (Figure 4A), which is in good agreement with previous experiments (*33*).

For the uncharged progesterone the maximum activity, V_1 (Figure 4A), and the concentration of half-maximum activation, K_1 (Figure 4B), were practically identical at two different pH values. However, for verapamil and promazine the maximum activity, V_1, increased with increasing pH (Figure 4A) and the concentration of half-maximum activation, K_1, decreased (Figure 4B). This is due to an increase
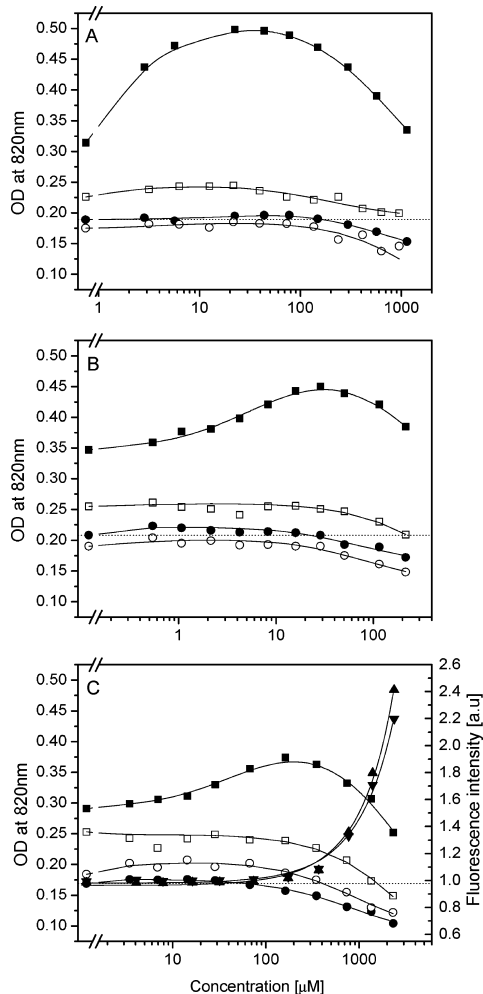
FIGURE 3: The amount of ATP hydrolyzed in plasma membrane vesicles of wild-type (open symbols, $\square$, $\bigcirc$)) and NIH-MDR1-G185 cells (filled symbols, $\blacksquare$, $\bullet$) with increasing concentration of verapamil (A), chlorpromazine (B), and promazine (C). Circles ($\bigcirc$, $\bullet$) refer to measurements in the presence of 0.5 mM vanadate and squares ($\square$, $\blacksquare$) in the absence of 0.5 mM vanadate. The results are expressed as optical densities at 820 nm (A−C, labels on left-hand side). The solid lines are fits to the modified Michaelis−Menten equation (eq 1). Labels at right-hand side in (C): 90° light scattering intensity at 550 nm as function of increasing concentration of promazine in the membrane-containing phosphate release assay buffer in the absence of 0.5 mM vanadate ($\blacktriangledown$) and in the presence of 0.5 mM vanadate ($\blacktriangle$). Light scattering intensities are normalized to the light scattering intensity of the sample without promazine. Data were fitted to an exponential curve. All measurements were performed at $T = 37\ °C$ and pH 7.0.

in the fraction of unprotonated drug and, in turn, to an increase in membrane partitioning and Pgp binding.

ECAR Measurements with Cytotoxic Compounds. The basal ECAR of NIH-MDR1-G185 cells in pyruvate containing DMEM flow medium was determined as $V_0 = ((1.4 \pm 0.6) \times 10^7)\ H^+ \cdot cell^{-1} \cdot s^{-1}$ ($n = 74$ measurements, passage number >4). In the absence of pyruvate the value is at least
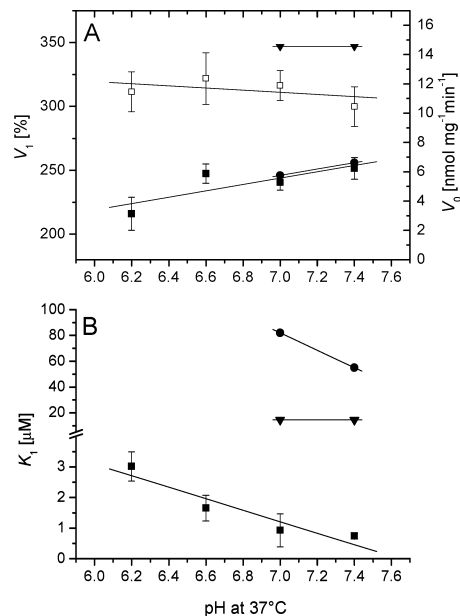
FIGURE 4: The effect of pH. A: Basal Pgp activity, V_0 ($\square$) (labels at the right-hand side), and maximum Pgp activity, V_1 (labels at left-hand side), for verapamil ($\blacksquare$), promazine ($\bullet$), and progesterone ($\blacktriangledown$) as a function of pH. B: Concentration of half-maximum Pgp activation, K_1, as a function of pH. Phosphate release measurements were performed in either 25 mM Tris-HCl or 25 mM Hepes-KOH buffer at 37 °C. The pH of phosphate release assay buffer was adjusted taking into account the temperature coefficient of the buffer. Data are expressed as the average of two to four measurements. Solid lines are linear regressions to the data. For data evaluation the average basal activity value in the pH range (pH 6.2 to pH 7.4) was used.

twice as large as shown previously (*2*). Figure 5A shows the stimulation of *MDR1*-transfected and wild-type cells with a single concentration of vinblastine (22.9 μM). First, cells were perfused with drug-free DMEM flow medium until a stable ECAR was reached. The first two points in Figure 5A correspond to the ECAR at the end of the equilibration phase (∼1 h) and were taken as basal values (100%). The ECAR comprises all the metabolic effects of the cell including basal Pgp activity. Cells were then stimulated for 3 min with vinblastine (hatched bar) during which two ECAR measurements (first and second stimulation point) were performed. The second stimulation point indicated as a solid symbol was used for the evaluation of Pgp activity (*24*). Cells were then again flushed with vinblastine-free flow medium. Nevertheless, the pronounced metabolic down regulation which had started already during the stimulation phase continued in wild-type and in transfected cells. Figure 5B shows the ECAR signals in *MDR1*-transfected cells as a function of time for different concentrations of vinblastine, and Figure 5C shows the evaluation of two different metabolic effects observed in *MDR1*-transfected cells. The upper solid line is the fit to the modified Michaelis−Menten equation (eq 1) and represents Pgp activation. The estimated concentration of half-maximum activation is somewhat higher than that for plasma membrane vesicles. The lower line is a fit to a Hill equation with an estimated half-
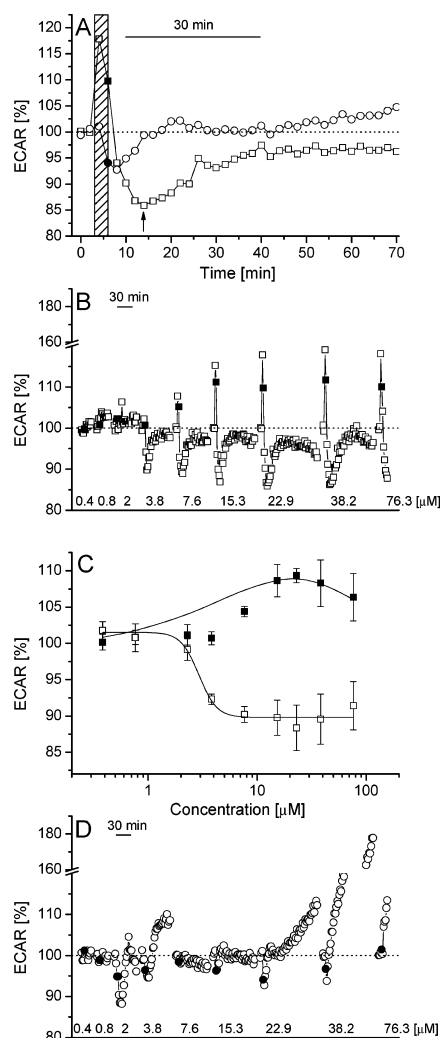
FIGURE 5: Time dependent ECAR of NIH-MDR1-G185 and NIH3T3 cells in response to increasing concentrations of vinblastine measured with a Cytosensor microphysiometer. A: ECAR of NIH-MDR1-G185 (squares) and NIH3T3 cells (circles) stimulated with 22.9 μM vinblastine as a function of time. The hatched box indicates the 3 min vinblastine stimulation period which comprises two measurement points, where the second measurement point is indicated as a filled symbol and is used for evaluation of Pgp activity if not otherwise stated. After the 3 min drug stimulation period cells were flushed again with drug-free flow medium. B: Time dependent ECAR of NIH-MDR1-G185 cells with increasing concentration of vinblastine (same type of measurement as in (A) but performed at different concentrations). C: ECAR of NIH-MDR1-G185 cells as function of vinblastine concentration. The second measurement point under vinblastine stimulation (■) most likely reflects Pgp activity and was fitted to a modified Michaelis–Menten equation (eq 1). The fit takes into account an estimated value for vinblastine adsorption to the Cytosensor tubing and debubbler membranes. Open squares (□) represent the fourth measurement point (indicated by arrow in (A)) and are fitted to a Hill equation. D: Time dependent ECAR of NIH3T3 cells with increasing concentration of vinblastine. The second measuring point is indicated as filled circles (●). Thirty minute time bars are included.

maximum inhibitory constant, IC$_{50}$ $\approx$ 2.9 μM, and may represent the inhibition of proton excretion by microtubules (*34*).

In wild-type cells (Figure 5D) low vinblastine concentrations caused a decrease in the ECAR which may again be attributed to the inhibition of proton excretion by microtubules starting, however, at even lower concentrations than in *MDR1*-transfected cells. Higher concentrations of vinblastine induced a strong continuous acidification which seems to be superimposed to the decrease in acidification at low concentrations. This strong continuous ECAR increase is typical for cell poisoning. Except daunorubicin, the other drugs measured so far showed no significant metabolic effects in wild-type cells (*24*).

DISCUSSION

We measured the activity of Pgp in inside-out vesicles formed from plasma membranes of mouse embryo fibroblasts (NIH-MDR1-G185) by monitoring the phosphate release rate for comparison with the Pgp activity measured previously in the corresponding living cells by monitoring the ECAR (*24*). For the present analysis Pgp was stimulated in a concentration-dependent manner with 19 different drugs, including cytotoxic compounds. Data were evaluated with a model proposed by Litman et al. (*19*) which assumes basal Pgp activity in the absence of drugs, activation of Pgp at low drug concentrations due to drug binding to a first binding region located in the cytosolic membrane leaflet, and inhibition at high drug concentrations due to drug binding to a second binding region (cf. eq 1). The large set of kinetic parameters is then used to get better insight into the relation between drug binding to the TMDs and ATP hydrolysis at the NBDs.

Comparison of the Kinetic Parameters from Plasma Membrane Vesicles and Living Cells. The comparison of Pgp activity in inside-out plasma membrane vesicles and living cells is shown in Figure 6A,B. The measurements in intact cells were performed at pH 7.4 (*24*), whereas the present phosphate release measurements were performed at pH 7.0. The slightly more acidic conditions were chosen to minimize drug association (cf. Materials and Methods) and vesicle aggregation (cf. Results). The basal activity of Pgp is practically not affected by the small pH difference as seen in Figure 4A which is in good agreement with previous investigations (*33*).

For the uncharged compounds or compounds with low ionization constants (pK_a $\leq$ 8.5) (open symbols) the *concentrations of half-maximum activation, K_1*, are identical within error limits, with the exception of three outliers, daunorubicin (*5*), lidocaine (*9*), and progesterone (*10*), which showed higher K_1 values in the phosphate release assay than expected. Daunorubicin and progesterone self-associate at high concentrations. Self-association may also partially explain the large divergence of published concentrations of half-maximum activation for daunorubicin (*19, 33, 35*). Daunorubicin moreover induces metabolic effects in living NIH3T3 and NIH-MDR1-G185 cells above 10 μM (*24*) which coincide with the concentration range of Pgp activity in plasma membrane vesicles. The hydrophilic local anesthetic, lidocaine, had to be applied up to high concentration (C_{sw} > 1 mM), which exhausted the buffer capacity of the
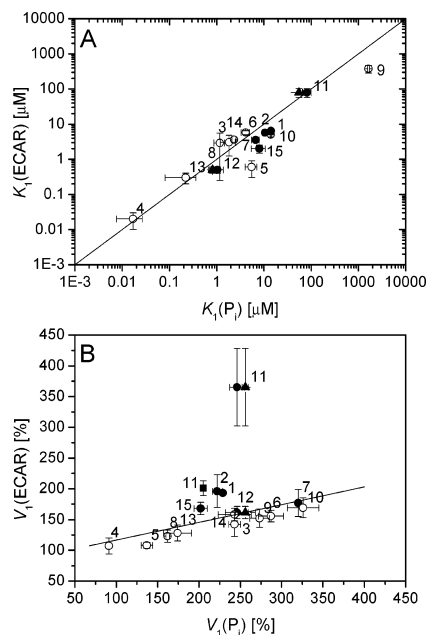
FIGURE 6: Comparison of kinetic data obtained with living cells (*24*) and inside-out membrane vesicles of NIH-MDR1-G185 cells. A: The concentration of half-maximum activation, K_1. B: Maximum Pgp activity, V_1. Phosphate release and ECAR assay, respectively, were performed at $T = 37$ °C, pH 7.0 and $T = 37$ °C, pH 7.4. Open circles (○) represent drugs with $pK_a \leq 8.5$, filled circles (●) drugs with $pK_a > 8.5$. Triangles (▲) represent values obtained with the phosphate release assay performed at pH 7.4. Data are expressed as the average of 2−15 measurements. The solid line in (A) is the diagonal to guide the eye, in (B) it is a linear fit without promazine (*11*). The Pgp activation profile for dibucaine (*6*) obtained from Cytosensor measurements was fitted to the simple Michaelis−Menten equation. In (B) the Pgp activation profiles for promazine (■) obtained from the Cytosensor and phosphate release assay, respectively, are also fitted to the simple Michaelis−Menten equation for comparison.

phosphate release buffer and led to an acidification of the solution (pH 6.83). As a result the lipid−water partition coefficient, K_{lw}, of the cationic compound decreased and the aqueous concentration required for half-maximum Pgp activation, K_1, increased concomitantly.

In the case of the highly charged compounds ($pK_a > 8.5$) (filled circles) the concentrations of half-maximum activation, K_1, were generally somewhat higher in the phosphate release assay (pH 7.0 at 37 °C) than in the ECAR assay (pH 7.4 at 37 °C), since the lipid−water partition coefficient, K_{lw}, was lower and the concentration for half-maximum Pgp activation, K_1, was higher. To illustrate the effect of the pH the K_1 values for verapamil and promazine obtained from phosphate release measurements performed at pH 7.4 (Figure 4B) were included in Figure 6A (filled triangles). As expected the K_1 values of the charged compounds moved to lower values and were in excellent agreement with those obtained by ECAR measurements (pH 7.4). In the pH range investigated the effect of pH on the activity of Pgp can therefore be attributed entirely to the pH dependence of the lipid−water partition coefficients, K_{lw}. Taking into account the possible artifacts and the pH difference, the concentra-

tions of half-maximum activation obtained in plasma membrane vesicles and living cells are in good agreement over the broad range investigated ($K_1 \sim 10^{-8}$ M for cyclosporin A to $K_1 \sim 10^{-3}$ M for lidocaine) (Figure 6A). The fact that exogenous substrates (e.g., drugs) approach Pgp from the extracellular side in living cells and from the cytosolic side in inside-out cellular membrane vesicles does not play a role, as long as the molecules can deprotonate and cross the bilayer in their uncharged form (*2*). The membrane concentration of substrates (which is much higher than the aqueous concentration) can thus be assumed to be identical in the two different systems.

Figure 6B shows a comparison of the maximum activities, V_1, expressed as relative values ([%] of the basal value). A good linear correlation is observed, whereby promazine (*11*) is an outlier. In the phosphate release assay the V_1 value of promazine was too low due to vesicle aggregation (cf. Figure 3). In the ECAR assay the V_2 value was too low due to an acidification of the medium at high promazine concentrations which led in turn to a too high V_1 value. Data evaluation using simple Michaelis−Menten kinetics (neglecting the inhibitory part) yields comparable V_1 values (see filled square in Figure 6B). Overall, the relative rates of Pgp activity, V_1, are higher in plasma membrane vesicles than in living NIH-MDR1-G185 cells since the basal phosphate release rates are lower than the basal ECARs which include basal Pgp activity and all other metabolic processes of the cell.

Pgp activity expressed as phosphate released per total protein concentration and time was determined as $V_0 = (12.3 \pm 1.3)$ nmol·mg^{-1}·min^{-1} ($n \approx 126$). Taking into account an average number of $(1.9 \pm 0.3) \times 10^8$ cells/mL, a molecular weight of 170 kDa, and 1.95×10^6 molecules of Pgp per cell, the basal and maximum verapamil-stimulated turnover number was calculated as 3.4 s^{-1} and 5.2 s^{-1}, respectively. Ambudkar et al. (*27*) and Al-Shawi et al. (*1*) obtained slightly lower basal (2.9 s^{-1} and 2.75 s^{-1}, respectively) and higher verapamil-stimulated values (9.9 s^{-1} and 8.8 s^{-1},[2] respectively). The differences may be due to the different lipid composition and the different lateral packing density of the membranes.

In living cells the ECAR was measured in the presence of pyruvate which reduces the basal value by (50−60)%. The basal ECAR obtained with the Cytosensor was in the absence and presence of pyruvate (($3.0 \pm 0.6) \times 10^7$) H$^+$·cell^{-1}·s^{-1} and (($1.4 \pm 0.6) \times 10^7$) H$^+$·cell^{-1}·s^{-1}, respectively (*2*). The drug-stimulated ECAR was linearly related to the basal value at low acidification rates. However, it flattened out at high basal acidification rates (Figure 9[3] in ref *2*). Since the buffer capacity of the medium was low, the solution acidified, which led in turn to a decrease in the ECAR (*36*, *37*). This negative feedback was recently corroborated by ^{13}C NMR measurements using ^{13}C-labeled glucose (unpublished result, G. Kohler, P. Äänismaa, A. Seelig, and J. Seelig). The maximum verapamil-stimulated turnover number measured with the Cytosensor in the

---

[2] The turnover number corresponds to the measured maximum Pgp activity for verapamil taken from Figure 1 in ref *1*.
[3] Verapamil-induced and basal ECAR in buffer with glucose without pyruvate (g+) is an average of data obtained with cells of low and high passage numbers whereas the other data points were obtained with cells of high passage numbers. If only data from high passage numbers were used, the value was higher (*2*).
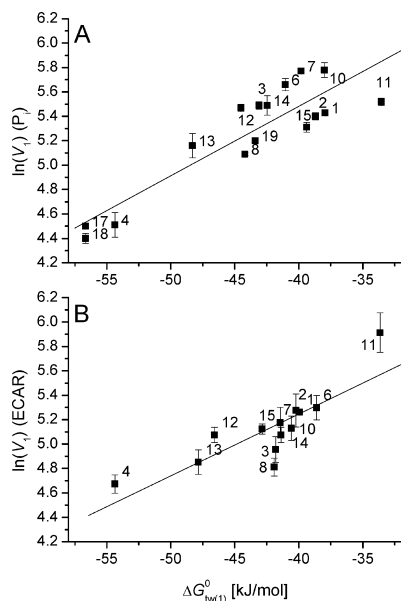
FIGURE 7: Correlation between the logarithm of the maximum Pgp activity, $\ln(V_1)$, obtained from phosphate release measurements at pH 7.0 (A) and from ECAR measurements at pH 7.4 (B) vs the free energy of drug binding from water to transporter, $\Delta G^0_{tw(1)}$. The maximum activity of Pgp, V_1, is expressed as a percentage of the basal rates taken as 100%. Data are presented as average of 2−15 measurements. Solid lines are linear regressions to the data with (A) a slope 0.06 ± 0.01 and an intercept 7.76 ± 0.34 ($R = 0.89 \pm 0.20$) and (B) a slope 0.05 ± 0.01 and an intercept 7.27 ± 0.44 ($R = 0.83 \pm 0.18$). Daunorubicin (*5*), lidocaine (*9*), and colchicine (*16*) are excluded from the fit in (A), and daunorubicin (*5*) and lidocaine (*9*) are excluded from the fit in (B) (cf. Results and Discussion).

presence of pyruvate (4.3 s^{-1}) was in close agreement with the number obtained with the phosphate release assay (5.2 s^{-1}). The effective value estimated from ECAR measurements in the absence of pyruvate must therefore be at least twice as large as supported by NMR measurements.

The Maximum Rate of ATP Hydrolysis by Pgp Depends on the Binding Affinity of the Drug from Water to the Transporter. To investigate the interplay between ATP hydrolysis at the NBDs and substrate binding and release at the TMDs, the maximum rate of Pgp activity, V_1 (Log scale), measured in inside-out membrane vesicles (at pH 7.0) and in living cells (at pH 7.4) was plotted as a function of the free energy of binding of the drug from the aqueous phase to the activating binding region of the transporter, $\Delta G^0_{tw(1)}$ (Figure 7A,B). The values of $\Delta G^0_{tw(1)}$ were derived from the concentration of half-maximum activation, K_1, as discussed previously (*24*). A linear correlation is observed which shows that the rate of phosphate release (Log scale) decreases with decreasing free energy of binding of the drug from water to the transporter, $\Delta G^0_{tw(1)}$ (or increasing binding affinity of the drug from water to the transporter).

A similar result was obtained previously by plotting the rate of Pgp activity either vs the free energy of binding from the lipid membrane to the transporter, $\Delta G^0_{tl(1)}$ (*17*), or vs the estimated free energy of hydrogen bond formation between

substrate and transporter (*10*, *38*). Since the value of ΔG^0_{lw} is rather constant for the majority of compounds, the two free energies, $\Delta G^0_{tl(1)}$ and $\Delta G^0_{tw(1)}$, tend to be linearly correlated (*24*). Litman et al. (*19*) have shown that the rate of intrinsic drug transport decreases with increasing molecular weight, which often correlates with the number of hydrogen bond acceptor groups in Pgp substrates and thus with the free energy, $\Delta G^0_{tl(1)}$. Exceptions are the so-called third generation inhibitors such as OC144-093 (cf. ref *17*) which show a very high affinity to the lipid membrane (E. Gatlik and A. Seelig, unpublished results) but only a moderate affinity from the lipid membrane to the transporter ($\Delta G^0_{lw} < \Delta G^0_{tl(1)}$). The classical "inhibitor" cyclosporin A exhibits in contrast an intermediate affinity for the lipid membrane and a high affinity from the lipid membrane to the transporter ($\Delta G^0_{lw} > \Delta G^0_{tl(1)}$). Since the free energy of binding from water to the transporter, $\Delta G^0_{tw(1)}$, which is the sum of ΔG^0_{lw} and $\Delta G^0_{tl(1)}$, is large for both, they are both effective so-called inhibitors.

The linear decrease of the rate of ATP hydrolysis (Log scale) with increasing binding affinity of the drug from water to the transporter (Figure 7A,B) suggests that drug release in the extracellular leaflet is the rate-determining step. This is consistent with the fact that high drug concentrations, which impede drug release, reduce the rate of ATP hydrolysis. It is also consistent with the fact that compounds such as cyclosporin A and OC144-093 with a high affinity from water to the transporter and thus a slow release from the TMDs function as inhibitors or modulators of Pgp. ATP hydrolysis to reset Pgp for a new transport cycle thus seems to start only after drug unloading.

REFERENCES

1. Al-Shawi, M. K., Polar, M. K., Omote, H., and Figler, R. A. (2003) Transition state analysis of the coupling of drug transport to ATP hydrolysis by P-glycoprotein, *J. Biol. Chem. 278*, 52629−52640.
2. Gatlik-Landwojtowicz, E., Aanismaa, P., and Seelig, A. (2004) The rate of P-glycoprotein activation depends on the metabolic state of the cell, *Biochemistry 43*, 14840−14851.
3. Gottesman, M. M., and Ambudkar, S. V. (2001) Overview: ABC transporters and human disease, *J. Bioenerg. Biomembr. 33*, 453−458.
4. Litman, T., Druley, T. E., Stein, W. D., and Bates, S. E. (2001) From MDR to MXR: new understanding of multidrug resistance systems, their properties and clinical significance, *Cell. Mol. Life Sci. 58*, 931−959.
5. Seelig, A., and Gerebtzoff, G. (2006) Enhancement of drug absorption by noncharged detergents through membrane and P-glycoprotein binding, *Expert Opin. Drug Metab. Toxicol. 2*, 733−752.
6. Urbatsch, I. L., Sankaran, B., Bhagat, S., and Senior, A. E. (1995) Both P-glycoprotein nucleotide-binding sites are catalytically active, *J. Biol. Chem. 270*, 26956−26961.
7. Senior, A. E., al-Shawi, M. K., and Urbatsch, I. L. (1995) The catalytic cycle of P-glycoprotein, *FEBS Lett. 377*, 285−289.
8. Raviv, Y., Pollard, H. B., Bruggemann, E. P., Pastan, I., and Gottesman, M. M. (1990) Photosensitized labeling of a functional multidrug transporter in living drug-resistant tumor cells, *J. Biol. Chem. 265*, 3975−3980.
9. Rosenberg, M. F., Callaghan, R., Modok, S., Higgins, C. F., and Ford, R. C. (2005) Three-dimensional structure of P-glycoprotein: the transmembrane regions adopt an asymmetric configuration in the nucleotide-bound state, *J. Biol. Chem. 280*, 2857−2862.
10. Omote, H., and Al-Shawi, M. K. (2006) Interaction of Transported Drugs with the Lipid Bilayer and P-Glycoprotein through a Solvation Exchange Mechanism, *Biophys. J. 90*, 4046−4059.

11. Urbatsch, I. L., Tyndall, G. A., Tombline, G., and Senior, A. E. (2003) P-glycoprotein catalytic mechanism: studies of the ADP-vanadate inhibited state, *J. Biol. Chem. 278*, 23171−23179.

12. Higgins, C. F., and Linton, K. J. (2004) The ATP switch model for ABC transporters, *Nat. Struct. Mol. Biol. 11*, 918−926.

13. Sauna, Z. E., and Ambudkar, S. V. (2001) Characterization of the catalytic cycle of ATP hydrolysis by human P-glycoprotein. The two ATP hydrolysis events in a single catalytic cycle are kinetically similar but affect different functional outcomes, *J. Biol. Chem. 276*, 11653−11661.

14. Dey, S., Ramachandra, M., Pastan, I., Gottesman, M. M., and Ambudkar, S. V. (1997) Evidence for two nonidentical drug-interaction sites in the human P-glycoprotein, *Proc. Natl. Acad. Sci. U.S.A. 94*, 10594−10599.

15. Sharom, F. J., Lugo, M. R., and Eckford, P. D. (2005) New insights into the drug binding, transport and lipid flippase activities of the p-glycoprotein multidrug transporter, *J. Bioenerg. Biomembr. 37*, 481−487.

16. Seelig, A. (2006) Unraveling membrane-mediated substrate-transporter interactions, *Biophys. J. 90*, 3825−3826.

17. Seelig, A., and Gatlik-Landwojtowicz, E. (2005) Inhibitors of multidrug efflux transporters: their membrane and protein interactions, *Mini-Rev. Med. Chem. 5*, 135−151.

18. Omote, H., and Al-Shawi, M. K. (2002) A novel electron paramagnetic resonance approach to determine the mechanism of drug transport by P-glycoprotein, *J. Biol. Chem. 277*, 45688−45694.

19. Litman, T., Zeuthen, T., Skovsgaard, T., and Stein, W. D. (1997) Structure-activity relationships of P-glycoprotein interacting drugs: kinetic characterization of their effects on ATPase activity, *Biochim. Biophys. Acta 1361*, 159−168.

20. Kerr, K. M., Sauna, Z. E., and Ambudkar, S. V. (2001) Correlation between steady-state ATP hydrolysis and vanadate-induced ADP trapping in Human P-glycoprotein. Evidence for ADP release as the rate-limiting step in the catalytic cycle and its modulation by substrates, *J. Biol. Chem. 276*, 8657−8664.

21. Garrigues, A., Nugier, J., Orlowski, S., and Ezan, E. (2002) A high-throughput screening microplate test for the interaction of drugs with P-glycoprotein, *Anal. Biochem. 305*, 106−114.

22. Broxterman, H. J., and Pinedo, H. M. (1991) Energy metabolism in multidrug resistant tumor cells: a review, *J. Cell. Pharmacol. 2*, 239−247.

23. Landwojtowicz, E., Nervi, P., and Seelig, A. (2002) Real-time monitoring of P-glycoprotein activation in living cells, *Biochemistry 41*, 8050−8057.

24. Gatlik-Landwojtowicz, E., Aanismaa, P., and Seelig, A. (2006) Quantification and characterization of P-glycoprotein-substrate interactions, *Biochemistry 45*, 3020−3032.

25. McConnell, H. M., Owicki, J. C., Parce, J. W., Miller, D. L., Baxter, G. T., Wada, H. G., and Pitchford, S. (1992) The cytosensor microphysiometer: biological applications of silicon technology, *Science 257*, 1906−1912.

26. Ambudkar, S. V. (1998) Drug-stimulatable ATPase activity in crude membranes of human MDR1-transfected mammalian cells, *Methods Enzymol. 292*, 504−514.

27. Ambudkar, S. V., Cardarelli, C. O., Pashinsky, I., and Stein, W. D. (1997) Relation between the turnover number for vinblastine transport and for vinblastine-stimulated ATP hydrolysis by human P-glycoprotein, *J. Biol. Chem. 272*, 21160−21166.

28. Sharom, F. J., Yu, X., and Doige, C. A. (1993) Functional reconstitution of drug transport and ATPase activity in proteoliposomes containing partially purified P-glycoprotein, *J. Biol. Chem. 268*, 24197−24202.

29. Fischer, H., Gottschlich, R., and Seelig, A. (1998) Blood-brain barrier permeation: molecular parameters governing passive diffusion, *J. Membr. Biol. 165*, 201−211.

30. Gerebtzoff, G., Li-Blatter, X., Fischer, H., Frentzel, A., and Seelig, A. (2004) Halogenation of drugs enhances membrane binding and permeation, *ChemBioChem 5*, 676−684.

31. Yahya, A. M., McElnay, J. C., and D'Arcy, P. F. (1988) Drug sorption to glass and plastics, *Drug Metab. Drug Interact. 6*, 1−45.

32. Meier, M., Blatter, X. L., Seelig, A., and Seelig, J. (2006) Interaction of verapamil with lipid membranes and P-glycoprotein: connecting thermodynamics and membrane structure with functional activity, *Biophys. J. 91*, 2943−2955.

33. Al-Shawi, M. K., and Senior, A. E. (1993) Characterization of the adenosine triphosphatase activity of Chinese hamster P-glycoprotein, *J. Biol. Chem. 268*, 4197−4206.

34. Arruda, J. A., Sabatini, S., Mola, R., and Dytko, G. (1980) Inhibition of H+ secretion in the turtle bladder by colchicine and vinblastine, *J. Lab. Clin. Med. 96*, 450−459.

35. Romsicki, Y., and Sharom, F. J. (1999) The membrane lipid environment modulates drug interactions with the P- glycoprotein multidrug transporter, *Biochemistry 38*, 6887−6896.

36. Kaminskas, E. (1978) The pH-dependence of sugar-transport and glycolysis in cultured Ehrlich ascites-tumour cells, *Biochem. J. 174*, 453−459.

37. Wilhelm, G., Schulz, J., and Hofmann, E. (1971) pH-dependence of aerobic glycolysis in ehrlich ascites tumour cells, *FEBS Lett. 17*, 158−162.

38. Seelig, A., and Landwojtowicz, E. (2000) Structure-activity relationship of P-glycoprotein substrates and modifiers, *Eur. J. Pharm. Sci. 12*, 31−40.

BI0619526

7.3 The Rate of P-glycoprotein Activation Depends on the Metabolic State of the Cell

Ewa Gatlik-Landwojtowicz, Päivi Äänismaa, and Anna Seelig*

Biophysical Chemistry, Biozentrum, University Basel, Klingelbergstrasse 70, CH-4056,
Basel, Switzerland
*Corresponding author, Phone: +41-61-267-22-06. Fax: +41-61-267-2-89. E-mail:
Anna.Seelig@unibas.ch

The Rate of P-Glycoprotein Activation Depends on the Metabolic State of the Cell[†]

Ewa Gatlik-Landwojtowicz, Päivi Äänismaa, and Anna Seelig*

Biophysical Chemistry, Biozentrum, University of Basel, Klingelbergstrasse 70, CH-4056 Basel, Switzerland

ABSTRACT: P-glycoprotein ATPase activity has been studied almost exclusively by measuring inorganic phosphate release from inside-out cellular vesicles. We have recently proposed a new method based on measurements of the extracellular acidification rate (ECAR) of living cells with a Cytosensor microphysiometer. This method allows for systematic investigation of the various factors influencing P-glycoprotein activation in living cells. Basal metabolic rates or ECARs of different *MDR1*-transfected cell lines were compared with those of the *Mdr1a$^{-/-}$1b$^{-/-}$* knockout, *MRP1*-transfected, and corresponding wild-type cell lines. Basal ECARs of all cells were on the order of 10^7 protons/cell/s, whereby those of genetically modified cells were on average (over all cell lines) slightly lower than those of wild-type cells. The expression level of P-glycoprotein in *MDR1*-transfected cells had no influence on basal ECARs. Verapamil-induced ECARs were specific for *MDR1*-transfected cells and increased with the expression level of P-glycoprotein. Moreover, ECARs were dependent on the metabolic state of the cell and were $(2.8 \pm 1.2) \times 10^6$ and $(8.0 \pm 1.5) \times 10^6$ protons/cell/s in glucose-deficient and glucose-fed NIH-MDR-G185 cells, respectively, after verapamil (10 μM) stimulation. The ECARs were practically identical to the rates of lactate extrusion and thus reflect the rates of ATP synthesis via glycolysis. Taking into account the number of P-glycoprotein molecules per cell, the rate of ATP hydrolysis in inside-out vesicles of the same cells was determined as $(9.2 \pm 1.5) \times 10^6$ phosphates/cell/s, in good agreement with the rate of ATP synthesized in glucose-fed cells. The energy required for P-glycoprotein activation *relative* to the basal metabolic energy was twice as large in glucose-deficient as in glucose-fed cells, suggesting cellular protection by P-glycoprotein even under conditions of starvation.

P-glycoprotein (Pgp),[1] a product of the multidrug resistance gene, *MDR1*, is an efflux transporter with broad substrate specificity. It binds a large variety of exogenous and endogenous toxic compounds within the plasma membrane and exports them to the extracellular environment (*1−3*). Transport of substrates by Pgp out of the cell is driven by metabolic energy. Per substrate transported one to two (or even three) molecules of ATP are hydrolyzed (*4−8*). The first molecule is proposed to drive drug transport and the second to reset the conformation of the transporter (*7*). However, even in the absence of exogenous substrates Pgp shows basal ATPase activity in plasma membrane vesicles (*9−11*) as well as in proteoliposomes (*12, 13*). Basal Pgp activity was suggested to arise either from transport of endogenous lipids (*14, 15*) or from uncoupled ATPase activity (*16, 17*).

Pgp activation can be measured with reconstituted proteoliposomes or inside-out membrane vesicles of *MDR1*-transfected cells by monitoring ATP hydrolysis via either inorganic phosphate release (*8, 9, 13*) or ADP formation (*10, 18*).

In intact *MDR1*-transfected cells Pgp activation can be analyzed noninvasively via extracellular proton secretion. As demonstrated, extracellular acidification rates, ECARs, of living cells can be quantified with a silicon-based potentiometric sensor (Cytosensor microphysiometer) (*19*), and the first systematic measurement of the effect of drugs on living *MDR1*-transfected cells has been published recently (*20*). Plots of the ECAR as a function of the logarithm of the drug concentration were bell-shaped, indicating activation at low and inhibition at high drug concentrations, and were consistent with Pgp activation/inhibition profiles measured previously by means of phosphate release measurements in inverted membrane vesicles for the same drugs (*9*). The concentrations of half-maximum activation for the different compounds investigated were practically identical for the two methods. Furthermore, a linear correlation between the rate of extracellular proton release and the intracellular phosphate release was obtained, indicating the quantitative equivalence of assays with plasma membrane vesicles and *living* cells (*20*).

Previous measurements of extracellular pH changes by conventional methods have led to conflicting results, arguing either in favor of (*21, 22*) or against extracellular acidification (*21, 23*). The bell-shaped activation/inhibition curves measured with the Cytosensor can partly explain these discrepancies since both activation and inhibition of extracellular acidification can be induced depending on the drug concentration employed.

* To whom correspondence should be addressed. Phone: +41-61 267 22 06. Fax: +41-61 267 21 89. E-mail: Anna.Seelig@unibas.ch.

[1] Abbreviations: ECAR, extracellular acidification rate; *MDR1*, multidrug resistance 1 gene; *MRP1*, multidrug resistance-associated protein gene; Pgp, P-glycoprotein, product of the *MDR1* gene.

Extracellular acidification reflects, in some general way, the *overall* metabolism of the cell (*24*). In contrast, the ATP hydrolysis assay involving proteoliposomes or inside-out vesicles is focused on a *single* metabolic event, analyzed without any relation to the metabolic state of the intact cell. Three general questions then emerge in this context. (i) To what extent is the metabolic activity of a living cell influenced by the expression level of Pgp? Whether Pgp overexpression influences the basal cellular metabolism is discussed controversially in the literature. Intracellular alkalization in cells overexpressing Pgp in comparison to wild-type cells has been observed by some investigators (*21*, *25*−*30*), whereas neither intracellular (*23*, *31*−*33*) nor extracellular basal pH changes were observed by others (*23*, *32*). Also no difference was found between cells overexpressing the multidrug resistance-associated protein, MRP1, and wild-type cells (*34*). (ii) How do variations of the metabolic state of the cell, such as starvation, regulate, in turn, the drug-induced activation of Pgp? ATP concentrations used in Pgp activation assays with inside-out membrane vesicles are rather high (3−7.5 mM) (*9*, *10*) since the Michaelis−Menten constant of ATP is $K_m = 0.33 \pm 0.04$ mM (*10*). In living cells, ATP concentrations are in a similar range or even higher under optimal conditions; however, they can vary with the metabolic state of the cell. Moreover, ATP has to be shared by different energy-dependent proteins. It is therefore of interest to test how the process of cellular detoxification by Pgp changes with the metabolic state of the cell. (iii) How is the general mechanism of extracellular acidification, under conditions of Pgp activation, linked to the specific process of Pgp-induced ATP hydrolysis?

The aim of the present work is therefore (i) to clarify the influence of the expression level of Pgp on basal metabolism, (ii) to measure the basal and verapamil-induced ECARs in living, *MDR1*-transfected cells under different metabolic conditions by means of a Cytosensor, (iii) to identify the export pathways of the acidic metabolites, and (iv) to compare the different ECARs obtained in living cells with the rate of Pgp ATP hydrolysis in inside-out vesicles of the same cells. Basal and verapamil-stimulated ECARs were assessed for different *MDR1*-transfected cell lines (*MDR1*-transfected pig kidney cells LLC-MDR1 (*35*), mouse embryo fibroblasts NIH-MDR-G185 (*36*)), for three other genetically modified cell lines (LLC-PK1 transfected with the human *MRP1* gene (*37*), cells 77.1 and 88.6, lacking functional Pgp, obtained from Mdr1a$^{-/-}$1b$^{-/-}$ mouse embryos (*38*)), and for the corresponding wild-type cell lines. In addition, special attention was given to the number of passages the various cell types had experienced since this turned out to be a further parameter influencing the basal extracellular acidification rates. The experiments will provide new insight into the mechanism of Pgp activation in living cells.

MATERIALS AND METHODS

Compounds. Colchicine, phloretin, and 2-deoxy-D-glucose were obtained from Fluka (Buchs, Switzerland), 4,4′-diisothiocyanatostilbene-2,2′-disulfonic acid, DIDS, verapamil, vincristine, and sodium pyruvate from Sigma (Steinheim, Germany), and lactate reagents and lactate standard solutions (Cat. Nos. 735-10 and 826-10, respectively) from Sigma Diagnostics Inc. (St. Louis, MO). The other chemicals were from Fluka, Merck, or Sigma. Complete EDTA-free

protease inhibitor cocktail tablets were obtained from Roche Diagnostics (Mannheim, Germany), 1,4-dithiol-DL-threit(ol), DTT, was from Applichem (Darmstadt, Germany), and BCA protein assay reagents were purchased from Pierce (Rockford, IL). DMEM (liquid and dry, Cat. Nos. 21969 and 52100, respectively) without pyruvate, IMDM medium, and other compounds required for cell culture such as fetal bovine serum, FBS, bovine serum albumin, BSA, and antibiotics were from Gibco-BRL (Basel, Switzerland). P-glycoprotein antibody, MRK16, and unspecific antibody, IgG$_{2ak}$, were from Kamiya Biomedical Co. (Seattle, WA), and the IgG$_{2a}$ FITC-labeled antibody was from PharMingen (San Diego, CA).

Cell Lines. The mouse embryo fibroblast wild-type lines (2ac.1 and 2ac.2) and lines lacking functional Pgp (77.1 and 88.6) from Mdr1a$^{-/-}$1b$^{-/-}$ mouse embryos were generously provided by Dr. A. H. Schinkel (The Netherlands Cancer Institute, Amsterdam, The Netherlands), the pig kidney epithelial cell lines LLC-PK1, LLC-PK1 transfected with the human *MDR1* gene (LLC-MDR1), and LLC-PK1 transfected with the human *MRP1* gene (LLC-MRP1) by Dr. P. Borst (The Netherlands Cancer Institute), and the mouse embryo fibroblast lines NIH3T3 and NIH3T3 transfected with the human *MDR1* gene (NIH-MDR-G185) by Dr. M. M. Gottesman (The National Institutes of Health, Bethesda, MD).

Cell Culture. All cell lines were grown under the same conditions in monolayer culture in DMEM medium (4.5 g/L glucose) supplemented with fetal bovine serum (10% v/v), penicillin (100 units/mL), streptomycin (100 μg/mL) and L-glutamine (146 mg/L) at 37 °C in an atmosphere containing CO_2 (5%). NIH-MDR-G185 and LLC-MDR1/V cells were grown in the presence of colchicine (0.15 μM) and vincristine, V (0.32 μM), respectively. The cells were passaged every 3−4 days. For quantitative comparisons cells with identical passage numbers were used. The cells were counted with a hemocytometer.

Detection of Pgp Expression. The expression level of Pgp in wild-type (LLC-PK1 and NIH3T3) and transfected (LLC-MDR1, LLC-MDR1/V, and NIH-MDR-G185) cells was estimated using the monoclonal antibody MRK16, which recognizes only human Pgp. Aliquots of (2−3) × 10^5 cells were incubated in IMDM containing 5% FBS at 37 °C for 30 min in the presence of MRK16 or the unspecific antibody IgG$_{2ak}$. After washing, the cells were reincubated at 37 °C for 30 min in the dark, in the presence of the fluorescent FITC-labeled antibody. The cells were resuspended in phosphate-buffered saline (containing 1% BSA), and the fluorescence intensities for 10000 events per cell sample were analyzed using a FACSort flow cytometer (Becktron, Dickinson) and the software Win MDI for data analysis.

Cytosensor Measurement. ECARs of intact cells were measured using an eight-channel Cytosensor microphysiometer (Molecular Devices, Menlo Park, CA) described elsewhere in detail (*20*, *39*). The cells were seeded into 12 mm diameter polycarbonate cell capsule cups at a density of 3 × 10^5 cells per cup in culture medium. Usually the cells were incubated overnight at 37 °C before the measurement (*20*). This protocol was followed for measurements of relative ECARs (data shown in Figures 4, 7, and 8). For quantification of ECARs (data shown in Figures 2, 3, 5, 6, and 9) the cells were prepared 4 h prior to the Cytosensor experiment,

Gatlik-Landwojtowicz et al.

since the number of cells seeded remained approximately constant within this period of time. After incubation, capsule spacers and inserts were put into the cups, and the cells were thus located between two polycarbonate membranes which together with the spacer ring form a tight chamber of 2.8 μL with fluid contact to the potentiometric sensor chip. Measurements were performed at 37 °C. The acidification rates were measured during periodic interruptions of the flow of the medium through the flow chambers (for details see ref *20*). Each pump cycle lasted 2 min, during which time the pumps were on for 1 min 40 s and were then switched off for the remaining 20 s. During the pump-off period (from 1 min 45 s to 1 min 58 s) in each pump cycle the rate of extracellular pH changes were calculated by the Cytosoft program. The ECAR was determined as the slope of a linear least-squares fit to pH versus time data (μV/s), where -1 μV/s corresponds to an acidification rate of 0.001 pH unit/min at pH 7.4. After a constant acidification rate was reached ($\sim$60–70 min), the flow medium was replaced by drug-containing medium. The cells were exposed to a 40 s pulse of a drug. The flow was then stopped, and the acidification rate was measured for 13 s. Perfusion with the drug solution was continued for another 2 min (the total drug perfusion interval was thus 160 s), and the ECAR was measured again (see ref *20*, Figure 1). The acidification rate was normalized to a basal acidification (defined as 100%) averaged over the two pump cycles before drug addition. The actual cellular response is given either in percentage over the basal activity or in absolute values of protons per cell, per second (H$^+$/cell/s).

Flow Medium and Buffer. The flow medium was prepared from the commercially available dry powder DMEM medium lacking sodium bicarbonate to have a low buffer capacity and to avoid formation of bubbles during the measurement. To preserve osmotic balance, sodium bicarbonate was replaced by sodium chloride (0.7 g of NaCl instead of 1 g of NaHCO$_3$). To adapt the cells to the conditions required for glucose deprivation and quantitative experiments, the flow medium was exchanged for flow buffer containing CaCl$_2$ (0.3 mM), MgCl$_2$ (0.6 mM), KH$_2$PO$_4$ (0.5 mM), KCl (3 mM), Na$_2$HPO$_4$ (0.5 mM), and NaCl (130 mM), with glucose (10 mM), buffer$_{g+}$, glucose and sodium pyruvate (1 mM), buffer$_{g+p+}$, no glucose but pyruvate, buffer$_{g-p+}$, or neither glucose nor pyruvate, buffer$_{g-p-}$. At the beginning of a measurement the pH of the solution was always adjusted to 7.4 at room temperature.

Quantification of Acid Export. To quantify the number of protons excreted by the cells within a certain time interval, the buffer capacity, β, and the number of cells in a flow chamber ($V = 2.8$ μL) have to be known. For flow buffer at pH 7.4 containing KH$_2$PO$_4$ (0.5 mM) and Na$_2$HPO$_4$ (0.5 mM) the buffer capacity was calculated according to Owicki (*24*) as $\beta = 0.40$ mM. For the phosphate salts we used a pK_a of 6.83 (6.865 at 25 °C) (*40*), which is in agreement with a value measured in our laboratory (X. Li Blatter, unpublished results) instead of the pK_a of 6.76 at 37 °C used previously (*20, 24*). The buffer capacity of the DMEM flow medium is $\beta = 0.56$ mM, calculated as the sum of the buffer capacities of phosphate salts (0.91 mM) and amino acids, in particular glutamine (4 mM), histidine (0.2 mM), and cysteine (0.4 mM).

Due to the space limitation by the spacer, the number of cells in the measuring chamber, which give rise to the ECAR recorded by the sensor chip, corresponds to about 25% of the total cells seeded, that is $N_c = 0.75 \times 10^5$ cells, provided the sensors are equally distributed in the capsule cup. Each of the sensors was calibrated at 37 °C with pH standard buffer solutions (Schott Glas, Mainz, Germany) within a range of pH of 6.81–8.87. According to the calibration, cal = 61.0 $\pm$ 1.1 mV corresponds to 1 pH unit. The ECARs (μV/s) recorded were transformed to protons released per cell per second as follows:

$$\text{ECAR (H}^+/\text{cell/s)} = [\text{ECAR (V/s)}][\beta \text{ (M)}][V \text{ (L)}]N_A/[\text{cal (V)}]N_c$$

where N_A is the Avogadro number. Units are given in parentheses.

Determination of Lactate Concentration. Total lactate production by NIH3T3 and NIH-MDR-G185 cells during basal and verapamil-induced metabolic rates was determined using a standard lactate spectrophotometric assay based on lactate oxidase and peroxidase activity (Sigma, Cat. No. 735-10, St. Louis, MO). The cells from 17–20 passages (9–10 weeks) were prepared as described before. The cells were perfused for $\sim$1 h in the Cytosensor with buffer$_{g+}$. Next, the cells were stimulated continuously for another 1 h with verapamil (6 μM) containing buffer$_{g+}$. The phosphate buffer leaving the Cytosensor chambers was collected, condensed by lyophilization, diluted 15 times with water, and assayed using the protocol provided by the lactic acid assay kit obtained from Sigma (which is adapted with minor changes from ref *41*). The number of lactate molecules produced per cell per second were calculated taking into account the total number of cells (3 $\times$ 10^5) placed on the capsule cup and an average flow rate of 83 μL/min, including pump-on and pump-off periods. In contrast to ECAR measurements where only about 25% of the cells are in contact with the sensor chip, all cells in the sensor chamber contribute to the acidification of the waste buffer leaving the sensor chamber.

Plasma Membrane Vesicle Preparation. The cell membranes were prepared as described previously (*42*) with some modifications. Briefly, cells washed once with PBS buffer were scraped into ice-cold PBS, pH 7.0, supplemented with protease inhibitors (1 tablet/50 mL of PBS). Next the cells were washed with hypotonic lysis buffer (10 mM Tris–HCl, pH 7.5, 10 mM NaCl, 1 mM MgCl$_2$, 1 protease inhibitor cocktail tablet/50 mL) by centrifugation at 2100g_{max} for 10 min at 4 °C. The pellet was resuspended in lysis buffer (5 mL per each of four 15 cm dishes) and was then frozen rapidly in dry ice. The frozen cell suspension was stored at -80 °C until later use. The cell suspension was thawed at room temperature and was then incubated on ice 30–45 min prior to the disruption of cells with a "One Shot" cell disrupter (Constant Systems Ltd., Warwickshire, U.K.) at 400 bar. The cell lysate was diluted 1:1 with ice cold isotonic buffer (10 mM Tris–HCl, pH 7.4, 250 mM sucrose, 50 mM *N*-methyl-D-glucamine, NMDG, 1 protease inhibitor cocktail tablet/50 mL buffer), and the unbroken cells and nuclei were precipitated by centrifugation at 800g_{max} for 10 min at 4 °C. Subsequently mitochondria were removed by centrifugation at 6000g_{max} for 10 min at 4 °C, and in the final centrifugation (100000g_{max}, 1 h, 4 °C) the crude membranes were pelleted.

P-Glycoprotein Activation and the Cellular Metabolic State

The pellet was resuspended with isotonic buffer, homogenized by aspiration through a 23-gauge syringe, and stored at -80 °C until use. The protein content of the membrane vesicles ($9-10$ mg/mL) was determined by BCA protein assay using bovine serum albumin as a standard.

ATPase Activation Assay. The P-glycoprotein-associated ATPase activity in plasma membrane vesicles was measured as described previously (*42*) with an adjustment to the assay carried out in a 96-well microtiter plate, with a reaction volume of 40 μL/well. The membrane suspension ($5-13$ μg of protein) was first incubated for 5 min at 37 °C with ATPase assay buffer (50 mM Tris$-$HCl, pH 7.5, 150 mM NMDG, 5 mM sodium azide, 1 mM EGTA, 1 mM ouabain, 2 mM DTT, and 10 mM MgCl$_2$) with or without 0.3 mM sodium vanadate. The reaction mixture was then incubated for 3 min at 37 °C with 5 μL of verapamil stock solution (80 μM in water, containing 5% DMSO). The final verapamil concentration was 10 μM and the final DMSO concentration was 0.625% (v/v). The reaction was initiated by addition of ATP solution (final concentration 5 mM in 40 μL). After 20 min of incubation at 37 °C the reaction was stopped by addition of 30 μL of 10% (w/v) SDS. For the estimation of released inorganic phosphate (P$_i$) 250 μL of ice-cold medium (0.2% (w/v) ammonium molybdate, 1.3% (v/v) sulfuric acid, 2.3% (w/v) trichloroacetic acid, and freshly prepared 1% (w/v) ascorbic acid) was added to each well. After 100 min of incubation at room temperature the absorbance at 820 nm was measured using a Spectramax M2 microplate reader (Molecular Devices, Sunnyvale, CA). Control measurements were performed with the appropriate DMSO concentrations.

Error Calculations. The error bars given in Figures 2, 3, and $5-9$ correspond to standard deviations, SDs. The statistical significance of the data in Figure 6 was calculated with the Student's *t* test.

RESULTS

Expression Level of Pgp in MDR1-Transfected Cell Lines. The level of Pgp expression in *MDR1*-transfected cells (LLC-MDR1, LLC-MDR1/V, and NIH-MDR-G185) and the corresponding wild-type cells (LLC-PK1 and NIH3T3) was studied by FACS using the monoclonal antibody MRK16 and a fluorescent, FITC-labeled second antibody. Figure 1 displays the cell count as a function of the relative fluorescence intensities (logarithmic scale) for the different cell lines studied. Cells overexpressing human Pgp (lines 1, 2, and 4) exhibit distinctly higher fluorescence intensity than wild-type cells (lines 3 and 5). Whereas LLC-MDR1/V cells grown in the presence of vincristine (line 1) and NIH-MDR-G185 grown in the presence of colchicine (line 4) show one population at high fluorescence intensity, LLC-MDR1 cells grown in the absence of vincristine show two populations, the first one at low ($\sim$25% of the cells) and the second one at high fluorescence ($\sim$75% of the cells) intensity. The content of human Pgp in the whole cell population was expressed as the ratio of the median fluorescence intensities (MFIs) of MRK16-labeled cells and isotype control IgG2a-labeled cells. It increases in the order wild-type cells (MFI = 1) < LLC-MDR1 (MFI = 23) < LLC-MDR1/V (MFI = 38) < NIH-MDR-G185 (MFI = 79). The expression level of endogenous Pgp in wild-type (2ac.1, 2ac.2, NIH3T3 (*38*), LLC-PK1 (*43*)), *Mdr1a$^{-/-}$1b$^{-/-}$* knockout (*38*), and LLC-

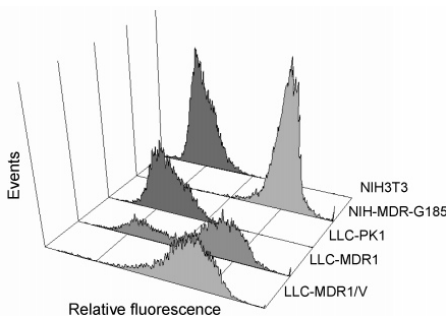

FIGURE 1: Expression of human Pgp monitored by immunoflow cytometry, FACS. Histograms represent the cell number versus fluorescence intensity expressed as the logarithm of the relative fluorescence intensity. Each distribution was obtained from collecting 10^4 cells labeled with MRK16 antibody. Transfected cell lines LLC-MDR1/V (grown in the presence of vincristine (0.32 μM)) (line 1), LLC-MDR1 (line 2), and NIH-MDR-G185 (grown in the presence of colchicine (0.15 μM)) (line 4) are shown in light gray and the corresponding wild-type cells LLC-PK1 (line 3) and NIH3T3 (line 5) in dark gray. Cells of high passage numbers (pn > 4) were used.

MRP1 (*37*) cells has been estimated previously by means of Western blot analysis and was not further analyzed. The expression level of Pgp thus increases in the order *Mdr1a$^{-/-}$1b$^{-/-}$* knockout cells (77.1, 88.6) < wild-type cells (2ac.1, 2ac.2, LLC-PK1, NIH3T3) $\approx$ LLC-MRP1 < LLC-MDR1 < LLC-MDR1/V < NIH-MDR-G185. Experiments were performed with cells of higher passage number (pn > 4). In the following we assume that the expression level of Pgp does not change with the passage number in the range of $2-20$ passages after defreezing.

Basal ECARs of the Different Genetically Modified Cell Lines. ECARs were monitored by means of a Cytosensor microphysiometer with four or eight parallel measuring chambers. Each chamber contained a potentiometric sensor chip measuring the extracellular acidification rate (μV/s) during periodic interruptions of the flow of the medium through the flow chambers (*19*). At 61 mV/pH unit and taking into account the buffer capacity, β, of the flow medium, the net flow of protons per second per cell was calculated (cf. Materials and Methods).

In our previous investigations MEM or DMEM was used as the flow medium to measure Pgp activation (*20*). However, since the effect of nutrients on the Pgp-induced cell activity was to be studied, the present measurements were made with simple buffer solutions. We first compared the basal ECARs of the different cell lines in DMEM with those obtained with phosphate buffer containing 10 mM glucose (buffer$_{g+}$) to test whether cellular metabolism was affected by the omission of the amino acids and vitamins present in DMEM. For this purpose, the cells were first exposed to DMEM (buffer capacity $\beta = 0.56$ mM) until stable basal ECARs were reached (75 min). DMEM was then replaced by glucose-containing buffer$_{g+}$ (buffer capacity $\beta = 0.40$ mM). Parts A (DMEM) and B (buffer$_{g+}$) of Figure 2 display the ECARs of the 10 cell lines employed in this study, ordered according to increasing expression levels of Pgp, that is, *Mdr1a$^{-/-}$1b$^{-/-}$* knockout cells (77.1, 88.6) < wild-type cells (2ac.1, 2ac.2, LLC-PK1, NIH3T3) $\approx$ LLC-MRP1 < LLC-MDR1 < LLC-MDR1/V < NIH-MDR-
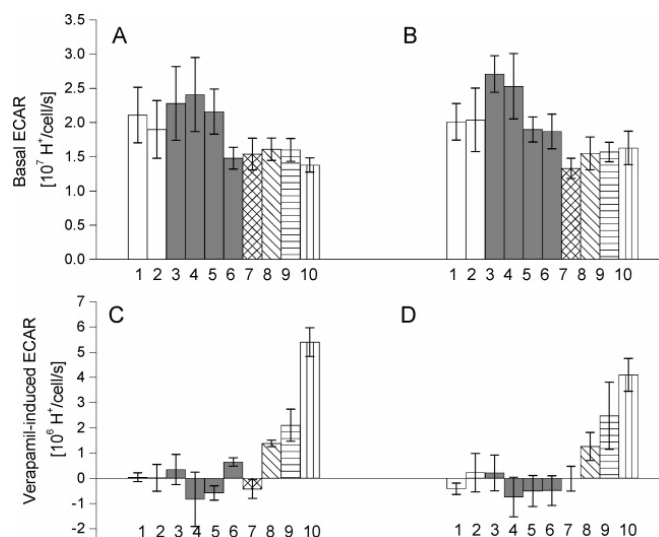
FIGURE 2: Basal extracellular acidification rates, ECARs (A, B), and verapamil (10 μM)-induced ECARs after subtraction of the basal ECARs (C, D) of *Mdr1a$^{-/-}$1b$^{-/-}$* knockout cells 77.1 (1) and 88.6 (2) (white columns), wild-type cells 2ac.1 (3) 2ac.2 (4), LLC-PK1 (5), and NIH3T3 (6) (gray columns), and cells transfected with *MRP1* or *MDR1* genes, LLC-MRP1 (7), LLC-MDR1 (8), LLC-MDR1/V (9), and NIH-MDR-G185 (10) (patterned columns). The cells were exposed to DMEM (A, C) or to phosphate buffer containing 10 mM glucose (B, D). The cells were defrozen 2−3 passages prior to the measurements. Error bars correspond to $n = 3-4$ measurements.

G185. After correction for the different buffer capacities, the ECARs of a given cell line in DMEM and in glucose buffer$_{g+}$ were practically identical. Furthermore, parts A and B of Figure 2 demonstrate that the basal ECARs of the different cell lines are similar and in the range of (1.4 ± 0.1) × 10^7 to (2.4 ± 0.5) × 10^7 H$^+$/cell/s (−66 ± 5 to −117 ± 26 μV/s) for DMEM and (1.3 ± 0.2) × 10^7 to (2.7 ± 0.3) × 10^7 H$^+$/cell/s (−89 ± 10 to −183 ± 18 μV/s) for buffer$_{g+}$. However, the ECARs of wild-type cells (gray columns) are on average 30 ± 10% larger than those of knockout (white columns) and transfected (patterned columns) cells. Considering only *MDR1*-transfected and the corresponding wild-type cells, the difference is lower (20 ± 4%). For the experiments shown in Figure 2 cells from a narrow range of cell passages after defreezing (pn = 2−3) were used to get optimal synchronization of cells.

The number of cell passages had a distinct influence on the ECAR as exemplified in Figure 3 for NIH-MDR-G185 cells, knockout cells (77.1), and the corresponding wild-type cells. At low passage numbers (pn = 2−3) the ECARs were lower than at higher passage numbers (pn ≥ 4). Basal ECARs of the second data set with high passage numbers, analogous to those in Figure 2, were on average over all cell lines 60 ± 40% higher than those of low passage numbers, whereby the difference between the basal ECARs of low and high passage numbers was lower (~20%) for *Mdr1a$^{-/-}$1b$^{-/-}$* knockout cells (77.1, 88.6) and the corresponding wild-type cells (2ac.1, 2ac.2) and higher (80−100%) for transfected cells (LLC-MRP1, LLC-MDR1, LLC-MDR1/V, NIH-MDR-G185). At higher passage numbers (pn > 4) the difference in ECARs between NIH-MDR-G185 and the corresponding wild-type cells therefore practically disappeared (Figure 5A).

Basal ECARs under Starvation Conditions. Next the activity of NIH-MDR-G185-transfected cells was tested after
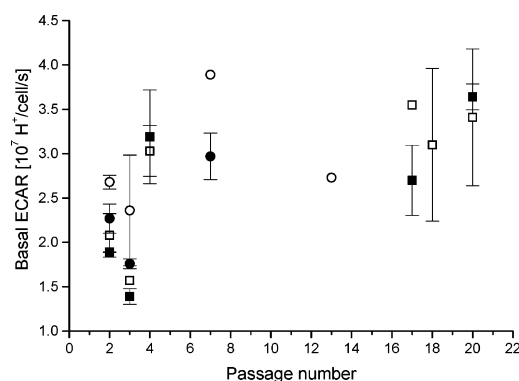

FIGURE 3: Basal extracellular acidification rate as a function of the passage number of NIH-MDR-G185 (■), NIH3T3 (□), *Mdr1a$^{-/-}$1b$^{-/-}$* knockout cells 77.1 (●) and 2ac.2 (○) cells as a function of the passage number. Measurements were performed in phosphate buffer containing 10 mM glucose. Error bars correspond to $n = 2-6$ measurements.

withdrawal of exogenous carbon sources. The metabolic response is seen in Figure 4. During period A, cells were perfused with buffer$_{g+}$ until a stable basal ECAR was reached. A preequilibration period of ~60 min is not shown. The basal ECAR was normalized and defined as 100%. As a control, perfusion with glucose buffer (buffer$_{g+}$) was continued in one chamber (■, no change in the ECAR occurring).

When sodium pyruvate (1 mM) was added to glucose buffer (buffer$_{g+p+}$, ▼), a significant decrease in the ECAR was observed. Pyruvate (1 mM) without glucose (buffer$_{g-p+}$, ○) led to an even larger decrease in the ECAR. Complete
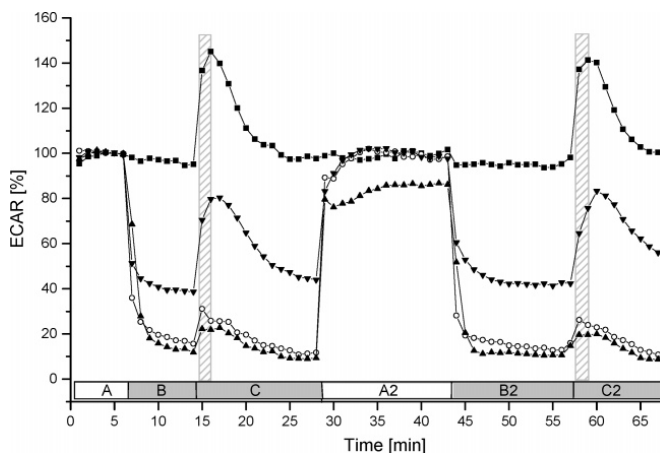
FIGURE 4: Effect of glucose and sodium pyruvate on the basal and verapamil-induced acidification rate of NIH-MDR-G185 cells. Cells of high passage numbers were used (pn > 20). During period A (indicated in white), the cells in all four chambers were exposed to phosphate buffer with glucose, buffer$_{g+}$. During periods B and C (indicated in gray) only one chamber was perfused with buffer$_{g+}$ (■); the others were perfused with buffer containing in addition 1 mM sodium pyruvate, buffer$_{g+p+}$ (▼), buffer containing 1 mM sodium pyruvate without glucose, buffer$_{g-p+}$ (○), or buffer containing neither glucose nor pyruvate, buffer$_{g-p-}$ (▲). Periods A−C were repeated (A2, B2, C2). Hatched bars indicate the interval (160 s) during which the cells were perfused with verapamil (6 μM). The basal ECAR of cells in buffer$_{g+}$ was defined as 100%. Results are normalized to the baseline and are expressed as a percent of the basal acidification rate.

elimination of all carbon sources (buffer$_{g-p-}$, ▲) caused a further small decrease.

Comparing the different cell lines, the average reduction of basal ECARs due to addition of pyruvate was more pronounced for mouse embryo fibroblasts ($50 \pm 10\%$, wild-type and transfected NIH cells) than for pig kidney cells ($15 \pm 4\%$, wild-type and transfected cells) (not shown). If glucose was removed or replaced by its nonmetabolizable analogue deoxyglucose, the basal ECARs of all cell lines tested were reduced by 75−90%.

Figure 5A then compares the basal ECARs of wild-type and transfected cells in the presence (□, ■) and absence (○, ●) of glucose, where open and closed symbols represent ECARs of cells with low (pn = 2−3) and high (pn = 4−20) passage numbers, respectively. Basal ECARs (logarithmic scale) are plotted as a function of the median fluorescence intensity representing the expression level of human Pgp. As a general conclusion it follows that under equivalent conditions of nutritional state and passage number wild-type and *MDR1*-transfected cells exhibit rather similar metabolic activity.

Verapamil-Induced Extracellular Acidification Rates. Figure 4, period C, displays the variation of the ECARs of NIH-MDR-G185 cells upon addition of verapamil under different nutritional conditions. We first discuss verapamil effects under normal nutritional conditions, that is, when the cells are perfused with buffer$_{g+}$ (uppermost curve in Figure 4, ■). At the beginning of period C, verapamil was added to buffer$_{g+}$ at a concentration of 6 μM during 160 s (hatched bar). After this stimulation interval the cells were again perfused with buffer$_{g+}$. Immediately after stimulation, the ECAR increases, indicating a distinct increase in acid production induced by verapamil. After the return to normal buffer$_{g+}$ the ECAR returns to basal values. Analogous measurements were performed for all 10 cell lines, and the quantitative evaluation for cells with pn = 2−3 is sum-

marized in Figure 2C,D. The values given correspond to the ECAR increase measured at the end of the 160 s stimulation interval. The verapamil-induced ECARs in DMEM (Figure 2C) and buffer$_{g+}$ (Figure 2D) are practically identical. Parts C and D of Figure 2 show that an increase in ECARs upon verapamil stimulation is observed only for cells overexpressing P-glycoprotein (columns 8−10), and that the increase in ECARs is proportional to the expression level of Pgp (see also Figure 5B,C).

We then tested whether Pgp activation by verapamil was still possible under starvation conditions. As seen in Figure 4, period C, verapamil stimulation induced a distinct ECAR increase under all buffer conditions, even in the absence of exogenous carbon sources. The stimulation cycle in Figure 4 (periods A−C) was then repeated. In period A2 the cells were again perfused with buffer$_{g+}$ in all four chambers. Cells treated with buffer$_{g+p+}$ (▼) and buffer$_{g-p+}$ (○) during periods B and C reversed to the initial ECARs within 5 min, whereas cells treated with buffer$_{g-p-}$ (▲) did not recover completely even after 15 min. Verapamil stimulation in period B2 yielded results very similar to those of period B. Even cells in buffer$_{g-p-}$ which had not recovered completely showed a similar ECAR upon the second verapamil stimulation.

The verapamil stimulation cycle in Figure 4 was repeated for a third time (data not shown) to test inhibition of verapamil-induced ECARs by cyclosporin A. For this purpose, cyclosporin A (1 μM) was added to the four different buffers and NIH-MDR-G185 cells were preincubated for 20 min followed by stimulation with verapamil, again in the presence of cyclosporin A. This led to an inhibition of the verapamil-induced ECARs by 50−60% under all buffer conditions, in agreement with previous inhibition values (*20*).

Parts B and C of Figure 5 display the *absolute* and *relative* increase in ECARs upon verapamil stimulation (10 μM) of *MDR1*-transfected and wild-type cells in the presence (□,
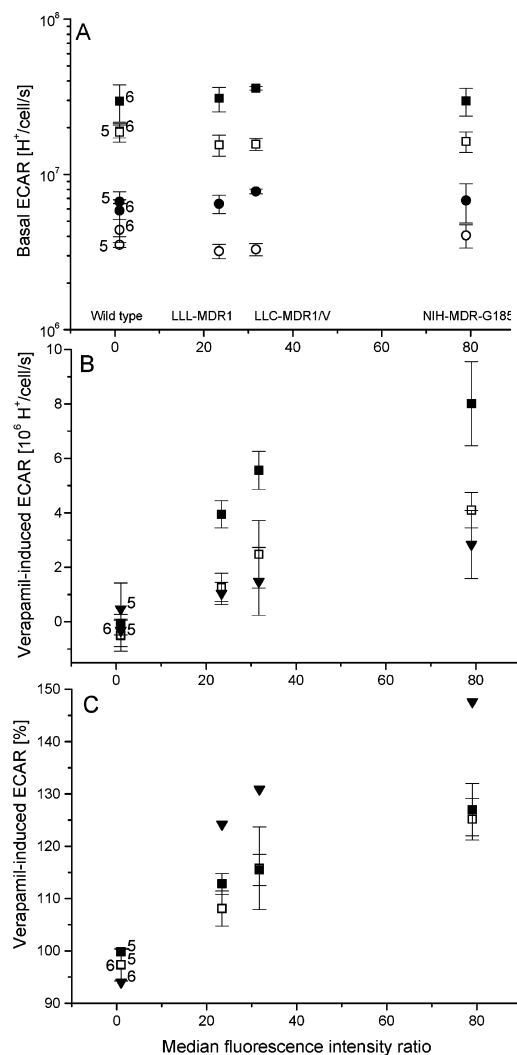
FIGURE 5: Basal (A) and verapamil (10 μM)-induced ECAR as a function of the expression level of human Pgp in cells given in absolute values (B) and relative values, where basal ECARs were taken as 100% (C). The expression level of Pgp was determined by FACS analysis and is expressed in MFIs for wild-type cells (MFI = 1) (LLC-PK1 (label 5), NIH3T3 (label 6)) and *MDR1*-transfected cells (LLC-MDR1 (MFI = 23), LLC-MDR1/V (MFI = 38), NIH-MDR-G185 (MFI = 79)). The cells for ECAR experiments were defrozen either 2−3 passages or 4−20 passages prior to the measurements, and the values given correspond to an average of $n = 3-4$ ($\square$, $\bigcirc$) or $n = 2-17$ ($\blacksquare$, $\bullet$) measurements. Both sets of data were measured in the presence (buffer$_{g+}$) (squares) and absence (buffer$_{g-p-}$) (circles) of glucose. Verapamil-induced ECARs (B, C) in the absence of glucose are shown as average values of all measurements ($n = 4-21$) for cells defrozen 2−20 passages prior to the measurements ($\blacktriangledown$).

$\blacksquare$) and absence ($\blacktriangledown$) of glucose plotted as a function of the expression level of Pgp. Under all conditions ECARs increased with the expression level of Pgp. *Absolute* ECARs (Figure 5B) were higher in the presence ($\square$, $\blacksquare$) than in the absence ($\blacktriangledown$) of glucose. However, if expressed as percent changes *relative* to the corresponding basal ECAR (Figure 5C), glucose-deprived cells showed a distinctly larger verapamil-induced stimulation than glucose-fed cells.

ECARs of cells with higher passage numbers (pn = 4−20) ($\blacksquare$) are higher than those of cells from low passage numbers (pn = 2−3) ($\square$) if given in absolute values (Figure 5B). However, if again expressed as percent changes of basal ECARs, the two data sets are practically identical (Figure 5C). For the sake of clarity, the data obtained for glucose-deprived cells with low and high passage numbers were averaged in Figure 5B,C ($\blacktriangledown$). The largest relative increase is clearly observed for cells under starvation conditions (cf. also Table 1).

Rate of Lactic Acid Efflux. NIH-MDR-G185 and NIH3T3 cells were perfused with glucose-containing buffer$_{g+}$ in the Cytosensor. The buffer was collected after leaving the chamber and was tested for lactate using a spectrophotometric assay based on lactate oxidase and peroxidase activity. Figure 6 shows the rate of lactate molecules exported (hatched columns) by NIH3T3 and NIH-MDR-G185 cells under basal conditions (−) and when stimulated continuously with 6 μM verapamil (+) for ∼1 h. The lactate rates are compared to the proton efflux rates (ECARs) measured in parallel (gray columns).

In the absence of verapamil, NIH3T3 and NIH-MDR-G185 cells exported $(3.5 \pm 0.5) \times 10^7$ and $(3.0 \pm 0.9) \times 10^7$ lactates/cell/s, respectively. The basal ECARs determined in parallel corresponded to $(3.4 \pm 0.1) \times 10^7$ and $(3.0 \pm 0.6) \times 10^7$ H$^+$/cell/s for NIH3T3 cells and NIH-MDR-G185 cells, respectively (see also Table 1).

Verapamil (6 μM) induced an increase in the rate of lactate export and in the ECAR of $(4.8 \pm 1.5) \times 10^7$ lactates/cell/s and $(4.5 \pm 0.4) \times 10^7$ H$^+$/cell/s, respectively, in Pgp-overexpressing cells. In wild-type cells, the rate of lactate export and the ECAR remained at $(3.4 \pm 0.5) \times 10^7$ lactates/cell/s and $(3.3 \pm 0.5) \times 10^7$ H$^+$/cell/s. Data in Figure 6 thus demonstrate that the rate of lactic acid leaving the measuring chambers of the Cytosensor corresponds to the rate of extracellular acidification registered by the pH-sensitive potentiometric sensor chip in the measuring chamber of the Cytosensor.

Route of Lactic Acid Efflux. To identify the pathway of lactic acid efflux, we incubated the cells in the Cytosensor chambers with DIDS and phloretin, which inhibit inorganic anion exchange mechanisms and monocarboxylate carriers, respectively (*44, 45*). Figure 7 shows the influence of DIDS and phloretin on basal ECARs of NIH-MDR-G185, LLC-MDR1, and NIH3T3 cells. Exposure of cells to increasing concentrations of DIDS (50−600 μM) leads to a slow decrease in basal ECARs. After 20 min of incubation with DIDS a reduction by about 10−15% was reached in wild-type and transfected cell lines. In contrast, exposure of NIH-MDR-G185 and NIH3T3 cells to phloretin leads to a fast decrease by ∼60% and ∼70%, respectively, which remained constant after 6 min.

Figure 8 shows the effect of DIDS and phloretin on verapamil-induced ECARs in NIH-MDR-G185 and NIH3T3 cells. The cells were preincubated with DIDS or phloretin for 20 and 6 min, respectively, and were then stimulated with 6 μM verapamil for 160 s in the presence of DIDS or phloretin. DIDS had no effect on the ECAR in the whole

Table 1: Basal and Verapamil-Induced Rate of Proton and Lactate Export by NIH-MDR-G185 and NIH3T3 Cells in Buffer$_{g+}$ under Different Conditions

no. of cell passages after defreezing	verapamil (μM)	10 mM glucose	stimulation time	basal ECAR for NIH3T3 [10^7 H$^+$/cell/s]	basal ECAR for NIH-MDR-G185 [10^7 H$^+$/cell/s]	verapamil-induced ECAR for NIH-MDR-G185 [10^6 H$^+$/cell/s]	verapamil-induced relative to basal (100%) ECAR for NIH-MDR-G185 (%)
2$-$3	10	+	160 s	1.87 $\pm$ 0.25 (3)[a]	1.63 $\pm$ 0.24 (4)[a]	4.1 $\pm$ 0.6 (4)[a]	125
4$-$20	10	+	160 s	2.97 $\pm$ 0.80 (10)	2.98 $\pm$ 0.60 (17)	8.0 $\pm$ 1.5 (16)	127
2$-$20[b]	10	$-$	160 s	0.54 $\pm$ 0.17 (13)	0.60 $\pm$ 0.21 (21)	2.8 $\pm$ 1.2 (20)	148
17$-$20	6[c]	+	60 min	3.40 $\pm$ 0.14 (3)	3.05 $\pm$ 0.58 (9)	14.7 $\pm$ 4.2 (9)	148
17$-$20	6	+	60 min	3.48 $\pm$ 0.45[d] (3)	3.03 $\pm$ 0.91[d] (9)	17.4 $\pm$ 15[d] (9)	157[d]

[a] Numbers in parentheses correspond to the numbers of measurements. [b] Since ECARs are relatively weak for glucoses-deprived cells, an average value of low (2$-$3) and high (>4) passage numbers is given. [c] ECAR measurements as a function of verapamil concentration have shown that ECAR values for 6 and 10 μM verapamil are very similar (*20*). [d] Amount of lactate determined spectrophotometrically (lactates/cell/s).
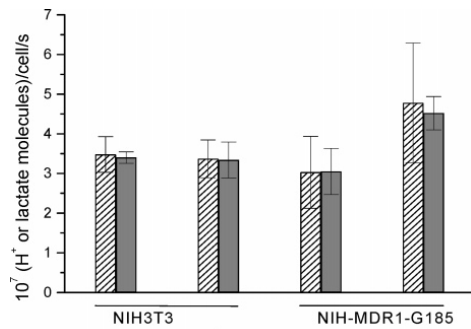

FIGURE 6: Comparison between the rate of lactic acid efflux as determined spectrophotometrically (hatched columns) and the extracellular acidification rate as determined by means of the Cytosensor microphysiometer (gray columns) for NIH3T3 ($n = 3$) and NIH-MDR-G185 ($n = 9$) cells in the absence ($-$) and presence ($+$) of 6 μM verapamil. The cells were defrozen 17$-$20 passages prior to the measurements. The differences in lactate efflux (and ECAR) between NIH-MDR-G185 without and with verapamil are statistically significant ($p < 0.05$) (and $p < 0.001$).
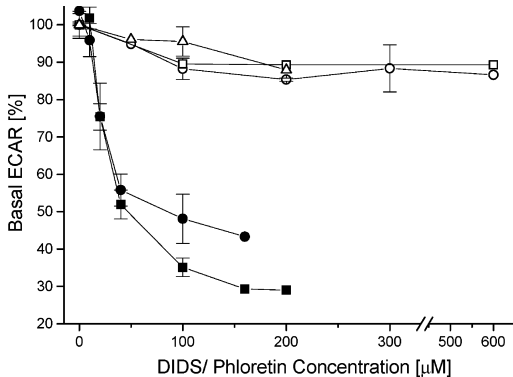

FIGURE 7: Effect of increasing concentrations of DIDS (open symbols) and phloretin (solid symbols) on the basal ECARs of NIH-MDR-G185 (circles), NIH3T3 (squares), and LLC-MDR1 (triangles) cells. The basal ECAR was defined as 100%. Results are normalized to the baseline and are expressed as a percent of the basal rate.

FIGURE 8: Effect of increasing concentrations of DIDS (A, open symbols) and phloretin (B, solid symbols) on verapamil (6 μM)-induced ECARs of NIH-MDR-G185 (circles) and NIH3T3 (squares). The ECARs of cells stimulated with verapamil for 160 s minus the corresponding basal ECARs (in the absence of inhibitors) were defined as 100%. Results are normalized and expressed as a percent of the verapamil-induced ECAR subtracted from the basal ECAR.

concentration range investigated (50$-$300 μM) (Figure 8A), suggesting that inorganic ion exchange mechanisms play no significant role in lactate efflux in intact cells. On the other hand, phloret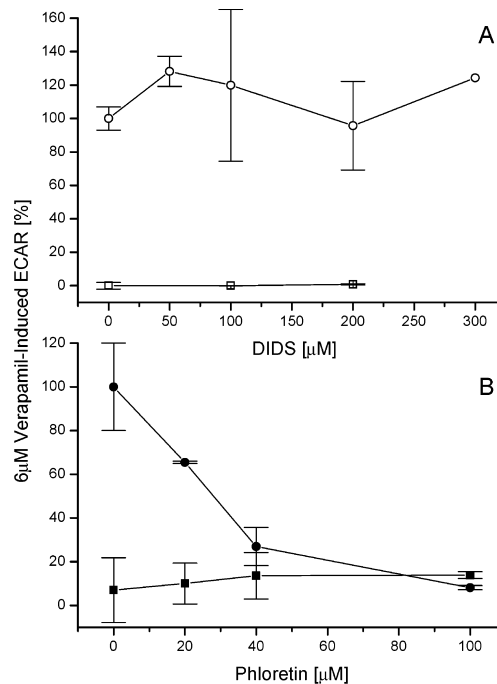in completely inhibited the Pgp-specific ECAR at a concentration of 100 μM, suggesting that monocarboxylate carriers are involved in lactate export (Figure 8B). As will be discussed below phloretin may, however, also affect glucose import. The concentration of 50% inhibition of lactate export by phloretin was IC$_{50}$ = 47 $\pm$ 20 μM (40 $\pm$ 19 μM) for wild-type (transfected) cells under basal conditions and IC$_{50}$ = 22 $\pm$ 8 μM for transfected cells upon drug activation.

ATPase Activation Assay. Basal Pgp activation led to a phosphate release of 10.7 $\pm$ 0.9 (nmol/mg of total protein)/min. Activation of the Pgp ATPase in plasma membrane vesicles of NIH-MDR1-G185 cells at pH 7.5 by verapamil

(10 μM) led to an increase in phosphate release by 14.1 $\pm$ 2.3 (nmol/mg of total protein)/min.

Taking into account the number of cells, the molecular mass of Pgp (170 kDa), and the total protein concentration determined experimentally, the content of Pgp was calculated as 0.85 $\pm$ 0.23% of total protein, in good agreement with previous results (*46, 47*). By combining these results with the estimate of the number of Pgp molecules per cell in NIH-MDR1-G185 (*8*), we calculated the turnover number of verapamil-induced activity as 4.7 $\pm$ 0.8 ATP hydrolyzed/Pgp/s. The errors correspond to four measurements.

DISCUSSION

Up to now, the classical method to determine Pgp-ATPase activation was based on inorganic phosphate release measurements made with inside-out vesicles prepared from Pgp-overexpressing cells. This method has the disadvantage that it is rather time-consuming and also requires destruction of the living cell. Therefore, little is known on the role of the basal metabolic state of the cell for Pgp activation. We have recently shown (*20*) that measuring the extracellular acidification rate of living *MDR1*-transfected cells by means of a Cytosensor (*19*) provides a much faster and more convenient method to monitor Pgp-ATPase activation. In the present study we have developed this method further. Our main interest is to investigate the influence of the metabolic state of the cell, which depends on the cell culture time (passage numbers) as well as on the nutritional state of the cell. We considered drug-induced stimulation of Pgp under conditions of starvation in some detail to understand the mechanism of extracellular acidification in relation to the general glycolytic metabolism of the cell and to show how it is linked to Pgp-induced ATP hydrolysis under conditions of Pgp activation.

The Different Genetically Modified Cell Lines Show Similar ECARs. For a comparison of the different cell lines the cells were kept in culture for identical periods of time after defreezing. Basal ECARs of wild-type (2ac.1, 2ac.2, LLC-PK1, NIH3T3) and genetically modified (*Mdr1a$^{-/-}$1b$^{-/-}$* knockout, *MDR1*- and *MRP1*-transfected (LLC-MDR1, LLC-MDR1/V, NIH-MDR-G185, LLC-MRP1)) cell lines were on the order of 10^7 H$^+$/cell/s, whereby those of genetically modified cells were on average slightly lower than those of wild-type cells (Figure 2 and 5, Table 1). The expression level of Pgp as such had no influence on the basal extracellular acidification rate of the different cell lines (Figures 2 and 5).

Basal Metabolic Rates Depend on Cell Culture Time. The rate of cellular metabolism reflected by the ECAR depends on many factors such as temperature, pH, ionic strength, and nutritional conditions (glucose concentration). The present data demonstrate that it also depends on the time which cells spend in culture after defreezing. For the comparison of different cell lines we collected two data sets, one for cells of low passage numbers (pn = 2−3) and one for cells of higher passage numbers (pn = 4−20), where the former show lower acidification rates than the latter (Figure 3, Table 1). A stable situation was reached after about two weeks in culture (pn $\geq$ 4). Basal ECARs in buffer$_{g+}$ as well as in medium (DMEM) were in the range of 1.3 $\times$ 10^7 to 2.7 $\times$ 10^7 H$^+$/cell/s for cells of low passage numbers (pn = 2−3).
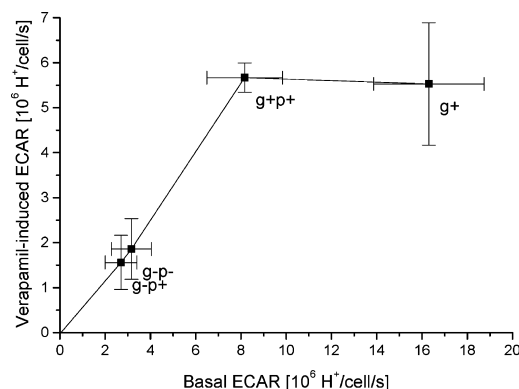

FIGURE 9: Contribution of exogenous carbon sources to the basal and verapamil-induced ECARs of NIH-MDR-G185 cells. The cells were perfused with phosphate buffer without any carbon sources (buffer$_{g-p-}$), with 1 mM pyruvate (buffer$_{g-p+}$), 1 mM pyruvate and 10 mM glucose (buffer$_{g+p+}$,), or 10 mM glucose (buffer$_{g+}$). Data in buffer$_{g-p+}$ correspond to an average of the data shown in Figure 4, data in buffer$_{g+}$ correspond to an average of the data from Figures 2B,D and 4, and data in buffer$_{g+p+}$ and buffer$_{g-p-}$ correspond to an average of the data from Figure 4 and two additional sets of measurements (n = 3−4), not shown. The line is drawn to guide the eyes.

The basal metabolism reflected by the ECAR is thus generally more affected by variations in the cell culture time (60 $\pm$ 40%, depending on the cell line) than by transfection (30 $\pm$ 10% for pn = 2−3, depending on the cell line).

ECARs due to Verapamil Stimulation Increase with the Expression Level of Pgp and Depend on the Metabolic State of the Cell. A metabolic response to verapamil stimulation was observed for *MDR1*-transfected cells only (Figures 2C,D and 5) and increased with the expression level of Pgp. In absolute terms, the response to verapamil stimulation was higher for cells of high passage numbers (pn = 4−20) than of low passage numbers (pn = 2−3). However, verapamil-induced ECARs relative to basal values were practically identical for the two data sets (cf. Figure 5C). This suggests that Pgp activation and the concomitant protection of cells against drugs and toxins are directly proportional to the basal metabolic state of the cell.

The metabolic conditions of the cells were modified by perfusing the cells in the Cytosensor either with buffers containing pyruvate in the presence or absence of glucose or with a buffer lacking a carbon source. To illustrate the amount of energy spent by NIH-MDR-G185 cells on detoxification by Pgp relative to the basal metabolic energy under different nutritional conditions, basal ECARs were plotted versus the verapamil-induced ECARs (Figure 9).

Addition of pyruvate (1 mM) to glucose-containing buffer (buffer$_{g+p+}$) led to a 50% decrease of the basal ECAR. Despite the decrease in basal metabolism, the verapamil-induced ECAR remained as high as in buffer$_{g+}$. The energy required to activate Pgp in the presence of pyruvate (buffer$_{g+p+}$) thus required on average ∼50% of the basal ECAR in contrast to only ∼25% in buffer$_{g+}$.

If pyruvate was the only carbon source (buffer$_{g-p+}$) or if exogenous carbon sources were lacking (buffer$_{g-p-}$), the absolute ECAR or the rate of basal metabolism decreased further (cf. Table 1). Nevertheless, Pgp activation by

verapamil was still possible and comprised again 50−60% of the basal value.

An analogous behavior was observed for LLC-MDR1 and LLC-MDR1/V cells. While the ECARs of LLC-MDR1 and LLC-MDR1/V cells upon verapamil stimulation (10 μM) were 108 ± 3% and 116 ± 7%, respectively, in the presence of glucose, they amounted to 124% and 131%, respectively, in the absence of exogenous carbon sources.

The reduction of the basal ECAR in the presence of high pyruvate concentrations led to substrate inhibition of lactate dehydrogenase (*48*). However, when Pgp was stimulated by verapamil and the ATP requirement was enhanced, glycolysis was up-regulated even in the absence of exogenous carbon sources. This suggests that endogenous carbon sources are used to drive Pgp under conditions of starvation.

Somewhat higher ECARs were also observed upon long-time (60 min) exposure to drugs (cf. Table 1). The value measured is in good agreement with previous results obtained in cancer cells under comparable conditions (*22*).

Glycolytic Pathway for Energy Production. For all cell lines basal ECARs were strongly reduced in the presence of pyruvate or deoxyglucose and in the absence of glucose as shown in Figure 4 for NIH-MDR-G185 cells, which is consistent with a primarily glycolytic pathway for energy production. Related results were obtained previously with Chinese hamster ovary cells CHO-K1 (*19*), swim bladder gas gland cells (*49*), and human rhabdomyosarcoma TE671 cells (*50*).

An analysis of the flow buffer leaving the Cytosensor measuring chambers containing NIH-MDR-G185 or NIH3T3 cells perfused with glucose-containing buffer$_{g+}$ revealed that the rate of lactate export was identical to the rate of proton export as determined by the potentiometric sensor chip (Figure 6), which further supports the primarily glycolytic pathway of these cells. We thus conclude that one molecule of lactate is exported per molecule of ATP synthesized.

To maintain cellular homeostasis, lactic acid molecules produced upon ATP synthesis must be transported across the cell membrane to the extracellular space. Multiple mechanisms exist, including facilitated transport by mono-carboxylate carriers and anion exchange proteins as well as diffusion of the protonated acid across the membrane (*24*). Whether facilitated lactate export occurs by inorganic anion exchange mechanisms or by monocarboxylate carriers was tested by treating the cells with increasing concentrations of DIDS or phloretin, respectively. While DIDS reduced basal ECARs only by about ∼10%, in agreement with previous measurements (*51*), phloretin reduced basal ECARs by about 70% in wild-type cells, and by about 60% in *MDR1*-transfected cells. The concentration of 50% inhibition of lactate export by phloretin was determined, in good agreement with previous measurements for other cell lines (IC$_{50}$ = 3−40 μM) (*45*, *52*, *53*), suggesting that monocarboxylate transporters play an important role in lactate−proton cotransport. However, phloretin also inhibits the glucose transporter with a similar concentration of half-maximum activation (IC$_{50}$ = 0.24−48 μM) (*49*, *54*, *55*). On the basis of the present experiments, it is therefore not possible to unambiguously decide to what extent inhibition of lactate export by phloretin is due to the inhibition of monocarboxylate transporters and to what extent it is due to the inhibition of

glucose import and the concomitant reduction in basal metabolism.

The amount of lactic acid leaving the cell by passive diffusion is determined by the pK_a value of lactic acid (pK_a = 3.8) and the pH close to the cytosolic membrane surface (pH ≈ 5.5). At pH ≈ 7.0 lactate is fully dissociated, which prevents passive diffusion. However, close to the inner cytosolic membrane surface, which exhibits a negative surface potential, the concentration of protons is higher and the pH is therefore lower. As a consequence about 1% of the lactate molecules produced are protonated in this environment and can leave the cell by passive diffusion.

Proton−Drug Symport? On the basis of the fact that the large majority of drugs transported by Pgp are cationic (pK_a ≈ 8) and that Pgp can transport permanently charged cations (*56*), we have previously (*20*) discussed the possibility that proton efflux in *MDR1*-transfected cells could also arise from the transport of protonated drugs (proton−drug symport). A drug molecule inserted into the negatively charged cytosolic membrane interface, which is assumed to be the site of interaction between Pgp and its substrates, is likely to be protonated due to the slightly acidic environment close to the membrane surface and might thus get transported in its charged form. Since the extracellular aqueous phase is slightly acidified by lactic acid efflux, the proton would not dissociate from the drug molecule and would therefore most likely remain undetected by the Cytosensor. For truncated LmrA, a bacterial transporter related to Pgp, a proton−ethidium symport was indeed demonstrated recently, and was also proposed for the native transporter (*57*).

ATP Synthesis and ATP Hydrolysis. We have demonstrated that drug-stimulated ECARs correspond to the rates of lactic acid export, which suggests that the ECARs reflect in turn the rates of ATP synthesis. To investigate the relationship between the rate of ATP synthesis and the rate of ATP hydrolysis in more detail, we compared the number of lactic acid molecules exported (or the number of ATP molecules synthesized) per NIH-MDR1-G185 cell with the number of phosphate molecules released upon ATP hydrolysis in inside-out vesicles of the same cells upon stimulation with 10 μM verapamil. To estimate the number of phosphate molecules, P$_i$, released per cell, we multiplied the turnover number, which gives the number of molecules of ATP hydrolyzed (or the number of inorganic phosphate molecules released) per molecule of Pgp, determined as 4.7 ± 0.8 P$_i$/Pgp/s in inside-out vesicles, with the number of Pgp molecules per NIH-MDR1-G185 cell determined previously as n = 1.95 × 10^6 Pgp/cell (*8*). This yields (9.2 ± 1.5) × 10^6 P$_i$/cell/s. For comparison the ECAR data obtained for intact NIH-MDR-G185 and NIH3T3 cells under different metabolic conditions are summarized in Table 1. The best agreement is found for cells with high passage numbers (pn = 4−20) in the presence of glucose. The excellent correlation between ECAR data and data from ATP hydrolysis suggests that ATP synthesis is kinetically linked to ATP hydrolysis.

Previous data from Pgp reconstituted into lipid vesicles are in the range of 10^6 to 10^7 P$_i$/cell/s (*8*, *15*, *58*, *59*). This variation in ATP hydrolysis data is due to the fact that many experimental steps are involved in Pgp purification and reconstitution into lipid membranes and that the lipid chosen for reconstitution plays a role (*60*). After careful standardization, the error range for ECARs under a given condition is

generally relatively small. ECAR measurements have moreover the advantage of giving an *in situ* determination of Pgp activation.

Conclusions. (i) Wild-type cells showed on average $30 \pm 10\%$ higher basal ECARs than genetically modified cells such as *MDR1*- and *MRP1*- transfected cells and *Mdr1a$^{-/-}$1b$^{-/-}$* knockout cells at least if measured at low passage numbers (pn = 2−3). The difference between the basal ECAR of wild-type and genetically modified cells was smallest for NIH-MDR1-G185 cells and almost vanished for cells of higher passage numbers (pn > 4). Although *MDR1*-transfected cells consume ATP at a high basal rate (perhaps due to an endogenous substrate), their basal ECARs were not higher than those of wild-type cells. Moreover, an increase in Pgp expression did not lead to an increase in basal ECARs. We thus conclude that a genetic modification, whether it is a *MDR1* or *MRP1* transfection or a *Mdr1a$^{-/}$ $^{-}$1b$^{-/-}$* knockout, tends to reduce the basal cellular metabolism. (ii) Stimulation of *MDR1*-transfected cells by verapamil (6−10 μM) induced an increase in metabolic rates which was proportional to the expression level of Pgp, whereas stimulation of wild-type, MRP1-transfected, or knockout cells gave no response. A comparison of *MDR1*-transfected cells of low and high passage numbers (exhibiting low and high basal metabolic rates, respectively) shows that the rate of Pgp activation and the concomitant protection of cells against drugs or toxins are proportional to the basal metabolic rate of the cell. In glucose-deficient (or pyruvate-fed) NIH-MDR1-G185 cells the energy spent on detoxification by Pgp *relative* to basal values is, however, 2-fold higher than in glucose-fed cells, suggesting that the energy required to drive Pgp can be derived from endogenous energy stores under conditions of starvation. Cells overexpressing Pgp thus seem to have an efficient mechanism of self-protection against toxic compounds even under starvation conditions and consequent low basal metabolic rates. (iii) ATP is generated mainly by glycolysis, producing one molecule of lactate per ATP molecule synthesized, whereby lactate seems to be exported mainly by monocarboxylate transporters. (iv) The excellent correlation between the number of protons or lactate molecules excreted per second per cell under optimal conditions (i.e., for cells with high passage numbers in glucose-containing buffer) and the number of ATP molecules hydrolyzed by Pgp in inside-out vesicles of the same cells suggests that ATP synthesis is kinetically linked to ATP hydrolysis.

REFERENCES

1. Ambudkar, S. V., Dey, S., Hrycyna, C. A., Ramachandra, M., Pastan, I., and Gottesman, M. M. (1999) Biochemical, cellular, and pharmacological aspects of the multidrug transporter, *Annu. Rev. Pharmacol. Toxicol. 39*, 361−398.
2. Stein, W. D. (1997) Kinetics of the multidrug transporter (P-glycoprotein) and its reversal, *Physiol. Rev. 77*, 545−590.
3. Seelig, A., and Gatlik-Landwojtowicz, E. (2004) Inhibitors of multidrug efflux transporters—their membrane and protein interactions, *Mini-Rev. Med. Chem.* (in press).
4. Urbatsch, I. L., Tyndall, G. A., Tombline, G., and Senior, A. E. (2003) P-glycoprotein catalytic mechanism. Studies of the ADP-vanadate inhibited state, *J. Biol. Chem. 2*, 2.
5. Eytan, G. D., Regev, R., Oren, G., and Assaraf, Y. G. (1996) The role of passive transbilayer drug movement in multidrug resistance and its modulation, *J. Biol. Chem. 271*, 12897−12902.
6. Shapiro, A. B., and Ling, V. (1998) Stoichiometry of coupling of rhodamine 123 transport to ATP hydrolysis by P-glycoprotein, *Eur. J. Biochem. 254*, 189−193.
7. Sauna, Z. E., and Ambudkar, S. V. (2001) Characterization of the catalytic cycle of ATP hydrolysis by human P-glycoprotein. The two ATP hydrolysis events in a single catalytic cycle are kinetically similar but affect different functional outcomes, *J. Biol. Chem. 276*, 11653−11661.
8. Ambudkar, S. V., Cardarelli, C. O., Pashinsky, I., and Stein, W. D. (1997) Relation between the turnover number for vinblastine transport and for vinblastine-stimulated ATP hydrolysis by human P-glycoprotein, *J. Biol. Chem. 272*, 21160−22166.
9. Litman, T., Zeuthen, T., Skovsgaard, T., and Stein, W. D. (1997) Structure−activity relationships of P-glycoprotein interacting drugs: kinetic characterization of their effects on ATPase activity, *Biochim. Biophys. Acta 1361*, 159−168.
10. Kerr, K. M., Sauna, Z. E., and Ambudkar, S. V. (2001) Correlation between steady-state ATP hydrolysis and vanadate-induced ADP trapping in Human P-glycoprotein. Evidence for ADP release as the rate-limiting step in the catalytic cycle and its modulation by substrates, *J. Biol. Chem. 276*, 8657−8664.
11. al-Shawi, M. K., and Senior, A. E. (1993) Characterization of the adenosine triphosphatase activity of Chinese hamster P-glyco-protein, *J. Biol. Chem. 268*, 4197−4206.
12. Ramachandra, M., Ambudkar, S. V., Chen, D., Hrycyna, C. A., Dey, S., Gottesman, M. M., and Pastan, I. (1998) Human P-glycoprotein exhibits reduced affinity for substrates during a catalytic transition state, *Biochemistry 37*, 5010−5019.
13. Sharom, F. J., Yu, X., Lu, P., Liu, R., Chu, J. W., Szabo, K., Muller, M., Hose, C. D., Monks, A., Varadi, A., Seprodi, J., and Sarkadi, B. (1999) Interaction of the P-glycoprotein multidrug transporter (MDR1) with high affinity peptide chemosensitizers in isolated membranes, reconstituted systems, and intact cells, *Biochem. Pharmacol. 58*, 571−586.
14. Raggers, R. J., Pomorski, T., Holthuis, J. C., Kalin, N., and van Meer, G. (2000) Lipid traffic: the ABC of transbilayer movement, *Traffic 1*, 226−234.
15. Romsicki, Y., and Sharom, F. J. (2001) Phospholipid flippase activity of the reconstituted P-glycoprotein multidrug transporter, *Biochemistry 40*, 6937−6947.
16. Krupka, R. M. (1999) Uncoupled active transport mechanisms accounting for low selectivity in multidrug carriers: P-glycoprotein and SMR antiporters, *J. Membr. Biol. 172*, 129−143.
17. Al-Shawi, M. K., Polar, M. K., Omote, H., and Figler, R. A. (2003) Transition state analysis of the coupling of drug transport to ATP hydrolysis by P-glycoprotein, *J. Biol. Chem. 278*, 52629−52640.
18. Garrigues, A., Nugier, J., Orlowski, S., and Ezan, E. (2002) A high-throughput screening microplate test for the interaction of drugs with P-glycoprotein, *Anal. Biochem. 305*, 106−114.
19. McConnell, H. M., Owicki, J. C., Parce, J. W., Miller, D. L., Baxter, G. T., Wada, H. G., and Pitchford, S. (1992) The cytosensor microphysiometer: biological applications of silicon technology, *Science 257*, 1906−1912.
20. Landwojtowicz, E., Nervi, P., and Seelig, A. (2002) Real-time monitoring of p-glycoprotein activation in living cells, *Biochemistry 41*, 8050−8057.
21. Goda, K., Balkay, L., Marian, T., Tron, L., Aszalos, A., and Szabo, G., Jr. (1996) Intracellular pH does not affect drug extrusion by P-glycoprotein, *J. Photochem. Photobiol., B 34*, 177−182.
22. Broxterman, H. J., Pinedo, H. M., Kuiper, C. M., Schuurhuis, G. J., and Lankelma, J. (1989) Glycolysis in P-glycoprotein-over-expressing human tumor cell lines. Effects of resistance-modifying agents, *FEBS Lett. 247*, 405−410.
23. Altenberg, G. A., Young, G., Horton, J. K., Glass, D., Belli, J. A., and Reuss, L. (1993) Changes in intra- or extracellular pH do not mediate P-glycoprotein-dependent multidrug resistance, *Proc. Natl. Acad. Sci. U.S.A. 90*, 9735−9738.
24. Owicki, J. C., and Parce, J. W. (1992) Biosensors based on the energy metabolism of living cells: the physical chemistry and cell biology of extracellular acidification, *Biosens. Bioelectron. 7*, 255−272.
25. Keizer, H. G., and Joenje, H. (1989) Increased cytosolic pH in multidrug-resistant human lung tumor cells: effect of verapamil, *J. Natl. Cancer Inst. 81*, 706−709.
26. Thiebaut, F., Currier, S. J., Whitaker, J., Haugland, R. P., Gottesman, M. M., Pastan, I., and Willingham, M. C. (1990) Activity of the multidrug transporter results in alkalinization of the cytosol: measurement of cytosolic pH by microinjection of a pH-sensitive dye, *J. Histochem. Cytochem. 38*, 685−690.

P-Glycoprotein Activation and the Cellular Metabolic State   *Biochemistry, Vol. 43, No. 46, 2004*   14851

27. Roepe, P. D. (1992) Analysis of the steady-state and initial rate of doxorubicin efflux from a series of multidrug-resistant cells expressing different levels of P-glycoprotein, *Biochemistry 31*, 12555−12564.

28. Boscoboinik, D., Gupta, R. S., and Epand, R. M. (1990) Investigation of the relationship between altered intracellular pH and multidrug resistance in mammalian cells, *Br. J. Cancer 61*, 568−572.

29. Hoffman, M. M., Wei, L. Y., and Roepe, P. D. (1996) Are altered pHi and membrane potential in hu MDR 1 transfectants sufficient to cause MDR protein-mediated multidrug resistance? *J. Gen. Physiol. 108*, 295−313.

30. Simon, S., Roy, D., and Schindler, M. (1994) Intracellular pH and the control of multidrug resistance, *Proc. Natl. Acad. Sci. U.S.A. 91*, 1128−1132.

31. Chen, Y., and Simon, S. M. (2000) In situ biochemical demonstration that P-glycoprotein is a drug efflux pump with broad specificity, *J. Cell Biol. 148*, 863−870.

32. Litman, T., Pedersen, S. F., Kramhoft, B., Skovsgaard, T., and Hoffmann, E. K. (1998) pH regulation in sensitive and multidrug resistant Ehrlich ascites tumor cells, *Cell Physiol. Biochem. 8*, 138−150.

33. Porcelli, A. M., Scotlandi, K., Strammiello, R., Gislimberti, G., Baldini, N., and Rugolo, M. (2002) Intracellular pH regulation in U-2 OS human osteosarcoma cells transfected with P-glycoprotein, *Biochim. Biophys. Acta 1542*, 125−138.

34. Marbeuf-Gueye, C., Priebe, W., and Garnier-Suillerot, A. (2000) Multidrug resistance protein functionality: no effect of intracellular or extracellular pH changes, *Biochem. Pharmacol. 60*, 1485−1489.

35. Schinkel, A. H., Wagenaar, E., van Deemter, L., Mol, C. A., and Borst, P. (1995) Absence of the mdr1a P-Glycoprotein in mice affects tissue distribution and pharmacokinetics of dexamethasone, digoxin, and cyclosporin A, *J. Clin. Invest. 96*, 1698−1705.

36. Cardarelli, C. O., Aksentijevich, I., Pastan, I., and Gottesman, M. M. (1995) Differential effects of P-glycoprotein inhibitors on NIH3T3 cells transfected with wild-type (G185) or mutant (V185) multidrug transporters, *Cancer Res. 55*, 1086−1091.

37. Evers, R., Zaman, G. J., van Deemter, L., Jansen, H., Calafat, J., Oomen, L. C., Oude Elferink, R. P., Borst, P., and Schinkel, A. H. (1996) Basolateral localization and export activity of the human multidrug resistance-associated protein in polarized pig kidney cells, *J. Clin. Invest. 97*, 1211−1218.

38. Allen, J. D., Brinkhuis, R. F., van Deemter, L., Wijnholds, J., and Schinkel, A. H. (2000) Extensive contribution of the multidrug transporters P-glycoprotein and Mrp1 to basal drug resistance, *Cancer Res. 60*, 5761−5766.

39. Parce, J. W., Owicki, J. C., Kercso, K. M., Sigal, G. B., Wada, H. G., Muir, V. C., Bousse, L. J., Ross, K. L., Sikic, B. I., and McConnell, H. M. (1989) Detection of cell-affecting agents with a silicon biosensor, *Science 246*, 243−247.

40. CIBA-GEIGY. (1979) *Wissenschaftliche Tabellen Geigy*, p 331, CIBA-GEIGY AG, Basel.

41. Wiley, C., and Beeson, C. (2002) Continuous measurement of glucose utilization in heart myoblasts, *Anal. Biochem. 304*, 139−146.

42. Ambudkar, S. V. (1998) Drug-stimulatable ATPase activity in crude membranes of human MDR1-transfected mammalian cells, *Methods Enzymol. 292*, 504−514.

43. Decorti, G., Rosati, A., Candussio, L., Giraldi, T., and Bartoli Klugmann, F. (2001) Characterization of multidrug transporters in a normal renal tubular cell line resistant to doxorubicin. Multidrug transporters in the LLC−PK(1) cell line and its resistant counterpart, *Biochem. Pharmacol. 61*, 61−66.

44. Restrepo, D., Cronise, B. L., Snyder, R. B., Spinelli, L. J., and Knauf, P. A. (1991) Kinetics of DIDS inhibition of HL-60 cell anion exchange rules out ping-pong model with slippage, *Am. J. Physiol. 260*, C535−C544.

45. Jackson, V. N., and Halestrap, A. P. (1996) The kinetics, substrate, and inhibitor specificity of the monocarboxylate (lactate) transporter of rat liver cells determined using the fluorescent intracellular pH indicator, 2′,7′-bis(carboxyethyl)-5(6)-carboxyfluorescein, *J. Biol. Chem. 271*, 861−868.

46. Sarkadi, B., Price, E. M., Boucher, R. C., Germann, U. A., and Scarborough, G. A. (1992) Expression of the human multidrug resistance cDNA in insect cells generates a high activity drug-stimulated membrane ATPase, *J. Biol. Chem. 267*, 4854−4858.

47. Ramachandra, M., Ambudkar, S. V., Gottesman, M. M., Pastan, I., and Hrycyna, C. A. (1996) Functional characterization of a glycine 185-to-valine substitution in human P-glycoprotein by using a vaccinia-based transient expression system, *Mol. Biol. Cell 7*, 1485−1498.

48. Hewitt, C. O., Eszes, C. M., Sessions, R. B., Moreton, K. M., Dafforn, T. R., Takei, J., Dempsey, C. E., Clarke, A. R., and Holbrook, J. J. (1999) A general method for relieving substrate inhibition in lactate dehydrogenases, *Protein Eng. 12*, 491−496.

49. Pelster, B., and Niederstatter, H. (1997) pH-dependent proton secretion in cultured swim bladder gas gland cells, *Am. J. Physiol. 273*, R1719−R1725.

50. Miller, D. L., Olson, J. C., Parce, J. W., and Owicki, J. C. (1993) Cholinergic stimulation of the Na+/K+ adenosine triphosphatase as revealed by microphysiometry, *Biophys. J. 64*, 813−823.

51. Hamilton, G., Cosentini, E. P., Teleky, B., Koperna, T., Zacheri, J., Riegler, M., Feil, W., Schiessel, R., and Wenzi, E. (1993) The multidrug-resistance modifiers verapamil, cyclosporine A and tamoxifen induce an intracellular acidification in colon carcinoma cell lines in vitro, *Anticancer Res. 13*, 2059−2063.

52. Dimmer, K. S., Friedrich, B., Lang, F., Deitmer, J. W., and Broer, S. (2000) The low-affinity monocarboxylate transporter MCT4 is adapted to the export of lactate in highly glycolytic cells, *Biochem. J. 350 Pt 1*, 219−227.

53. Wilson, M. C., Jackson, V. N., Heddle, C., Price, N. T., Pilegaard, H., Juel, C., Bonen, A., Montgomery, I., Hutter, O. F., and Halestrap, A. P. (1998) Lactic acid efflux from white skeletal muscle is catalyzed by the monocarboxylate transporter isoform MCT3, *J. Biol. Chem. 273*, 15920−15926.

54. Tse, C. M., and Young, J. D. (1990) Glucose transport in fish erythrocytes: variable cytochalasin-B-sensitive hexose transport activity in the common eel (Anguilla japonica) and transport deficiency in the paddyfield eel (Monopterus albus) and rainbow trout (Salmo gairdneri), *J. Exp. Biol. 148*, 367−383.

55. Krupka, R. M. (1985) Asymmetrical binding of phloretin to the glucose transport system of human erythrocytes, *J. Membr. Biol. 83*, 71−80.

56. Schmid, D., Ecker, G., Kopp, S., Hitzler, M., and Chiba, P. (1999) Structure−activity relationship studies of propafenone analogs based on P-glycoprotein ATPase activity measurements, *Biochem. Pharmacol. 58*, 1447−1456.

57. Venter, H., Shilling, R. A., Velamakanni, S., Balakrishnan, L., and Van Veen, H. W. (2003) An ABC transporter with a secondary-active multidrug translocator domain, *Nature 426*, 866−870.

58. Shapiro, A. B., and Ling, V. (1994) ATPase activity of purified and reconstituted P-glycoprotein from Chinese hamster ovary cells, *J. Biol. Chem. 269*, 3745−3754.

59. Urbatsch, I. L., al-Shawi, M. K., and Senior, A. E. (1994) Characterization of the ATPase activity of purified Chinese hamster P-glycoprotein, *Biochemistry 33*, 7069−7076.

60. Romsicki, Y., and Sharom, F. J. (1999) The membrane lipid environment modulates drug interactions with the P-glycoprotein multidrug transporter, *Biochemistry 38*, 6887−6896.

BI048761S

7.4 Metabolic Rate of Mouse Embryo Fibroblasts Determined by ^{13}C-NMR

Unpublished manuscript

Götz Kohler and Päivi Äänismaa

Unpublished Manuscript

INTRODUCTION

Nuclear magnetic resonance (NMR) has been established as a powerful tool in many fields of science. The great advantage of NMR is its non-invasive character. As the object of interest does not need to be destructed repeated investigations of the same object are possible. This property of NMR can be used to perform additional measurements with NMR beside other techniques. In this manner accuracy of an experiment can be enhanced and the risk of systematic errors can be diminished.

The metabolic rate of mouse embryo fibroblasts NIH3T3, wild -type (NIH-WT) and *MDR1*-gene transfected (NIH-MDR1-G185), has been studied in our lab with and without P-glycoprotein (ABCB1, Pgp) stimulation (Chapter 7.3 (*1*)). The usually used method in our lab to determine the metabolic rate of cells is the observation of the extracellular acidification rate (ECAR) with a Cytosensor microphysiometer (*2*) under anaerobic conditions. Without aerobic metabolism anaerobic glycolysis is the only pathway for ATP production in the studied cells. Thus every mol of glucose (Gluc) is metabolized to two mol of lactic acid which dissociates to lactate (Lac$^-$) and protons (H$^+$) at the physiological pH. The most important membrane transporters for Lac$^-$ release are the monocarboxylate transporters (MCTs) which transport Lac$^-$ together with H$^+$ (*3, 4*). However, MCTs are not the only transporters involved in H$^+$ release and also a small amount of undissociated lactic acid is able to cross the cell membrane by diffusion (*5*). Furthermore, only the extracellular protons can be detected with the Cytosensor microphysiometer. Therefore the ECAR is a rather indirect method to detect the metabolic rate of the cells and even if the Cytosensor microphysiometer is an established method a more direct method is desirable to validate the results obtained with the Cytosensor.

NMR spectroscopy seems to be an adequate method to measure the metabolic rate of cells directly by monitoring the Gluc consumption and the Lac production. In contrast to the ECAR, extra- as well as intracellular Gluc and Lac are observed with NMR. Furthermore, NMR spectroscopy might offer the possibility to distinguish between the intra- and the extracellular Lac. The separation of the intra- and the extracellular Lac is of interest to proof whether the Lac transport systems of the used cells are fast enough to avoid the intracellular Lac accumulation upon Pgp stimulation. The accumulation of intracellular Lac would result in an inhibition of the metabolic rate (*3*). Gatlik-

Landwojtowicz et al. (*1*) (Chapter 7.3) observed an increased ECAR until at least 10 min after the stimulation with verapamil was stopped. To exclude that this enhanced ECAR after the stimulation is due to a delayed release of lactate because of a limited MCT capacity it would be of interest to distinguish between the intra- and the extracellular Lac.

Chemistry has developed a huge amount of shift reagents (*6*). These compounds are often used to divide NMR signals which are very close together within a spectrum rather than to distinguish between the different compartments. However, in biological applications it is often of interest to separate the signals of the same substance in the different compartments. Therefore the shift reagents which are used to distinguish between the intra- and the extracellular volume need to have certain properties. These compounds are not allowed to cross the cell membrane. Furthermore, the shift reagents for living cells must not be toxic and should not influence the viability or the metabolic rate of the observed cells. Even if the shift reagents have already been used to distinguish the NMR signals of intra- and extracellular compartments the usage is still not routine. Aime et al. (*7*) have developed a shift reagent (Pr-DO3A) that especially binds to Lac. Thus, the needed amount of shift reagent can be kept small. Pr-DO3A has been tested with the ghosts of human red blood cells, but up to now its applicability has not been proofed with the intact cells.

In the current study NMR spectroscopy is used as an additionally technique to observe the metabolic rate and the Pgp activation in mouse embryo fibroblast cells under the stimulation with verapamil. Furthermore, the shift reagent Pr-DO3A was used to separate intra- and extracellular Lac to get additional information about the transport capacity of MCTs and simultaneously the bio-compatibility of the shift reagent was tested.

MATERIALS AND METHODS

Cell Lines and Cell Preparation. Mouse embryo fibroblasts NIH3T3, wild-type (NIH-WT) and transfected with human *MDR1*-gene (NIH-MDR1-G185) were used with various numbers of cell passages (pn) after defreezing. The cells were maintained as described previously in details (*1*) (Chapter 7.3). For NMR measurements cells were suspended in 0.4 ml self-made degassed PBS-buffer (50 mM, 35 mM NaCl, 4 mM KCl, pH 7.4, 154 mM ionic strength) containing 10 mM single 1-^{13}C or double labeled 1,6-^{13}C Gluc. Thereafter, the cells were transferred in a 5 mm NMR tube which was filled with Ar in order to avoid

contact with oxygen. Cell viability was tested with trypan blue and counting the viable and not viable cells with a hemocytometer. NMR measurements were performed at two different temperatures and with two different cell quantities. The metabolic rate of both cells was measured with $3.6 \cdot 10^6$ cells at 37 °C in the presence and absence of verapamil (9 µM). Single labeled Gluc was used for these experiments because no homonuclear couplings occur on the 1-^{13}C-Gluc NMR signal. To determine the intracellular Lac content the measurements with and without Pr-DO3A were performed. For measuring the intracellular Lac content a higher number of NIH-MDR1-G185 cells were used ($18 \cdot 10^6$) in order to increase the total cell volume and the NMR signal intensity. These experiments were performed with a double labeled Gluc to observe all Lac produced. The metabolism of cells was lowered in these experiments by reducing the temperature to 23 °C in order to avoid fast acidification. With these settings pH of the cell suspensions in the NMR tube did not decrease below pH 7.0 during the total experimental time of 90 min. After the experiments a small droplet of the cell suspension was used to test the cell viability. The remaining suspension was used to determine the cell volume proportion by centrifugation at 4000×g for 20 min.

NMR Measurements.^{13}C-NMR spectroscopy was performed on a 9 T Bruker Avance spectrometer. Distortionless Enhancement by Polarization Transfer (DEPT) sequence was used to enhance ^{13}C-NMR signal intensity. Pulse parameters were optimized for the Lac methyl group resonance. Repetition time (T_R) was 1.7 s. Continuous broad band decoupling was used to avoid multiplets. 256 scans were accumulated during 7:30 min. Before each NMR measurement magnetic field homogeneity was optimized. The intensity of Gluc signal was calibrated with the starting Gluc concentration of 10 mM. The quantification of Lac concentration was determined by a constant which was determined by a standard solution containing 10 mM 1,6-^{13}C-Gluc and 10 mM 3-^{13}C-Lac in buffer. Because of the sedimentation of the cells during the scans the cells were resuspended after each NMR measurement. Resuspension was performed by a soft tilting the NMR tube with a little gas bubble.

Shift Reagent. To separate intra- and extracellular NMR Lac signals the shift reagent Pr-DO3A was used. Pr-DO3A was prepared as reported previously by Aime et al. (*7*). The basic substance DO3A was kindly provided by Bracco (S.p.A, Milan,Italy). An active shift reagent concentration of 7 mM was used to shift extracellular 3-^{13}C-Lac NMR signal 0.2 ppm towards low field direction.

RESULTS

Metabolic rate. The Gluc and the Lac content as well as the total metabolic rate of both cell suspensions in the presence and in the absence of verapamil (9 µM) are shown in the Figures 1-4. The absolute Gluc consumption and the Lac production per NIH-WT and NIH-MDR1-G185 cell in the presence and absence of verapamil (9 µM) are shown in Table 1. Verapamil (9 µM) stimulation at 37 °C increases the metabolic rate of wild-type cells only slightly (Gluc consumption 104 % and Lac production 101 % compared to the values measured in the absence of verapamil) whereas the metabolic rate of NIH-MDR1-G185 cells increased more than 50% (Gluc consumption 152 % and Lac production 161 % compared to the values measured in the absence of verapamil). By decreasing the temperature from 37 °C to 23 °C the metabolic rate of the NIH-MDR-G185 cells was reduced to a fifth. The Gluc consumption in NIH-MDR1-G185 cells with Pr-DO3A was 112 % of the value in the absence of Pr-DO3A (Table 1). The Lac production in the presence of Pr-DO3A was not calculated due to the signal bleaching of the extracellular NMR signal. The pH of the cell suspensions in the NMR tubes did not fall below pH 7.0 during all measurements.

<div align="center">

FIGURES 1-4

TABLE 1

</div>

Intracellular Lac concentration (high cell density only). The intra- and the extracellular NMR 3-^{13}C-Lac signals were separated by 0.2 ppm in the presence a shift reagent Pr-DO3A (Figure 5). However, the intensity of the extracellular 3-^{13}C-Lac NMR signal was bleached significantly due to the used shift reagent and therefore the extracellular Lac concentration was not quantified. The intracellular Lac concentration was calculated by taking into account the cell volume and the intracellular NMR signal intensity which was not affected by Pr-DO3A. The Gluc and the Lac content as well as the total metabolic rate of NIH-MDR1-G185 cells in the presence and absence of Pr-DO3A are shown in Figures 6-7. The total cell volume was determined by centrifugation to be 10.7 % of the total suspension volume, corresponding to a single NIH-MDR1-G185 cell volume of 2.4 pl. The cell volume was not affected by Pr-DO3A. In the presence of Pr-DO3A the total Lac was calculated according to the Gluc consumption (1 mol Gluc → 2 mol Lac). The total Lac production was 7.2 mM·h^{-1} whereas the intracellular Lac concentration increased by 7.5 mM·h^{-1}. The total and the intracellular Lac content are shown in Figure 8. The ratio of the

intracellular Lac to the total Lac seems to be constant at an average of (10.2 ± 1.3) % ($\pm$SD). Students t-test shows that there is no significant difference ($p > 0.05$) between the intra- and the total Lac concentrations.

FIGURES 5-8

Cell viability. After each NMR experiments the cell viability was tested with trypan blue exclusion. At low cell density and 37 °C the cell viability was 95 % in the presence as well in the absence of verapamil. At high cell density and 23 °C the cell viability with the shift reagent Pr-DO3A was 94 % after the experimental period of 90 min and 96 % without Pr-DO3A.

DISCUSSION

The aim of the current study was to investigate further the metabolic rate of mouse embryo fibroblasts, and to understand better the previous observations from the ECAR measurements (*1*) (Chapter 7.3). The previous ECAR measurements revealed that the basal ECAR of *MDR1*-transfected cells correlated linearly with the verapamil-stimulated ECAR under conditions where the metabolic state of cells was low, whereas under conditions where the metabolic state of cells was high the correlation flattened out. The increase in the verapamil-stimulated ECAR was suppressed compared to the increase in the basal ECAR. Therefore the question rose whether the flattening of the linear correlation is due to the acidification of the weakly buffered flow medium and, thus, due to the suppression of glycolysis by feedback mechanism. As another possibility it was hypothyzed that the transport capacity of the MCTs might become a limiting factor when the metabolic rate of cells is high (*3*). In order to better understand these issues the metabolic rate of wild-type and *MDR1*-transfected mouse embryo fibroblasts were further studied with the NMR spectroscopy. Furthermore, the intracellular Lac concentration of mouse embryo fibroblast cells was determined and the bio-compatibility of the Lac specific NMR shift reagent Pr-DO3A was tested.

Gatlik-Landwojtowicz et al. (*1*) (Chapter 7.3) determined the metabolic rate of NIH3T3 mouse embryo fibroblast cells by monitoring the ECAR with a Cytosensor microphysiometer. In the current study the metabolic rate (Gluc consumption and Lac

production) of the same cells was determined directly with NMR spectroscopy. Under anaerobic conditions all three rate aspects are connected by the following formula: 1 Gluc → 2 Lac$^-$ + 2 H$^+$. Therefore, the amount of Lac molecules and the protons produced should be the same. The *absolute* metabolic rate of the mouse embryo fibroblasts, wild-type and *MDR1*-transfected, measured with a NMR spectroscopy is about three fold higher than determined with a Cytosensor microphysiometer ($1.0 \cdot 10^8$ molecules Lac·cell^{-1}·s^{-1} compared to $3.0 \cdot 10^7$ H$^+$·cell^{-1}·s^{-1} for NIH-MDR1-G185 cells without verapamil stimulation). Because the amount of lactate extruded in previous investigation (*1*) (Chapter 7.3) was determined also with the spectrophotometric measurements and the results were very close to that obtained with the Cytosensor microphysiometer a systematic error was excluded.

Presently, we can only speculate for the reasons of the difference. One possible explanation could be the different cell preparation. It was observed in the preliminary tests that the small changes of the cell preparation can affect the metabolic rate of cells significantly. The NMR measurements were performed with suspended cells, whereas the cells are attached on the surface of a sensor chip during the Cytosensor measurements. A further difference in these two methods is the buffer concentration. The NMR measurements were performed with a stronger phosphate buffer (50 mM) to avoid the acidification during the measurement period. On the other hand, in the ECAR measurements the weak buffer is mandatory in order to observe the changes in extracellular pH (1 mM) (Chapter 7.3). This could be the reason for the higher *absolute* metabolic rates observed with NMR measurements. The higher buffer concentration reduces the acidification of the extracellular medium and, thus, diminishes the suppression of glycolysis by a feedback mechanism. This could further give an explanation for the previous observations from the ECAR measurements. However, further investigations are needed to confirm this. Despite the difference in the absolute values, the *relative* metabolic rate enhancement during the longtime verapamil stimulation (9 μM) of NIH-MDR1-G185 cells (161 %) determined with the NMR is very close to the values reported by Gatlik-Landwojtowicz et al. (Chapter 7.3 (*1*)) (Cytosensor microphysiometer: 148 %; Spectrophotometric assay: 157 %).

The intra- and the extracellular NMR Lac signals are well separated by the shift reagent Pr-DO3A (Figure 5). The metabolic rate and the cell viability are not affected by Pr-DO3A. Since the extracellular ^{13}C-Lac NMR signal is highly influenced by Pr-DO3A it can hardly be used to determine the extracellular Lac content. However, the extracellular Lac concentration can be estimated from the total Lac concentration which can be

determined from the Gluc consumption if anaerobic conditions are hold. Our measurements show that the intracellular Lac concentration is not constant but it increases as the total Lac concentration increases. Furthermore, the intracellular Lac concentration does not differ from the extracellular Lac concentration significantly. This result indicates that transmembrane Lac transport is fast enough to avoid intracellular Lac accumulation.

We conclude that even if the *absolute* basal metabolic rates determined by the two different methods were not identical the *relative* rate enhancement by verapamil was very close. Therefore, both methods fulfill our purpose to determine the changes in the metabolic rate of living cells. Additionally, the shift reagent Pr-DO3A can be used to observe the intracellular Lac content of living cells without affecting the metabolic rate and the cell viability.

REFERENCES

(1)   Gatlik-Landwojtowicz, E., Aanismaa, P., and Seelig, A. (2004) The rate of P-glycoprotein activation depends on the metabolic state of the cell. *Biochemistry 43*, 14840-14851.

(2)   McConnell, H. M., Owicki, J. C., Parce, J. W., Miller, D. L., Baxter, G. T., Wada, H. G., and Pitchford, S. (1992) The cytosensor microphysiometer: biological applications of silicon technology. *Science 257*, 1906-1912.

(3)   Halestrap, A. P., and Price, N. T. (1999) The proton-linked monocarboxylate transporter (MCT) family: structure, function and regulation. *Biochem J 343 Pt 2*, 281-99.

(4)   Poole, R. C., and Halestrap, A. P. (1993) Transport of lactate and other monocarboxylates across mammalian plasma membranes. *Am J Physiol 264*, C761-82.

(5)   Walter, A., and Gutknecht, J. (1984) Monocarboxylic acid permeation through lipid bilayer membranes. *J Membr Biol 77*, 255-64.

(6)   Sanders, J., and Williams, D. (1972) Shift Reagents in NMR Spectroscopy. *Nature 240*, 385-390.

(7)   Aime, S., Botta, M., Mainero, V., and Terreno, E. (2002) Separation of intra- and extracellular lactate NMR signals using a lanthanide shift reagent. *Magn Reson Med 47*, 10-3.

TABLE

Table 1. The glucose (Gluc) consumption and the lactate (Lac) production of NIH-WT and NIH-MDR1-G185 cells with and without verapamil (9 μM) ($3.6 \cdot 10^6$ cells in 0.4 ml) at 37 ^{o}C and with and without shift reagent Pr-DO3A (7 mM) ($18 \cdot 10^6$ cells in 0.4 ml) at 23 ^{o}C.

cell	T [^{o}C]	pn	Gluc consumption [10^6 molecules·cell^{-1}·s^{-1}]		Lac production [10^6 molecules·cell^{-1}·s^{-1}]	
			no ver	ver	no ver	ver
NIH-WT	37	12	55	57	100	101
NIH-MDR1-G185	37	12	56	85	106	170
			no Pr-DO3A	Pr-DO3A	no Pr-DO3A	Pr-DO3A
NIH-MDR1-G185	23	19	11.2	12.6	22.3	nd

FIGURE LEGENDS

FIGURE 1. Glucose concentration in a suspension of NIH-WT cells ($3.6 \cdot 10^6$) in a phosphate buffer (50 mM, pH 7.4) at 37 °C.

FIGURE 2. Lactate concentration in a suspension of NIH-WT cells ($3.6 \cdot 10^6$) in a phosphate buffer (50 mM, pH 7.4) at 37 °C.

FIGURE 3. Glucose concentration in a suspension of NIH-MDR1-G185 cells ($3.6 \cdot 10^6$) in a phosphate buffer (50 mM, pH 7.4) at 37 °C.

FIGURE 4. Lactate concentration in a suspension of NIH-MDR1-G185 cells ($3.6 \cdot 10^6$) in a phosphate buffer (50 mM, pH 7.4) at 37 °C.

FIGURE 5. ^{13}C-NMR spectra of NIH-MDR1-G185 cells ($18 \cdot 10^6$ cells) in the absence and presence of the shift reagent Pr-DO3A at 23°C. Time separation between the stacked spectra is about 17 min. Intra- and extracellular lactate methyl group signals are separated 22 Hz. Lactate NMR signal intensity in both compartments increases due to glucose consumption.

FIGURE 6. Glucose and lactate concentration in a suspension of NIH-MDR1-G185 cells ($18 \cdot 10^6$) without the shift reagent Pr-DO3A in a phosphate buffer (50 mM, pH 7.4) at 23 °C.

FIGURE 7. Glucose and lactate concentration in a suspension of NIH-MDR1-G185 cells ($18 \cdot 10^6$) with the shift reagent Pr-DO3A in a phosphate buffer (50 mM, pH 7.4) at 23 °C.

FIGURE 8. Intracellular and the total lactate content of NIH-MDR1-G185 cells ($18 \cdot 10^6$) with the shift reagent Pr-DO3A in a phosphate buffer (50 mM, pH 7.4) at 23 °C. Total lactate content was calculated according to glucose consumption.
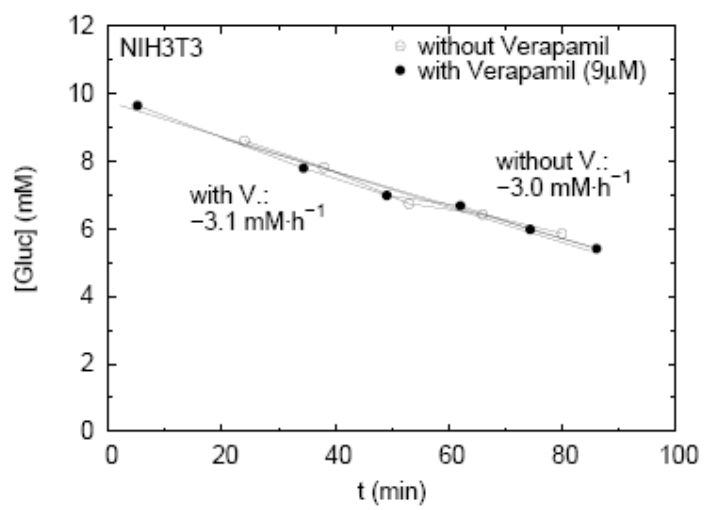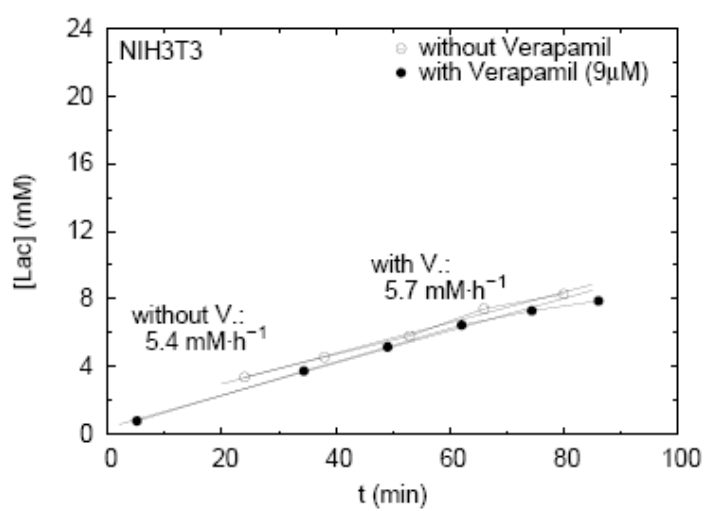
FIGURES

FIGURE 1

FIGURE 2
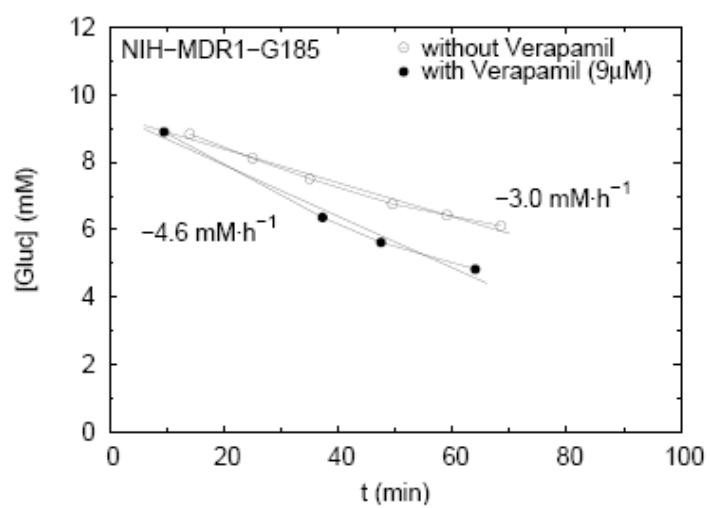
FIGURE 3
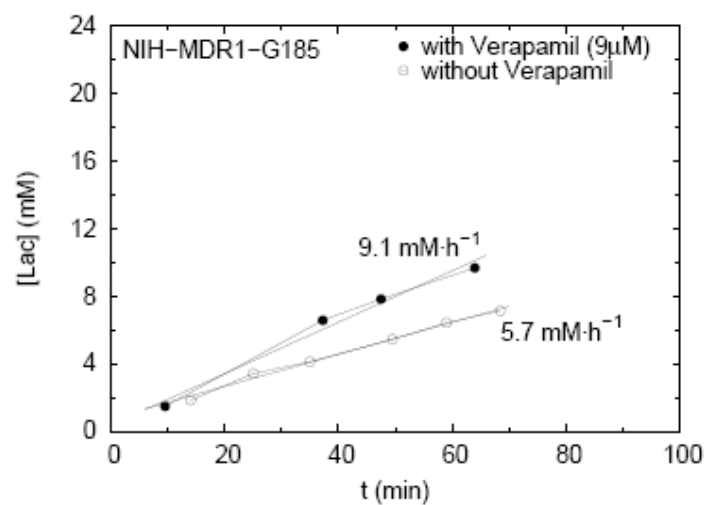
FIGURE 4
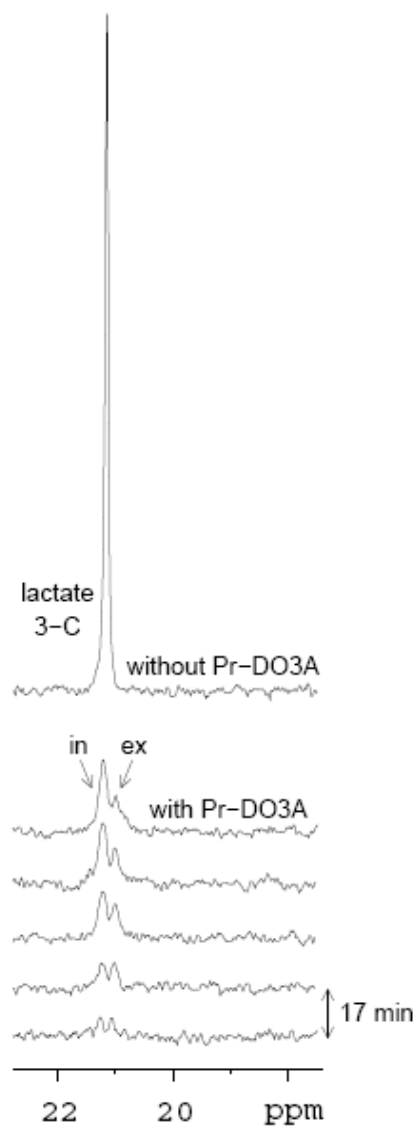
FIGURE 5
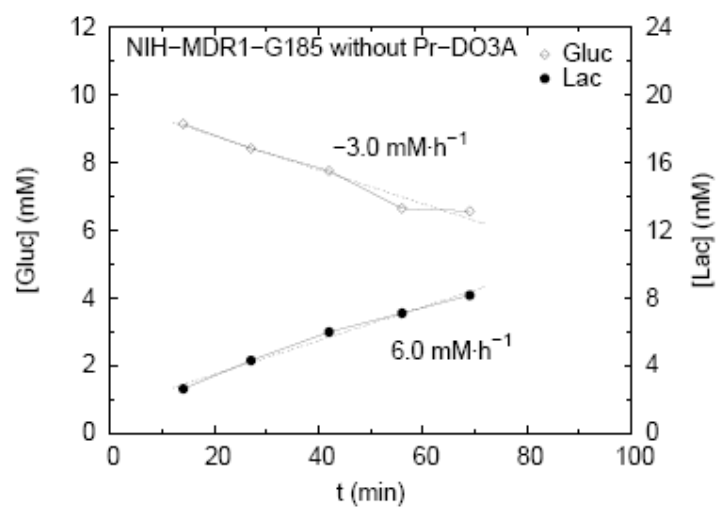
FIGURE 6
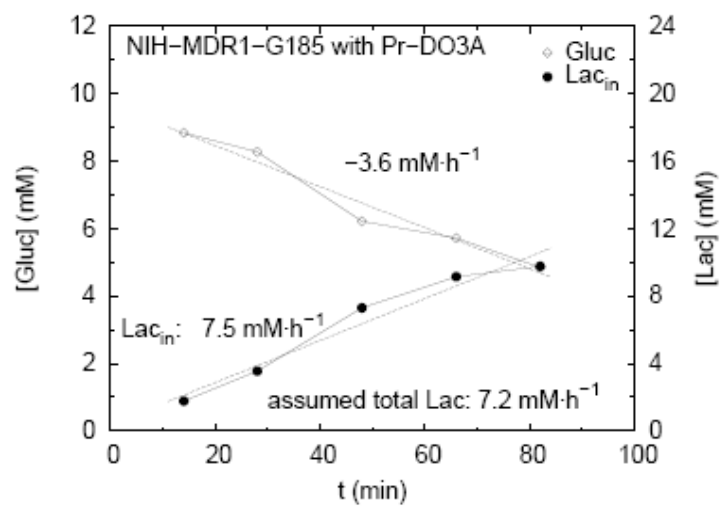
FIGURE 7
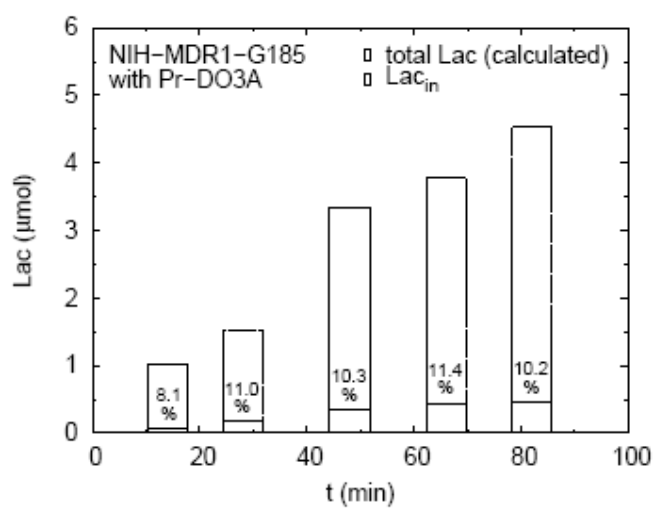
FIGURE 8

7.5 P-glycoprotein Senses Its Substrates and the Lateral Membrane Packing Density: Consequences for the Catalytic Cycle

Päivi Äänismaa, Ewa Gatlik-Landwojtowicz, and Anna Seelig*

Biophysical Chemistry, Biozentrum, University Basel, Klingelbergstrasse 70, CH-4056, Basel, Switzerland
*Corresponding author, Phone: +41-61-267-22-06. Fax: +41-61-267-2-89. E-mail: Anna.Seelig@unibas.ch

RUNNING TITTLE: Transition State Thermodynamics of P-Glycoprotein

Manuscript, *Biochemistry, in press*

ABBREVIATIONS

ABC,	ATP binding cassette transporters in humans include 7 subfamilies ABCA to ABCG
ECAR,	extracellular acidification rate
MDR,	multidrug resistance
NBD,	nucleotide binding domain
Pgp,	human P-glycoprotein-ATPase (MDR1, ABCB1)
PGP1,	hamster P-glycoprotein-ATPase
TMD,	transmembrane domain

ABSTRACT

P-glycoprotein (ABCB1) prevents absorption (e.g. blood-brain barrier) or enhances excretion (e.g. kidney) by moving substrates from the cytosolic to the extracellular membrane leaflet at the expense of ATP hydrolysis. It translocates various drugs and functions in membranes exhibiting different lateral packing densities. To gain more functional insight we measured the temperature dependence of the P-glycoprotein ATPase activity in NIH-MDR1-G185 cell membranes in the absence and presence drugs (Promazine, verapamil and PSC833) exhibiting significantly different transporter affinities. Activation enthalpies ($\Delta H^{\ddagger}$) and entropies ($\mathrm{T}\Delta S^{\ddagger}$) were derived from Eyring plots. In the absence of drugs, the activation enthalpy and the free energy of activation for P-glycoprotein ATPase activity was determined as $\Delta H^{\ddagger} = 92.6 \pm 4.2$ kJ/mol and $\Delta G^{\ddagger} = 73.1 \pm 7.2$ kJ/mol, respectively. Increasing the drug concentration reduced the activation enthalpy, whereby the drug with the highest transporter affinity had the strongest effect ($\Delta\Delta H^{\ddagger} = -21$ %). The free energy of activation decreased for activating ($\Delta\Delta G^{\ddagger} = \sim -3.8$ %) and increased for inhibitory compounds ($\Delta\Delta G^{\ddagger} = \sim +0.7$ %). The drug-specific changes of the free energy of activation are thus barely above thermal energy. A comparison with literature data revealed that a decrease of the lateral membrane packing density reduces the enthalpic and the entropic contribution to the free energy of activation. Although, the P-glycoprotein ATPase activity increases only slightly with decreasing lateral membrane packing density the mode of action changes from strongly entropy-driven at high, to essentially enthalpy-driven at low packing densities. This suggests that the transporter and the membrane form a functional entity.

Footnote

[1] Based on the previously measured Michaelis-Menten constants, K_m, (*23*) and eq. (8) the free energy of ATP binding from water to the transporter, ΔG_b^0, was estimated as $\Delta G_{ATP,b}^0$ ≈ -31.1 kJ/mol and $\Delta G_{ATP,b}^0$ ≈ -30.1 kJ/mol in the presence and absence of drugs, respectively. The free energy of drug binding from water to the activating binding regions of the transporter was estimated as $\Delta G_{tw(1)}^0$ ≈ (- 30 to - 54) kJ/mol, and the free energy of drug binding from the lipid bilayer to the activating binding region of the transporter as $\Delta G_{tl(1)}^0$ ≈ (-7 to -27) kJ/mol (*11*). It should be noted that the Michelis-Menten constants and the dissociation constants are similar for ATP (*49*) as well as for substrates (*14*). Under physiological conditions the free energy of ATP hydrolysis is $\Delta G_{ATP,h}^0$ = - 55 kJ/mol (*50*).

INTRODUCTION

The human ATP-binding cassette transporter, P-glycoprotein, Pgp (MDR1, ABCB1) is highly expressed in absorptive membrane barriers such as the intestinal barrier and the blood-brain barrier where it reduces or even prevents absorption of drugs and toxins. It is also present in membranes of excretory organs such as the liver and the kidney, where it enhances excretion (for review see (*1*)). Moreover, it is abundant in many tumor cells contributing to multidrug resistance (MDR) (for review see (*2*)). The transporter (170 kDa) consists of two transmembrane domains (TMDs) each comprising six putative transmembrane helices and two nucleotide binding domains (NBDs) exposed to the cytosol. The latter dimerize upon nucleotide binding which leads to the formation of an outward-facing conformation by the TMDs (*3*).

The analysis of substrate binding and transport by Pgp is complex for several reasons. First, Pgp transports chemically very different compounds (*4*) at different rates (*5-7*). This is in contrast to most well-known transporters which move one single substrate or one class of substrates at a constant rate. An example for the latter case is the related heterodimer TAP1/TAP2 (ABCB2/ABCB3) associated with antigen processing (*8*).

Second, Pgp binds its substrates in the lipid membrane (*9*) and more precisely in the cytosolic membrane leaflet (*10*) and flips them to the outer leaflet, whereas most well-known transporters, including TAP1/TAP2, (*8*) bind and release their substrates in the aqueous phase. This implies that exogenous compounds have to cross the membrane by passive diffusion to reach the Pgp binding site. It also implies that the concentration of half-maximum activation depends on the nature of the lipid membrane (*11*).

Although, transport by Pgp has long been suggested to correlate with ATP hydrolysis (*12*), the stoichiometry is still discussed. Compounds that diffuse rapidly across the membrane partially escape to the cytosol before they are caught by Pgp. Therefore apparent transport tends to be lower than intrinsic transport (*13*). The direct correlation between transport and ATP hydrolysis was demonstrated using permanently charged compounds such as fluorescent dyes (*14*) or a spin-labeled verapamil analog (*15*) that cannot cross the membrane by passive diffusion. However, these compounds partially remain bound to the extracellular membrane leaflet after transport, and therefore the question of whether one molecule of ATP is required to transport one substrate molecule (*16*) or whether two molecules are required as demonstrated for TAP1/TAP2 (*17*) is difficult to resolve. We quantified the apparent transport of drugs across a cell membrane

as the sum of passive influx and active efflux by Pgp, assuming that the rate of transport equals the rate of ATP hydrolysis. The excellent agreement with data from transport assays provided clear evidence for the direct correlation between the rate of ATP hydrolysis and the rate of effective transport by Pgp (*13, 18*).

Pgp ATPase activity was assessed by measuring the release of inorganic phosphate from inside-out plasma membrane vesicles and proteoliposomes (*5, 7, 19*) or by measuring the release of lactate from living cells (*11*). In the absence of drugs the Pgp ATPase shows basal activity. Upon titration with drugs the activity increases up to a maximum and then decreases again at high concentrations for. The bell-shaped activity profiles have been analyzed by modified Michaelis-Menten kinetics (*5, 7, 11, 19*). The kinetic models used to evaluate the bell-shaped activity curves take into account an activating drug binding step at low and an inhibitory drug binding step at high concentrations, followed by a catalytic ATP hydrolysis step. These models provide an adequate description of the drug-induced variation of Pgp ATPase activity as discussed in detail elsewhere (*11*), however, the catalytic step includes further steps such as substrate translocation and transporter resetting. Despite extensive efforts it is still controversial whether ATP hydrolysis drives only the substrate translocation (*16, 19, 20*), only transporter resetting after release of the substrate (*21*), or both, substrate translocation and transporter resetting (*22, 23*).

Insight into the reaction mechanism can be gained by measuring the temperature dependence of ATP hydrolysis rates which allows determination of the transition state parameters. The first comprehensive transition state analysis for Pgp and hamster P-glycoprotein (PGP1) was performed by Al-Shawi et al. (*19*). They determined the transition state parameters for ATPase activity in liposomes of different composition in the absence and presence of drugs and suggested that the activation enthalpy, $\Delta H^{\ddagger}$, (or activation energy, E_a) as a function of drug concentration first decreases and then increases (*19*). No or only negligibly small effects were observed by others (*5, 24, 25*).

The activation energies, E_a, reported for basal Pgp ATPase activity in various membranes or membrane mimicking systems differ significantly (*19, 24, 26*). Although, several investigators have shown that Pgp senses the lipid composition (*19, 27*) and the phase state of the lipid membrane (*14*) the role of the lipid membrane in modulating basal Pgp ATPase activity has not yet been investigated systematically.

We therefore first analyzed how the drug, its concentration and its affinity to the transporter influence the transition state parameters (i.e the activation enthalpy, $\Delta H^{\ddagger}$, the activation entropy, $\Delta S^{\ddagger}$, and the free energy of activation, $\Delta G^{\ddagger}$) for Pgp ATPase activity.

As test compounds we used promazine, verapamil, and the Pgp inhibitor PSC833, an analog of cyclosporin A, which differ considerably in their affinity to the transporter (*11*). All three compounds are transported by Pgp, although, only verapamil and PSC833 appear as substrates in transport assays (*13, 18*). As membrane system we used inside-out plasma membrane vesicles of NIH-MDR1-G185 cells. Second, we analyzed how the nature of the membrane influences the activity of the Pgp ATPase. To this purposes we compared the transition state parameters for basal Pgp ATPase activity in plasma membranes of NIH-MDR1-G185 cells with transition state parameters for basal Pgp ATPase activity in other systems. A meaningful comparison is possible if the Pgp ATPase containing membranes are characterized by the same physical chemical parameter. Parameters used to characterize lipid membranes are e.g. fluidity, the order parameter, and the lateral membrane packing density. A decrease in fluidity generally correlates with an increase in the order parameter and the lateral membrane packing density. Here, we characterized the membranes in terms of the lateral packing density, π_M, (*28, 29*) since it can be directly estimated from ATPase activity measurements (*11*).

Our investigation shows that all three drugs, even those which reduce the Pgp ATPase activity such as PSC833, reduced the activation enthalpy, $\Delta H^{\ddagger}$, (and the activation energy, E_a) for ATP hydrolysis, whereby the effect was considerable at high drug concentrations. The free energy of activation, $\Delta G^{\ddagger}$, for Pgp ATPase activity decreased at low and increased at high drug concentrations. The free energy of activation, $\Delta G^{\ddagger}$, for Pgp ATPase activity as a function of concentration thus yielded the mirror image of the bell-shaped activity profiles in good agreement with the Eyring theory. The comparison of the transition state parameters for Pgp ATPase activity in the different membrane systems revealed that the activation enthalpy, $\Delta H^{\ddagger}$, and the free energy of activation, $\Delta G^{\ddagger}$ for Pgp ATPase activity decrease with decreasing lateral membrane packing density, π_M, whereby the effect is significant in the former and small in the latter case. The catalytic cycle of the Pgp ATPase is discussed in the light of the present data.

MATERIALS AND METHODS

Materials. PSC833 was a gift from Novartis AG (Basel, Switzerland). Promazine·HCl was obtained from Sigma-Aldrich (Steinheim, Germany), (R/S)-verapamil·HCl from Fluka (Buchs, Switzerland), complete EDTA-free protease inhibitor

cocktail tablets from Roche Diagnostics (Mannheim, Germany), 1,4-dithiol-DL-threitol, DTT, from Applichem (Darmstadt, Germany), and bicinchoninic acid, BCA, protein assay reagents from Pierce (Rockford, IL). All other chemicals were either obtained from Sigma, Fluka or Merck. Cell culture media DMEM with pyruvate (Cat. No. 21969) as well as other compounds required for cell culture such as fetal bovine serum, FBS, L-glutamine, and antibiotics were purchased from Gibco-BRL (Basel, Switzerland).

Stock solutions for the phosphate release assay were made with nanopure water in the case of promazine and verapamil and with DMSO in the case of PSC833. The samples for measurements were prepared by adding 5 µL of the aqueous drug solution or 1 µL of the DMSO/drug solution to the phosphate release assay buffer (total sample volume per well = 60 µL). The final DMSO concentration was constant c = 1.7 % (v/v).

NIH-MDR1-G185 Cells and the Corresponding Plasma Membrane Vesicles. Wild-type (NIH3T3) and *MDR1*-transfected mouse embryo fibroblasts (NIH-MDR1-G185) were generous gifts from Dr. M.M. Gottesman and Dr. S.V. Ambudkar (The National Institutes of Health, Bethesda, MD). Cells were grown in the presence of 0.15 µM colchicine and were maintained as described previously (*30*). The crude plasma membrane vesicles were prepared as described in detail elsewhere (*7*).

Monitoring Pgp ATPase Activity in Plasma Membrane Vesicles with Colorimetric Phosphate Release Assay. The Pgp associated ATP hydrolysis was measured according to Litman et al. (*5*) in 96-well microtiter plate (Nunc F96 MicroWell™ plate, non-treated) with small modifications. Briefly, the plasma membrane vesicles were diluted to a protein concentration of 0.1 mg/mL in ice-cold phosphate release assay buffer (25 mM Tris-HCl including 50 mM KCl, 3 mM ATP, 2.5 mM MgSO$_4$, 3 mM DTT, 0.5 mM EGTA, 2 mM ouabain, and 3 mM sodium azide) unless otherwise stated. The buffer was adjusted to pH 7.0 at the respective temperatures by taking into account the temperature coefficient of the buffer. Each sample contained ~5 µg of protein per total assay volume of 60 µL. Incubation with drugs was started by transferring the plate from ice to a water bath kept at the temperature of choice for 1 h, and was terminated by rapidly cooling the plate on ice. The inorganic phosphate, P$_i$, concentration was determined by addition of ice-cold solution (200 µL) containing ammonium molybdate (0.2 % (w/v)), sulphuric acid (1.43 % (v/v)), freshly prepared ascorbic acid (1 % (w/v)) and SDS (0.9 % (w/v)). After incubation at room temperature (30 min) the released phosphate was quantified colorimetrically at 820 nm using a Spectramax M2 (Molecular Device, Sunnyvale, USA). Reference phosphate standards were included to each 96-well plate. Samples incubated with 0.5 mM vanadate to

determine the vanadate-sensitive Pgp activity were obtained in parallel and were subtracted from the measured values.

Reaction Mechanism. The basic reaction for ATP hydrolysis by Pgp at low drug concentration where only the activating binding region is occupied is shown in Scheme (1). The reaction including the second binding step is shown in detail elsewhere (*11*). The ATP-substrate stoichiometry is still discussed (see Introduction). For simplicity we assume a stoichiometry of 1:1 as suggested previously (*16*). The transporter, T(ATP), binds the transport substrate, S (in the inner leaflet of the lipid membrane), moreover, it binds a second ATP molecule from the aqueous phase, yielding the transporter-ATP-substrate complex, T(ATP)$_2$S. The catalytic step includes, ATP hydrolysis, the release of P$_i$, ADP, and substrate and yields the starting complex T(ATP), where k is the measured catalytic rate constant, and $\Delta G^{\ddagger}$ is the corresponding free energy of activation. In the absence of drugs T(ATP) also binds a second molecule of ATP yielding the complex, T(ATP)$_2$, ATP is then hydrolyzed and the starting complex T(ATP) is formed.

Scheme 1

Data Evaluation Using Modified Michaelis-Menten Kinetics. For data evaluation we used modified Michaelis-Menten kinetics (*5*) which considers two substrate binding steps

$$V_{\text{sw}} = \frac{K_1 K_2 V_{\text{bas}} + K_2 V_1 C_{\text{sw}} + V_2 C_{\text{sw}}^2}{K_1 K_2 + K_2 C_{\text{sw}} + C_{\text{sw}}^2}, \tag{1}$$

where V_{sw} is the rate of P$_i$ release (Pgp ATPase activity) as a function of the substrate concentration in aqueous solution, C_{sw}; V_{bas} is the basal activity of Pgp in the absence of drugs, V_1 is the maximum transporter activity (if only activation occurred) and V_2 is the minimum activity at large substrate concentration. At a substrate concentration, K_1, half-maximum Pgp activation, and at a substrate concentration, K_2, half-maximum Pgp inhibition is reached. The catalytic rate constant, k_1 or turnover number corresponds to $V_1/[\text{T}]_0$, where $[\text{T}]_0$ is the transporter concentration. According to eq. (1) the rate, V_{sw}, can be measured in the presence ($C_{\text{sw}} > 0$) or in the absence of substrates ($C_{\text{sw}} = 0$). In the absence of substrates the rate of the reaction corresponds to the basal rate ($V_{\text{sw}} = V_{\text{bas}}$). For practical reasons, i.e. to investigate the role of drug concentration, we further define $V_{\text{sw}}/[\text{T}]_0$ as k_{sw}.

Temperature Dependence of Pgp ATPase Activity and Evaluation of the Transition State Parameters. The bell-shaped activity curve described by eq. (1) was measured in the present study as a function of temperature yielding the temperature dependence of the different rate parameters such as V_{sw} or k_{sw}. We evaluate the experimental data according to the Eyring equation (2),

$$k = \kappa \frac{k_B T}{h} e^{-\frac{\Delta G^{\ddagger}}{RT}} = \kappa \frac{k_B T}{h} e^{-\frac{\Delta H^{\ddagger}}{RT}} e^{\frac{\Delta S^{\ddagger}}{R}} , \tag{2}$$

where κ is the transmission factor assumed to be unity, k_B is Boltzmann's constant, h Planck's constant, R the gas constant, T the absolute temperature, $\Delta G^{\ddagger}$ the free energy of activation, $\Delta S^{\ddagger}$ the activation entropy, and $\Delta H^{\ddagger}$ the activation enthalpy. It is assumed that all transition states break down with the same rate, $k_B T/h$. On the assumption that the entropy, $\Delta S^{\ddagger}$, of activation, the enthalpy, $\Delta H^{\ddagger}$, of activation, and the constant k_B are temperature independent and, moreover, a single process is monitored, a plot of $\ln(k/T)$ vs. $1/T$ (Eyring plot) yields the activation enthalpy, from the slope and the activation entropy, $\Delta S^{\ddagger}/R$, from the y-axis intercept. This equation permits a calculation of the free energy of activation, $\Delta G^{\ddagger}$, from measured rate constants as

$$\Delta G^{\ddagger} = \Delta H^{\ddagger} - T\Delta S^{\ddagger} \tag{3}$$

The relationship between the activation enthalpy, $\Delta H^{\ddagger}$, and the activation energy, E_a, can be expressed as

$$\Delta H^{\ddagger} = E_a - RT \tag{4}$$

The Isokinetic Relationship. It was proposed that for any single rate-limiting transition state there is a linear free energy relationship between two rate constants for the reaction, k_{T1} and k_{T2}, measured at two different temperatures, $(T_1 < T_2)$ (*19, 31*)

$$\ln k_{T2} = a + b \ln k_{T1}, \tag{5}$$

where a and b are constants. A plot of $\ln k_{T2}$ as a function of $\ln k_{T1}$ yields a preliminary test of a common mechanism in related reactions. When the plots deviate from one another it follows to a high probability that the mechanisms of the two related reactions are different.

Estimation of the Free Energies of Drug and ATP Binding to Pgp. The free energies of drug binding, $\Delta G_{tw(1)}^{0}$, were calculated from concentrations of half-maximum activity, K_1. Based on the assumption that the binding step is much faster than the subsequent catalytic step (*11*), K_1 can be considered as dissociation constant and the inverse $1/K_1$ as transporter-water binding constant, $K_{tw(1)}$ to a first approximation.

$$1/K_1 \cong K_{tw(1)} \tag{6}$$

The assumption made in eq. (6) is supported by the similarity of the concentrations of half-maximum activation, K_m, for ATP hydrolysis and the dissociation constant, K_d determined for ATP binding to MIANS-labelled Pgp. Moreover, the K_m for tetramethylrosamine also compared favorably with the K_d for MIANS-labelled Pgp (*14*).

The corresponding free energy relationship is shown below,

$$\Delta G_{tw(1)}^{0} \cong - RT\ln(C_w K_{tw(1)}) \cong - RT\ln(C_w (1/K_1)). \tag{7}$$

The superscript zero refers to a biological standard state (pH 7.4 and 37°C), and $C_w = 55.3$ mol/L corresponds to the molar concentration of water at 37°C. The constants $K_{tw(1)}$ and $1/K_1$ with the units [L/mol] are multiplied by the concentration of water, C_w [mol/L], to obtain mole fraction units (*32*). A corresponding expression was formulated for ATP binding,

$$\Delta G_{b}^{0} = - RT\ln(C_w (1/K_m)). \tag{8}$$

RESULTS

Pgp ATPase Activity in Inside-Out Plasma Membrane Vesicles as a Function of Drug Concentration and Temperature. The test compounds, promazine, verapamil, and PSC833 are listed in Table 1 together with their molecular weight, cross-sectional area, A_D, concentration of half-maximum Pgp ATPase activation, K_1, maximum activity, V_1, and free energy of binding from water to the activating binding region of the transporter, $\Delta G_{tw(1)}^{0}$.

The more negative the free energy of binding, $\Delta G^{0}_{tw(1)}$, the higher is the binding affinity to the transporter as shown previously (*11*). The molecular weight, the cross-sectional area, A_D, and the binding affinity to the transporter increase considerably in the order: promazine < verapamil < PSC833 and the concentrations of half maximum activation, K_1, differ by orders of magnitude.

The basal, V_{bas}, and drug-induced Pgp ATPase activity, V_{sw}, in inside-out vesicles formed from plasma membranes of NIH-MDR1-G185 cells were measured by monitoring the phosphate release rate with a colorimetric assay (*7*). Titrations were performed as a function of concentration at different temperatures over the temperature range, $\Delta T = (25 - 37)$ ^{o}C, with the buffer adjusted to pH 7.0 at each temperature. The titration curves are shown in Figure 1A-C.

The first point in each titration curve (Figure 1A-C) corresponds to basal activity, V_{bas}, and the subsequent points to drug-induced ATPase activity, V_{sw}. The solid lines drawn in Figure 1 are fits to the measured data using the kinetic model given in eq. (1).Each drug shows a specific ATPase activity profile that is characterized by four parameters (see eq. (1)), the concentration of half-maximum activation, K_1, (with one molecule bound to the transporter) the concentration of half-maximum inhibition, K_2, (with two molecules bound to the transporter), and the maximum, V_1, and minimum, V_2, ATPase activity, respectively (see also ref. (*5*)). Promazine (Figure 1A) and verapamil (Figure 1B) exhibit the typical bell-shaped activity curves as a function of concentration, whereas PSC833 (Figure 1C) reduces the ATPase activity relative to basal values in the whole concentration range measured. With increasing temperature basal, V_{bas}, and drug-induced ATPase activity, V_{sw}, increase. However, the shape of the activity curves remains approximately constant for a given drug. For comparison with literature data (see below, Figure 8), we also measured the Pgp ATPase activity as a function of verapamil concentration at pH 7.5 (Tris buffer) and T = 35 °C (see Table 1). The concentration of half-maximum activation, K_1, is lower than at pH 7.0 due to the higher lipid-water partition coefficient, K_{lw}, of the drug at the higher pH, however, the maximum activity, V_1, is similar (Table 1).

TABLE 1

FIGURE 1A-D

The Thermodynamic Transition State Parameters for Pgp ATPase Activity in the Presence of Different Drugs. Figure 2A-C displays plots of $\ln(k_{sw}/T)$ vs. the reciprocal absolute temperature (Eyring plot) in the absence and presence of drugs for inside-out plasma membrane vesicles of NIH-MDR1-G185 cells. Each line corresponds to a specific concentration in the activity profiles (Figure 1). The lines are linear fits to the data. The activation enthalpy, $\Delta H^{\ddagger}$, and activation entropy, $\Delta S^{\ddagger}$, for Pgp ATPase activity were determined from the slope and the y-axis intercept, respectively. The transition state parameters determined from Eyring plots are summarized in Table 1. As previously pointed out by Al-Shawi et al. (*19*) data derived from these plots have to be considered as apparent values, valuable for the particular membrane and the temperature range indicated.

FIGURE 2A-D

Figure 3 shows $\ln V_1$ for promazine and verapamil as a function of the reciprocal absolute temperature. The maximum rate, V_1, is expressed relative to basal value at the corresponding temperature. In this representation the maximum rate, V_1, decreases with increasing temperature. Because the change in activity with temperature is more pronounced in the absence than in the presence of drugs.

Transition State Parameters of the Pgp ATPase Activity as a Function of Drug Concentration. We have measured the transition state parameters for the Pgp ATPase activity in NIH-MDR1-G185 plasma membranes over a large range of concentrations (Figure 2) covering the full activity profiles (Figure 1). Figure 4A-C shows the thermodynamic transition state parameters, $\Delta H^{\ddagger}$, $T\Delta S^{\ddagger}$ and $\Delta G^{\ddagger}$, derived for Pgp ATPase activity as a function of promazine, verapamil and PSC833 concentration, respectively. The concentration of half-maximum activation for promazine and verapamil and the concentration of half-maximum inhibition for PSC833 are indicated by arrows. In the absence of drugs the activation enthalpy for ATPase activity in plasma membrane vesicles of NIH-MDR1-G185 cells was determined as $\Delta H^{\ddagger} = 92.6 \pm 4.2$ kJ/mol. Increasing the drug concentration reduced the activation enthalpy, $\Delta H^{\ddagger}$, and the activation entropy, $T\Delta S^{\ddagger}$, for both, activating and inhibitory compounds as seen in Figure 4A-C. The reduction in the enthalpy increased in the order verapamil ($\Delta\Delta H^{\ddagger} = -14$ kJ/mol, (-15 %) < PSC833 ($\Delta\Delta H^{\ddagger} = -19.2$ kJ/mol, (-21 %) < promazine ($\Delta\Delta H^{\ddagger} = -27.6$ kJ/mol (-30 %) at the highest concentrations investigated. At high drug concentrations the entropy contribution almost vanished, and the Pgp ATPase was therefore essentially enthalpy driven under these

conditions. Figure 4A-C shows that the drug-induced changes are not negligible as assumed previously (*5, 24, 25*) but depend on the drug concentration applied. Data in Figure 4A-C also differ from those observed by Al-Shawi et al. (*19*).

The free energy of activation was determined as $\Delta G^{\ddagger} = 73.1$ kJ/mol (at T = 37 °C) in the absence of drugs. With increasing promazine and verapamil concentration (Figure 4D, E) the free energy of activation, $\Delta G^{\ddagger}$, first decreased and then increased again, while it increased already at low concentrations of PSC833 (Figure 4F). The decrease relative to the basal value was $\Delta\Delta G^{\ddagger} = -2.8$ kJ/mol (-3.8%) for verapamil, and the increase relative to the basal value was $\Delta\Delta G^{\ddagger} = +0.5$ kJ/mol (+0.7%) for PSC833. The drug-induced changes in the free energy of activation, $\Delta G^{\ddagger}$, relative to basal values are thus small, but drug specific.

To test the relevance of the $\Delta G^{\ddagger}$ values we inserted them into the Eyring eq. (2) and calculated the activity profiles (i.e. the rate constants, k_{sw}, as a function of concentration) for comparison with the ATPase activity profiles measured directly at a given temperature (Figure 4G-I). Since the $\Delta G^{\ddagger}$ values change with concentration the calculated curve is not a simple exponential (see eq. (2)) but is indeed bell-shaped. The resulting activity profiles showed a two to three fold increase and a somewhat smaller decrease in rate depending on the concentration in excellent agreement with the experimentally determined activity profiles.

The temperature dependence of the Pgp ATPase activity was also measured in living NIH-MDR1-G185 cells by monitoring the extracellular acidification rate, ECAR, (*11*) in the absence and in the presence of verapamil. Below 35°C similar Eyring plots were obtained (*33*).

FIGURE 4A-F

One or More than One Rate-Limiting Transition State? As seen in Figure 1 the Pgp ATPase works (i) under basal conditions (in the absence of drugs), (ii) under conditions of drug-induced activation (at low and intermediate concentrations) and (iii) under conditions of drug-induced inhibition (at high concentrations). To see whether the three different modes of Pgp ATPase activity are rate-limited by the same transition state we applied the isokinetic equation (eq. (5)) (*31*) as proposed by Al-Shawi *et al*. (*19*). The logarithm of the rate constants, $\ln V_{sw}$, measured as a function of the drug concentration at $T_2 = 31$°C and $T_3 = 37$°C were plotted as a function of the corresponding rate constants, $\ln V_{sw}$, measured at

$T_1 = 25°C$ according to eq. (5) (Figure 5). As seen in Figure 5, data fit linear regression lines with a slope, m ≈ 1 (m = 0.99 and m = 0.90, respectively). From these data no indication of more than one rate-limiting transition state can be observed which suggests that the basal, the drug-induced and the drug-inhibited Pgp ATPase activity are rate-limited by the same transition state.

In a previous investigation (*19*) data for low and high drug concentrations also fell to the same regression line (slope of m ≈ 0.8) which is close to that in the present analysis. However, the values for basal ATPase activity deviated and the regression line revealed a slope of m ≈ 0.5 only. As a consequence two different transition states, one associated with uncoupled basal activity and the other with coupled drug transport activity, were proposed. It should be noted that the investigation was performed with membranes exhibiting different lateral packing densities which might affect the slope of the curve measured under basal conditions (see Discussion).

FIGURE 5

DISCUSSION

We measured the basal and drug-induced Pgp ATPase activity in inside-out plasma membrane vesicles of NIH-MDR1-G185 cells over a broad concentration range using promazine with low, verapamil with intermediate, and PSC833 with high affinity to the transporter. The activity profile for each drug was measured at different temperatures which allowed assessment of the transition state parameters, $\Delta H^{\ddagger}$, $T\Delta S^{\ddagger}$, and $\Delta G^{\ddagger}$ for Pgp ATPase activity from Eyring plots in the absence and presence of drugs. The relevance of the free energies of activation, $\Delta G^{\ddagger}$, determined was demonstrated by inserting the values into the Eyring equation (eq. (2)) which yielded the rate constants in excellent agreement with the primary data. In the following we compare the transition state parameters for Pgp ATPase activity in plasma membranes of NIH-MDR1-G185 cells in the absence of drugs with those obtained previously in other systems and analyze the influence of the lateral membrane packing density, π_M. We then discuss the changes in the transition state parameters observed upon titration with the different drugs and estimate to which extent they are due to direct substrate-transporter interactions and to which extent they are

membrane mediated. Models for the catalytic cycle of the Pgp ATPase are discussed on the basis of the present data.

   The Transition State Parameters for Pgp ATPase Activity in the Absence of Drugs. The transition state parameters for basal Pgp ATPase activity measured in different lipid membranes or membrane mimicking systems (*19, 26*) differ considerably. A meaningful comparison with the transition state parameters for Pgp ATPase activity determined in plasma membranes of NIH-MDR1-G185 cells is possible if data are plotted as a function of the lateral packing density, π_M, of the different membranes or membrane mimicking systems as seen in Figure 6.

   The lateral membrane packing density, π_M, is not directly measurable, but can be assessed in comparison to the lateral membrane packing density or surface pressure, π, of a lipid monolayer which is directly measurable. Monolayer-bilayer equivalence packing densities (or equivalence pressures) were obtained by comparing binding isotherms to lipid bilayers with binding isotherms to lipid monolayers at different lateral packing densities (*28*). To assess the lateral packing density, π_M, of a lipid membrane containing the Pgp ATPase we measured the concentration of half-maximum Pgp ATPase activation, K_1, for verapamil and compared it with the K_1, value for verapamil measured in a membrane with known lateral membrane packing density (for details see (*11*)). For bilayer membranes the lateral packing density varied between $\pi_M \cong 51$ mN/m as estimated for mixed liposomes composed of 60 % (w/w) *E. Coli* lipids, 17.5 % egg phopshatidylcholine, 10% bovine brain phosphatidylserine, and 12.5% cholesterol (*19*) and $\pi_M = 30.5 \pm 1.0$ mN/m as estimated for plasma membranes of NIH-MDR1-G185 cells (*11*). For CHAPS micelles the lateral packing density was estimated as $\pi_M \cong 10$ mN/m in analogy to that of SDS micelles (*34*). The extrapolation to zero lateral membrane packing density ($\pi_M = 0$ mN/m) can be considered as the hypothetical situation of Pgp working in an isotropic solvent. For comparison the transition state parameters for ATP hydrolysis by the water soluble NBD of the glucose ABC transporter of the extreme thermoacidophile Sulfolobus solfataricus, GlcV (*35*) were included in Figure 6. The soluble NBDs of GlcV dimerize upon ATP binding and hydrolyze both ATP molecules in the interface (*35*).

   The free energy of activation for Pgp ATPase activity appears at first sight almost packing density independent. However, it slightly decreases from $\Delta G^{\ddagger} = 73.9$ kJ/mol at $\pi_M \cong 51$ mN/m to $\Delta G^{\ddagger} = 72.2$ kJ/mol at $\pi_M \cong 0$ mN/m ($\Delta\Delta G^{\ddagger} = -1.7$ kJ/mol) which translates into an approximately 2 fold acceleration of ATP hydrolysis. This is in good agreement with previous observations showing that basal Pgp ATPase activity is higher in more

disordered lipids with low phase transition temperatures, T_c, than in more ordered lipids with a higher phase transition temperature (see Figure 7 in ref. (*36*)). The free energy of activation, $\Delta G^{\ddagger}$, has contributions from both, enthalpy, $\Delta H^{\ddagger}$, and entropy, $T\Delta S^{\ddagger}$, the transporter can thus function either by lowering the enthalpy or enhancing the entropy of activation (i.e. decreasing $-T\Delta S^{\ddagger}$) (eq. (2)). In membranes or membrane mimicking systems with the lowest lateral packing density, π_M, the activation entropy, $T\Delta S^{\ddagger}$, is close to zero and the Pgp ATPase thus functions in an essentially enthalpy-driven manner. A similar situation is observed for the soluble NBDs of GlcV (*35*) which is also enthalpy-driven. With increasing lateral membrane packing density, π_M, the enthalpy, $\Delta H^{\ddagger}$, and the entropy, $T\Delta S^{\ddagger}$, contribution increase and the latter becomes significant. This suggests that the lipid membrane plays a crucial role in the mode of activation of the Pgp ATPase. The function of proteins embedded in densely packed lipid bilayers may thus be supported by the high "entropy-producing potential" of lipid membranes as suggested previously (*37*).

FIGURE 6

All over, the activation energy, E_a, and activation enthalpy, $\Delta H^{\ddagger}$, for Na/K-ATPase seem to be smaller than those of the Pgp ATPase. The activation energy was determined as $E_a \approx 19$ kJ/mol for the Na/K-ATPase in the foot muscle of land snails (*38*). The activation enthalpy was determined as $\Delta H^{\ddagger} \approx 67$ kJ/mol and $\Delta H^{\ddagger} \approx 74$ kJ/mol for the Na/K-ATPase from the shark rectal gland reconstituted into dioleoylphosphatidylcholine and into dioleoylphosphatidylcholine containing 40% cholesterol, respectively (*39*). Land snail membranes with a high content of highly unsaturated lipids (*40*) exhibit most likely the lowest lateral packing density, membranes formed from dioleoylphosphatidylcholine exhibit an intermediate and the cholesterol containing membranes the highest lateral packing density of the three membranes cited. Provided the Na/K-ATPases from the different sources are comparable the activation energy, E_a, seems again to increase with the lateral packing density of the membrane. For the sarcoplasmic reticulum Ca-ATPase it was shown that the lipid fluidity directly modulates the overall protein rotational mobility and the ATPase activity (*41*) which again supports the trends observed in Figure 6.

The Transition State Parameters as a Function of the Drug Affinity to the Transporter and Drug Concentration. Figure 7 displays the drug-induced Pgp ATPase activity in plasma membrane vesicles formed from NIH-MDR1-G185 cells, ln k_1 (indicated as ln*k* in Figure 7), as a function of the binding affinity of the drug to the

transporter (i.e. the free energy of drug binding from water to the transporter, $\Delta G^0_{tw(1)}$) for promazine, verapamil, and PSC833 in comparison to other compounds measured previously under the same conditions (*7*). The Pgp ATPase activity, $\ln k_1$, decreases linearly with increasing affinity of the drug from water to the transporter (or decreasing free energy of drug binding from water to the transporter, $\Delta G^0_{tw(1)}$). A similar linear correlation between the rate constant, $\ln k$, and the affinity to the transport system was observed previously for maltoporin LamB of *E.coli* (*42*) as shown for comparison in Figure 7. Maltoporin is a much simpler transport system which allows the translocation of maltodextrins of different lengths.

Maltodextrins interact with maltoporin essentially via transient hydrogen bond formation, whereby the substrates provide the hydrogen bond donor groups and the transporter the hydrogen bond acceptor groups (*42*). A related mechanism has been proposed for the interaction of the Pgp ATPase with transport substrates. However, in the case of the Pgp ATPase the substrate provides the hydrogen bond acceptor groups and Pgp the hydrogen bond donor groups (*4, 11, 43*). It is interesting to note that the overall rate of translocation by maltoporin is in the millisecond range, whereas, the rate of substrate translocation by Pgp is in the range of seconds. The low rate of transport by the Pgp ATPase seems to be due to the requirement for a conformational switch between the binding- and the release-competent conformation, respectively.

According to the Eyring equation (eq. 2) the rate, *k*, decreases with increasing free energy of activation, $\Delta G^{\ddagger}$. Figure 7 thus suggests that the free energy of activation, $\Delta G^{\ddagger}$, for Pgp ATPase activity increases with increasing substrate affinity to the transporter (or decreasing free energy of activation, $\Delta G^0_{tw(1)}$). PSC833, the compound with the highest affinity to the transporter indeed shows the highest activation energy, $\Delta G^{\ddagger}$, as seen in Table 2.

FIGURE 7

In addition to the drug affinity, the drug concentration also plays a substantial role for the Pgp ATPase activity (Figure 1A-D and Figure 4 G-I) and the corresponding free energy of activation, $\Delta G^{\ddagger}$ (Figure 4D-F). The change in the free energy of activation varied from $\Delta\Delta G^{\ddagger} \sim$ -3.8% to $\Delta\Delta G^{\ddagger} \sim$ +0.7%. The activation enthalpy, $\Delta H^{\ddagger}$, and the activation entropy, $T\Delta S^{\ddagger}$, for the Pgp ATPase activity in NIH-MDR1-G185 plasma membranes decreased with increasing concentration for both activating and inhibitory compounds as

seen in Figure 4A-C. At the highest concentrations measured the reduction in the enthalpy, $\Delta\Delta H^{\ddagger}$, increased in the order verapamil < PSC833 < promazine. However, if the compounds are compared at identical concentrations the "inhibitor" PSC833 has the strongest and promazine the weakest enthalpy lowering effect. The strong effect of promazine at the high concentrations measured (Figure 4A-C) may be twofold. First, more than one molecule of the drug may be bound to the transporter and the transporter my thus feel a cargo of "higher affinity". The low activation entropy in the presence of more than one molecule with low affinity or of one molecule with high affinity may be due to a loss of residual motion of the substrate-transporter complex. Moreover, the high drug concentration in the membrane (in the case of promazine) may slightly lower the order parameter and the lateral packing density of the membrane.

The Lateral Packing Density of the Membrane May Vary in the Course of the Experiment. Drug partitioning into membranes leads to a reduction of the fatty acyl chain order of lipids and a concomitant decrease of the lateral lipid packing density, π_M, of the membrane, as has been shown by deuterium NMR for verapamil (*44*), local anesthetics (*45*) and also for cyclosporin A, an analog of PSC833, however, to a lesser extent (*46*). Since the mole fraction of drugs in the lipid membrane at the concentrations of half-maximum Pgp ATPase activation is rather high (*11*) a reduction of the membrane order and the lateral membrane packing density can be expected for most drugs.

The fatty acyl chain order of lipid bilayers and the lateral packing density of the lipid bilayer, π_M, also decrease with increasing temperature as shown by deuterium NMR (*47*). In the limited temperature intervals, ΔT, the lateral membrane packing density changes may, however, be small as suggested by the apparently linear Arrhenius or Eyring plots for Pgp ATPase activity ($\Delta T = 18$ ^{o}C for crude membrane preparations of Chinese hamster ovary cells, CR1R12 (*5*), $\Delta T = 17$ ^{o}C for HeLa cells (*22*), and $\Delta T = 12$ ^{o}C for proteoliposomes (*19*) and plasma membrane of NIH-MDR1-G185 cells (present investigation)). A much broader temperature range ($\Delta T = 40$ °C) was accessible by using radioactively labeled ATP and yielded a convex Arrhenius plot for the Pgp ATPase in crude membranes of CH^{R}B30 (*25*). It is interesting to note that if the activation energy, E_a, for crude membranes of CH^{R}B30 (*25*) is assessed in the temperature range used in the present investigation a comparable value is obtained. The water soluble NBD of the glucose ABC transporter of the extreme thermoacidophile Sulfolobus solfataricus, GlcV, shows in contrast an Eyring plot which is linear over a much broader temperature range

($\Delta T = 60$ °C) (*35*). Nevertheless, the change in the lipid packing density with temperature may not be the only factor responsible for the non-linear Eyring plot of the Pgp ATPase.

     Differentiation between Drug-Induced and Packing Density-Induced Effects. As discussed, the enthalpy of activation, $\Delta H^{\ddagger}$, for Pgp ATPase activity decreases with decreasing lateral membrane packing density, π_M, (Figure 6) as well as with increasing drug concentration (Figure 4A-C). The question arises to which extent the decrease in the activation enthalpy in the present experiments is due to a drug-induced reduction in the membrane packing density, π_M, and to which extent it is due to the direct drug-transporter interaction. To address this question in more detail we compared the basal rates of ATP hydrolysis with the drug-induced rates, both measured at different lateral membrane packing densities (Figure 8A). In Figure 8A all data are given relative to the basal rate at the highest lateral packing density, taken as 100 %. The comparison in Figure 8A reveals that the maximum possible acceleration achieved by loosening the lateral membrane packing density, π_M, is lower than that induced by concentrations of verapamil yielding the maximum activity, V_1, but higher than the effect induced by the inhibitory PSC833. This implies that a significant part of the activity modulating effect of drugs is due to the direct substrate-transporter interaction and that the acceleration of ATP hydrolysis due to drug-induced membrane loosening is small. Figure 8A moreover reveals that a specific drug (e.g. verapamil) induces approximately the same rate of ATP hydrolysis in different membranes if compared to a single reference state, (e.g. the basal rate at the highest lateral packing density). This further supports the assumption that the substrate transporter interaction is independent of the lateral membrane packing density (*11*). Generally, drug-induced Pgp ATPase activity is expressed relative to the basal activity in the respective system as shown in Figure 8B. This representation gives the impression that the Pgp ATPase works better in densely packed, than in loosely packed membranes which is misleading (for review see also Introduction in ref. (*48*)). A comparable situation is seen in Figure 3 which shows a decrease of the fold activity with increasing temperature, due to the fact that the basal activity shows stronger temperature dependence than the drug-induced activity.

     Discussion of the Catalytic Cycle - Does Drug Transport Occur before or after ATP hydrolysis by the Pgp ATPase? We first consider the Pgp ATPase as a simple enzyme, ignoring its transport function. Under these conditions ATP is the substrate which is transformed to inorganic phosphate and ADP. For this reaction three transition states can be assumed, one for ATP binding (with the free energy of activation, $\Delta G^{\ddagger}_1$), a second one

for ATP hydrolysis (with the free energy of activation, $\Delta G^{\ddagger}_2$), and a third one for ADP release (with the free energy of activation, $\Delta G^{\ddagger}_3$), whereby the second step is rate-limiting ($\Delta G^{\ddagger}_2 \gg \Delta G^{\ddagger}_1$ and $\Delta G^{\ddagger}_3$). The free energies of ATP binding and ATP hydrolysis are similar[1] and are dissipated. The energy levels of the substrate decrease from one step to the other, whereas the energy level of the enzyme remains unchanged. A model with a rate-limiting ATP hydrolysis step could also be considered in the presence of a transport substrate (i.e. a drug) which lowers the activation energy, $\Delta G^{\ddagger}_2$. If we assume that this model is appropriate for the Pgp ATPase, drugs must still be bound when the transition state for ATP hydrolysis has formed and drugs are released only after ATP is hydrolyzed. On the basis of the apparent linearity of Eyring plots an analogous model was suggested by Al-Shawi et al. (*19*).

A different interpretation is possible if we assume a model analogous to that proposed previously for Na,K-ATPases (*50*) and adopted for the Pgp ATPase by Higgins and Linton (*21*). In this model ATP binding and hydrolysis serve to switch the protein between two conformational states with a high- and a low-affinity binding site for the substrate, respectively. The free energy of ATP binding and ATP hydrolysis may be transformed into potential energy which is stored in the protein and is then used to drive the two conformational changes. If we further assume that the two conformational changes of the Pgp ATPase exhibit similar free energies of activation, $\Delta G^{\ddagger}$, the transition state for the first conformational change could be modulated by the presence of drugs, and drugs could then be released before the ATP-driven resetting step occurs. Based on the observation that the rate of ATP hydrolysis depends in an exponential manner on the drug affinity to the transporter (Figure 7) we previously suggested that drugs may be released before ATP is hydrolyzed (*7*), which is consistent with the second model. However, for a conclusive answer, further experiments are required.

FIGURE 8

Summary. To test how Pgp senses its substrates we measured the temperature dependence of the Pgp ATPase activity in inside-out plasma membrane vesicles of NIH-MDR1-G185 cells over a broad concentration range using three drugs with different affinities to the transporter and determined the transition state parameters from Eyring plots in the temperature range, $\Delta T = (25 - 37)$ °C. To investigate how the Pgp senses the lipid composition of the membrane we compared the transition state parameters for basal

ATPase activity in inside-out plasma membrane vesicles of NIH-MDR1-G185 cells with the transition state parameters for Pgp ATPase activity in other systems exhibiting different lateral membrane packing densities, π_M. This revealed that the free energy of activation, $\Delta G^{\ddagger}$, decreases slightly with decreasing lateral membrane packing density, π_M (corresponding to a maximally two-fold increase in activity). Moreover, it revealed that the transporter works in an essentially enthalpy driven manner at low, and in a more entropy driven manner at high lateral packing densities.

Addition of low-affinity drugs at low and intermediate concentrations lead to a small decrease (maximally $\Delta\Delta G^{\ddagger} = \sim$ -3.8 %) in the free energy of activation, $\Delta G^{\ddagger}$ relative to basal values (corresponding to an increase in ATPase activity). Addition of high-affinity drugs at low concentrations, or low-affinity drugs at high concentrations, lead, in contrast, to a small increase ($\Delta\Delta G^{\ddagger} = \sim$ +0.7 %) in the free energy of activation, $\Delta G^{\ddagger}$, (corresponding to a decrease in the rate of transport). The activation enthalpy, $\Delta H^{\ddagger}$ (or activation energy E_a), and the activation entropy, $T\Delta S^{\ddagger}$, decreased significantly with increasing concentration, and increasing transporter affinity of the drug. At high drug concentrations the Pgp ATPase worked in an essentially enthalpy-driven manner which may be due to the loss of residual motion of the transporter and, however, to lower extent, to the loosening of the lateral membrane packing density upon drug partitioning into the membrane.

Although, basal activity seems to increases slightly with decreasing lateral packing density, π_M, the effective transport rate seems not to decrease. The Pgp ATPase is thus able to efficiently transport cargo of considerable size at almost constant rate in membranes of different lateral packing densities, π_M, whereas uncatalyzed flip-flop and diffusion of molecules across a lipid membrane decrease exponentially with increasing lateral packing density, π_M, and increasing cross-sectional area, A_D (*13, 29*). Densely packed lipid membranes, expressing a high level of the Pgp ATPase thus guarantee excellent barrier properties. The catalytic cycle may be similar to that of Na,K-ATPases, where cargo is released before ATP is hydrolyzed, however, further experiments are required to get a conclusive answer.

REFERENCES

1. Glavinas, H., Krajcsi, P., Cserepes, J., and Sarkadi, B. (2004) The role of ABC transporters in drug resistance, metabolism and toxicity, *Curr Drug Deliv 1*, 27-42.
2. Gottesman, M. M., Ludwig, J., Xia, D., and Szakacs, G. (2006) Defeating drug resistance in cancer, *Discov Med 6*, 18-23.
3. Rosenberg, M. F., Callaghan, R., Modok, S., Higgins, C. F., and Ford, R. C. (2005) Three-dimensional structure of P-glycoprotein: the transmembrane regions adopt an asymmetric configuration in the nucleotide-bound state, *J Biol Chem 280*, 2857-2862.
4. Seelig, A. (1998) A general pattern for substrate recognition by P-glycoprotein, *Eur J Biochem 251*, 252-261.
5. Litman, T., Zeuthen, T., Skovsgaard, T., and Stein, W. D. (1997) Structure-activity relationships of P-glycoprotein interacting drugs: kinetic characterization of their effects on ATPase activity, *Biochim Biophys Acta 1361*, 159-168.
6. Al-Shawi, M. K., and Senior, A. E. (1993) Characterization of the adenosine triphosphatase activity of Chinese hamster P-glycoprotein, *J Biol Chem 268*, 4197-4206.
7. Aanismaa, P., and Seelig, A. (2007) P-Glycoprotein Kinetics Measured in Plasma Membrane Vesicles and Living Cells, *Biochemistry 46*, 3394-3404.
8. Gorbulev, S., Abele, R., and Tampe, R. (2001) Allosteric crosstalk between peptide-binding, transport, and ATP hydrolysis of the ABC transporter TAP, *Proc Natl Acad Sci U S A 98*, 3732-3737.
9. Raviv, Y., Pollard, H. B., Bruggemann, E. P., Pastan, I., and Gottesman, M. M. (1990) Photosensitized labeling of a functional multidrug transporter in living drug-resistant tumor cells, *J Biol Chem 265*, 3975-3980.
10. Shapiro, A. B., and Ling, V. (1997) Extraction of Hoechst 33342 from the cytoplasmic leaflet of the plasma membrane by P-glycoprotein, *Eur J Biochem 250*, 122-129.
11. Gatlik-Landwojtowicz, E., Aanismaa, P., and Seelig, A. (2006) Quantification and characterization of P-glycoprotein-substrate interactions, *Biochemistry 45*, 3020-3032.
12. Ambudkar, S. V., Cardarelli, C. O., Pashinsky, I., and Stein, W. D. (1997) Relation between the turnover number for vinblastine transport and for vinblastine-stimulated ATP hydrolysis by human P-glycoprotein, *J Biol Chem 272*, 21160-21166.
13. Seelig, A. (2007) The role of size and charge for blood-brain barrier permeation of drugs and fatty acids, *J Mol Neurosci 33*, 32-41.
14. Lu, P., Liu, R., and Sharom, F. J. (2001) Drug transport by reconstituted P-glycoprotein in proteoliposomes. Effect of substrates and modulators, and dependence on bilayer phase state, *Eur J Biochem 268*, 1687-1697.
15. Omote, H., and Al-Shawi, M. K. (2002) A novel electron paramagnetic resonance approach to determine the mechanism of drug transport by P-glycoprotein, *J Biol Chem 277*, 45688-45694.
16. Senior, A. E., al-Shawi, M. K., and Urbatsch, I. L. (1995) The catalytic cycle of P-glycoprotein, *FEBS Lett 377*, 285-289.
17. Chen, M., Abele, R., and Tampe, R. (2003) Peptides induce ATP hydrolysis at both subunits of the transporter associated with antigen processing, *J Biol Chem 278*, 29686-29692.

18. Seelig, A., and Gatlik-Landwojtowicz, E. (2005) Inhibitors of multidrug efflux transporters: their membrane and protein interactions, *Mini Rev Med Chem 5*, 135-151.

19. Al-Shawi, M. K., Polar, M. K., Omote, H., and Figler, R. A. (2003) Transition state analysis of the coupling of drug transport to ATP hydrolysis by P-glycoprotein, *J Biol Chem 278*, 52629-52640.

20. Qu, Q., Chu, J. W., and Sharom, F. J. (2003) Transition state P-glycoprotein binds drugs and modulators with unchanged affinity, suggesting a concerted transport mechanism, *Biochemistry 42*, 1345-1353.

21. Higgins, C. F., and Linton, K. J. (2004) The ATP switch model for ABC transporters, *Nat Struct Mol Biol 11*, 918-926.

22. Sauna, Z. E., and Ambudkar, S. V. (2001) Characterization of the catalytic cycle of ATP hydrolysis by human P-glycoprotein. The two ATP hydrolysis events in a single catalytic cycle are kinetically similar but affect different functional outcomes, *J Biol Chem 276*, 11653-11661.

23. Kerr, K. M., Sauna, Z. E., and Ambudkar, S. V. (2001) Correlation between steady-state ATP hydrolysis and vanadate-induced ADP trapping in Human P-glycoprotein. Evidence for ADP release as the rate-limiting step in the catalytic cycle and its modulation by substrates, *J Biol Chem 276*, 8657-8664.

24. Sauna, Z. E., Smith, M. M., Muller, M., and Ambudkar, S. V. (2001) Functionally similar vanadate-induced 8-azidoadenosine 5'-[alpha-(32)P]Diphosphate-trapped transition state intermediates of human P-glycoprotin are generated in the absence and presence of ATP hydrolysis, *J Biol Chem 276*, 21199-21208.

25. Buxbaum, E. (1999) Co-operating ATP sites in the multiple drug resistance transporter Mdr1, *Eur J Biochem 265*, 54-63.

26. Romsicki, Y., and Sharom, F. J. (1998) The ATPase and ATP-binding functions of P-glycoprotein--modulation by interaction with defined phospholipids, *Eur J Biochem 256*, 170-178.

27. Omote, H., Figler, R. A., Polar, M. K., and Al-Shawi, M. K. (2004) Improved energy coupling of human P-glycoprotein by the glycine 185 to valine mutation, *Biochemistry 43*, 3917-3928.

28. Seelig, A. (1987) Local anesthetics and pressure: a comparison of dibucaine binding to lipid monolayers and bilayers, *Biochim Biophys Acta 899*, 196-204.

29. Fischer, H., Gottschlich, R., and Seelig, A. (1998) Blood-brain barrier permeation: molecular parameters governing passive diffusion, *J Membr Biol 165*, 201-211.

30. Gatlik-Landwojtowicz, E., Aanismaa, P., and Seelig, A. (2004) The rate of P-glycoprotein activation depends on the metabolic state of the cell, *Biochemistry 43*, 14840-14851.

31. Exner, O. (1973) The enthaly-entropy relationship, *Prog.Phys.Org.Chem. 10*, 411-482.

32. Cantor, C. R., and Schimmel, P. R. (1980) *Biophysical Chemistry, Part I: The conformation of biological macromolecules*, Vol. 1, p. 283, Freeman, W.H. and Company, San Francisco.

33. Landwojtowicz, E. (2002) Multidrug Transporter P-Glycoprotein: From Kinetics of Drug-Induced ATPase Activation in Intact Cells to Structure-Activity Relationships, in *Biozentrum* p121, University of Basel, Basel.

34. Seelig, A. (1992) Interaction of a substance P agonist and of substance P antagonists with lipid membranes. A thermodynamic analysis, *Biochemistry 31*, 2897-2904.

35.   Pretz, M. G., Albers, S. V., Schuurman-Wolters, G., Tampé, R., Driessen, A. J., and van der Does, C. (2006) Thermodynamics of the ATPase cycle of GlcV, the nucleotide-binding domain of the glucose ABC transporter of sulfolobus solfataricus, *Biochemistry 45*, 15056-15067.
36.   Doige, C. A., Yu, X., and Sharom, F. J. (1993) The effects of lipids and detergents on ATPase-active P-glycoprotein, *Biochim Biophys Acta 1146*, 65-72.
37.   Seelig, J., and Ganz, P. (1991) Nonclassical hydrophobic effect in membrane binding equilibria, *Biochemistry 30*, 9354-9359.
38.   Ramnanan, C. J., and Storey, K. B. (2006) Suppression of Na+/K+-ATPase activity during estivation in the land snail Otala lactea, *J. Exp. Biol. 209*, 677-688.
39.   Cornelius, F. (2001) Modulation of Na,K-ATPase and Na-ATPase activity by phospholipids and cholesterol. I. Steady-state kinetics, *Biochemistry 40*, 8842-8851.
40.   Zhu, N., Dai, X., Lin, D. S., and Connor, W. E. (1994) The lipids of slugs and snails: evolution, diet and biosynthesis, *Lipids 29*, 869-875.
41.   Squier, T. C., Bigelow, D. J., and Thomas, D. D. (1988) Lipid fluidity directly modulates the overall protein rotational mobility of the Ca-ATPase in sarcoplasmic reticulum, *J Biol Chem 263*, 9178-9186.
42.   Andersen, C., Jordy, M., and Benz, R. (1995) Evaluation of the rate constants of sugar transport through maltoporin (LamB) of Escherichia coli from the sugar-induced current noise, *J Gen Physiol 105*, 385-401.
43.   Seelig, A., Blatter, X. L., and Wohnsland, F. (2000) Substrate recognition by P-glycoprotein and the multidrug resistance-associated protein MRP1: a comparison, *Int J Clin Pharmacol Ther 38*, 111-121.
44.   Meier, M., Blatter, X. L., Seelig, A., and Seelig, J. (2006) Interaction of verapamil with lipid membranes and P-glycoprotein: connecting thermodynamics and membrane structure with functional activity, *Biophys J 91*, 2943-2955.
45.   Auger, M., Jarrell, H. C., and Smith, I. C. (1988) Interactions of the local anesthetic tetracaine with membranes containing phosphatidylcholine and cholesterol: a 2H NMR study, *Biochemistry 27*, 4660-4667.
46.   Schote, U., Ganz, P., Fahr, A., and Seelig, J. (2002) Interactions of cyclosporines with lipid membranes as studied by solid-state nuclear magnetic resonance spectroscopy and high-sensitivity titration calorimetry, *J Pharm Sci 91*, 856-867.
47.   Seelig, A., and Seelig, J. (1977) Effect of a single cis double bond on the structures of a phospholipid bilayer, *Biochemistry 16*, 45-50.
48.   Seelig, A., and Gerebtzoff, G. (2006) Enhancement of drug absorption by noncharged detergents through membrane and P-glycoprotein binding, *Expert Opin Drug Metab Toxicol 2*, 733-752.
49.   Sharom, F. J., Liu, R., Romsicki, Y., and Lu, P. (1999) Insights into the structure and substrate interactions of the P-glycoprotein multidrug transporter from spectroscopic studies, *Biochim Biophys Acta 1461*, 327-345.
50.   Läuger, P., (Ed.) (1991) *Electrogenic Ion Pumps.* , Sinauer, Sunderland, MA.

TABLES

Table 1. Characteristic Parameters for Test Compounds and Transition State Parameters for ATP Hydrolysis by the Pgp ATPase in the Absence and Presence of Different Drugs.

Drug	MW_{base} [g/mol]	$A_D{}^a$ [$Å^2$]	K_1 [μM]	V_1 [%]	$\Delta G_{tw(1)}^0$ [kJ/mol]	$Conc^d$ [μM]	$\Delta H^{\ddagger e}$ [kJ/mol]	$T\Delta S^{\ddagger e}$ (37 °C) [kJ/mol]	$\Delta G^{\ddagger e}$ (37 °C) [kJ/mol]
Basal	-	-	-	-	-	0	92.6 ± 4.2	19.5 ± 1.0	73.1
promazine	284.4	42	214.5 ± 28.6^b	378 ± 15^b	-31.2^b	160.6	83.5 ± 6.5	11.9 ± 1.1	71.6
verapamil	454.6	90	1.0 ± 0.2	250 ± 28	-44.5	0.8	88.5 ± 12.7	17.2 ± 2.8	71.2
PSC833	1214.6	140	0.008 ± 0.001	84 ± 10	-56.6	1.9	73.4 ± 7.7	-0.2 ± 0.1	73.6
verapamil	454.6	90	0.67 ± 0.09^c	274 ± 10^c	-45.6^c	-	-	-	-

[a]The cross-sectional area of drugs, A_D, were determined from the surface activity measurements in 50 mM Tris-HCl, 114 mM NaCl, pH 8.0 at ambient temperature; the cross-sectional area, A_D, of PSC833 was assumed to be identical to that of cyclosporin A (11). The concentration of half-maximum Pgp activation, K_1, and the maximum Pgp activity, V_1, were determined at 37 °C and pH 7.0. [b]Data for promazine were obtained with a membranes prepared from older cells and gave higher values for the concentration of half-maximum Pgp activation, K_1, than given in ref. (7). [c]Measurements performed at pH 7.5, T = 35 °C. [d]Transition state data are given at the concentrations closest to the concentration of half-maximum activation, K_1, for promazine and verapamil and for the concentration of half-maximum inhibition, K_2, for PSC833. [e]The transition state parameters are evaluated from Figure 2A-C. The parameters are apparent values and are valid in the given temperature range. The $\Delta G^{\ddagger}$ values have to be considered as estimates. Thermodynamic parameters for basal values are the average of seven different temperature dependence measurements with multiple samples (number of samples, n > 140, four different membrane preparations). Thermodynamic parameters for drug stimulated values are the average of one temperature dependence measurement with multiple samples. The errors for basal and drug stimulated values represent the goodness of the linear fit.

SCHEMES

Scheme 1: Pgp ATPase activity at low substrate concentration considering one ATP hydrolyzed per cycle (16). The dotted arrow indicates that the catalytic step is more complex than observed by Pgp ATPase measurements.
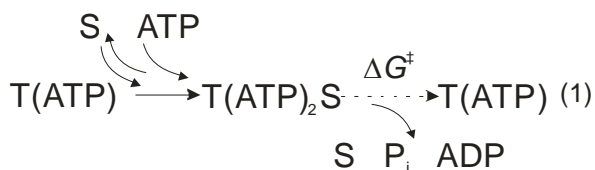
$$S \quad ATP$$
$$T(ATP) \longrightarrow T(ATP)_2 S \xrightarrow{\Delta G^{\ddagger}} T(ATP) \quad (1)$$
$$S \quad P_i \quad ADP$$

FIGURE LEGENDS

FIGURE 1A-C: Temperature dependence of the Pgp ATPase activity, V_{sw}, as a function of drug concentration in inside-out plasma membranes of NIH-MDR1-G185 cells (A-C): Promazine (A), verapamil (B), and PSC833, an "inhibitor" of the Pgp ATPase (C). The filled and open symbols represent basal and drug induced Pgp ATPase activity, respectively. Pgp ATPase activity was measured by means of a colorimetric phosphate release assay at (◆, ◇) 25, (▼, ▽) 28, (▲, △) 31, (●, ○) 34 and (■, □) 37 ^{o}C, either in 25 mM Tris-HCl or 25 mM Hepes-KOH buffer. Buffer were adjusted to pH 7.0 taking into account the temperature coefficient of the buffer. Data are expressed as the average of two to four experiments. Solid lines are fits to the modified Michaelis-Menten equation (eq. (1)).

FIGURE 2A-C: Analysis of the thermodynamic transition state parameters by means of Eyring plots for Pgp ATPase activity in plasma membrane vesicles: Eyring plots for Pgp ATPase activity under basal conditions (◆) and increasing concentrations of promazine (A), verapamil (B), and PSC833 (C) (open symbols and stars). Each symbol corresponds to a specific concentration in Figure 1. Pgp ATPase activity is expressed in absolute values (s^{-1}) and was calculated as described previously (7). The amount of the Pgp ATPase in plasma membrane vesicle preparations used in verapamil and PSC833 measurements was estimated as 0.9 % and in promazine measurements as 1.1 % of total protein. The straight lines are linear fits to the data.

FIGURE 3:   Temperature dependence of maximum Pgp ATPase activity, $\ln V_1$ (where V_1 is given in % values) for verapamil (□) and promazine (○). The straights lines are the linear regressions to the data. Data are expressed as the average of two to six experiments.

FIGURE 4A-I: The thermodynamic transition state parameters for Pgp ATPase activity in plasma membrane vesicles of NIH-MDR1-G185 cells as a function of drug concentration: Promazine (A, D, G), verapamil (B, E, H) and PSC8333 (C, F, I). A-F: Activation enthalpy, $\Delta H^{\ddagger}$, (●●○); activation entropy, $T\Delta S^{\ddagger}$, (■■□); and free energy of activation, $\Delta G^{\ddagger}$, (▲▲△) at T = 37°C. Filled and open symbols represent data in the absence and presence of drugs, respectively. Filled black and open symbols represent data from one temperature dependence measurement with multiple samples and filled gray symbols represent the average of seven temperature dependence measurements with

multiple samples. G-I: Measured Pgp ATPase activity at 37°C ($\ast$) (data from Figure 1); Pgp ATPase activity ($\blacklozenge\,\lozenge\,\diamondsuit$) calculated according to eq. 2 using $\Delta G^{\ddagger}$ values given in D-F. The arrows indicate the concentrations of half-maximum activation for verapamil and promazine and the concentration of half-maximum inhibition for PSC833. The straight lines were drawn to guide the eye. For clarity the error bars were omitted. For the activation enthalpy and the activation entropy, the error (representing the goodness of the fit) was $\sim 20\%$ at very low concentrations and $\sim 10\%$ at higher concentrations.

FIGURE 5: Isokinetic relationship. The logarithm of Pgp ATPase activity, $\ln V_{sw}$ (at $T_2 = 31$ °C) (lower data set) and $\ln V_{sw}$ (at $T_3 = 37$ °C) (upper data set) is plotted as a function of $\ln V_{sw}$ (at $T_1 = 25$ °C). Filled symbols ($\bullet$) basal activity and open symbols drug-induced activity, measured over the whole concentration range given in Figure 1A-C: promazine ($\bigcirc$), verapamil ($\square$) and PSC833 ($\triangle$).

FIGURE 6: The thermodynamic transition state parameters for basal Pgp ATPase activity as a function of the lateral packing density, π_M, of the membrane surrounding the transporter. The lateral membrane packing densities were derived from the concentrations of half-maximum Pgp activation, K_1, determined at pH 7.4 or pH 7.5 according to ref. (*11*). Different reconstitutions may provide slightly different lateral packing densities. Activation enthalpy, $\Delta H^{\ddagger}$ ($\bullet$, $\bigcirc$), the product of the absolute temperature and the activation entropy, $T\Delta S^{\ddagger}$ ($\blacksquare$, $\square$), and the free energy of activation, $\Delta G^{\ddagger}$, ($\blacktriangle$, $\triangle$) for Pgp ATPase activity at $T = 35$ °C. 1: MDR1 in native NIH-MDR1-G185 membranes (pH 7.0), (present data is an average of seven different temperature dependence measurements with multiple samples); 2: MDR1 in mixed *E. coli* lipids (pH 7.5) (*19*); 3: PGP1 (hamster Pgp), in dimyristoylphosphatidylcholine (*26*), 4: PGP1 in CHAPS (*26*). The open symbols represent the transition state parameters measured for the water-soluble NBD of Glucose ABC transporters, GlcV, (pH 6.5). It works as a dimer and hydrolyzes one ATP per monomer (*35*). The solid lines are the linear regressions to the data presented as filled symbols.

FIGURE 7: Correlation between the rate of substrate transport and substrate affinity to the Pgp ATPase and maltoporin. For the Pgp ATPase the logarithm of the rate constants, k_1, for ATP hydrolysis taken as k is plotted as a function of the free energy of substrate binding from water to the activating binding region of the transporter, $\Delta G_{tw(1)}^{0}$, taken from ref. (*7*) ($\bigcirc$). Data obtained from the present investigation are indicated as ($\ast$). Substrates:

amitriptyline (1), chlorpromazine (2), cis-Flupenthixol (3), cyclosporin A (4), dibucaine (5), diltiazem (6), glivec (7), progesterone (8), promazine (9), (R/S)-verapamil (10), reserpine (11), trifluoperazine (12), triflupromazine (13), OC144-093 (14), PSC833 (15), vinblastine (16). For comparison, the logarithm of the rate constants, k, for transport across maltoporin is plotted as a function of the free energy of substrate binding from water to maltoporin, ΔG_{tw}^{0} ($\square$) (42): Maltotriose (17), maltotetraose (18), maltopentaose (19), maltohexaose (20), and maltoheptaose (21).

FIGURE 8: The rate of ATP hydrolysis by the Pgp ATPase in membranes with different lateral packing densities. A) Pgp ATPase activity is normalized to the basal activity in the membrane with the highest lateral packing density, $\pi_M = 51$mN/m. B) Pgp ATPase activity is normalized to the basal Pgp ATPase activity at the corresponding lateral membrane packing density. Basal Pgp ATPase activity is shown as black bars, and verapamil and PSC833 stimulated Pgp ATPase activity as hatched and cross-hatched bars, respectively. The Pgp ATPase activity at $\pi_M = 51$mN/m was calculated from the free energies of activation, $\Delta G^{\ddagger}$, at T = 35 ^{o}C according the eq. (2), data were taken from ref (19) at pH 7.5. For comparison, the basal and verapamil induced Pgp ATPase activity was measured at T = 35 ^{o}C and at pH 7.5 in NIH-MDR1-G185 cell membranes exhibiting an estimated lateral packing density of $\pi_M = 30.5$ mN/m. The Pgp ATPase activity in the presence of PSC833 at $\pi_M = 30.5$ mN/m was calculated from the free energies of activation, $\Delta G^{\ddagger}$, at T = 35 ^{o}C according to eq. (2). The amount of the Pgp ATPase in plasma membrane vesicle preparation used in the measurements at pH 7.5 and T = 35 ^{o}C was estimated as 1.1 %.
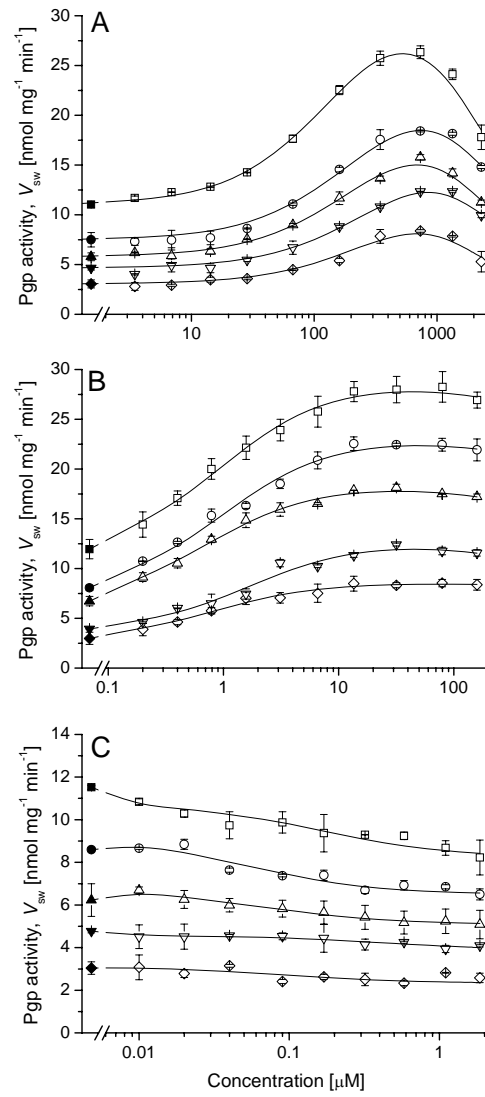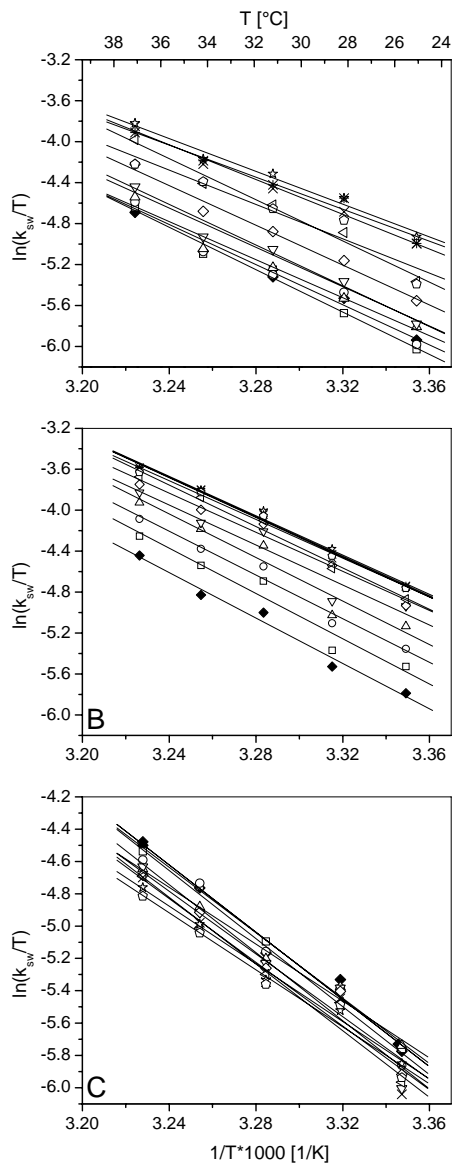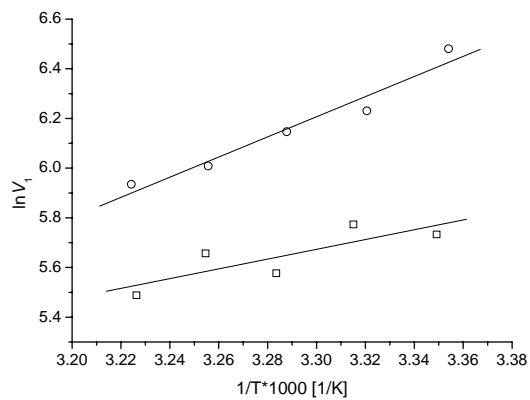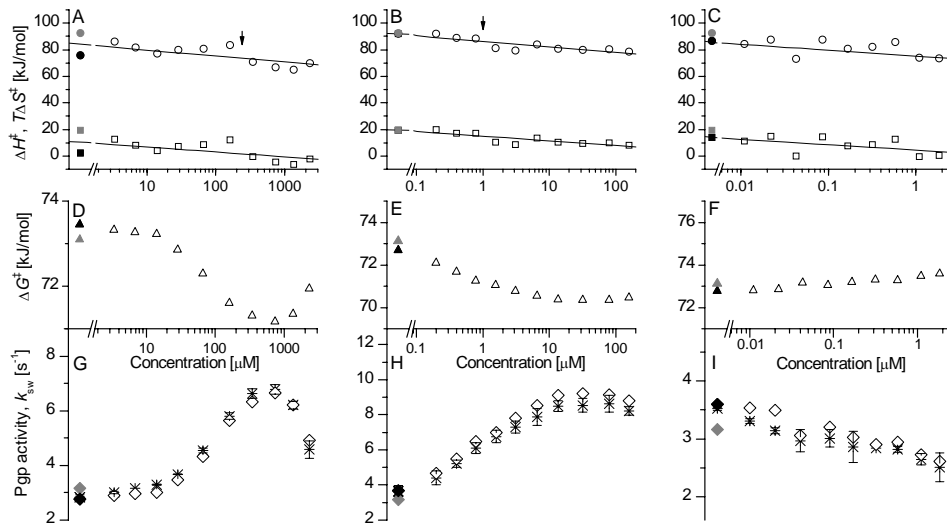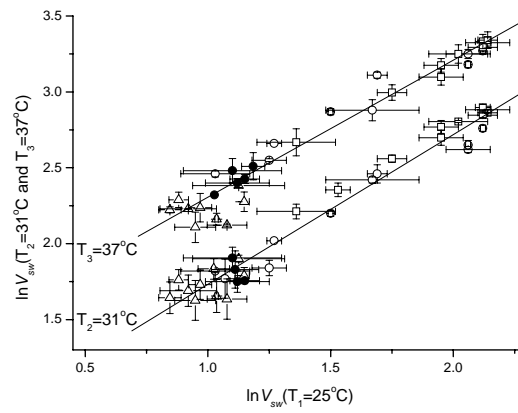
FIGURES

FIGURE 1A-C

FIGURE 2A-C

FIGURE 3

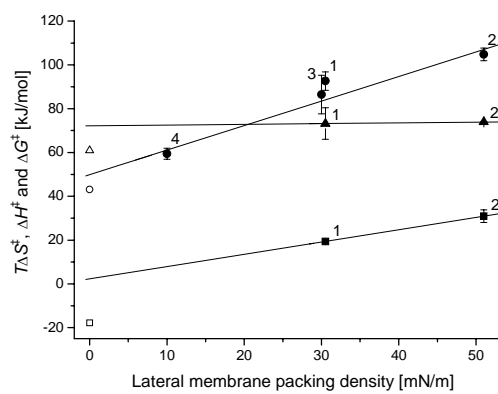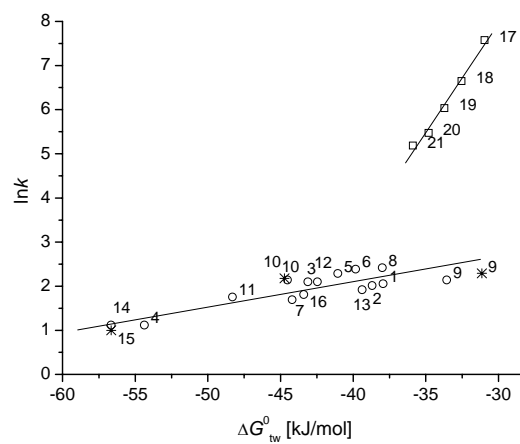FIGURE 4A-I

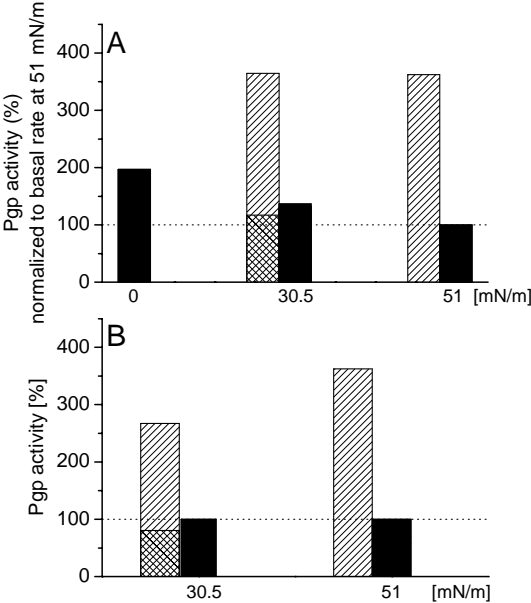FIGURE 5

FIGURE 6

FIGURE 7

FIGURE 8

7.6 Prediction and Validation of P-glycoprotein-Substrates Exemplified with Ehrlich´s Dyes

Unpublished manuscript

Unpublished manuscript

INTRODUCTION

The first synthetic dye, aniline, was discovered in the 19th century. Since then in the field of biology and medicine synthetic dyes have been used for histological studies because they provide the possibility for a visual examination of cell and tissue physiology and morphology at the microscopic level. Due to their selectivity and furthermore the biological activity they formed a basis of modern chemotherapy initiated by Paul Ehrlich. In 1891 Ehrlich and Guttmann used for the first time methylene blue for the treatment of malaria in humans (*1-4*).

Methylene blue, MB, stains cellular nuclei blue. The mechanism of staining is based on the electrostatic interactions between the positive charge of MB and the anionic oxygens in DNA and RNA (*5*). *Acridine orange*, AO, is a cell permeant cationic dye which interacts with DNA and RNA. AO has been used in cell-cycle studies because it emits green fluorescence when bound to the double stranded DNA and red fluorescence when bound to the single stranded DNA or RNA (*6, 7*). *Basic fuchsin*, Fu, is used for carbohydrate staining together with periodic acid. Periodic acid opens the sugar rings of carbohydrate forming two aldehyde groups and iodate. The $=NH_2^+$ group of fuchsin forms a Schiff base bond with aldehyde binding the dye to carbohydrate (*5*). *Eosin*, Eo, and its derivatives stain protein rich regions of cells red. At physiological pH eosin has one to two negative charges and, thus, it binds electrostatically to the positively charged amino acids. Figure 1 shows the structures of MB, AO, Fu and Eo.

The applicability of dyes as anticancer and antimicrobial drugs in photodynamic therapy, PDT, has also been tested. PDT combines a nontoxic photoactivable dye, also called as photosensitizer, PS, with the harmless visible light of relevant wavelength to excite the dye to its reactive triplet state, which will then generate reactive oxygen species that are toxic to cells (*8-11*).

A serious problem in the cancer and antimicrobial chemotherapy is the development of multidrug resistance, MDR, for several drugs simultaneously (*12, 13*). One reason for MDR is the overexpression of ATP binding cassette, ABC, efflux transporters that reduce the accumulation of active agents inside cells below their therapeutic concentration. In mammalian cells P-glycoprotein (Pgp, MDR1, ABCB1) is best characterized among them

(for reviews see (*14, 15*)). Similar efflux transporters are expressed in bacteria (e.g. Sav1866 (*16*), LmrA (*17, 18*), for review see (*19*)) and in fungi (e.g Cdr1p (*20*)).

Pgp (170 kDa) is a transmembrane protein which transports a wide variety of structurally diverse compounds out of the cell membrane extruding them either directly to the extracellular medium or flipping them from the inner to the outer leaflet of the lipid bilayer (*21*). The substrate translocation occurs at the expense of ATP hydrolysis (*22-25*). Taking together our previous investigations with the research made in other laboratories reveals three requirements for Pgp substrates (*26*): 1) Pgp substrates have to partition into the cytosolic leaflet of the lipid bilayer before they can reach the Pgp binding site (*27-30*), 2) Pgp substrates have to be positively charged or non-charged at physiological pH (negatively charged compounds are not generally interacting with Pgp), and 3) Pgp substrates have to carry a minimum binding element which is composed of two or three hydrogen bond acceptor groups in a specific distance ((2.5 ± 0.5) Å or (4.6 ± 0.6) Å) (*31, 32*). The third requirement was revealed by screening the 3D structures of hundreds of Pgp substrates. It was suggested that Pgp recognize its substrates via hydrogen bonding. Furthermore, the importance of hydrogen bonds was supported by the fact that transmembrane domains of Pgp contain a high density of hydrogen bond donor side chains.

Recently, using 15 structurally diverse Pgp substrates as a calibration set we demonstrated that Pgp activity depends mainly on the nature and the concentration of the substrates as well as on the packing density of membrane, π_M, and on the pH of environment (*33, 34*). We further showed that the air-water partition coefficient, K_{aw}, correlated linearly with the inverse of the concentration of half-maximum Pgp activity, $1/K_1$, indicating that the substrate concentration in the membrane is relevant for Pgp activity (*34*). Furthermore, we demonstrated that the logarithm of maximum Pgp activity, $\ln V_1$, increases linearly with increasing free energy of drug binding from the aqueous phase to the transporter, $\Delta G^0_{tw(1)}$ (*33*), which in turn depends on the number and the strength of the hydrogen bonds formed between the drug and the transporter and on the lipid-water partition coefficient of the drug (*35*).

The present investigation was made in order to answer the following questions. At first, we asked whether MB, AO, Fu, and Eo are substrates for Pgp. This is relevant since MB, AO, Fu, and Eo are commonly used in histological studies and the potency of MB and AO as PS in PDT for the treatment of cancer and microbial infections has been tested (*8, 36-39*). Secondly, we tested whether the three requirements for Pgp substrates hold for MB, AO, Fu, and Eo. To our knowledge Fu and Eo were not tested earlier for Pgp interactions

and MB and AO have only been tested with indirect methods (*37, 40-43*). For this purpose we measured the Pgp activity in living mouse embryo fibroblasts, NIH-WT and *MDR1*-transfected, and in plasma membrane vesicles formed from the same cells. The measurements were performed in living cells with a Cytosensor microphysiometer and in plasma membrane vesicles with colorimetric phosphate release assay.

MATERIALS AND METHODS

Materials. Methylene blue (Cat. No. M9140) and acridine orange (Cat. No. 318337) were from Sigma-Aldrich (Steinheim, Germany). Basic fuchsin (Cat. No. 47860) and ethyl eosin (Cat. No. 45230) were obtained from Fluka (Buchs, Switzerland). Complete EDTA-free protease inhibitor cocktail tablets were obtained from Roche Diagnostics (Mannheim, Germany), 1,4-dithiol-DL-threitol, DTT, from Applichem (Darmstadt, Germany), and bicinchoninic acid, BCA, protein assay reagents from Pierce (Rockford, IL). All other chemicals were either from Sigma, Fluka or Merck. Cell culture media DMEM with and without pyruvate (liquid and dry, Cat. No. 21969 and Cat. No. 52100, respectively) as well as other compounds required for cell culture such as fetal bovine serum, FBS, L-glutamine, and antibiotics were from Gibco-BRL (Basel, Switzerland).

Cell Lines and Cell Culture. The mouse embryo fibroblasts NIH3T3, NIH-WT (NIH-WT) and *MDR1*-transfected (NIH-MDR1-G185) (grown in the presence of 0.15 µM colchicine) were generous gifts from Dr. M.M. Gottesman and Dr. S.V. Ambudkar (The National Institutes of Health, Bethesda, MD). Cells were maintained as described previously (Chapter 7.3 (*44, 45*)).

Plasma Membrane Preparation. The crude plasma membrane vesicles were prepared as described previously (cf. Chapter 7.4 (*33*)).

Phosphate Release Assay. The Pgp associated vanadate-sensitive ATPase activity was determined according to Litman et al. (*24*) in 96-well microtiter plate (Nunc F96 MicroWell^{TM} plate, non-treated). The measurements were performed at pH 7.0 and T=37 °C as described earlier (cf. Chapter 7.4 (*33*)).

Cytosensor Measurements. Cytosensor microphysiometer detects the changes in extracellular acidification rate, ECAR, of living cells. The measurements were performed at pH 7.4 and T=37 °C as described earlier in detail (Chapters 7.1 and 7.3 (*34, 44*)). The DMEM flow medium was prepared from DMEM dry powder supplemented with NaCl (2.6

g/L) and pyruvate (1 mM). MB, AO, Fu, and Eo concentrations were corrected for the adsorption to the Cytosensor tubes and debubbler membranes via UV-spectroscopy measurements.

Light Microscope Pictures. NIH-MDR1-G185 and NIH-WT cells ($8 \cdot 10^5$ cells) were seeded to 35-mm dishes and at the same time colchicine was removed from NIH-MDR1-G185 cells. The cells were incubated at 37°C ~6h in order to let the cells attach to the dish. After cell attachment 10 μL of MB stock solution (19.3 mM) was added to the cells in 3 mL of culture medium obtaining the final MB concentration 64.3 μM. Next the cells were incubated at 37°C for 1h and thereafter the light microscope pictures were taken. The control pictures were taken just before the addition of MB. For MB and PSC833 pictures $1.0 \cdot 10^5$ cells were seeded on glass-bottom dishes one day before the pictures were taken. One hour before the addition of the test compounds (MB alone (64.5 μM) or together with PSC833 (1μM)) the cells were washed with PBS and fresh DMEM without colchicine was added to cells. Next the cells were incubated at 37°C one hour and thereafter the pictures were taken.

The Kinetic Model. The data from proton and phosphate release measurements are fitted to a modified Michaelis-Menten equation (eq. (1)) proposed by Litman et al. (*24*) assuming basal Pgp activity in the absence of drugs, activation with one and inhibition with two drug molecules bound to Pgp

$$V_{sw} = \frac{K_1 K_2 V_{bas} + K_2 V_1 C_{sw} + V_2 C_{sw}^2}{K_1 K_2 + K_2 C_{sw} + C_{sw}^2} \qquad (1)$$

where V_{sw} is the rate of phosphate release, P_i, or the rate of proton, H^+, release as a function of substrate concentration in aqueous solution, C_{sw}, and V_{bas} is the basal activity of Pgp in the absence of drug. K_1 is the concentration of half-maximum Pgp activation, K_2 is the concentration of half-maximum inhibition, V_1 is the maximum Pgp activity and V_2 the minimum Pgp activity at infinite substrate concentration.

Surface Activity Measurements. Surface activity measurements were performed in 50 mM Tris/HCl buffer containing 114 mM NaCl, pH 7.4 and temperature (24 ± 1)°C. For details see (*46, 47*). Shortly, by measuring the surface pressure, π, as a function of tissue dye concentration (Gibbs adsorption isotherm) allows determination of air-water partition coefficient, K_{aw}, the surface area of the molecule at the air-water interface, A_d, and the critical micelle concentration, CMC_D. Lipid-water partition coefficient, K_{lw}, can be then

estimated according the (eq. (2)) where membrane packing density, π_M, (30 mN/m for NIH-MDR1-G185 cells), the negative surface potential, ψ, of the cytosolic lipid leaflet (-30 mV) and the charge of the drug, z, are taken into account.

$$K_{lw} = K_{aw} e^{-\pi_M A_d / kT} e^{-\psi Fz / RT} \tag{2}$$

Thermodynamics of Substrate Binding to Pgp. The binding constant of substrate to the activating binding region of Pgp from the aqueous phase, $K_{tw(1)}$, is expressed as a product of lipid-water partition coefficient, K_{lw}, and the substrate binding constant from the lipid phase to the activating binding region of Pgp, $K_{tl(1)}$ ($K_{tw(1)} = K_{lw} \cdot K_{tl(1)}$). Correspondently, the free energy of substrate binding from the aqueous phase to the activating binding region of Pgp, $\Delta G_{tw(1)}^0$, is a sum of the free energy of substrate partitioning to the lipid bilayer, ΔG_{lw}^0, and the free energy of substrate binding from the lipid phase to the activating region of the transporter, $\Delta G_{tl(1)}^0$ ($\Delta G_{tw(1)}^0 = \Delta G_{lw}^0 + \Delta G_{tl(1)}^0$) (for details cf. Chapter 7.1 (*34, 35*)). The substrate binding constant from the aqueous phase to the activating binding region of Pgp, $K_{tw(1)}$, can be estimated as an inverse of concentration of half-maximum Pgp activity ($K_{tw(1)} \sim 1/K_1$). The lipid-water partition coefficient, K_{lw}, is determined from the surface activity measurements according (eq. (2)).

Stock Solutions of Dyes. Dyes were used as they were obtained from the commercial sources. For the *Cytosensor measurements* the stock solutions of MB and AO were made in DMEM flow medium. Fu and Eo were dissolved in DMSO which were then diluted with flow medium to the final DMSO concentration (0.5 % (v/v)). DMSO concentration was decreasing upon further dilution with flow medium. For the *phosphate release assay* MB and AO were solubilized in nano-pure water and Fu and Eo in DMSO. From the stock solutions the intermediate dye solutions were prepared by further diluting them either with water or DMSO. The measured concentrations were obtained by adding 5 μL aqueous or 1 μL DMSO dye solution into the phosphate release assay buffer (total sample volume 60 μL). Final DMSO concentration was 1.7 % (v/v). DMSO did not have effect on the ECAR or the phosphate release rate measurements.

RESULTS

Dye-Induced ECAR of Wild-Type and MDR1-Transfected Mouse Embryo Fibroblasts. The effect of four dyes MB, AO, Fu, and Eo, on the ECAR of mouse embryo fibroblast, wild-type (NIH-WT) and *MDR1*-transfected (NIH-MDR1-G185), cells were studied with a Cytosensor microphysiometer. Figure 1 shows the structures of dyes. The cells $(4 \cdot 10^5)$ trapped between two polycarbonate membranes in a flow chamber were in diffusive contact with a pH sensitive silicon chip. First cells were flushed with the dye-free flow medium to reach a stable ECAR. Thereafter they were flushed with the dye-containing flow medium for 3 min comprising two measuring points (indicated as hatched bar in Figure 2D). After the 3-min stimulation the cells were again flushed with the dye-free flow medium until the basal ECAR was reached. Thereafter a new stimulation with a higher dye concentration was performed. The ECAR measurements were performed in every two minutes by halting the pumps for 20s, during which the acidic metabolites excreted by cells accumulated inside the sensor chamber. The change in pH was then measured during 13s. Figures 2A-D display the changes in the ECAR of NIH-WT and NIH-MDR1-G185 cells upon stimulation with increasing concentration of MB, AO, Fu, and Eo as function of time. The ECAR is normalized to the basal ECAR which is defined as 100 %.

FIGURE 1

FIGURE 2A-D

As seen in Figure 2A-D all dyes except Fu affected the energy metabolism of living cells in complex manner. Upon stimulation with *MB* (Figure 2A) the ECAR increased in NIH-MDR1-G185 cells as well as in NIH-WT cells, however, the increase in NIH-WT cells was higher and moreover; the maximum ECAR in NIH-WT cells was reached at lower MB concentration than in NIH-MDR1-G185 cells.

AO stimulated the ECAR of NIH-MDR1-G185 and NIH-WT cells in concentration dependent manner (Figure 2B). The increase in the ECAR of NIH-MDR1-G185 cells was significantly higher than that in NIH-WT cells. Kinetics for reaching the basal ECAR after AO stimulation was considerably slower than for other tested dyes. After stimulating the NIH-MDR1-G185 cells with 22.6 μM AO, it took approximately two hours to reach the basal ECAR again.

Fu induced a modest increase in the ECAR of NIH-MDR1-G185 cells (maximally ~120%), but not in NIH-WT cells (Figure 2C). However, the highest Fu concentration studied caused a fast transient increase in the ECAR of NIH-WT cells (up to ~125%) which decreased back to the basal value immediately after a 3-min dye-stimulation period.

Eo caused a sharp decrease in the ECAR that was similar in NIH-WT and in NIH-MDR1-G185 cells (Figure 2D). Kinetics for reaching the basal ECAR of both cells after Eo stimulation was fast (~6 min for 6.5 μM Eo).

Tissue Dye-Induced Pgp Activation Measured in Plasma Membrane Vesicles Prepared from Wild-Type and MDR1-Transfected Mouse Embryo Fibroblasts. Figure 3A displays the Pgp activity profiles as a function of tissue dye concentration (log scale) obtained from phosphate release rate measurements in the plasma membrane vesicles of NIH-MDR1-G185 and NIH-WT cells. The tissue dye-induced Pgp activation is expressed as a percentage of the basal Pgp activity. For comparison the ECARs measured in living NIH-WT and NIH-MDR1-G185 cells at the end of the 3-min stimulation period (indicated as solid symbols in Figures 2A-D) are shown in Figure 3B.

FIGURE 3A-B

As seen in Figure 3A Pgp activity increased at a low concentration of *MB*, at the intermediate concentration the maximum Pgp activity was reached and at the high MB concentration Pgp activity decreased again. Similar bell-shaped Pgp activity profiles were obtained previously for typical Pgp substrates (cf. Chapter 7.2 (*33*)) indicating that MB is an intrinsic substrate for Pgp. In the plasma membrane vesicles formed from NIH-WT cells no increase in the phosphate release rate with increasing concentration of MB was observed. A bell-shaped Pgp activity profile was also obtained with increasing concentrations of *AO* in plasma membrane vesicles of NIH-MDR1-G185 cells. *Fu* stimulated Pgp activity; however, the maximum Pgp activity was very modest. *Eo,* in contrary, did not stimulate Pgp activity at all. Only a slight decrease in the phosphate release rate was observed at high concentrations. A similar ATPase activity profile was observed for Eo in the plasma membrane vesicles of NIH-WT cells (results not shown).

The data from the phosphate release and the ECAR measurements were fitted to the rate equation (eq. (1)) proposed by Litman et al. (*24*). It assumes basal Pgp activity in the absence of exogenous substrates, Pgp activation upon binding of one substrate molecule at a low aqueous concentration and Pgp inhibition upon binding of two substrate molecules to

transporter at a high aqueous concentration. Data evaluation yielded the concentration of half-maximum activation (inhibition), K_1 (K_2), and the maximum (minimum) Pgp activity, V_1 (V_2). The kinetic parameters are summarized in Table 1. Only the data from the phosphate release measurements were evaluated because AO, MB and Eo also affected strongly the ECAR of NIH-WT cells. Several metabolic processes are superimposed in the ECAR of NIH-MDR1-G185 cells and their differentiation was not possible. The ECAR of NIH-WT cells can not be used as a blank sample to subtract them from the ECAR of NIH-MDR1-G185 cells, because Pgp creates intracellular concentration gradient between the NIH-WT and NIH-MDR1-G185 cells.

TABLE 1

Visualization of Wild-Type and MDR1-Transfected Mouse Embryo Fibroblasts after Incubation with MB. Figures 4A-D show the light microscopy pictures of NIH-WT and NIH-MDR1-G185 cells in the absence and in the presence of MB (64.5 μM). After 1h incubation with MB a clear difference between NIH-WT and NIH-MDR1-G185 cells is observed. The majority of NIH-WT cells have taken up MB and they were stained blue whereas the majority of NIH-MDR1-G185 cells remained uncolored. After 2h incubation with MB the pictures were similar (data not shown). We further tested the effect of PSC833 (1 μM) on the uptake of MB in NIH-MDR1-G185 cells. PSC833 is a known inhibitor of Pgp and if the MB uptake is dependent on the function of Pgp, we should observe more blue cells after when Pgp is inhibited by PSC833. In Figure 5A-F NIH-WT and NIH-MDR1-G185 cells in the absence of MB, after 1h incubation with MB and after 1h incubation together with MB and PSC833 are shown. Inhibition of Pgp with PSC833 clearly increased the number of blue NIH-MDR1-G185 cells. In preliminary tests we also visualized the cells with fluorescence microscopy after incubation with AO (7.6 μM) at various time points. No visible difference was observed between the NIH-WT and *MDR1*-transfected fibroblasts after AO incubation. Already after few minutes incubation AO was observed in the nucleus of both cells.

FIGURE 4A-D

FIGURE 5A-F

DISCUSSION

In the first step of the present investigation we studied whether the dyes, MB, AO, Fu and Eo are intrinsic substrates for Pgp. MB, AO, Fu, and Eo are widely used in histological studies and more recently their applicability in photodynamic therapy, PDT, for the treatment of cancer and microbial infections was tested. To this purpose we measured the Pgp activity as a function of dye concentration in living mouse embryo fibroblasts, NIH-WT (NIH-WT) and *MDR1*-transfected (NIH-MDR1-G185) cells, by monitoring the changes in the ECAR and in the plasma membrane vesicles obtained from the same cells by monitoring the phosphate release rate. In the second step, we tested whether the Pgp activity for unknown compounds can be predicted using as a guideline our previous investigations with a large set of well-known Pgp substrates. Furthermore, we utilized the staining properties of the dyes and visualized the cells after incubation with various dyes.

Pgp Activation with Dyes in Living MDR1-transfected Cells and in Plasma Membrane Vesicles Derived from the Same Cells. Previously, we have shown that the stimulation of NIH-MDR1-G185 cells with the well-known Pgp substrates caused increase in the ECAR at a low substrate concentration, the maximum ECAR was reached at an intermediate substrate concentration and at a high substrate concentration the ECAR was decreasing again. The ECAR of NIH-WT cells were not affected or only a fast transient decrease at a high substrate concentration was observed. Therefore the effect of Pgp substrates on the ECAR of NIH-MDR1-G185 cells was entirely associated to the activity of Pgp (Chapter 7.1 (*34, 45*)). In the present investigation only Fu induced a typical Pgp activity profile in NIH-MDR1-G185 cells, however, the inhibition part was not seen most likely due to the low solubility of the compound (Figure 2C). Three other dyes MB, AO and Eo, caused *not* only changes in the ECAR of NIH-MDR1-G185 cells but also in the ECAR of NIH-WT cells (Figure 2A, 2B and 2D).

As seen in Figure 2A the MB stimulated increase in the ECAR of NIH-WT cells was higher and it occurred at lower MB concentration than that in NIH-MDR1-G185 cells suggesting that MB is an intrinsic substrate for Pgp. The other MB induced metabolic effect is overwhelming in both cells but its effect is delayed in NIH-MDR1-G185 cells because of lower intracellular MB concentration. The lower intracellular MB concentration is caused by the active efflux of MB by Pgp. The increase in the ECAR of NIH-WT cells upon MB stimulation might be related to the activation of pentose phosphatase pathway that causes an oxidative stress in cells (*48*).

AO caused an increase in the ECAR of both cells at similar concentration range, but in contrary to MB, the ECAR of NIH-MDR1-G185 cells were higher than in NIH-WT cells indicating that AO is an intrinsic substrate for Pgp. AO is known to intercalate to between the base pairs of DNA and RNA (*49-51*) which may contribute to the observed increase in the ECAR of NIH-WT cells.

Eo, in contrary, suppressed the ECAR of both cells below basal ECARs with a similar extent and at the same concentration range.

Since effect of AO, MB and Eo on the ECAR of living cells are complex a more direct method was used to investigate the influence of the tissue dyes on Pgp activity in order to better understand their interactions. This was done spectroscopically by measuring the phosphate release rate from ATP hydrolysis by Pgp (Figure 3A). As seen in Figure 3A AO and MB induced an increase in the phosphate release rate in the plasma membrane vesicles of NIH-MDR1-G185 cells. MB was also measured in plasma membrane vesicles of NIH-WT cells and no increase in the phosphate release rate was observed. These results supported the conclusion that both AO and MB are the intrinsic substrates for Pgp. *Eo,* on the other hand, did not stimulated the phosphate release rate at all in the plasma membrane vesicles prepared either from NIH-MDR1-G185 or NIH-WT cells. However, high Eo concentrations inhibited the phosphate release rate in both membranes with a similar extent. The decrease observed in the ECAR of NIH-WT and NIH-MDR1-G185 cells, and also in the phosphate release rate upon Eo stimulation may be due to the interaction of eosin with the ATP binding sites of other ATPases eg. Ca-, Na/K- and K/H-ATPases (*52-55*). From the present data it could not conclusively decide whether eosin also interacts with NBDs of Pgp.

Visualization of NIH-WT and NIH-MDR1-G185 cells in the Presence of MB. When NIH-WT and NIH-MDR1-G185 were incubated with MB for 1h at 37°C a clear difference in the uptake rate of MB was observed. NIH-WT cells were getting more blue than NIH-MDR1-G185 cells, however when Pgp was inhibited by PSC833 the difference disappeared. These results further suggest that MB is a substrate for Pgp. When cells were incubated with AO, no similar difference could be observed (results not shown). This is most likely due to the different uptake mechanisms. It has been suggested that positively charged MB is reduced at the surface of the cell by an enzyme ''thiazine dye reductase'' (*56*) (cf. below). Most likely the enzyme coupled reaction is much slower than the passive influx rate of AO.

Requirements for Pgp Substrates and Prediction of Interactions between Pgp and Substrates. Three requirements for the intrinsic Pgp-substrates are (*26*): 1) they have to be able to partition into the cytosolic leaflet of the lipid bilayer (*27, 29, 30*), 2) they are positively charged or non-charged (*31, 57*)), and 3) they carry hydrogen bond acceptor groups in a specific distance ((2.5 ± 0.5) Å or (4.6 ± 0.6) Å) (*31, 32*) . All four tissue dyes fulfilled the *first requirement*. This was tested with the surface activity measurements that allow the estimation of the air-water partition coefficient, K_{aw}, the cross-sectional area of compound, A_d, in the lipid bound orientation. However, due to the low solubility of Fu and Eo and the high charge of MB and AO, the concentration of surface activity onset, C_0, that correlates with the air-water partition coefficient, K_{aw}, was determined (*46, 58*). Same reasons abolished the determination the cross-sectional area, A_d, and, therefore the estimates are used in the present calculations (Table 1).

The C_0 was increasing for tissue dyes in order MB, AO, Fu, and Eo. Previously, the linear correlation between the air-water partition coefficient, K_{aw}, (~ the concentration of surface activity onset, C_0) and the inverse of the concentration of half-maximum Pgp activation, $1/K_1$, were found (Chapter 7.1 (*34*)). Therefore, it was expected that the concentration of half-maximum Pgp activation, K_1, for the studied tissue dyes are increasing in same order, as they indeed are doing. Figure 6 shows the air-water partition coefficient, K_{aw}, (the inverse of the concentration of surface activity onset, $1/C_0$, for the dyes) obtained from the surface activity measurements versus the inverse of the concentration of half-maximum Pgp activation, $1/K_1$, obtained from the phosphate release measurements. The reported values for dyes are rough estimates and give only the tendency. For more rigorous evaluation further investigations are needed. It was observed that e.g the K_{aw} of AO depends on the stock solution concentration.

FIGURE 6

The *second requirement* is fulfilled by MB, AO, and Fu. Eo instead has a negative charge at pH 7.0 and pH 7.4 and therefore it was excepted that Eo is not transported by Pgp. The experimental data supported the expectations (Figures 2D and 3). However, it is not clear from the present data whether Eo interacts with the NBDs of Pgp. Here, it also has to be noted that pH of the local environment effects on the protonation state of drugs, which usually are weak acids or bases. Thus the compounds which has a negatively charge at pH 7.4 can be substrates for Pgp at acidic conditions. Interestingly, *MB* has a fixed positive

charge. In inside-out Pgp vesicles permanently charged compounds are able to stimulate Pgp activity because the drug binding site is located towards extracellular medium (*59*). In living cells this is unexpected because drugs have to diffuse through the hydrophobic lipid bilayer in order to reach the drug binding site of Pgp. Only uncharged compounds diffuse through hydrophobic lipid core (*60*). However, as seen in the microscope pictures (Figure 4 and 5) MB has clearly been taken up the cells and therefore another uptake mechanism has to exist. May et al. (*56*) suggested that MB enters into the human erythocytes via an enzyme ''thiazine dye reductase'' that reduces the oxidized, charged MB (MB+, or ''blue'') on the extracellular surface of cell. Thus the non-charged form (MBH or ''colorless'') can diffuse passively across the plasma membrane. Similar uptake mechanism has been proposed for endothelial cells (*61-63*) and it also may exist in mouse embryo fibroblasts.

The *third requirement* for Pgp substrates is also fulfilled by all studied tissue dyes as seen in Figure 1. Also Eo carries at least three hydrogen bond acceptor patterns in the distance ((2.5 ± 0.5) Å or (4.6 ± 0.6) Å), but a negative charge abolishes the possible interactions with the transmembrane helices Pgp. The binding affinity of drug to Pgp can be estimated as the free energy of hydrogen bond formation between the substrate and the transporter, EU_H, according to the differently weighted hydrogen bond acceptor patterns. For the strong (oxygen), the intermediate (nitrogen, sulfur, phenyl ring), and the weak hydrogen bond acceptor groups (fluorine) were given the weight 1, 0.5, and 0.25, respectively. Fu has only one hydrogen bond acceptor pattern composed of two phenyl rings whereas MB and AO have two patterns composed of two phenyl rings and one composed of sulfur-nitrogen and nitrogen-nitrogen atoms, respectively. Thus, it was expected that the total hydrogen bond energy between Pgp and Fu is weaker than between Pgp and MB/AO and correspondently the maximum Pgp activity, V_1, for Fu is smaller than for MB and AO. In Figure 7 is shown the logarithm of maximum activity of Pgp, $\ln V_1$, as a function of the free energy of drug binding from the aqueous phase to the transporter, $\Delta G^0_{tw(1)}$. The previously studied Pgp substrates are indicated as stars, and the tissue dyes as open squares. As seen the tissue dyes are in good agreement with the previously reported results and with the expectations.

FIGURE 7

Free-Energy of Substrate Binding to the Transporter Evaluated According to a Two-Step Substrate Binding Mechanism. The free energy of substrate binding to the activating binding region of Pgp from the lipid phase, $\Delta G^0_{tl(1)}$, were calculated as a difference between the free energy of drug binding from the aqueous phase to the transporter, $\Delta G^0_{tw(1)}$, and the free energy of drug partitioning into the lipid bilayer, ΔG^0_{lw}. For MB, AO, and Fu $\Delta G^0_{tl(1)}$ were -7.8 kJ/mol, -5.8 kJ/mol, and -4.4 kJ/mol, respectively. Eo did not interact with Pgp as seen in Figure 3. By dividing the experimental free energies, $\Delta G^0_{tl(1)}$, by the weighted hydrogen bonds (for details cf. Chapter 7.1) we estimated the free energy of binding per potential hydrogen bond formed, ΔG^0_{Hi}, for AO, MB and Fu as -2.9 kJ/mol, -3.8 kJ/mol, and -4.4 kJ/mol, respectively (Table 1). These results are in good agreement with the values calculated previously with a similar approach for the 15 well-known Pgp substrates and they are reasonable values for the weak hydrogen bonds (Chapter 7.1 (*34*)). However, it has to be emphasized that these values have to be taken as rough estimates since the experimental difficulties in the determination of the lipid-water partition coefficient of the dyes.

Conclusions. We showed that by applying the established rules for intrinsic Pgp-substrates the Pgp-substrate interaction can be predicted in reasonable manner. In accordance with the established rules it was assumed that MB, AO, and Fu are intrinsic substrates for Pgp, whereas Eo is not. This prediction was validated experimentally with the phosphate release measurements in plasma membrane vesicles of NIH-MDR1-G185 cells and with the ECAR measurements in living cells. Furthermore, ECAR measurements revealed that MB, AO and Eo influence the energy metabolism of NIH-WT and *MDR1*-transfected cells in complex manner. Thus, by evaluating Pgp activity in living cells gives further valuable information about the cytotoxicity of drugs.

REFERENCES

1.   Guttmann, P., and Erhlich, P. (1891) Ueber die Wirkung des Methylenblau bei Malaria., *Berlin Klin. Wochehschr. 28*, 953-956.
2.   Vennerstrom, J. L., Makler, M. T., Angerhofer, C. K., and Williams, J. A. (1995) Antimalarial dyes revisited: xanthenes, azines, oxazines, and thiazines, *Antimicrob. Agents Chemother. 39*, 2671-2677.
3.   Wainwright, M. (2003) The use of dyes in modern biomedicine, *Biotech. Histochem. 78*, 147-155.
4.   Wainwright, M., and Amaral, L. (2005) The phenothiazinium chromophore and the evolution of antimalarial drugs, *Trop. Med. Int. Health 10*, 501-511.
5.   Kuchel, P., and Ralston, G. (1998) *Schaum's Outline of Theory and Problems of Biochemistry*, McGraw-Hill.
6.   Darzynkiewicz, Z., and Crissman, H. A. (1990) *Methods In Cell Biology*, Vol. 33, Academic Press, San Diego.
7.   Poot, M., Rizk-Rabin, M., Hoehn, H., and Pavlovitch, J. H. (1990) Cell size and RNA content correlate with cell differentiation and proliferative capacity of rat keratinocytes, *J. Cell. Physiol. 143*, 279-286.
8.   Capella, M. A., and Capella, L. S. (2003) A light in multidrug resistance: photodynamic treatment of multidrug-resistant tumors, *J. Biomed. Sci. 10*, 361-366.
9.   Dolmans, D. E., Fukumura, D., and Jain, R. K. (2003) Photodynamic therapy for cancer, *Nat. Rev. Cancer 3*, 380-387.
10.   Sibata, C. H., Colussi, V. C., Oleinick, N. L., and Kinsella, T. J. (2000) Photodynamic therapy: a new concept in medical treatment, *Braz. J. Med. Biol. Res. 33*, 869-880.
11.   Sibata, C. H., Colussi, V. C., Oleinick, N. L., and Kinsella, T. J. (2001) Photodynamic therapy in oncology, *Expert Opin. Pharmacother. 2*, 917-927.
12.   Gottesman, M. M., Fojo, T., and Bates, S. E. (2002) Multidrug resistance in cancer: role of ATP-dependent transporters, *Nat. Rev. Cancer 2*, 48-58.
13.   Harbottle, H., Thakur, S., Zhao, S., and White, D. G. (2006) Genetics of antimicrobial resistance, *Anim. Biotechnol. 17*, 111-124.
14.   Ambudkar, S. V., Dey, S., Hrycyna, C. A., Ramachandra, M., Pastan, I., and Gottesman, M. M. (1999) Biochemical, cellular, and pharmacological aspects of the multidrug transporter, *Annu. Rev. Pharmacol. Toxicol. 39*, 361-398.
15.   Litman, T., Druley, T. E., Stein, W. D., and Bates, S. E. (2001) From MDR to MXR: new understanding of multidrug resistance systems, their properties and clinical significance, *Cell. Mol. Life Sci. 58*, 931-959.
16.   Dawson, R. J., and Locher, K. P. (2006) Structure of a bacterial multidrug ABC transporter, *Nature 443*, 180-185.
17.   Konings, W. N., and Poelarends, G. J. (2002) Bacterial multidrug resistance mediated by a homologue of the human multidrug transporter P-glycoprotein, *IUBMB Life 53*, 213-218.
18.   van Veen, H. W., Margolles, A., Muller, M., Higgins, C. F., and Konings, W. N. (2000) The homodimeric ATP-binding cassette transporter LmrA mediates multidrug transport by an alternating two-site (two-cylinder engine) mechanism, *EMBO J. 19*, 2503-2514.
19.   Poole, K. (2005) Efflux-mediated antimicrobial resistance, *J. Antimicrob. Chemother. 56*, 20-51.

20.   Shukla, S., Rai, V., Banerjee, D., and Prasad, R. (2006) Characterization of Cdr1p, a major multidrug efflux protein of Candida albicans: purified protein is amenable to intrinsic fluorescence analysis, *Biochemistry 45*, 2425-2435.

21.   Higgins, C. F., and Gottesman, M. M. (1992) Is the multidrug transporter a flippase?, *Trends Biochem. Sci. 17*, 18-21.

22.   Al-Shawi, M. K., Polar, M. K., Omote, H., and Figler, R. A. (2003) Transition state analysis of the coupling of drug transport to ATP hydrolysis by P-glycoprotein, *J. Biol. Chem. 278*, 52629-52640.

23.   Ambudkar, S. V., Cardarelli, C. O., Pashinsky, I., and Stein, W. D. (1997) Relation between the turnover number for vinblastine transport and for vinblastine-stimulated ATP hydrolysis by human P-glycoprotein, *J. Biol. Chem. 272*, 21160-21166.

24.   Litman, T., Zeuthen, T., Skovsgaard, T., and Stein, W. D. (1997) Structure-activity relationships of P-glycoprotein interacting drugs: kinetic characterization of their effects on ATPase activity, *Biochim. Biophys. Acta 1361*, 159-168.

25.   Sharom, F. J., Yu, X., and Doige, C. A. (1993) Functional reconstitution of drug transport and ATPase activity in proteoliposomes containing partially purified P-glycoprotein, *J. Biol. Chem. 268*, 24197-24202.

26.   Seelig, A., and Gerebtzoff, G. (2006) Enhancement of drug absorption by noncharged detergents through membrane and P-glycoprotein binding, *Expert Opin Drug Metab Toxicol 2*, 733-752.

27.   Chen, Y., Pant, A. C., and Simon, S. M. (2001) P-glycoprotein does not reduce substrate concentration from the extracellular leaflet of the plasma membrane in living cells, *Cancer Res. 61*, 7763-7769.

28.   Raviv, Y., Pollard, H. B., Bruggemann, E. P., Pastan, I., and Gottesman, M. M. (1990) Photosensitized labeling of a functional multidrug transporter in living drug-resistant tumor cells, *J. Biol. Chem. 265*, 3975-3980.

29.   Shapiro, A. B., and Ling, V. (1997) Extraction of Hoechst 33342 from the cytoplasmic leaflet of the plasma membrane by P-glycoprotein, *Eur. J. Biochem. 250*, 122-129.

30.   Shapiro, A. B., and Ling, V. (1998) Transport of LDS-751 from the cytoplasmic leaflet of the plasma membrane by the rhodamine-123-selective site of P-glycoprotein, *Eur. J. Biochem. 254*, 181-188.

31.   Seelig, A. (1998) A general pattern for substrate recognition by P-glycoprotein, *Eur. J. Biochem. 251*, 252-261.

32.   Seelig, A., Blatter, X. L., and Wohnsland, F. (2000) Substrate recognition by P-glycoprotein and the multidrug resistance-associated protein MRP1: a comparison, *Int. J. Clin. Pharmacol. Ther. 38*, 111-121.

33.   Aanismaa, P., and Seelig, A. (2007) P-Glycoprotein Kinetics Measured in Plasma Membrane Vesicles and Living Cells, *Biochemistry*.

34.   Gatlik-Landwojtowicz, E., Aanismaa, P., and Seelig, A. (2006) Quantification and characterization of p-glycoprotein-substrate interactions, *Biochemistry 45*, 3020-3032.

35.   Seelig, A., and Gatlik-Landwojtowicz, E. (2005) Inhibitors of multidrug efflux transporters: their membrane and protein interactions, *Mini-Rev. Med. Chem. 5*, 135-151.

36.   Kusuzaki, K., Minami, G., Takeshita, H., Murata, H., Hashiguchi, S., Nozaki, T., Ashihara, T., and Hirasawa, Y. (2000) Photodynamic inactivation with acridine orange on a multidrug-resistant mouse osteosarcoma cell line, *Jpn. J. Cancer Res. 91*, 439-445.

37.   Trindade, G. S., Farias, S. L., Rumjanek, V. M., and Capella, M. A. (2000) Methylene blue reverts multidrug resistance: sensitivity of multidrug resistant cells to this dye and its photodynamic action, *Cancer Lett. 151*, 161-167.

38.   Wainwright, M., Phoenix, D. A., Marland, J., Wareing, D. R., and Bolton, F. J. (1997) A study of photobactericidal activity in the phenothiazinium series, *FEMS Immunol. Med. Microbiol. 19*, 75-80.

39.   Wainwright, M., Phoenix, D. A., Marland, J., Wareing, D. R., and Bolton, F. J. (1998) A comparison of the bactericidal and photobactericidal activities of aminoacridines and bis(aminoacridines), *Lett. Appl. Microbiol. 26*, 404-406.

40.   Kwon, Y., Kamath, A. V., and Morris, M. E. (1996) Inhibitors of P-glycoprotein-mediated daunomycin transport in rat liver canalicular membrane vesicles, *J Pharm Sci 85*, 935-939.

41.   Rumjanek, V. M., Trindade, G. S., Wagner-Souza, K., de-Oliveira, M. C., Marques-Santos, L. F., Maia, R. C., and Capella, M. A. (2001) Multidrug resistance in tumour cells: characterization of the multidrug resistant cell line K562-Lucena 1, *An. Acad. Bras. Cienc. 73*, 57-69.

42.   Thalhammer, T., Stapf, V., Gajdzik, L., and Graf, J. (1994) Bile canalicular cationic dye secretion as a model for P-glycoprotein mediated transport, *Eur J Pharmacol 270*, 213-220.

43.   Zamora, J. M., Pearce, H. L., and Beck, W. T. (1988) Physical-chemical properties shared by compounds that modulate multidrug resistance in human leukemic cells, *Mol Pharmacol 33*, 454-462.

44.   Gatlik-Landwojtowicz, E., Aanismaa, P., and Seelig, A. (2004) The rate of P-glycoprotein activation depends on the metabolic state of the cell, *Biochemistry 43*, 14840-14851.

45.   Landwojtowicz, E., Nervi, P., and Seelig, A. (2002) Real-time monitoring of P-glycoprotein activation in living cells, *Biochemistry 41*, 8050-8057.

46.   Fischer, H., Gottschlich, R., and Seelig, A. (1998) Blood-brain barrier permeation: molecular parameters governing passive diffusion, *J. Membr. Biol. 165*, 201-211.

47.   Gerebtzoff, G., Li-Blatter, X., Fischer, H., Frentzel, A., and Seelig, A. (2004) Halogenation of drugs enhances membrane binding and permeation, *Chembiochem 5*, 676-684.

48.   May, J. M., Qu, Z. C., and Whitesell, R. R. (2003) Generation of oxidant stress in cultured endothelial cells by methylene blue: protective effects of glucose and ascorbic acid, *Biochem Pharmacol 66*, 777-784.

49.   Kapuscinski, J., and Darzynkiewicz, Z. (1983) Increased accessibility of bases in DNA upon binding of acridine orange, *Nucleic Acids Res 11*, 7555-7568.

50.   Kapuscinski, J., Darzynkiewicz, Z., and Melamed, M. R. (1983) Interactions of acridine orange with nucleic acids. Properties of complexes of acridine orange with single stranded ribonucleic acid, *Biochem Pharmacol 32*, 3679-3694.

51.   Lerman, L. S. (1963) The structure of the DNA-acridine complex, *Proc Natl Acad Sci U S A 49*, 94-102.

52.   Gatto, C., and Milanick, M. A. (1993) Inhibition of the red blood cell calcium pump by eosin and other fluorescein analogues, *Am. J. Physiol. 264*, C1577-1586.

53.   Helmich-de Jong, M. L., van Duynhoven, J. P., Schuurmans Stekhoven, F. M., and De Pont, J. J. (1986) Eosin, a fluorescent marker for the high-affinity ATP site of (K+ + H+)-ATPase, *Biochim Biophys Acta 858*, 254-262.

54.   Kennedy, B. G., and Mangini, N. J. (1996) Plasma membrane calcium-ATPase in cultured human retinal pigment epithelium, *Exp. Eye Res. 63*, 547-556.

55.   Skou, J. C., and Esmann, M. (1981) Eosin, a fluorescent probe of ATP binding to the (Na+ + K+)-ATPase, *Biochim Biophys Acta 647*, 232-240.

56.   May, J. M., Qu, Z. C., and Cobb, C. E. (2004) Reduction and uptake of methylene blue by human erythrocytes, *Am J Physiol Cell Physiol 286*, C1390-1398.

57.   Seelig, A., and Landwojtowicz, E. (2000) Structure-activity relationship of P-glycoprotein substrates and modifiers, *Eur. J. Pharm. Sci. 12*, 31-40.

58.   Seelig, A., Gottschlich, R., and Devant, R. M. (1994) A method to determine the ability of drugs to diffuse through the blood-brain barrier, *Proc. Natl. Acad. Sci. U.S.A. 91*, 68-72.

59.   Omote, H., and Al-Shawi, M. K. (2002) A novel electron paramagnetic resonance approach to determine the mechanism of drug transport by P-glycoprotein, *J Biol Chem 277*, 45688-45694.

60.   Saparov, S. M., Antonenko, Y. N., and Pohl, P. (2006) A new model of weak acid permeation through membranes revisited: does Overton still rule?, *Biophys J 90*, L86-88.

61.   Bongard, R. D., Merker, M. P., Shundo, R., Okamoto, Y., Roerig, D. L., Linehan, J. H., and Dawson, C. A. (1995) Reduction of thiazine dyes by bovine pulmonary arterial endothelial cells in culture, *Am. J. Physiol. 269*, L78-84.

62.   Merker, M. P., Bongard, R. D., Kettenhofen, N. J., Okamoto, Y., and Dawson, C. A. (2002) Intracellular redox status affects transplasma membrane electron transport in pulmonary arterial endothelial cells, *Am J Physiol Lung Cell Mol Physiol 282*, L36-43.

63.   Merker, M. P., Bongard, R. D., Linehan, J. H., Okamoto, Y., Vyprachticky, D., Brantmeier, B. M., Roerig, D. L., and Dawson, C. A. (1997) Pulmonary endothelial thiazine uptake: separation of cell surface reduction from intracellular reoxidation, *Am. J. Physiol. 272*, L673-680.

64.   Kurz, T., Gustafsson, B., and Brunk, U. T. (2006) Intralysosomal iron chelation protects against oxidative stress-induced cellular damage, *Febs J 273*, 3106-3117.

65.   Mukumoto, I., Matsukawa, H., Tabata, H., and Omura, M. (1956) Absorption spectrum and dissociation constant of fuchsin solution. , *Osaka Daigaku Igaku Zassi 8* 749-751.

66.   Majima, E., Yamaguchi, N., Chuman, H., Shinohara, Y., Ishida, M., Goto, S., and Terada, H. (1998) Binding of the fluorescein derivative eosin Y to the mitochondrial ADP/ATP carrier: characterization of the adenine nucleotide binding site, *Biochemistry 37*, 424-432.

67.   Gerebtzoff, G., and Seelig, A. (2006) In silico prediction of blood-brain barrier permeation using the calculated molecular cross-sectional area as main parameter, *J Chem Inf Model 46*, 2638-2650.

TABLES

Table 1. The kinetic parameters of Pgp activation for the dyes measured with the phosphate release measurements in plasma membrane vesicles of NIH-MDR1-G185. K_1 (K_2) is the concentration of the half-maximum Pgp activation (inhibition), and V_1 (V_2) is the maximum (minimum) Pgp activity. ΔG_{Hi}^0 is the estimated free energy per hydrogen bond formed between Pgp and its substrate.

Dye	MW [g/mol]	pK_a	weighted number of H-bond acceptors	$1/C_0$ [a] [mM^{-1}] pH 7.4	A_d [b] [Å^2]	K_1 [μM] pH7.0	K_2 [μM] pH7.0	V_1 [fold] pH7.0	V_2 [fold] pH7.0	ΔG_{Hi}^0 [kJ/mol]
MB	284.4	~13-14[2]	2	14	55	46.5	825	3.1	0.1	-3.8
AO	265.4	10.3[64]	2	13-455	55	6.2	801.2	3.3	0	-2.9
Fu	337.9	2.5 7.8[65] 12.5	1	1280	70	5.7	50.0	1.75	0.3	-4.4
Eo	714.0	3.2[66]	5	1650	70	-	-	-	-	-

[a] The concentration of the surface activity onset is obtained from the surface activity measurements at pH 7.4. Eo was dissolved in DMSO, MB, AO, and Fu in H$_2$O. C_0 for AO is affected by the association state of the molecule in solution which depends on the stock solution concentration. C_0 for Eo and Fu are affected by the low solubility of the compounds. [b] The cross-sectional area of the molecule are the estimates. They will be modelled according to (67).

FIGURE LEGENDS

FIGURE 1. Chemical structures of methylene blue, MB, acridine orange, AO, basic fuchsin, Fu, and ethyl eosin, Eo. The dashed line circles and the asterisks indicate the hydrogen bond acceptor groups in the distance ((2.5 ± 0.5) Å or (4.6 ± 0.6) Å).

FIGURE 2A-D. Time dependent ECAR of NIH-WT (circles) and NIH-MDR1-G185 (squares) cells as a function of increasing concentration of A) MB, B) AO, C) Fu, and D) Eo. The ECAR is measured with a Cytosensor microphysiometer (37°C, pH 7.4). The cells were stimulated with dyes for 3 min which is indicated as a hatched bar in 2D. Each segment is normalized to a basal ECAR (the average of two data points before dye-stimulation period is taken as 100 %). The solid symbols indicate the second stimulation point during the 3-min stimulation period which is used for the evaluation of Pgp activity (cf. Chapter 3). The time bars (30 min) are shown. Note the difference in the scale of Y-axis.

FIGURE 3A-B. Dye-induced Pgp activity profiles measured in living NIH-MDR1-G185 cells (filled symbols) and NIH-WT cells (open symbols) and B) in plasma membrane vesicles prepared thereof. MB ($\bullet$, $\bigcirc$), AO ($\blacksquare$, $\square$), Fu ($\blacktriangledown$, $\triangledown$), and D) Eo ($\blacktriangle$, $\triangle$). Vanadate-sensitive Pgp activation was measured with the phosphate release assay (37°C, pH 7.0). The basal vanadate-sensitive Pgp activity is taken as 100%. The ECAR was measured with a Cytosensor microphysiometer (37°C, pH 7.4). The second measuring point during 3-min stimulation period indicated in Figure 2A-D as filled symbols are shown. The solid lines are the fits to the modified Michaelis-Menten equation (eq. (1)). The data points correspond to the average of 1-4 measurements.

FIGURE 4A-D. Light microscopy pictures (20x magnification) of NIH-WT (A and C) and NIH-MDR1-G185 cells (B and D) before (top row) and after 1h incubation with 64.5 µM MB (bottom row).

FIGURE 5A-F. Light microscopy pictures (40x magnification) of NIH-WT (A, B, C) and NIH-MDR1-G185 cells (D, E, F). A and D: without drug; B and E: after 1h incubation at 37°C with MB (64.5 µM); C and F: after 1h incubation at 37°C with PSC833 (1 µM) and MB (64.5 µM).

FIGURE 6. Correlation between the air-water partition coefficient, K_{aw}, and the inverse of the concentration of half-maximum Pgp activation, $1/K_1$. The concentrations of half-maximum Pgp activation, K_1, are obtained from the phosphate release measurements (pH 7.0, 37°C) in plasma membrane vesicles of NIH-MDR1-G185 cells. The air-water partition coefficient, K_{aw}, and the concentration of surface activity onset, C_0, are determined from the surface activity measurements (pH 7.4, $(24 \pm 1)^{o}$C). Tissue dyes are shown as filled squares, and the previously studied Pgp substrates are indicated as stars (adapted from the studies presented in Chapters 7.1 and 7.2). 1) amitriptyline, 2) chlorpromazine, 3) cis-flupenthixol, 4) cyclosporin A, 5) daunorubicin 6) dibucaine, 7) diltiazem, 8) glivec, 9) lidocaine 10) progesterone, 11) promazine, 12) (R/S)-verapamil, 13) reserpine, 14) trifluoperazine, 15) triflupromazine.

FIGURE 7. Logarithm of maximum Pgp activity, $\ln V_1$, as a function of the free energy of binding of substrate from the aqueous phase to the activating binding region of the transporter, $\Delta G^0_{tw(1)}$. Pgp activity was measured in the inverted plasma membrane vesicles of NIH-MDR1-G185 cells (pH 7.0, 37°C). Tissue dyes are shown as filled squares, and the previously studied Pgp substrates are indicated as stars (adapted from the study presented in Chapter 7.2). 1) amitriptyline, 2) chlorpromazine, 3) cis-flupenthixol, 4) cyclosporin A, 6) dibucaine, 7) diltiazem, 8) glivec, 10) progesterone, 11) promazine, 12) (R/S)-verapamil, 13) reserpine, 14) trifluoperazine, 15) triflupromazine, 16) colchicine, 17) OC144-093, 18) PSC-833, and 19) vinblastine.

FIGURES

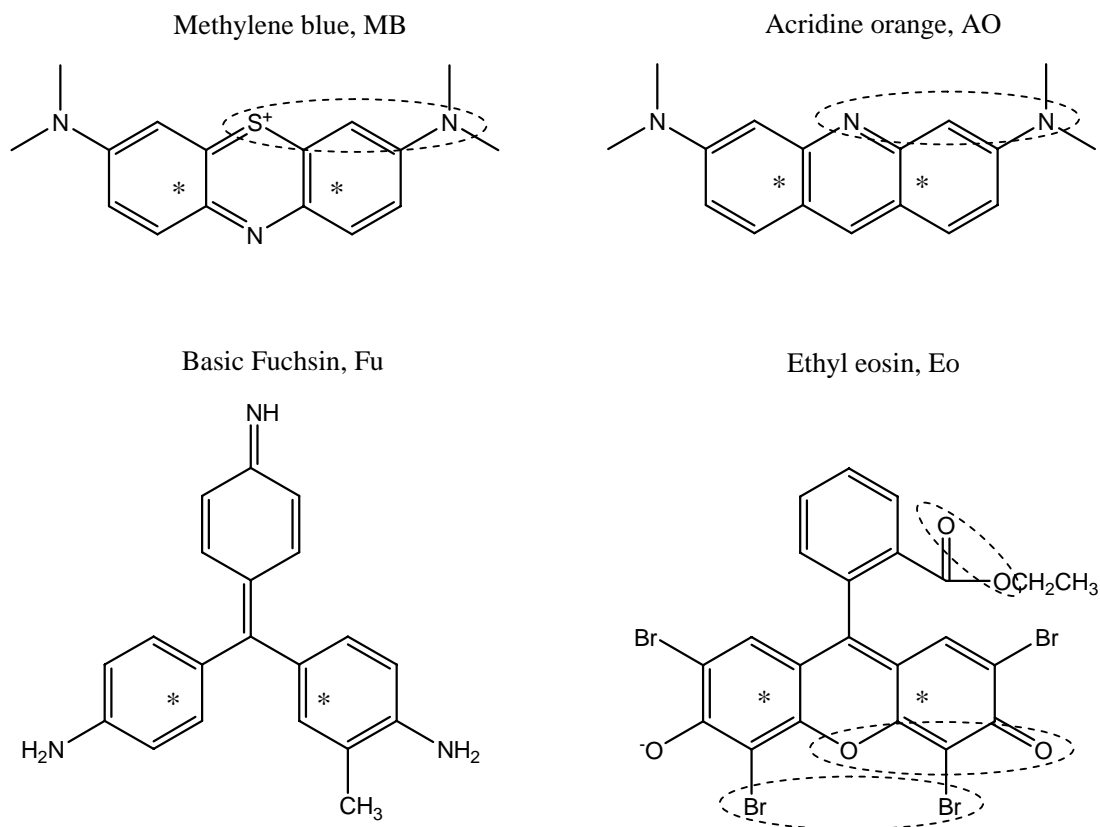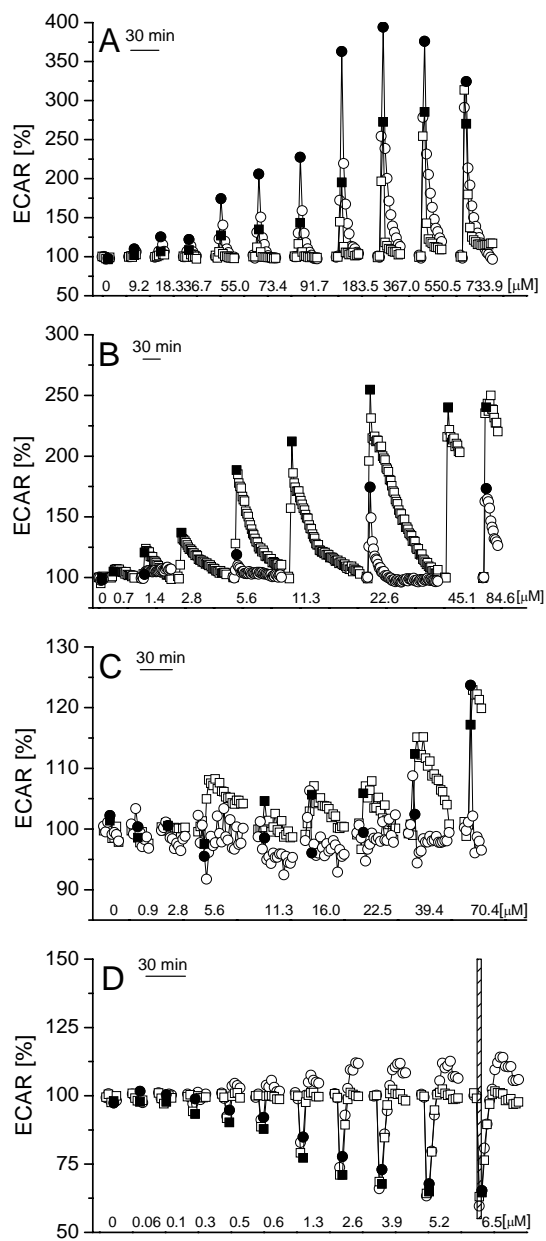Methylene blue, MB

Acridine orange, AO
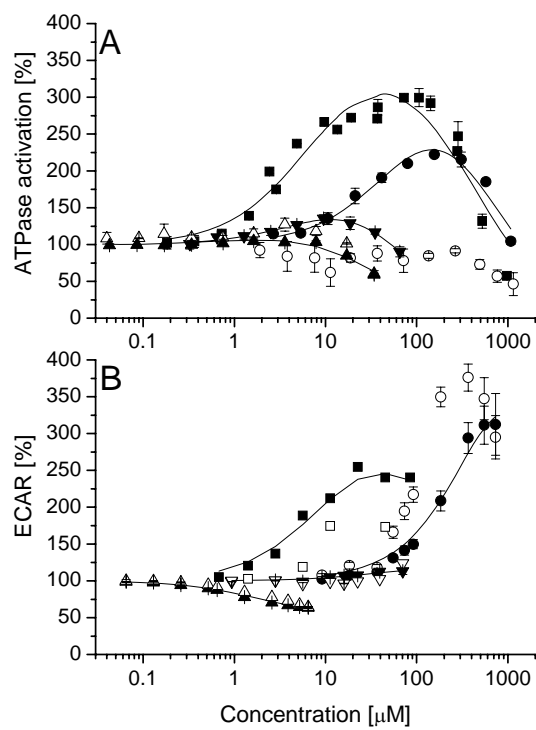
Basic Fuchsin, Fu

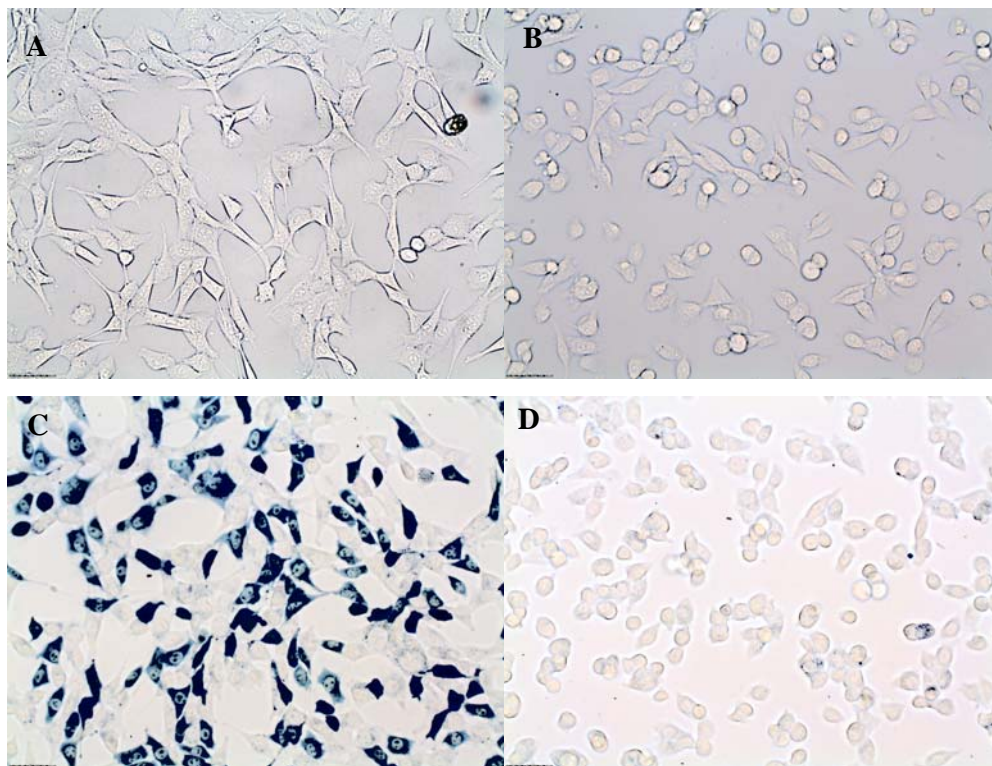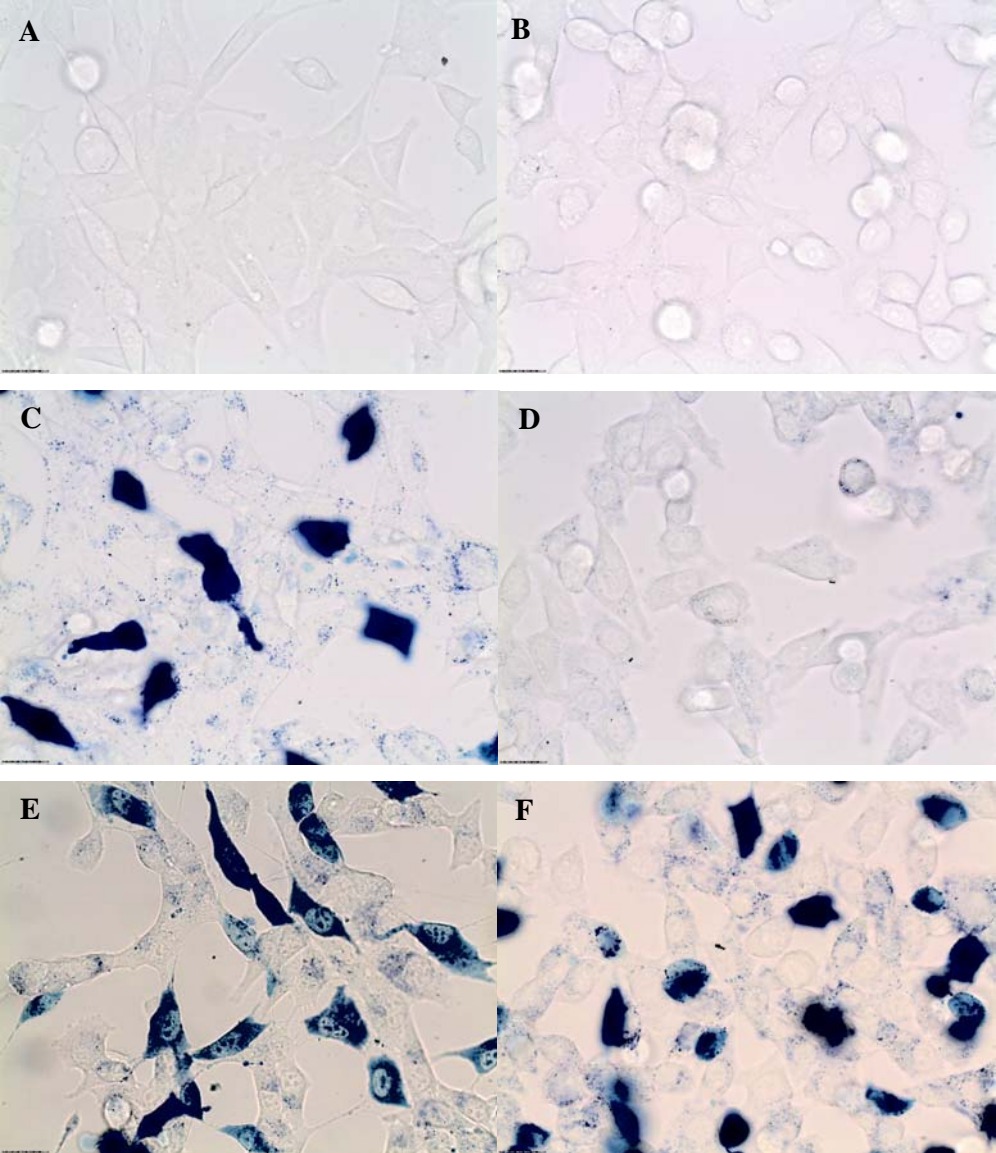Ethyl eosin, Eo

FIGURE 1

FIGURE 2A-D

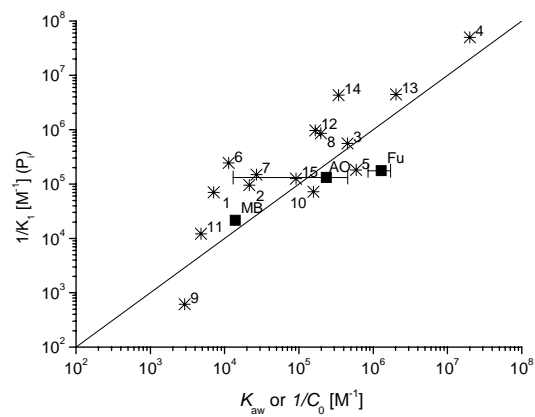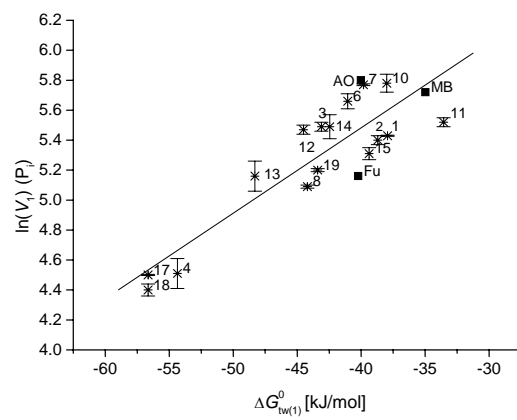FIGURE 3A-B

FIGURE 4A-D

FIGURE 5A-F

FIGURE 6

FIGURE 7

8. Curriculum Vitae

Päivi Äänismaa
Institute of Biophysical Chemistry
Biozentrum, University Basel
Klingelbergstrasse 50-70
CH-4056 Basel
Tel +41 612672192
paivi.aanismaa@unibas.ch

CURRICULUM VITAE

Personal data:

Date and place of birth: 11.10.1974, Savonlinna, Finland

Nationality: Finnish

Education:

04/2003-03/2007:	Graduate (PhD) studies at the Department of Biophysical Chemistry, Biozentrum, University of Basel, Switzerland
	Thesis Supervisor: PD. Dr. Anna Seelig
	PhD Thesis: Thermodynamics and Kinetics of P-Glycoprotein-Substrate Interactions
2000:	M. Sc in Chemical Technology, Applied Chemistry, Lappeenranta University of Technology, Finland
	Master Thesis: Characterization of Acrylic based ion exchange resins and their applicability to chromatographic separation
1998-1998:	Exchange student at Technical University of Dresden, Germany

Publications and Poster Presentations:

2007:   P-glycoprotein Kinetics Measured in Plasma Membrane Vesicles and Living
          Cells, Päivi Äänismaa and Anna Seelig, *Biochemistry*, web released,
          05.02.2007

2006:   Quantification and Characterization of P-Glycoprotein-Substrate Interactions,
          Ewa Gatlik-Landwojtowicz, Päivi Äänismaa, and Anna Seelig, (2006)
          Biochemistry, *45*, 3020-3032.

2004:   The rate of P-glycoprotein activation depends on the metabolic state of the cell,
          Ewa Gatlik-Landwojtowicz, Päivi Äänismaa, and Anna Seelig, (2004)
          Biochemistry 43, 14840-14851.

2002:   Modeling the Sorption of Water-Ethanol Mixtures in Cross-linked Ionic and
          Neutral Polymers, Jari Tiihonen, Ismo Markkanen, Ari Kärki, Päivi Äänismaa,
          Markku Laatikainen and Erkki Paatero, (2002), *Chem. Eng. Sci*, 57 (11), 2885-
          1897

2006:   Poster Presentation at the MipTec Event in Basel, Switzerland, 2006
          Basel Award for best poster: ''P-glycoprotein Activation Monitored via ATP
          Hydrolysis and ATP Synthesis''

2004:   Poster Presentation at the PGRD Drug Discovery European Postgraduate Poster
          Symposium, Pfizer Global Research and Development, Sandwich, UK
          Poster Price, highly commended: '' P-glycoprotein Activation: Intact Cells
          versus Inside-Out Vesicles''